CLOSED-LOOP CONTROL AND VARIABLE CONSTRAINT MECHANISMS OF A HYBRID NEUROPROSTHESIS TO RESTORE GAIT AFTER SPINAL CORD INJURY

by

CURTIS SAI-HAY TO

Submitted in partial fulfillment of the requirements

For the degree of Doctor of Philosophy

Dissertation Adviser: Dr. Ronald J. Triolo

Department of Biomedical Engineering

CASE WESTERN RESERVE UNIVERSITY

May, 2010

CASE WESTERN RESERVE UNIVERSITY

SCHOOL OF GRADUATE STUDIES

We hereby approve the thesis/dissertation of

Curtis Sai-Hay To

candidate for the Ph.D. degree *.

(signed) Robert F. Kirsch, Ph.D.
(chair of the committee)

Ronald J. Triolo, Ph.D.

Roger D. Quinn, Ph.D.

Patrick E. Crago, Ph.D.

(date) March 19, 2010

*We also certify that written approval has been obtained for any proprietary material contained therein.

THIS WORK IS DEDICATED TO MY MOTHER AND FATHER,

WINNIE YEUK-BIG TO & BYRON HIN-LEUNG TO.

TABLE OF CONTENTS

CHAPTER 4

DEVELOPMENT AND IMPLEMETATION OF A CLOSED-LOOP CONTROLLER FOR THE REAL-TIME MODULATION OF ELECTRICAL STIMULATION AND JOINT CONSTRAINTS OF A PROTOTYPE HYBRID NEUROPROSTHESIS FOR RESTORING GAIT

CHAPTER 5

THE HYBRID NEUROPROSTHESIS: CONSTRAINTS WITHOUT LIMITATIONS

LIST OF TABLES

GLOSSARY

CHAPTER 2

CHAPTER 3

CHAPTER 4

LIST OF FIGURES

CHAPTER 1

CHAPTER 2

CHAPTER 3

CHAPTER 4

CHAPTER 5

APPENDIX A

APPENDIX B

PREFACE

This dissertation constitutes the entirety of my doctoral work in the Department of Biomedical Engineering at Case Western Reserve University from January 2004 to May 2010. This work has been done in association with the Advanced Platform Technology (APT) Center and Cleveland Functional Electrical Stimulation (FES) Center at the Louis Stokes Cleveland Department of Veterans Affair Medical Center.

ACKNOWLEDGEMENTS

The whole of this work has been influenced by and comprised of the cumulative efforts of many individuals. This work was funded by the Department of Defense (Grant #PR043074) and the Department of Veterans Affairs (Grant #B3463R and #A6404R).

First I would like to thank the principal investigators of this research, Dr. Ronald J. Triolo and Rudi Kobetic. Their original vision of this research is truly inspirational and their continued guidance throughout my graduate career has been a critical component to making this work possible. I am grateful for Dr. Triolo's and Mr. Kobetic's trust and confidence in me to explore and implement my own ideas through a wealth of available resources.

I would like to show my gratitude to the study participants. Their generosity and commitment to this research has been exceptional.

I would like to thank the members of my Ph.D. Guidance Committee, Drs. Robert F. Kirsch, Patrick E. Crago, Roger D. Quinn, and Musa L. Audu for their advice and participation in this work. I would especially like to extend my appreciation to Dr. Audu. He is unquestionably a pleasure to work with and has always been able and eager to help me.

I am indebted to John R. Schnellenberger for his involvement in this work. An invaluable contributor to this research, he was responsible for designing and developing all the electronics required for the feasible implementation of my work. Thomas C. Bulea, a fellow graduate student working on related research, has not only helped me

through a majority of my experiments, but was a valuable source for advice and new ideas.

I am truly grateful to the following individuals for their friendship and making working at Case Western Reserve University, the APT Center, and the Cleveland FES Center an awesome experience: Stephanie Nogan Bailey, Arden Bartlett, Lisa Boggs, Jim Buckett, Alex Campean, Dr. Dwight T. Davy, Dr. Anirban Dutta, Vanessa Q. Everding, Lee E. Fisher, Kevin Foglyano, Steve Gartman, Dr. Elizabeth Hardin, Dr. Juan Gabriel Hincapie, Suzana C. Iveljic, Joris Lambrecht, Nicole Kern, Dr. Jose Luis Lujan, Wendy Lujan, Michael E. Miller, Brian Murphy, Raviraj Nataraj, Arkady Polinkovsky, Mark Renfrew, Lori Rohde, Jonathan L. Sakai, Dr. Matthew Schiefer, Barb Seitz, Paula Shelton, Cathy Walker, Merien Washington, Jeff Weisgarber, and Gary A. Wu.

I would like to thank Dan Adams and Timothy O'Shaughnessy at Shamrock Hose and Fittings, Inc., Cleveland, OH, USA, for their advice, generosity, and introducing me to the state of the art in fluid connectors.

Most importantly, I would like to thank my family for their love, encouragement, and support. I would like to give my deepest appreciation to my mother and father, to whom this work is dedicated to, brother, Dr. Ambrose Jing-Hay To, sister-in-law, Dr. Renee Pui-San Wong, twin sister, Dr. Vivien Ngah-Tse To, and brother-in-law, Yuriy Krichevskiy.

LIST OF ABBREVIATIONS

AFO = ankle-foot orthosis
APT = Advanced Platform Technology

BLEEX = Berkeley lower extremity exoskeleton

CAD = computer-aided design

DOF = degree of freedom
DSKM = dual-state knee mechanism

ESw = early swing

FES = functional electrical stimulation
FIS = fuzzy inference system
FNS = functional neuromuscular stimulation
FSKC = finite state knee controller
FSPC = finite state postural controller
FSR = force sensitive resistor

GED = gait event detector
GUI = graphical user interface

HAL-5 = Hybrid Assistive Leg
HFECR = hip flexion/extension coupling ratio
HGO = Hip Guidance Orthosis
HKAFO = hip-knee-ankle-foot orthosis
HNP = hybrid neuroprosthesis
HRA = hydraulic rotary actuator

IPI = inter-pulse interval
IRGO = Isocentric Reciprocating Gait Orthosis
ISw = initial swing

KAFO = knee-ankle-foot orthosis

LLB = long leg braces
LR = loading response
LSDCVAMC = Louis Stokes Cleveland Department of Veterans Affair Medical Center
LSw = late swing

MSL = Motion Study Laboratory
MSt = mid stance

NC = normally closed
NO = normally open

PC = personal computer
PSw = pre-swing
PW = pulse width

RGO = Reciprocating Gait Orthosis
ROM = range of motion

SCI = spinal cord injury

TDL = Technical Development Laboratory
THKAFO = trunk-hip-knee-ankle-foot orthosis
TSt = terminal stance

UECU = Universal External Control Unit
UPS = uninterruptible power supply

VCHM = variable constraint hip mechanism

GLOSSARY

FNS-only – The use of only a lower extremity FNS system for assistive gait.

HNP – The combined use of a lower extremity exoskeleton and FNS system for assistive gait.

HNP-hip1 – The combined use of a VCHM, pair of DSKMs, and the hip module of the FNS controller for assistive gait.

HNP-hip2 – The combined use of a VCHM, pair of DSKMs, and a FNS system with pre-programmed baseline stimulation parameters for assistive gait.

HNP-knee1 – The combined use of a 1:1 hip reciprocator, pair of DSKMs, and the knee module of the FNS controller for assistive gait.

HNP-knee2 – The combined use of a 1:1 hip reciprocator, pair of DSKMs, and a FNS system with pre-programmed baseline stimulation parameters for assistive gait.

Hysteresis thresholding – The input must exceed a first threshold for the digital output to transition high and a second threshold must be subceeded for the digital output to transition back to low.

IRGO-only – The use of only an IRGO for assistive gait.

Mechanical compliance – The change in motion in the direction in which the motion is impeded against.

Muscle duty cycle – The duration of time in which the target muscle is activated by the electrical stimulation relative to the total duration of the stride.

Passive resistance – The torque required to move a constraint mechanism, contributed by the deleterious factors against motion inherent to the mechanism (i.e., viscous or frictional effects), at a known angular velocity while the constraint mechanism is in a state not intended to resist motion.

Table G.1
Sign Conventions of Human Motion

Sign → Motion of ↓	**negative**	**positive**
trunk	posterior orientation	anterior orientation
hip	extension	flexion
knee	extension	flexion

Closed-Loop Control and Variable Constraint Mechanisms
of a Hybrid Neuroprosthesis to Restore Gait after
Spinal Cord Injury

Abstract

by

CURTIS SAI-HAY TO

A hybrid neuroprosthesis (HNP) was developed with the goal of providing improved gait to individuals with paraplegia relative to existing assistive gait systems. The HNP is an approach to restoring gait by combining a lower extremity exoskeleton with functional neuromuscular stimulation (FNS). Individually, exoskeletons apply constraints for support, but provide limited step length and depend on upper extremity actions on a walker for forward propulsion. Conversely, FNS mobilizes the limbs through electrical pulses to paralyzed muscles. However, muscles targeted for stimulation quickly fatigue and provide inadequate postural support. The HNP was designed to functionally combine the supportive features of the exoskeleton and joint mobility of FNS.

Controllable knee and hip joint mechanisms were developed to support the user while allowing for functional motion from FNS for forward progression. These mechanisms were optimized for maximal torque when supporting a joint and minimal resistance when driven by FNS. A closed-loop controller based on sensor measurements of joint dynamics was developed to synchronize exoskeletal operation with muscle stimulus activity. The objectives were to modulate joint constraints to provide continual

support to the user while minimizing the deleterious effects of the constraints on joint mobility, deactivate stimulus to target muscles when certain exoskeletal constraints are engaged to allow the target muscles to rest, and modulate FNS from baseline levels to achieve functional joint positions.

The operational response of the controller and mechanisms were characterized through simulation, bench, and able-bodied testing. Implementation of the HNP with an individual with paraplegia respectively showed a 40 % and 16 % reduction in maximum exerted upper extremity forces relative to exoskeleton-only and FNS-only gait. Step lengths were shown to be comparable between HNP and FNS-only gait. When comparing the HNP with and without the FNS modulation, the average gait speed was increased by 16 % with FNS modulation due to a 10 % increase in the hip range of motion. Reductions in muscle activity were feasible when the exoskeletal constraints were enabled.

Future work to optimize joint coordination or apply an active mechanism to the exoskeleton to assist hip extension may improve postural control and forward progression.

CHAPTER 1

INTRODUCTION: CURRENT TECHNIQUES FOR ASSISTIVE GAIT

1.1 MOTIVATION AND SIGNIFICANCE OF WORK

This research centers on developing and evaluating the feasibility of a new hybrid neuroprosthesis (HNP) to provide functional reciprocal gait to individuals with paraplegia after spinal cord injury (SCI). The objective is to use an exoskeleton with controllable joint constraints to provide support while activating the paralyzed muscles via functional neuromuscular stimulation (FNS) to provide mobility. The new HNP will address specific limitations in existing gait assist systems. Gait systems that utilize FNS to restore walking electrically activate paralyzed muscles such that the forces generated are used for both limb mobility and support. FNS gait systems also demand that the user apply high upper extremity forces on a walking aid to support the upper body. Both of these factors lead to increased energy consumption, resulting in short walking durations. A mechanical orthosis known as a reciprocating gait orthosis (RGO) has been demonstrated to be effective in maintaining upright trunk posture. However, the reciprocating hip mechanism of the RGO limits the achievable stride length of the user

which limits gait speed. Furthermore, mechanical orthoses constrain the knees in extension, requiring upper extremity exertion to facilitate proper foot-to-ground clearance during the swing phases of gait. The knee constraints of mechanical orthoses can be manually unlocked, but the knees would then need to be controlled continuously throughout the entire gait cycle by FNS. Currently, no commercialized mechanism exists that is capable of achieving the dependable operation required for the intended user population.

This work consists of the development and implementation of three components of a prototype HNP: 1) a variable constraint hip mechanism (VCHM) [1, 2], 2) a dual-state knee mechanism (DSKM), and 3) a sensor-based feedback control algorithm to synchronously coordinate exoskeleton constraints with the real-time modulation of electrical stimulation patterns to target muscles during gait. The trunk instability of FNS systems and the hip constraint limitation of the RGO are being addressed with a new hip mechanism that was designed to provide postural stability while allowing uninhibited sagittal hip movement during gait. The fundamental function of the VCHM is to modulate each hip constraint independently among four states during gait: 1) reciprocally coupled, 2) freed, 3) bidirectionally locked, and 4) unidirectionally locked. A new knee mechanism was designed to support the knee in extension during the stance phases of gait while allowing the knee to move freely via FNS during the swing phases of gait. The application of a real-time closed-loop controller to modify FNS patterns during gait has yet to be realized partially due to establishing a practical sensor set that can be easily and reliably donned and aligned by the user. The lower extremity exoskeleton provides a convenient structure to instrument a variety of sensors. Thus, difficulties in sensor

donning and alignment should not be a factor in sensor selection. The function of the closed-loop controller is to coordinate the states of the prototype exoskeletal joint constraints with the electrical stimulation to target muscles so that 1) when an exoskeleton constraint is supporting a joint, stimulation to target muscles controlling the joint can be deactivated, 2) stimulation to target muscles can be increased from nominal levels when necessary to achieve the joint movements functional for gait, and 3) the exoskeleton constraints do not impede the functional joint motion. Accordingly, muscle activation via FNS could be focused exclusively on producing the functional movements of joints to reduce the effects of fatigue. The combined implementation of the all three systems should have the effect of minimizing the user voluntary upper extremity effort and stimulated lower extremity muscle activity while facilitating functional limb mobility. Thus, this prototype HNP has the potential of providing energy efficient gait to individuals with paraplegia.

1.2 BACKGROUND

1.2.1 Restoring Gait to Individuals with Paraplegia

Approximately 250,000 people in the US live with SCI with 11,000 new injuries every year [3]. Approximately 50 % of these injuries result in paraplegia. This work will focus on restoring gait to individuals with SCI levels between T5 and T12. Restoring ambulatory function to these individuals is important not only to enhance mobility, but to improve overall health and wellbeing. Gait has been shown to improve bone density, psychological health, cardiopulmonary status, and bladder and bowel function and is

associated with the reduction of spasticity, joint contractures, and pressure sores. Current techniques for facilitating walking in individuals with paraplegia include the use of 1) passive or actively powered exoskeletons (i.e. braces and orthoses), 2) FNS, or 3) hybridizations of both modalities (i.e. HNP). To date, all gait-assist devices require the concurrent use of some form of walking aid (i.e. walker, rollator, crutches, or quad canes) for additional stability.

1.2.2 Lower Extremity Exoskeletons

Conventional braces or orthoses are typically passive exoskeletal devices that reduce the number of degrees of freedom (DOF) of the lower extremities by imposing kinematic constraints to maximize joint stability. Numerous lower extremity exoskeletons have been developed that differ primarily in which DOFs are constrained and how ambulation is achieved. The type of mechanical orthosis prescribed depends on the level and severity of the injury. Four classes of lower extremity exoskeletons have been predominantly employed for ambulation after SCI: 1) ankle-foot orthosis (AFO), 2) knee-ankle-foot orthosis (KAFO), 3) hip-knee-ankle-foot orthosis (HKAFO), and 4) trunk-hip-knee-ankle-foot orthosis (THKAFO).

AFOs, such as the Vannini-Rizzoli Stabilizing Limb Orthosis [4, 5], are typically custom shaped lower leg braces that constrains all DOFs of the ankle. The ankle is medio-laterally fixed at neutral while the sagittal ankle angle can be adjusted to aid in foot-ground clearance during swing or to redirect the ground reaction vector to help extend the knee during standing. KAFOs, such as long leg braces (LLB) or the Scott-Craig Orthosis [6], provide constraints to both the knee and ankle joints. During

ambulation, the knee is locked in extension while the ankle is constrained as in an AFO. Ambulation is typically achieved through a simultaneous swing-to or swing-through motion of both limbs, but reciprocal gait can also be achieved with KAFOs. Because of low walking speeds of 0.147 m/s, high energy expenditure and overall difficulty of use, KAFOs are utilized most often for standing and exercise purposes [8, 9, 10]. Additional stability in the form of HKAFOs or THKAFOs can be obtained by fitting a pelvic band or trunk corset to KAFOs, respectively. One HKAFO known as the Walkabout Orthosis [11] incorporates a medially located hip joint that links the KAFOs of both limbs together to constrain hip movement to the sagittal plane. Commercially available THKAFOs such as the Hip Guidance Orthosis (HGO) and RGO have been developed as standalone mechanical systems for assisted reciprocal gait.

The laterally located hip joints of the HGO [12], also known to as the Parawalker, only permit sagittal hip rotation and include flexion stops to limit the range of motion. A rigid trunk brace links sagittal trunk motion to hip motion. With average speeds of 0.213 m/s, it was shown that users with thoracic lesions (T4-T11) could ambulate with an HGO at a significantly greater efficiency than with KAFOs [13]. The HGO has also been shown to produce improved user compliance over the existing KAFOs, although functional usage rates for the HGO are still low [14].

The RGO incorporates a hip mechanism that reciprocally couples hip extension with contralateral hip flexion. This hip reciprocator therefore passively prevents bilateral hip rotation in the same direction. Various types of RGOs exist with hip coupling facilitated by dual Bowden cables (Louisiana State University RGO [15]), a single Bowden cable (Advanced RGO [16]), or pivoting bar/tie rod design (Isocentric RGO

[17]). A corset stabilizes the trunk laterally and links sagittal trunk motion with hip motion through lateral joints attached to each KAFO. Average gait speeds with an RGO have been shown to be approximately 0.2 m/s [18]. Reciprocal gait with an RGO was shown to be more energy efficient than KAFOs [20]. Individuals with paraplegia (T9-T12) walking with the RGO achieved double the gait speed and half the energy cost of walking with the Walkabout Orthosis [21]. However, user compliance is low and walking duration is limited by the extensive energy required [19].

Multiple comparative studies have evaluated the performances of the RGO and HGO. The average gait speed of subjects with T3-T12 injuries with either the RGO or HGO was approximately 0.24 m/s [22]. Ijzerman *et al*. [23] showed a significant increase in oxygen cost in individuals with high levels of paraplegia when the hip reciprocator was removed from the RGO due to the reduced ability to flex the hip during swing and increased exertion required to maintain upright posture during double stance. Hirokawa *et al*. [18] inferred that since the RGO prevents bilateral hip flexion during double stance, less energy is expended by the user in applying upper extremity forces against the walking aid than with the HGO. However, this effect is reduced as gait speed increases since the duration of the double stance phases decrease relative to the swing phase. Furthermore, during the swing phase of RGO gait the swing limb is constrained by the dynamics of the contralateral stance limb, whereas in HGO gait the swing limb is unconstrained which facilitates faster and more ballistic movements. As a result, at slow gait speeds the energy cost of walking with a RGO is less than a HGO, whereas at fast gait speeds HGO gait is more energy efficient.

Dall *et al*. [24] assessed the function of the RGO by measuring the forces applied to the hip reciprocator during gait with individuals with paraplegia. The study concluded that hip extension during stance does not necessarily drive contralateral hip flexion during swing as commonly assumed. The reciprocator acts primarily to prevent bilateral hip flexion during the double support phases of gait and to restrict hip flexion and slow the swinging limb during the later half of the swing phase.

Overall, reciprocal gait with a lower extremity exoskeleton demands that the user apply high upper body forces on the walking aid during the swing and double support phases due to the pelvic thrust necessary to swing the leg forward [25]. Furthermore, since the knees and ankles are fixed in extension and neutral respectively, the swing limb cannot shorten to allow for proper foot-to-ground clearance. As a result, significant upper body exertion on the walking aid is necessary to elevate the body to allow the swing limb to clear the floor [26]. This awkward and unintuitive form of ambulation requires five times the energy costs of normal walking [27] at gait speeds approaching only 16 % of nominal able-bodied values, and limits typical walking distances to less than 100 m [19, 28, 29].

1.2.3 Functional Neuromuscular Stimulation

FNS is a method for restoring lost motor function after SCI by eliciting muscle contractions through the application of electrical pulses to the peripheral nerves innervating the paralyzed muscle. Significant effort has been made to develop FNS as a viable means to provide functional gait to individuals with paraplegia [30-35]. Early FNS systems for individuals with paraplegia applied electrical stimulation via surface

electrodes to the afferent nerves in order to facilitate the flexion withdrawal reflex to initiate a step [31]. Additional channels of surface stimulation have been incorporated for hip extension, hip abduction, or plantar flexion during walking [36, 37] with the maximum number of stimulation channels generally limited to less than eight. Such a surface FNS system has been commercialized under the name ParaStep®. Users of the ParaStep® were able to walk at an average speed of 0.2 m/s up to an average maximum distance of approximately 73 m [33]. The ParaStep® was found to be effective for restoring standing and walking in individuals paralyzed by SCI [38, 39], maintaining physical and psychological fitness [40], increasing the resting arterial inflow volume to the lower extremities [41], improving physical self-concept, and decreasing depression [42]. Unfortunately, surface electrodes complicate donning and doffing, provide poor muscle selectivity and cannot activate deep muscles such as hip flexors [43, 44]. Furthermore, habituation of the flexion withdrawal response occurs with repeated activation [45]. Other drawbacks of surface stimulation are poor repeatability and skin irritation.

As a result of the complications associated with surface stimulation, intramuscular electrodes with percutaneous leads [46, 47] and outpatient methods for implanting them in all major muscles of lower extremities and trunk [48-50] for safe stimulation of paralyzed muscles [51] have been developed. They provide selective and repeatable lower limb muscle stimulation [32, 52], and with an external multi-channel stimulator have enabled multiple ambulatory functions in subjects with paraplegia. The electrodes are suitable for system development [34, 53, 54], clinical assessment and limited home use [55]. The energy cost of individuals with complete SCI at T4 and T8 implanted with

a multichannel percutaneous intramuscular FNS system were measured to be 11 times normal at an average gait speed of 0.24 m/s, 18 % normal [56]. Approximately 80 % of the energy cost was due to upper extremity exertion and other voluntary muscle contractions while stimulation accounted for only roughly 20 %. Higher stimulation levels were used than that required for functional muscle contraction to compensate for muscle fatigue and provide support [18, 56]. An average maximum walking distance of about 150 m was attained with thoracic level subjects equipped with percutaneous intramuscular FNS systems [32].

Essentially, two limitations have restricted existing FNS-gait systems from practical everyday use. First, the multiple DOFs of the lower extremities and multiplanar actions of the lower extremity muscles complicate control strategies and require the selective activation of a large number of muscles to achieve functional joint dynamics. Second, paralyzed muscles fatigue rapidly during FNS since motor unit recruitment patterns and firing frequencies are not adapted to maintain force output as compared to voluntary contractions [57].

1.2.4 Hybrid Systems

A HNP is an active system that combines the advantages of the exoskeletal and FNS approaches with the goal of eliminating the disadvantages of each taken individually. The exoskeletal component of HNPs has been generally a passive device to provide joint support while the FNS component generates active limb motion. The exoskeleton is intended to constrain joint motion to reduce the amount of stimulation required to achieve ambulation, thus delaying the onset of muscle fatigue and allowing

for increased walking distance and duration. Furthermore, the secondary and tertiary actions of the muscles targeted for FNS are eliminated by the exoskeletal constraints, removing the need to compensate for unintended actions through the activation of antagonist muscles.

Surface [26, 29, 58-65] and intramuscular [66-68] FNS systems have been used in combination with THKAFOs for reciprocal gait in individuals with complete thoracic level SCI. Marsolais *et al*. [67] demonstrated that individuals unable to use a RGO could be trained to use a HNP. Hirokawa *et al*. [18] combined a RGO with a 4-channel surface FNS system to show a 16 % reduction in energy expenditure for subjects with SCI between T1 and T10 relative to RGO walking. Petrofsky and Smith [26] showed that for paraplegic subjects (T4-T12), 70 % of the aerobic capacity of the upper extremities is required for walking with an RGO, while walking with a RGO combined with FNS required only 32 %. Accordingly, it has been shown that individuals with paraplegia could walk significantly farther with an HNP than with either exoskeleton-only or FNS-only systems [29, 65, 67], with HNP users achieving an average maximum walking distance of 800 m [29].

FNS-only systems require the user to maintain trunk stability by using significant upper extremity forces on a walking aid. This increases energy consumption and thus reduces walking duration. Stimulation of the hip flexors during the initiation of the swing phase of gait often destabilized the trunk in FNS-only walking [18]. Anterior trunk tilt of 23-40^{o} has been associated with FNS-only gait systems [67]. The RGO combined with FNS has been shown to reduce anterior trunk tilt to 8-18^{o}. However, the RGO has a fixed 1:1 hip flexion/extension coupling ratio (hip flexion is limited by the

degree of contralateral hip extension). Yang *et al*. [64] constructed a RGO that allowed for pre-set hip flexion/extension coupling ratios (HFECR). Individuals with paraplegia walking with the RGO-only at a 2:1 HFECR exhibited a 15 % reduction in physiological cost index and 4 % increase in stride length relative to a RGO with a 1:1 HFECR. Tests with FNS-assisted hip flexion and the RGO at a 2:1 HFECR further reduced the physiological cost index and increased stride length and walking speed. In a study by Marsolais *et al*. [67] a multichannel FNS system was combined with a RGO fitted with a controllable locking mechanism at the knee joint to allow for knee flexion during swing. With the RGO at a 1:1 HFECR the average stride length and gait speed was 0.64 m and 0.32 m/s respectively. With the hip reciprocator of the RGO disengaged both the average stride length and gait speed increased by 47 % (to 0.94 m) and 53 % (to 0.49 m/s) respectively at the expense of an increase in the maximum forward trunk tilt of 22^{o} (to 40^{o}).

Various prototype lower extremity exoskeletons specifically designed for hybrid systems utilize auxiliary passive mechanisms to reduce the burden of controlling joint motion on electrically stimulated muscles. These joint constraint mechanisms must be properly controlled to provide stability when needed, without restricting functional joint motion necessary for ambulation. The controlled-brake orthosis [69, 70] incorporates magnetic particle brakes at the hip and knee joints to refine the sagittal limb dynamics driven by FNS. A cam-slider mechanism [71] that synchronizes knee flexion with ankle dorsiflexion was developed to assure proper foot-ground clearance during swing. The spring brake orthosis [72] utilizes excess spring energy stored from FNS driven knee extension to facilitate knee flexion and assist hip flexion in the succeeding ipsilateral

swing period. Similarly, a conceptual design of an energy storing orthosis [73] employs a pneumatic system to harness and transfer excess energy from knee extension to facilitate ipsilateral hip extension during stance.

1.3 Specific Aims and Hypotheses

The general objective of this work was to develop and evaluate a new HNP that would minimize overall user muscle activity and facilitate functional stepping for individuals with paraplegia. This objective was divided into three specific aims.

Aim 1: Develop and implement a DSKM to maintain extension during the stance phases of gait and allow for unimpeded flexion during the swing phases of gait.

Aim 2: Develop and implement a VCHM to maintain the upper body postural stability of individuals with paraplegia while allowing for unimpeded functional stepping. The following hypotheses were tested as part of this aim.

- **Hypothesis 1:** The trunk orientation of individuals with SCI walking with the prototype HNP is comparable to walking with a RGO.
- **Hypothesis 2:** The maximum upper extremity effort applied to a walking aid while an individual with paraplegia ambulates with the prototype HNP is less than walking with a RGO alone.
- **Hypothesis 3:** The sagittal hip range of motion allowed by the HNP during gait is comparable to FNS-only gait.
- **Hypothesis 4:** An individual with SCI walking with the prototype HNP will achieve a stride length comparable to walking with a FNS-only gait system.

Aim 3: Develop and evaluate a closed-loop controller for modifying the muscle stimulation patterns synchronously with the constraint states of a prototype exoskeleton with the goal of minimizing the duty cycle of the electrical stimulation to target muscles and achieving functional kinematics for gait. The following hypotheses will be tested as part of this aim.

- **Hypothesis 5:** The DSKM can adequately support the user during gait, such that the gait dynamics observed with stimulation to the knee extensors deactivated is comparable to those observed with baseline knee extensor stimulation.
- **Hypothesis 6:** The synchronous implementation of the VCHM and closed-loop control of FNS to target hip extensors will provide improved gait dynamics relative to the utilization of baseline hip extensor stimulation.

The systems involved in the prototype exoskeleton of the HNP, which are discussed in the preceding chapters, are summarized in **Figure 1.1**.

1.4 RESEARCH RESOURCES

This research was conducted in collaboration with the Advanced Platform Technology (APT) Center and Cleveland Functional Electrical Stimulation (FES) Center. These Rehabilitation Research & Development Centers of Excellence represent collaborations between Louis Stokes Cleveland Department of Veterans Affair Medical Center (LSCDVAMC), Case Western Reserve University Schools of Medicine and Engineering, and MetroHealth Medical Center. This research was conducted primarily at the Motion Study Laboratory (MSL) of the LSCDVAMC.

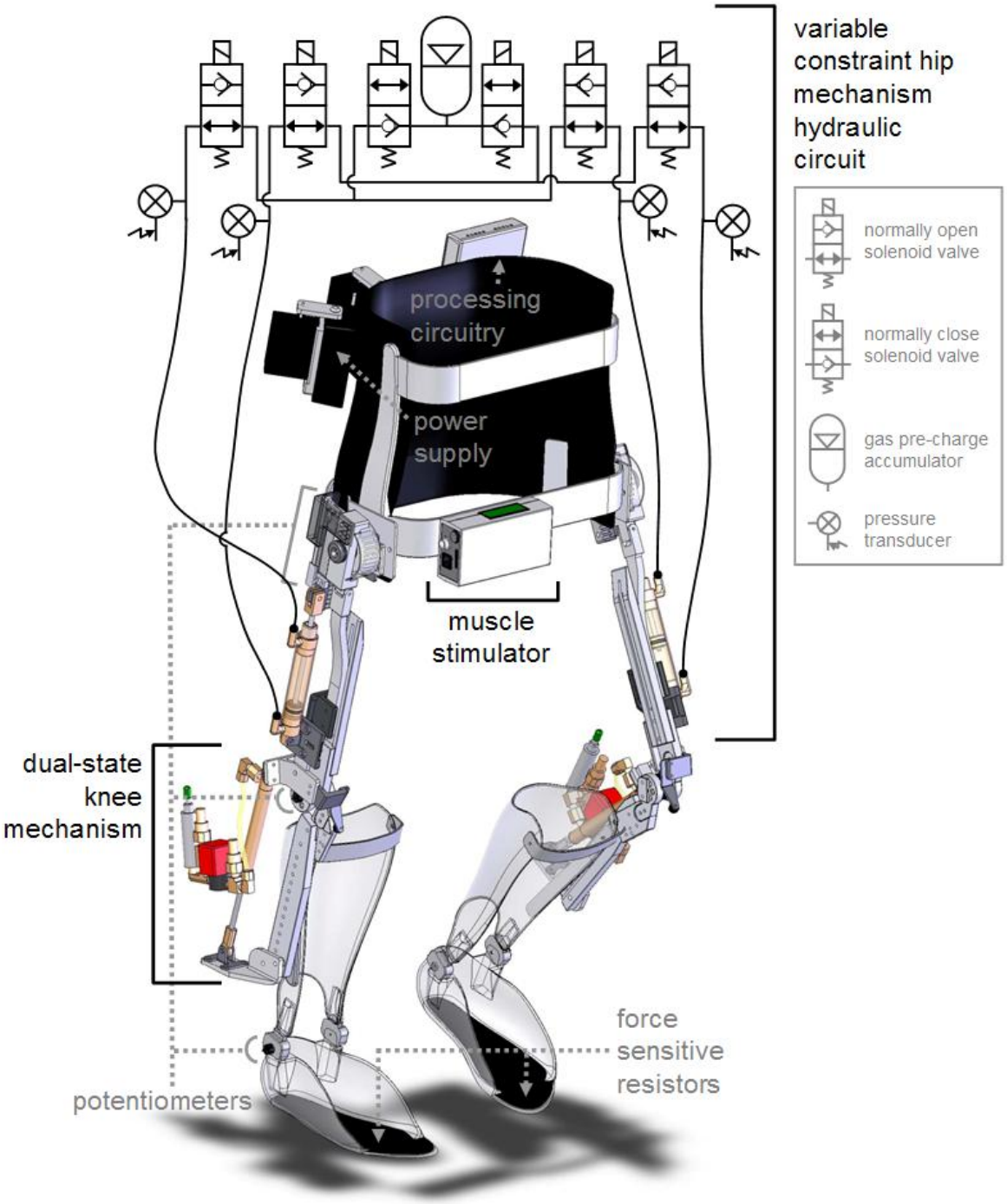

Figure 1.1. Systems of the HNP exoskeleton: dual-state knee mechanism (**Chapter 2**), variable constraint hip mechanism (**Chapter 3**), and muscle stimulator (**Chapter 4**).

The MSL contains state-of-the-art equipment for biomechanical, metabolic and functional assessment of human movement. The available instrumentation in the MSL

includes a sixteen camera Vicon MX40 (Vicon, Inc., Oxford, UK) digital motion capture and analysis system and three biomechanics platforms (AMTI, Inc., Watertown, MA, USA) embedded in an eight by three meter walkway. The three-dimensional coordinates of reflective markers, fixed to key locations on the study participant, are captured by the motion analysis system within the work volume (**Figure 1.2**). With these marker coordinates, the motion of the body segments under study can then be fully reproduced for later analysis to calculate the joint angles or segment trajectories. When the kinematic data from the Vicon system are appropriately combined with the kinetic data from the biomechanics platforms, joint moments and powers can be calculated to determine the energetics of ambulation.

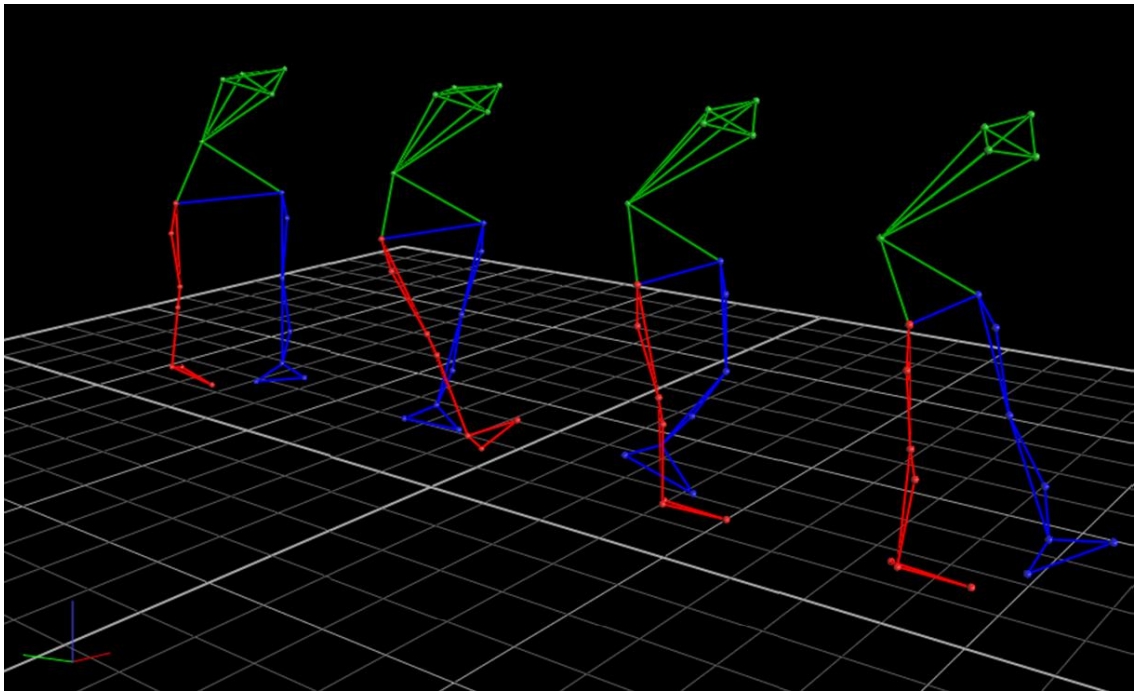

Figure 1.2. Vicon Nexus 3-D motion capture of reflective markers during gait with the HNP.

The MSL also houses a Biodex Pro System 3 (Biodex Medical Systems, Inc., Shirley, NY, USA) robotic dynamometer. The Biodex can be torque or position controlled and is

fully programmable allowing for diverse ways of testing orthotic devices. A state of the art 64-channels data acquisition system in the MSL allows for the prototyping of real-time controller applications.

All software applications for data acquisition, real-time control, and data analysis were custom developed in Matlab®/Simulink® (The MathWorks, Inc., Natick, MA, USA). Specifically, the control applications were prototyped using the xPC Target real-time environment. Two desktop computers are used, a target PC and a host PC. The target PC runs the real-time application while the host PC acts as a user interface for controlling the target PC. Refer to **Chapter 4** for the specific software and hardware setup used in this work.

The research machine shop at the LSDCVAMC provides an onsite location for the customization, fabrication, alteration, and machining of exoskeleton mechanisms and parts. SolidWorks 3-D CAD Design Software (Dassault Systèmes SolidWorks Corp., Concord, MA) was used to design all custom parts of the exoskeleton depicted in **Figure 1.1**. All custom components of the exoskeleton were machined with a Smithy® Midas 1220 LTD lathe-mill-drill (Smithy Company, Ann Arbor, MI, USA) or Sherline 5400/5410 tabletop mill (Sherline Products, Inc., Vista, CA, USA).

1.5 OVERVIEW OF THE CHAPTERS

Chapter 2 and **Chapter 3** respectively discuss the development of the DSKM and VCHM. The conceptualization and design for each mechanism are first considered. Each chapter then presents the methods that were used to optimize the respective

mechanism. The control methodologies are then described, followed by system characterization through bench testing. Finally, the operation of each mechanism is validated through testing with able-bodied individuals.

Chapter 4 discusses the development of the closed-loop FNS controller and the implementation of the entire prototype HNP. The control algorithm and hardware configurations are first examined. The FNS controller is then validated through simulation using joint kinematics and exoskeleton control data collected from the previous able-body experiments. Finally, the implementation of the complete HNP with an individual with paraplegia is assessed.

Chapter 5 summarizes all the results, examines them collectively and considers the implications for future development of the technology.

1.6 REFERENCES

1. C. S. To, R. Kobetic, J. R. Schnellenberger, M. L. Audu, and R. J. Triolo, "Design of a variable constraint hip mechanism for a hybrid neuroprosthesis to restore gait after spinal cord injury," *IEEE/ASME Trans Mechatronics*, vol. 13, no. 2, pp. 197-205, 2008.

2. R. Kobetic, C. S. To, J. R. Schnellenberger, M. L. Audu, T. C. Bulea, R. Gaudio, G. Pinault, S. Tashman, and R. J. Triolo, "Development of a hybrid orthosis for standing, walking, and stair climbing after spinal cord injury" *J. Rehabil. Res. Dev.*, vol. 46, no. 3, pp. 447-462, 2009.

3. "Spinal Cord Injury Facts & Statistics." Spinal Cord Injury Information Pages. 25 June 2006. 23 Dec. 2007 <http://www.sci-info-pages.com/facts.html>.

4. H. O. Kent, "Vannini-Rizzoli Stabilizing Orthosis (Boot): Preliminary report on a new ambulatory aid for spinal cord injury," *Arch. Phys. Med. Rehabil*., vol. 73, pp. 302-307, Mar. 1992.

5. M. Lyles and J. Munday, "Report on the evaluation of the Vannini-Rizzoli Stabilizing Limb Orthosis," J. *Rehab. Res. & Dev*., vol. 29, no. 2, pp. 77-104, 1992.

6. J. F. Lehmann, C. G. Warren, D. Hertling, M. McGee, B. C. Simons, and A. Dralle, Craig-Scott orthosis: a biochemical and functional evaluation," *Arch. Phys. Med. Rehabil*., vol. 57, no. 9, pp. 438-442, Sep. 1976.

7. K. D. Merkel, N. E. Miller, P. R. Westbrook, and J. L. Merritt, " Energy expenditure of paraplegic patients standing and walking with two knee-ankle-foot orthoses," *Arch. Phys. Med. Rehabil.*, vol. 65, pp. 121-124, Mar. 1984.

8. N. Rosman and E. Spira, "Paraplegic use of walking braces: A survey," *Arch. Phys. Med. Rehabil.*, vol. 55, pp. 310-314, July 1974.

9. R. Mikelberg and S. Reid, "Spinal cord lesions and lower extremity bracing: An overview and follow-up study," *Paraplegia*, vol. 19, pp. 379-385, 1981.

10. C. Hong, E. B. San Luis, and S. Chung, "Follow-up study on the use of leg braces issued to spinal cord injury patients," *Paraplegia*, vol. 28, pp. 172-177, 1990.

11. J. W. Middleton, J. D. Yeo, L. Blanch, V. Vare, K. Peterson, and K. Brigden, "Clinical evaluation of a new orthosis, the 'Walkabout', for restoration of functional standing and short distance mobility in spinal paralysed individuals," *Spinal Cord*, vol. 35, pp. 574-579, 1997.

12. G. K. Rose, "The principles and practice of hip guidance articulations," *Prosth. & Orth. Intnl*., vol. 3, pp. 37-43, 1979.

13. A. V. Nene and J. H. Patrick, "Energy cost of paraplegic locomotion with the ORLAU Parawalker," *Paraplegia*, vol. 27, pp. 5-18, 1989.

14. P. Moore and J. Stallard, "A clinical review of adult paraplegia patients with complete lesions using the ORLAU Parawalker," *Paraplegia*, vol. 29, pp. 191-196, 1991.

15. R. Douglas, P. F. Larson, R. D'Ambrosia, R. E. McCall, "The LSU reciprocating gait orthosis," *Orthopedics*, vol. 6, pp. 834-839, 1983.

16. R. J. Jefferson, M. W. Whittle, "Performance of three walking orthosis for the paralyzed: a case study using gait analysis," *Prosth. & Orth. Intnl*., vol. 14, pp. 103-110, 1990.

17. W. M. Motloch, "Principles of orthotic management for child and adult paraplegia and clinical experience with the isocentric RGO," *Proc. 7th World Congress of the International Society for Prosthetics and Orthotics*, Chicago, pp. 28, Jun 28 - July 3, 1992.

18. S. Hirokawa, M. Grimm, T. Le, M. Solomonow, R. V. Baratta, H. Shoji, and R. D. D'Ambrosia, "Energy consumption in paraplegic ambulation using the reciprocating gait orthosis and electrical stimulation of the thigh muscles," *Arch. Phys. Med. Rehabil*., vol. 71, pp. 687-694, Aug. 1990.

19. L. Sykes, J. Edwards, E. S. Powell, and E. R. S. Ross, "The reciprocating gait orthosis: Long-term usage patterns," *Arch. Phys. Med. Rehabil.*, vol. 76, pp. 779-783, Aug. 1995.

20. J. L. Merritt, N. E. Miller, and T. J. Hanson, "Preliminary studies of energy expenditures in paraplegics using swing-thru and reciprocating gait patterns," *Arch. Phys. Med. Rehabil.*, vol. 64, pp. 510, Oct. 1983.

21. L. A. Harvey, G. M. Davis, M. B. Smith, and S. Engel, "Energy expenditure during gait using the Walkabout and Isocentric Reciprocating Gait orthoses in persons with paraplegia," *Arch. Phys. Med. Rehabil.*, vol. 79, pp. 945-949, Aug. 1998.

22. M. W. Whittle, G. M. Cochrane, A. P. Chase, A. V. Copping, R. J. Jefferson, J. Staples, P. T. Fenn, and D. C. Thomas, "A comparative trial of two walking systems for paralysed people," *Paraplegia*, vol. 29, pp. 97-102, 1991.

23. M. J. Ijzerman, G. Baardman, H. J. Hermens, P.H. Veltink, H. B. K. Boom, and G. Zilvold, "The influence of the reciprocal cable linkage in the advanced reciprocating gait orthosis on paraplegic gait performance," *Prosth. & Orth. Intnl*., vol. 21, pp. 52-61, 1997.

24. P. M. Dall, B. Muller, I. Stallard, J. Edwards, and M. H. Granat, "The functional use of the reciprocal hip mechanism during gait for paraplegic patients walking in the Louisiana State University reciprocating gait orthosis," *Prosth. & Orth. Intnl*., vol. 23, pp. 152-162, 1999.

25. S. Tashman, F. E. Zajac, and I. Perkash, "Modeling and simulation of paraplegic ambulation in a reciprocating gait orthosis," *J. Biomech. Eng.*, vol. 117, pp. 300-308, Aug. 1995.

26. J. S. Petrofsky and J. B. Smith, "Physiologic costs of computer-controller walking in persons with paraplegia using a Reciprocating-Gait Orthosis," *Arch. Phys. Med. Rehabil*., vol. 72, pp. 890-896, Oct. 1991.

27. R. Blessey, "Energy cost of normal walking," *Orthopedic Clinics of North America*, vol. 9, pp. 356-358, 1978.

28. H. Natvig, and R. McAdam, "Ambulation without wheelchairs for paraplegics with complete lesions," *Paraplegia*, vol. 16, pp. 142-146, 1978.

29. M. Solomonow, R. Baratta, S. Hirokawa, N. Rightor, W. Walker, P. Beaudette, H. Shoji, and R. D'Ambrosia, "The RGO Generation II: Muscle stimulation powered orthosis as a practical walking system for thoracic paraplegics," *Orthopedics*, vol. 12, pp. 1309-1315, 1989.

30. A. Kralj, T. Bajd, R. Turk, "Electrical stimulation providing functional use of paraplegic patient muscles," *Med. Prog. Technol*., vol. 7, pp. 3-9, 1980.

31. T. Bajd, A. Kralj, R. Turk, H. Benko, J. Sega, "The use of a four-channel electrical stimulator as an ambulatory aid for paraplegic patients," *Physical Therapy*, vol. 63, no. 7, pp. 1116-1120, July 1983.

32. E. B. Marsolais and R. Kobetic, "Development of a practical electrical stimulation system for restoring gait in the paralyzed patient," *Clin. Orthop.*, no. 233, pp. 64-74, Aug. 1988.

33. P. Gallien, R. Brissot, M. Eyssette, L. Tell, M. Barat, L. Wiart, H. Petit, "Restoration of gait by functional electrical stimulation for spinal cord injured patients," *Paraplegia*, vol. 33, no. 11, pp. 660-664, Nov. 1995.

34. R. Kobetic, R. J. Triolo, and E. B. Marsolais, "Muscle selection and walking performance of multichannel FES systems for ambulation in paraplegia," *IEEE Trans. Rehab. Eng.*, vol. 5, no. 1, pp. 23-29, Mar. 1997.

35. R. Kobetic, R. J. Triolo, J. P. Uhlir, C. Bieri, M. Wibowo, G. Polando, E. B. Marsolais, J. A. Davis, K. A. Ferguson, and M. Sharma, "Implanted functional

electrical stimulation system for mobility in paraplegia: A follow-up case report," *IEEE Trans. Rehab. Eng.*, vol. 7, no. 4, pp. 390-398, Dec. 1999.

36. A. Kralj, R. J. Jaeger, and T. Bajd, "Posture switching enables prolonged standing in paraplegic patients functionally electrically stimulated," *Proc. Fifth. Ann. Conf. on Rehab. Eng.*, pp. 60, Houston, 1982.

37. Kralj, T. Bajd, R. Turk, J. Krajnik, and H. Benko, "Gait restoration in paraplegic patients: a feasibility demonstration using multichannel surface electrode FES," *J. Rehabil. Res. Dev.*, vol. 20, pp. 3-20, 1983.

38. D. Graupe and K. H. Kohn, "Transcutaneous functional neuromuscular stimulation of certain traumatic complete thoracic paraplegics for independent short-distance ambulation," *Neurol. Res.*, vol. 19, no. 3, pp. 323-333, June 1997.

39. D. Graupe and K. H. Kohn, "Functional neuromuscular stimulator for short-distance ambulation by certain thoracic-level spinal-cord-injured paraplegics," *Surg. Neurol.*, vol. 50, no. 3, pp. 202-207, Sep. 1998.

40. R. Brissot, P. Gallien, M. P. Le Bot, A. Beaubras, D. Laisne, J. Beillot, and J. Dassonville, "Clinical experience with functional electrical stimulation-assisted gait with Parastep in spinal cord-injured patients," *Spine*, vol. 25, no. 4, pp. 501-508, 2000.

41. M. S. Nash, P. L. Jacobs, B. M. Montalvo, K. J. Klose, R. S. Guest, and B. M. Needham-Shropshire, "Evaluation of a training program for persons with SCI paraplegia using the Parastep 1 ambulation system: part 5. Lower extremity blood flow and hyperemic response to occlusion are augmented by ambulation training," *Arch. Phys. Med. Rehabil*., vol. 78, no. 8, pp. 808-814, 1997.

42. R. S. Guest, K. J. Klose, B. M. Needham-Shropshire, and P. L. Jacobs, "Evaluation of a training program for persons with SCI paraplegia using the Parastep 1 ambulation system: part 4. Effect on physical self-concept and depression," *Arch. Phys. Med. Rehabil*., vol. 78, no. 8, pp. 804-807, 1997.

43. U. Stanic, R. Acimovic-Janezic, N. Gros, A. Trnkoczy, T. Bajd, and M. Kljajic, "Multichannel electrical stimulation for correction of hemiplegic gait," *Scand. J. Rehabil. Med.*, vol. 10, pp. 175-192, 1977.

44. J. S. Petrofsky and C. A. Phillips, "Closed-loop control of movement of skeletal muscle," *CRC Crit. Rev. Biomed. Eng*., vol. 13, pp. 35-96, 1985.

45. D. J. Nicol, M. H. Granat, S. J. Tuson, and R. H. Baxendale, "Variability of the dishabituation of flexion reflexes for FES assisted gait in spinal injured man," *Med. Eng. Phys.*, vol. 20, no. 3, pp. 182-187, 1998.

46. A. Scheiner, G. Polando, and E. B. Marsolais, "Design and clinical application of a double helix electrode for functional electrical stimulation," *IEEE Trans. Biomed. Eng.*, vol. 41, no. 5, pp. 425-431, 1994.

47. H. Kagaya, M. Sharma, G. Polando, and E. B. Marsolais, "Reliability of closed double helix electrode for totally implantable FES system," *Clin. Orthop.*, vol. 233, pp. 64-74, 1998.

48. E. B. Marsolais and R. Kobetic, "Functional electrical stimulation for walking in paraplegia," *J. Bone. Joint. Surg.*, vol. 69A, pp. 728-733, 1987.

49. E. B. Marsolais and R. Kobetic, "Implantation techniques and experience with percutaneous intramuscular electrodes in the lower extremities," *J. Rehabil. Res. Dev.*, vol. 23, pp. 1-8, 1986.

50. S. Nandurkar, E. B. Marsolais, and R. Kobetic, "Percutaneous implantation of iliopsoas for functional neuromuscular stimulation," *Clin. Orthop.*, vol. 389, pp. 210-217, 2001.

51. J. T. Mortimer, D. Kaufman, and U. Roessmann, "Intramuscular electrical stimulation: Tissue damage," *Ann. Biomed. Eng*., vol. 8, pp. 235-244, 1980.

52. R. J. Triolo, M. Q. Liu, R. Kobetic, and J. P. Uhlir, "Selectivity of intramuscular stimulating electrodes in the lower limbs," *J. Rehabil. Res. Dev.*, vol. 38, no. 5, pp. 533-544, 2001.

53. J. P. Uhlir, R. J. Triolo, and R. Kobetic, "The use of selective electrical stimulation of the quadriceps to improve standing function in paraplegia," *IEEE Trans. Rehabil. Eng.*, vol. 8, no. 4, pp. 514-522, 2000.

54. R. J. Triolo, M. Wibowo, J. Uhlir, R. Kobetic, and R. Kirsch, "Effects of stimulated hip extension moment and position on upper-limb support forces during FES-induced standing – A technical note," *J. Rehabil. Res. Dev.*, vol. 38, no. 5, pp. 545-555, 2001.

55. Y. Shimada, K. Sato, E. Abe, H. Kagaya, K. Ebata, M. Oba, M. Sata, "Clinical experience of functional electrical stimulation in complete paraplegia," *Spinal Cord*, vol. 34, pp. 615-619, 1996.

56. E. B. Marsolais and B. G. Edwards, "Energy costs of walking and standing with functional neuromuscular stimulation and long leg braces," *Arch. Phys. Med. Rehabil*., vol. 69, pp. 243-249, April 1988.

57. M. Gregory and C. S. Bickel, "Recruitment patterns in human skeletal muscle during electrical stimulation," *Physical Therapy*, vol. 85, no. 4, pp. 358-364, 2005.

58. J. H. Patrick and M. R. McClelland, “Low energy cost reciprocal walking for the adult paraplegic,” *Paraplegia*, vol. 23, pp. 113-117, 1985.

59. J. Stallard, R. E. Major, R. Poiner, I. R. Farmer, and N. Jones, “Engineering design considerations of the ORLAU Parawalker and FES hybrid system,” *Eng. Med.*, vol. 15, no. 3, pp. 123-129, 1986.

60. M. McClelland, B. J. Andrews, J. H. Patrick, P. A. Freeman, and W. S. El Masri, “Augmentation of the Oswestry Parawalker Orthosis by means of surface electrical stimulation: Gait analysis of three patients,” *Paraplegia*, vol. 25, pp. 32-38, 1987.

61. A. V. Nene and J. H. Patrick, “Energy cost of paraplegic locomotion using the Parawalker – Electrical stimulation “hybrid” orthosis,” *Arch. Phys. Med. Rehabil.*, vol. 71, pp. 116-120, Feb. 1990.

62. C. A. Phillips and D. M. Hendershot, “A systems approach to medically prescribed functional electrical stimulation. Ambulation after spinal cord injury,” *Paraplegia*, vol. 29, pp. 505-513, 1991.

63. E. Isakov, R. Douglas, and P. Berns, “Ambulation using the reciprocating gait orthosis and functional electrical stimulation,” *Paraplegia*, vol. 30, pp. 239-245, 1992.

64. L. Yang, M. H. Granat, J. P. Paul, D. N. Condie, and D. I. Rowley, “Further development of hybrid functional electrical stimulation orthoses,” *Spinal Cord*, vol. 34, no. 10, pp. 611-614, Oct. 1996.

65. M. Solomonow, E. Aguilar, E. Reisin, R. V. Baratta, R. Best, T. Coetzee, and R. D’Ambrosia, “Reciprocating gait orthosis powered with electrical muscle stimulation (RGO II). Part I: Performance evaluation of 70 paraplegic patients,” *Orthopedics*, vol. 20, no. 4, pp. 315-324, April 1997.

66. A. V. Nene and S. J. Jennings, “Hybrid paraplegic locomotion with the Parawalker using intramuscular stimulation: A single subject study,” *Paraplegia*, vol. 27, pp. 125-132, 1989.

67. E. B. Marsolais, R. Kobetic, G. Polando, K. Ferguson, S. Tashman, R. Gaudio, S. Nandurkar, and H. R. Lehneis, “The Case Western Reserve University hybrid gait orthosis,” *J. Spinal Cord Med*., vol. 23, no. 2, pp. 100-108, 2000.

68. R. Kobetic, E. B. Marsolais, R. J. Triolo, D. T. Davy, R. Gaudio, and S. Tashman, “Development of a hybrid gait orthosis: A case report,” *J. Spinal Cord Med*., vol. 26, no. 3, pp. 254-258, 2003.

69. M. Goldfarb and W. Durfee, “Design of a controlled-brake orthosis for FES-added gait,” *IEEE Trans. Rehab. Eng.*, vol 4, no. 1, pp. 13-24, Mar. 1996.

70. M. Goldfarb, K. Korkowski, B. Harrold, and W. Durfee, "Preliminary evaluation of a controlled-brake orthosis for FES-aided gait," *IEEE Trans. Neur. Sys. Rehab. Eng.*, vol. 11, no. 3, pp. 241-248, Sept. 2003.

71. P. J. Greene and M. H. Granat, "A knee and ankle flexing hybrid orthosis for paraplegic ambulation," *Med. Eng. Phys*., vol. 25, pp. 539-545, 2003.

72. S. Gharooni, B. Heller, and M. O. Tokhi, "A new hybrid spring brake orthosis for controlling hip and knee flexion in the swing phase," *IEEE Trans. Neur. Sys. Rehab. Eng.*, vol. 9, no. 1, pp. 106-107, Mar. 2001.

73. W. K. Durfee and A. Rivard, "Design and simulation of a pneumatic stored-energy, hybrid orthosis for gait restoration," *J. Biomech. Eng*., vol. 127, pp. 1014-1019, Nov. 2005.

CHAPTER 2

DESIGN OF A DUAL-STATE KNEE MECHANISM FOR A HYBRID NEUROPROSTHESIS FOR LOAD BEARING AND FREE STEPPING

2.1 INTRODUCTION

There has been considerable effort to develop a constraint mechanism exclusively for supporting the knee joint during the stance phase of gait and allowing for free movement during swing. These dual-state knee mechanisms (DSKM) have utilized a myriad of design approaches which include bail locking [1], pin locking [2-4], a ratchet/pawl (Otto Bock Free Walk/Becker UTX and Fillauer Swing Phase Lock Orthosis) [5, 6], cam locking (Horton Stance Control Orthotic Knee Joint [7]), belt clamping (Ottawalk) [8], hydraulics [9], a wrap-spring clutch (dynamic knee-brace system/Otto Bock Sensor Walk) [10], a dog clutch via circular ratchet plates (Becker Orthopedic E-Knee) [11], a roller clutch [3], lever locking, and spring stiffness switching [12]. Many of these design approaches require the removal of the flexion moment about the mechanism before unlocking of the knee joint can be achieved [3, 8, 10, 13].

However, this may not be achieved consistently over multiple strides with users with weak knee extensors or once the knee extensors have fatigued. The commercially available knee mechanisms do not provide sufficient control and support for the intended user population. Specifically, both the Otto Bock Free Walk/Becker UTX and Fillauer Swing Phase Lock Orthosis lock only when the knee has reached full extension. For the target user population, full extension may not occur at the end of swing due to the inconsistent force output or fatigue of electrically stimulated muscle. Furthermore, the pawl of the Fillauer Swing Phase Lock Orthosis is actuated by gravity, which depends on the thigh to flex/extend to a preset orientation to lock/unlock the mechanism. This again requires consistent gait kinematics, which is currently not realizable by FNS. The Becker Orthopedic E-Knee, which depends on engagement of a pair of ratchet plates to lock the knee, only offers discrete locking angles at 6^o intervals [13]. Thus, up to 6^o of unsupported knee flexion can occur from the knee angle at which the mechanism is triggered to lock, due to the slipping of the ratchet teeth to full engagement.

This chapter presents the development of a new DSKM, from the design concepts to the validation with able-bodied individuals. The aim of this new DSKM is to provide improved reliability and functionality over existing mechanisms for individuals paralyzed by SCI.

2.2 Design Description of the Dual-State Knee Mechanism

The objective of the DSKM is to fully support the knee joint during load bearing instances, such as quiet standing and the stance phases of gait, while allowing for

uninhibited knee movement during stepping actions. The overall goal is to eliminate the need for FNS of target knee extensor muscles during static load supporting tasks.

Consequently, the DSKM must possess a wide mechanical impedance range. High device mechanical impedance is necessary during stance to resist against flexion under the user's weight in addition to any dynamic loading (i.e., heel strike event at the beginning of the stance phase) applied to the device. This is important to prevent the knee from buckling which would lead to either collapse or the lowering of the user's center of mass, resulting in insufficient foot-to-ground clearance for contralateral swing. To counter either adverse event, the user may have to increase reliance on a walking aid, resulting in an inefficient form of gait. Low device mechanical impedance is critical during swing so that the knee can move through the desired trajectory as efficiently as possible. This is particularly important when utilizing FNS to drive limb motion. The electrical stimulation of paralyzed muscle is weaker and fatigues more rapidly than normal, volitionally controlled muscle. Thus, any resistance imposed by the device against knee motion during swing may adversely affect the desired trajectory or hasten the onset of muscle fatigue.

The fundamental design of the DSKM incorporates a single rod, double-acting cylinder with a 2-way, 2-position, normally closed solenoid valve inline between the cylinder ports (**Figure 2.1**). A normally closed valve was chosen so that the knee mechanism can be locked without consuming power. **Figure 2.1** shows that the solenoid valve behaves as a check valve when pressure is applied to port A (Refer to **Figure 3.6** for a detailed valve schematic). When this pressure rises beyond a critical maximal value

(valve cracking pressure) the valve will be forced to open. As a result, the mechanism was designed to be locked only against knee flexion.

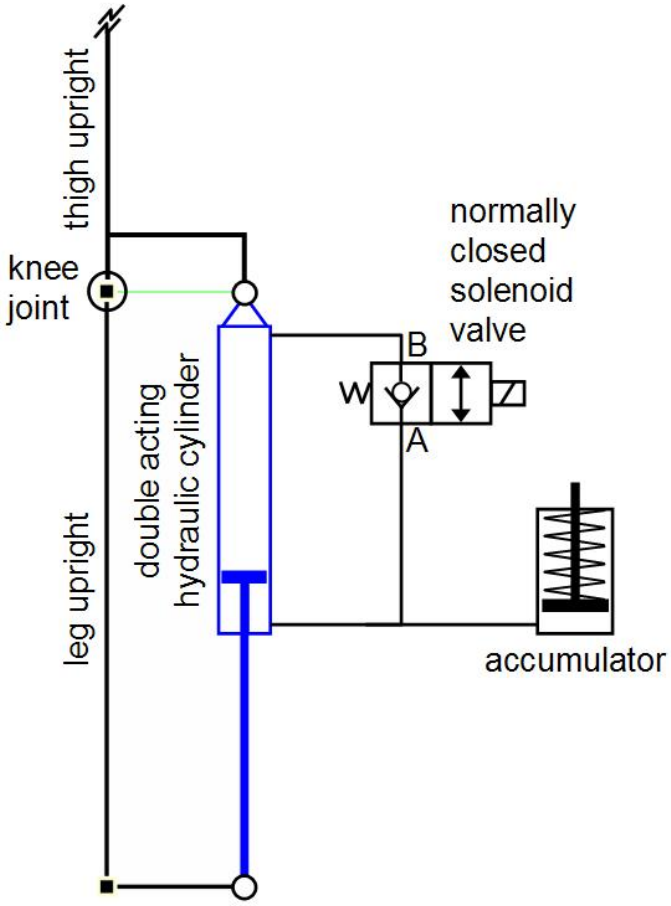

Figure 2.1. Schematic of the hydraulic dual-state knee mechanism (DSKM).

Since hydraulic fluids are relatively incompressible, as expressed by the bulk modulus of the liquid, an accumulator was included to take up the fluid volume of the piston rod when flow is directed from the blind to the rod side of the cylinder (i.e., mechanism is moved into flexion). However, the accumulator prevents the pressure differential across the valve from exceeding the valve cracking pressure when an unpowered DSKM is extended. During knee extension, fluid flow will move into the accumulator (until the pressure differential across the valve exceeds the cracking

pressure), decreasing the pressure and increasing the volume (due to the expansion of existing air bubbles) of the system blind side. The DSKM cannot effectively lock against flexion until the resting volume of the blind side is restored. To prevent this effect, the solenoid valve must be powered and opened during knee extension by feedback control. A four-bar linkage approach was used for linear-to-rotary transmission.

2.3 COMPONENT SELECTION, OPTIMIZATION, AND FABRICATION

The design goal was to maximize the locking torque of the DSKM. Since a linkage was used to transmit between linear and rotary motion, the moment arm and thus the maximum locking torque will vary with joint angle. Consequently, the objective was to optimize the moment arm versus joint angle profile such that the maximum moment arm occurred at or near full knee extension. To test the feasibility of the design and to minimize cost, the knee mechanism was optimized around available off-the-shelf hydraulic component specifications. The following optimization constraints were considered in maximizing the operating torque of the knee mechanism. 1) Cylinder geometry (i.e., bore and stroke) was minimized to maintain low flow rates and low mechanism weight. 2) The maximum operating pressure of the hydraulic components must be relatively high to accommodate the small actuator. 3) The solenoid valve flow coefficient was maximized to minimize the pressure losses through the opened valve at the system flow rates generated during gait. Specifically, the contribution of the pressure losses through the opened valve to user applied knee torque was constrained to be less than 1 Nm. 4) The power consumption of the solenoid valve was minimized to allow for

sustained use. 5) The position of the linkage mechanism at which the singularity occurs (i.e., moment arm is equal to zero) was kept outside the angle range at which the mechanism has a high probability of supporting a high static load. Sagittal knee kinematic data from preliminary gait experiments with able-bodied individuals were used in the mechanism optimization.

Table 2.1
Knee Mechanism Hydraulic Components

	cylinder	**valve**	**accumulator**
manufacturer	Clippard Minimatic	Allenair	Clippard Minimatic
type	double acting	solenoid 2/2	single acting spring return
bore	9/16”	-	3/4”
port	1/16” NPT	1/8” NPT	1/8” NPT
orifice	-	2.38 mm	-
stroke	3”	-	1”
rod diameter	0.25”	-	0.25”
voltage	-	12 VDC	-
power consumption	-	7 W	-
C_V	-	0.176 B➔A 0.166 A➔B	-
response time (no load)	-	12 ms (on) 43 ms (off)	-
max operating pressure	2000 psi	-	250 psi
spring force	-	-	3 lbs installed 6 lbs compressed
cracking pressure	-	46 ± 7 psi	-

Table 2.1 lists the specifications for the selected hydraulic components. Custom circuitry was developed to drive the valves for a pair of DSKMs (**Figure 2.2**). A 12 VDC supply, boost converted from a Sony NP-F970 lithium ion rechargeable battery (Sony Corp., Tokyo, Japan), was used to power the valves (**Figure 2.2**). Originally, a small amount of air was maintained in the hydraulic system in an attempt to eliminate the need for a physical accumulator in order to minimize system size and weight. The difference in volume between the rod and blind sides of the cylinder was taken up by the

compression of the internal air bubbles. However, bench and human testing of this initial prototype revealed an excessive amount of compliance (i.e., change in flexion angle) when locked against flexion. Ultimately, a single acting, spring-loaded cylinder was used as an accumulator. A small spring force was selected for the accumulator to keep the passive resistance low when the accumulator is pressurized during free knee flexion.

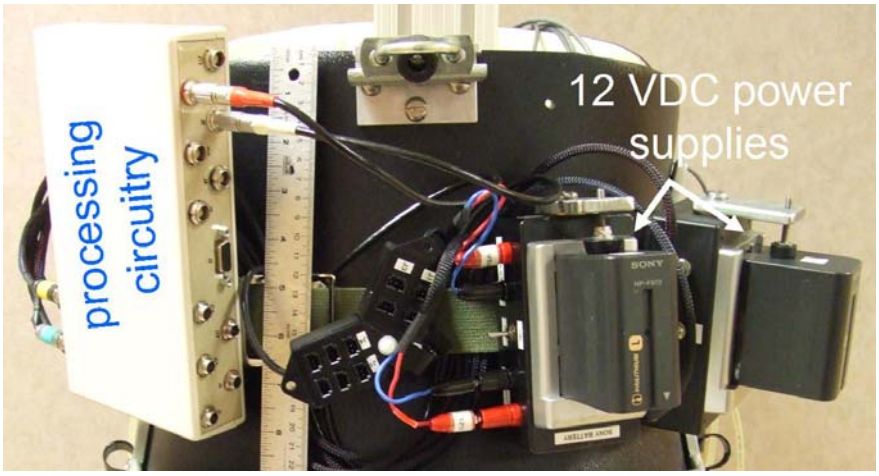

Figure 2.2. Processing circuitry and power supply (Technical Development Laboratory, Advanced Platform Technology (APT) Center, Cleveland, OH, USA) of the DSKM.

Table 2.2
Hydraulic Knee Mechanism Specifications

type	linkage
voltage	12 VDC
power consumption	7 W
response time (no load)	12 ms (unlock) 43 ms (lock)
max operating pressure	1000 psi
extension cracking pressure	46 ± 7 psi
maximum operating torque	69.5 Nm @ 0^{o}
range of motion	-5^{o} to 106^{o}
maximum tested speed	330^{o}/s

Table 2.2 summarizes the optimized specifications of the hydraulic DSKM. **Figure 2.3** shows a CAD (Dassault Systèmes SolidWorks Corp., Concord, MA, USA) representation of the DSKM. The knee-ankle-foot orthosis (KAFO) equipped with the DSKM as pictured in **Figure 2.3** weights approximately 5 kg (11 lbs).

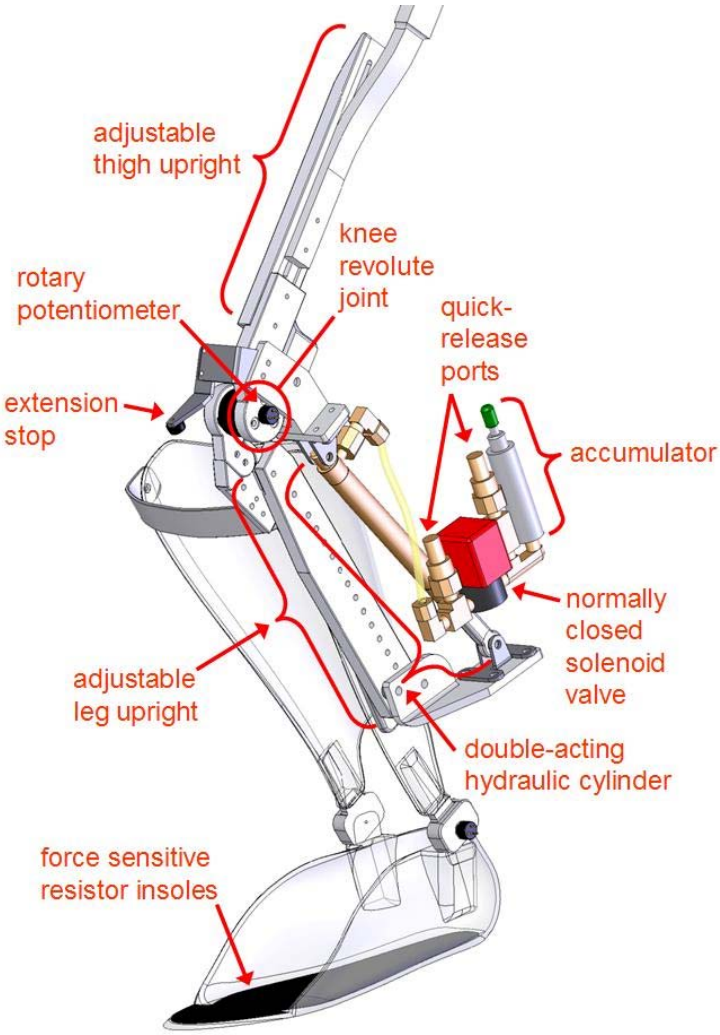

Figure 2.3. CAD representation of the DSKM.

The structural components of the KAFO were fabricated from a combination of 6061 and 6063 aluminum alloy and 4142 and galvanized low-carbon steel alloys (Refer to **Appendix C** for the material of each component). Note that the range of motion (ROM) of the DSKM in flexion was limited by the off-the-shelf clevis components used to simplify construction. A mechanical extension stop was incorporated to prevent hyperextension of the knee. The KAFO was made adjustable for different users. Hydraulic quick-release nipples were installed at each cylinder port to allow for pressure

measurements or serve as system fluid priming points (Refer to **Chapter 5** for details on system priming). Hydraulic oil, ISO VG 46, was used as the fluid media. The Reynolds number was calculated to be 721 (less than 2000, indicating laminar flow) at an estimated maximum internal fluid velocity of 13.92 m/s.

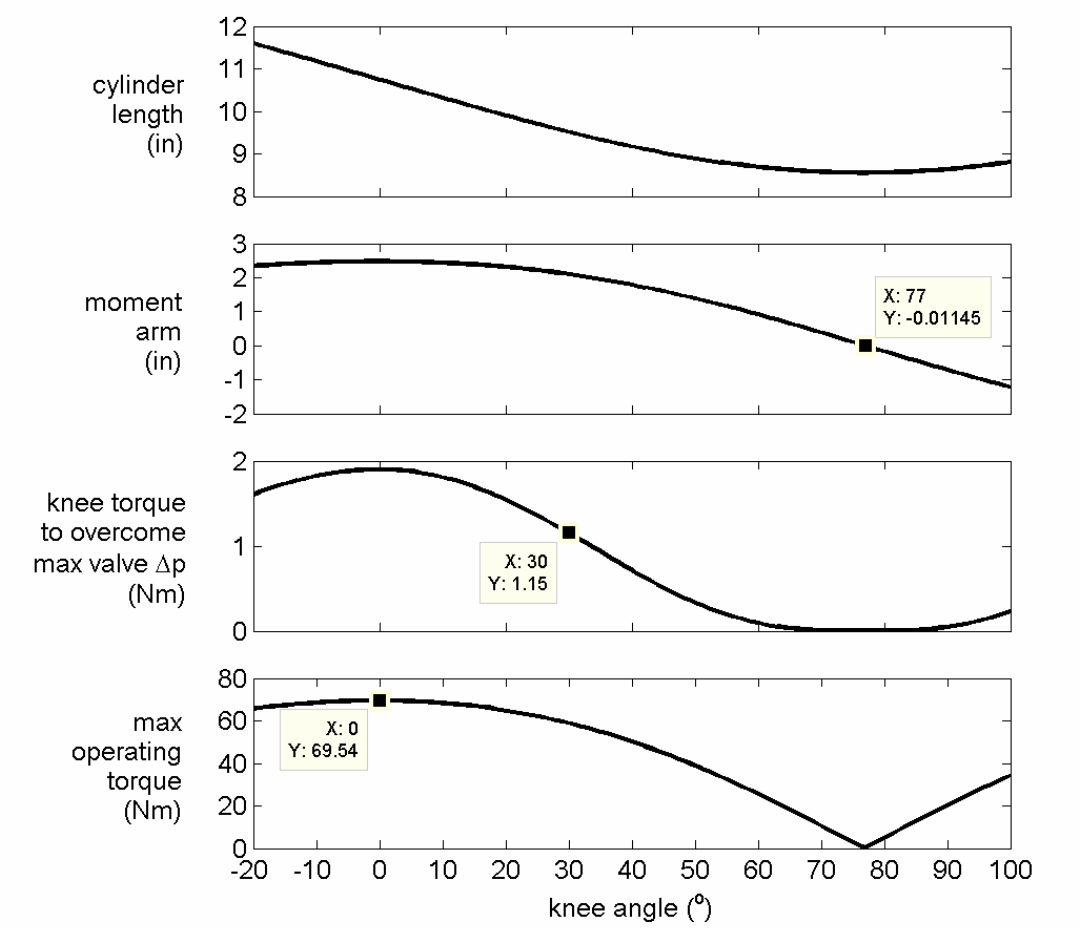

Figure 2.4. Design parameters of the DSKM.

Figure 2.4 shows the design parameters with respect to joint angle (negative angle = extension, positive angle = flexion) for the optimized DSKM design. Since torque is directly proportional to the moment arm, the maximum operating torque is largest (approximately 70 Nm) at full extension (0^o) and decreases with increased knee flexion. With a linkage mechanism, a singularity occurs when the moment arm is equal

to zero. At the singularity, the maximum operating torque is zero, thus the DSKM should never be locked at this angle.

Attempts at removing the singularity entirely from the knee ROM resulted in an overall decrease in the maximum operating torque of the mechanism. The strategy used in the current design was to move the singularity to a point where knee locking has the lowest probability of occurring. During walking, the knee typically moves between 0^o and 65^o [14]. Within this range, locking can happen anywhere if power failure or control problems arise. During sitting, the knee angle is between 90^o and 110^o. The knee may be locked during sitting to conserve power or to prevent the solenoid valve from overheating. The solution was to move the singularity in between 65^o and 90^o. The passive resistance is represented as the applied knee torque necessary to overcome the maximum pressure differential across the valve (when the valve is open) induced by a maximum knee angular velocity of 330^o/s (determined from able-bodied gait experiments) over the entire ROM of the knee. This is only hypothetical, since the maximum angular velocity of the knee typically occurs at around 30^o knee flexion during swing phase of gait. In the current design, the applied knee torque necessary to overcome the maximum valve pressure differential has been constrained to approximately 1 Nm.

2.4 CLOSED-LOOP CONTROL

A controller was developed to unlock the DSKM during the swing phases of gait and lock the knee mechanism in full extension when the limb is being loaded upon and supporting the weight of the user. The controller for the DSKM was designed as finite

state machine based on feedback signals, which include 1) state of the solenoid valve, 2) foot-to-ground contact, 3) knee angle, 4) knee angular velocity, and 5) a signal from the FNS controller (**Chapter 4**). The knee controller and data acquisition software was developed and implemented in the Simulink®/xPC Target real-time environment (The Mathworks, Inc., Natick, MA, USA). Refer to **Chapter 4** for details on the overall hybrid neuroprosthesis system control software and graphical user interface.

2.4.1 Sensors for Signal Feedback

Feedback control of the DSKM was based on signals from the following sensors (**Figure 2.3**). 1) Force sensitive resistors (B & L Engineering, Tustin, CA, USA) embedded in the soles of the shoes were used to measure foot-ground contact instances. One force sensitive resistor (FSR) was positioned under the 1st metatarsal, 1st phalange, 5th metatarsal, and heel of each foot. For the purposes of the current controller, the only information required from the FSRs is whether or not the heel or forefoot is in contact with the ground. The recordings from FSRs under the forefoot (1st metatarsal, 1st phalange, and 5th metatarsal) of impaired gait were observed to be inconsistent relative to normal gait. Thus, to increase robustness, the output of the three forefoot FSRs were summed into a single forefoot FSR signal with a saturation value equal to one. 2) A precision rotary potentiometer (Vishay Spectrol, Malvern, PA, USA) measured joint angle. The joint angle was differentiated to determined knee angular velocity. **Figure 2.2** shows the custom processing circuitry and power supply for all sensors. Foot-to-ground contact information and joint angle signals were chosen for the controller inputs as they have been shown to contain enough information to discriminate among the phases

of gait [15, 16]. All signals were sampled at a frequency of 200 Hz and low-pass filtered through software. The potentiometer signal was low-pass filtered (5^{th}-order Butterworth) at a cut-off frequency of 10 Hz and the pressure and FSR signals was low-pass filtered (7^{th}-order Butterworth) at a cut-off frequency of 20 Hz.

2.4.2 Finite State Knee Controller

Table 2.3 diagrams the finite state knee controller (FSKC). The finite state machine uses seven feedback signals to control the state of the DSKM, 1) contralateral knee valve state control signal, 2) contralateral forefoot ground contact 3) contralateral heel ground contact, 4) ipsilateral heel ground contact, 5) ipsilateral knee angle, 6) ipsilateral knee angular velocity, and 7) a FNS controller output signal. The finite state machine essentially incorporates four rules that can act independently or mutually to designate if the DSKM should be unlocked. For each rule, all the IF conditions must be satisfied in order for the THEN clause to be executed, otherwise the ELSE clause is implemented. The execution of the THEN clause of a rule takes precedence over the ELSE clause of other rules.

Rule 1 states that as long as the knee is extending, the mechanism is unlocked. An extending knee is indicated by an angular velocity subceeding a preset threshold (extension is negative). This threshold was set to be two standard deviations above the steady state angular velocity signal. An angular velocity in the extension direction can always be achieved even if the knee mechanism is in a locked state since the solenoid valve allows for flow from the rod to the blind side (if the valve cracking pressure is exceeded) and the rod side of the system is always open to the accumulator. This rule

was established to prevent unpowered DSKM extension, which can compromise the responsiveness of the device locking against flexion. The FNS controller (**Chapter 4**) utilizes the output of the FSKC to modulate electrical stimulation pulses to the target muscles. In general, stimulation is activated and deactivated when the DSKM is unlocked and locked respectively. The implementation of the **Rule 1** of the FSKC can allow for brief moments of DSKM unlocking during load bearing instances. This will subsequently lead to short bursts of muscle stimulation that are nonfunctional and may destabilize the user.

Table 2.3
Dual-State Knee Mechanism Finite State Machine

rule	IF	THEN	ELSE*
1	ipsilateral knee angle has not crossed below threshold 1	unlock	lock
	ipsilateral knee angle has crossed above threshold 2		
	ipsilateral knee angular velocity < angular velocity threshold		
2	contralateral DSKM valve state is closed+	unlock	lock
	either contralateral forefoot or heel FSR is high		
	ipsilateral heel FSR is low		
3	FNS controller signal is high	unlock	**Rule 4**
4	FNS controller signal is low	lock	**Rule 1** or **Rule 2**
	ipsilateral knee angle < threshold 1		

***** The execution of the THEN clause of a rule takes precedence over the ELSE clause of other rules.
+ The contralateral valve does not need to be closed to unlock the ipsilateral DSKM if the contralateral DSKM is unlocked via **Rule 1**.

To prevent this effect, **Rule 1** is disabled once full knee extension is achieved and enabled when full extension needs to be restored. The disabling/enabling of **Rule 1** uses hysteresis thresholding. The input knee angle must exceed a first threshold for an output

to be high and a second threshold must be subceeded for an output to be low. When the knee has extended beyond angle threshold 1, indicating full extension, **Rule 1** is disabled. When the knee is flexed beyond angle threshold 2, **Rule 1** is enabled. Angle threshold 2 must be greater than the sum of the magnitude of angle threshold 1 and the maximum mechanical compliance of the DSKM when locked against flexion (as defined in **Section 2.4**). **Rule 1** facilitates uninhibited knee extension during the mid and terminal swing phases of gait and the sit-to-stand transition.

Rule 2 states that the DSKM unlocks if all the following conditions are met. 1) The contralateral knee valve must be closed, indicating that the contralateral knee is locked. Note that the contralateral valve does not need to be closed to unlock the ipsilateral knee if the contralateral knee is unlocked via **Rule 1**. 2) The ipsilateral heel is off the ground (FSR is low), indicating either terminal stance or pre-swing. 3) Either the contralateral forefoot or heel is in contact with the ground (FSR is high), indicating that the contralateral limb is in stance. The designation of whether a FSR signal is high or low was determined by hysteresis thresholding, with the second threshold greater than the first threshold to increase response time. **Rule 2** coordinates locking/unlocking of the DSKM with gait events derived from the feedback of selected signals.

Rule 3 utilizes an output signal from the FNS controller which is derived from the timing of the pre-programmed ipsilateral knee flexor and extensor muscle stimulation patterns. This signal dictates when the DSKM must be unlocked during the swing phases of gait. This rule was established to prevent the knee mechanism from locking (due to **Rule 2**) during mid swing in the event that the foot contacts the ground, resulting in a high FSR signal.

Rule 4 states that once the FNS controller output signal is low, the DSKM is unlocked until the knee has returned to a fully extended position (determined by a knee angle below a preset threshold, consistent with angle threshold 1 for **Rule 1**) or if both **Rules 1** and **2** dictate that locking should occur.

Table 2.4 shows the threshold values used for the FSKC. Unless stated otherwise, the thresholds were determined empirically during bench and human testing.

Table 2.4
FSKC Threshold Values

signal	threshold 1	threshold 2
FSR (normalized)	0.1	0.2
angle	3^o	13^o
angular velocity	$-6^o/s$	-

2.5 SYSTEM CHARACTERIZATION

Bench testing was conducted on the prototype knee mechanism to 1) quantify the passive resistance as a function of knee angle and angular velocity, 2) verify that the knee mechanism can hold a static torque of at least 50 Nm [14] at/near full knee extension, 3) test if the knee mechanism can responsively unlock (i.e., open the valve) at relatively high static loads, and 4) quantify the mechanical compliance when the knee mechanism is locked (i.e., valve closed) against flexion. Here, passive resistance is the torque required to move the knee mechanism, contributed by the viscous and frictional effects of the hydraulics, at a known angular velocity while the knee mechanism is unlocked. Mechanical compliance is defined as the variation in knee angle into flexion while the valve of the mechanism is closed.

All bench testing was completed with the knee mechanism secured to the actuator of a Biodex System 3 (Biodex Medical Systems, Inc., Shirley, NY, USA) robotic dynamometer (**Figure 2.5**). In addition to the feedback sensors and valve control signals, knee angle, angular velocity, and torque were collected from the dynamometer, and cylinder blind and rod side pressures were measured with pressure transducers installed via the quick-release couplers (**Figure 2.3**). The dynamometer signals were low-pass filtered (5^{th}-order Butterworth) at a cut-off frequency of 10 Hz during data collection. The torque data were further low-pass filtered at a cut-off frequency of 3 Hz during analysis. The pressure signals were low-pass filtered (7^{th}-order Butterworth) online at a 20 Hz cut-off frequency. The experimental setup limited the ROM of the DSKM to 90^{o}.

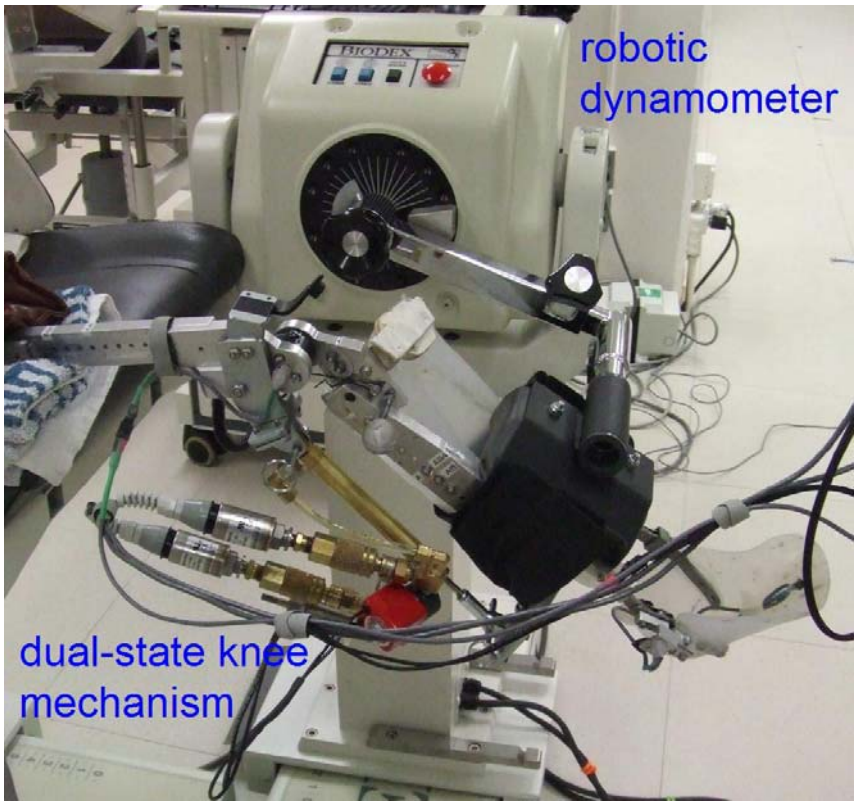

Figure 2.5. Bench testing experimental setup of the DSKM. A Biodex System 3 (Biodex Medical Systems, Inc., Shirley, NY) robotic dynamometer was used to drive the DSKM at a specified angular velocity.

2.5.1 Passive Resistance

To determine the passive resistance, the knee mechanism was unlocked (valve opened) and actuated by the dynamometer at various angular velocities, ranging from 5^o/s to 150^o/s, through the set ROM. The maximum tested angular velocity was limited by the angular acceleration of the dynamometer to the specified angular velocity within the ROM. The inertial component of the measured torque necessary to accelerate the mass of the dynamometer attachment and mechanism was subtracted from the total measured torque to obtain the passive resistance torque.

Figure 2.6a and **2.6b** shows the passive resistance torque magnitude relative to joint angular velocity at a knee flexion angle near 30^o for flexion and extension motion respectively. Able-bodied gait kinematics show that the maximum angular velocity during gait occurs near a knee angle of 30^o. Since passive resistance is proportional to angular velocity, it was assumed that the maximum passive resistance occurred at a knee angle of 30^o as well. The mean for the torque magnitudes for all the tested angular velocities were below 2.0 Nm in flexion and 1.0 Nm in extension. **Figure 2.6c** shows the passive resistance torque magnitude relative to joint angle at a knee angular velocity of 5^o/s for flexion and extension motion. A low angular velocity was chosen to minimize the velocity contribution to the total mechanism passive resistance. A linear regression (thick line) was fit to each data series with corresponding 95% confidence intervals (thin lines).

An analysis of variance was done over both the influence of direction (flexion/extension) and angular velocity on the passive resistance. A statistical difference was found between flexion and extension directions ($p = 0.0000$). The passive resistance

is larger in the flexion direction because 1) the blind side of the piston, which has a larger area than the rod side of the piston, is pressurized during cylinder retraction (coincident with the flexion of the DSKM) and 2) the accumulator is being pressurized during flexion, whereas during extension the pressure from the accumulator is being released. The accumulator pressure opposes DSKM flexion but assists DSKM extension.

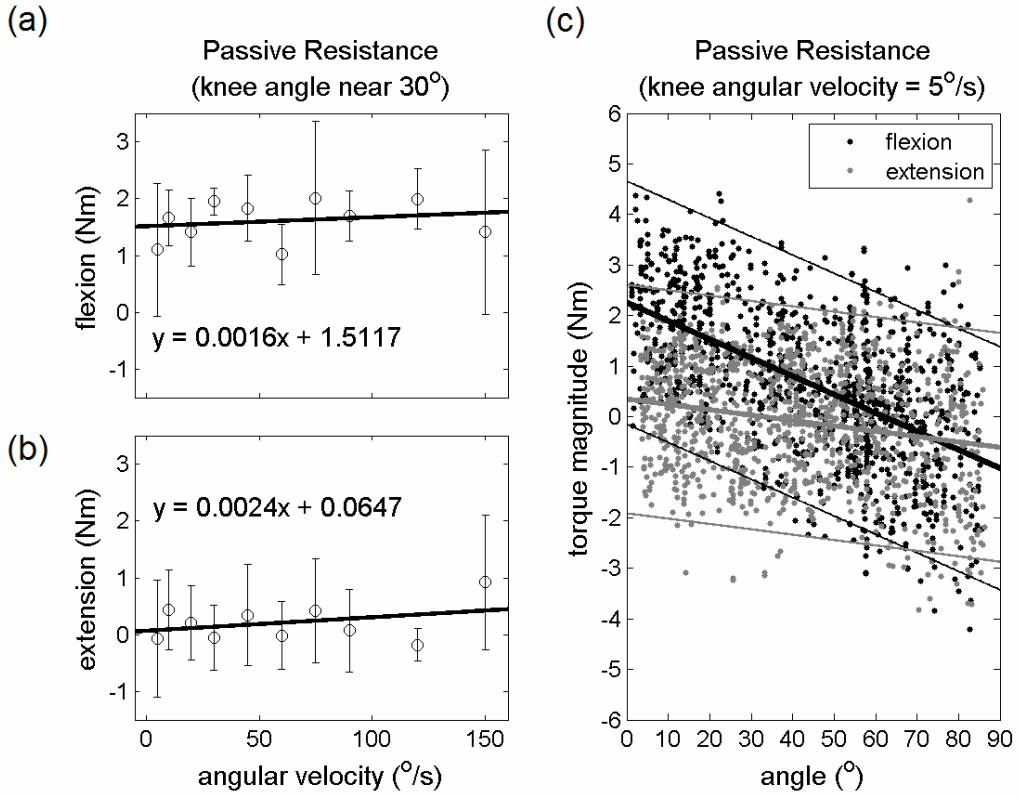

Figure 2.6. Passive resistance of the DSKM with respect to knee angular velocity for **(a)** flexion and **(b)** extension directions at a knee angle near 30°. **(c)** Passive resistance of the DSKM with respect to knee angle at a knee angular velocity of 5°/s.

There was no statistical difference in applied torque among the angular velocities in the flexion direction ($p = 0.1335$). In the extension direction, there was a no statistical difference between the applied torques at angular velocities up to 120°/s ($p = 0.3548$). However, a statistical difference was found between the low angular velocities and 150°/s ($p = 0.0000$). The minimal influence of angular velocity on the passive resistance torque

suggests that angular velocities higher than the values tested should not substantially increase passive resistance. Extrapolated from 1st-order least squares regressions fitted to both the flexion and extension torque versus angular velocity data, the applied passive resistance was 2.07 Nm and 0.90 Nm at a maximum knee angular velocity of 350°/s [14] for flexion and extension, respectively.

Kobetic and Marsolais [17] measured the average isometric knee flexion and extension moments produced by FNS in 23 subjects with paraplegia to be 15 Nm (90° flexion) and 80 Nm (45° flexion) respectively. A combination of percutaneous intramuscular, subfascial, and surface electrodes were used to activate knee flexor (hamstrings, biceps femoris (short head), sartorius, and gracilis) and extensor (vastus lateralis, vastus medialis, and vastus intermedius) muscles. For knee flexion, about 13 % of the achievable knee flexion torque generated by FNS is required to overcome mechanism passive resistance. Only 1 % of the achievable knee extension torque generated by FNS is required to overcome the mechanism passive resistance in the extension direction.

2.5.2 Dynamic Parameters

Figure 2.7 illustrates the knee angle, angular velocity, differential pressure, and applied torque (measured by the dynamometer and calculated from the measured pressure) measured in a typical trial. The horizontal bar under each curve indicates when the DSKM was locked. The valve was initially opened to allow the dynamometer to freely actuate the DSKM. A signal to close the valve was sent to lock the DSKM while the DSKM was extending. According to **Rule 1** of the FSKC, the DSKM would lock

against flexion after the knee has fully extended. After the DSKM had reached a steady state, a signal to open the valve was sent to unlock the DSKM. The dynamometer was set to apply a different maximum torque magnitude for each trial. The flexion torque contributed by gravity, from the mass of the dynamometer attachment and DSKM, was added to the measured torque applied by the dynamometer to determine the total applied torque to the locked DSKM. As a result of this gravitational component, it was not possible to apply less than 12 Nm of flexion torque on the DSKM.

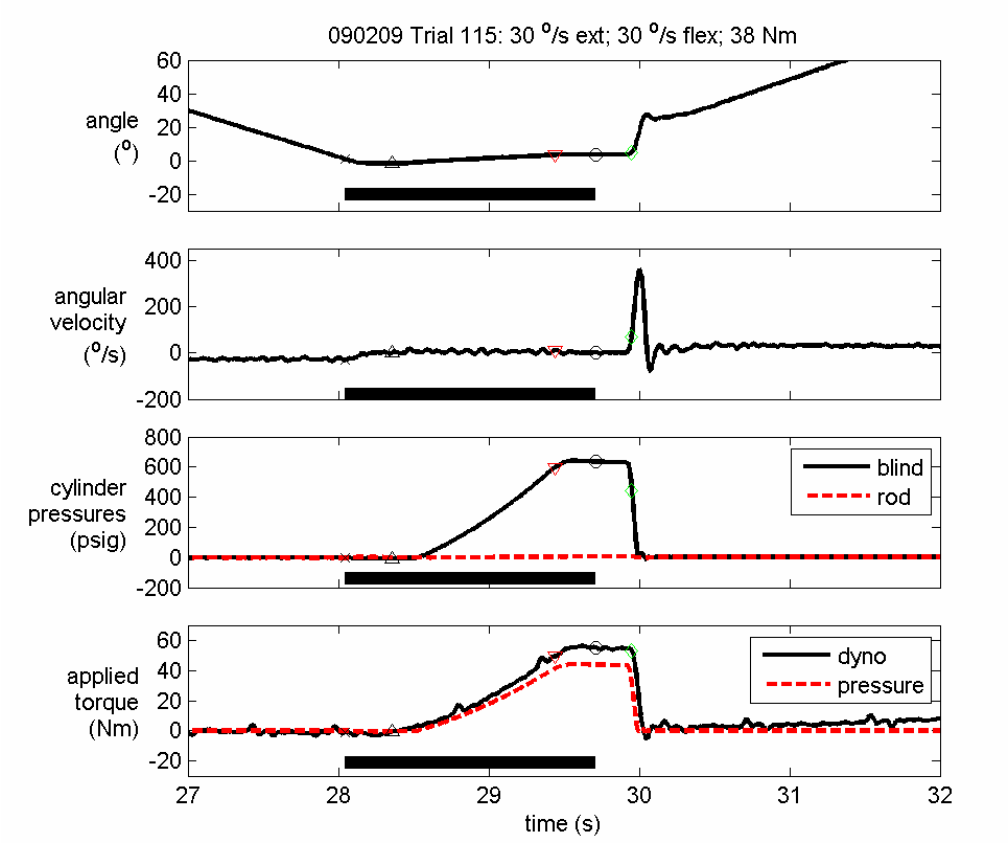

Figure 2.7. Sensor measurements from a typical bench test trial to quantify the dynamic parameters of the DSKM.

A maximum flexion torque of 71 Nm was applied on the locked DSKM. **Figure 2.8** shows the duration to open the valve (unlock the knee), Δt_{open}, with respect to the pressure differential across the valve. The DSKM was able to unlock consistently with a

valve pressure differential of up to approximately 700 psi. This maximum unlocking valve pressure differential corresponds to a flexion torque magnitude of approximately 49 Nm at full knee extension. When unloaded, the DSKM requires only 12 ms to unlock. However, once loaded, the DSKM requires a minimum of just under 200 ms to unlock.

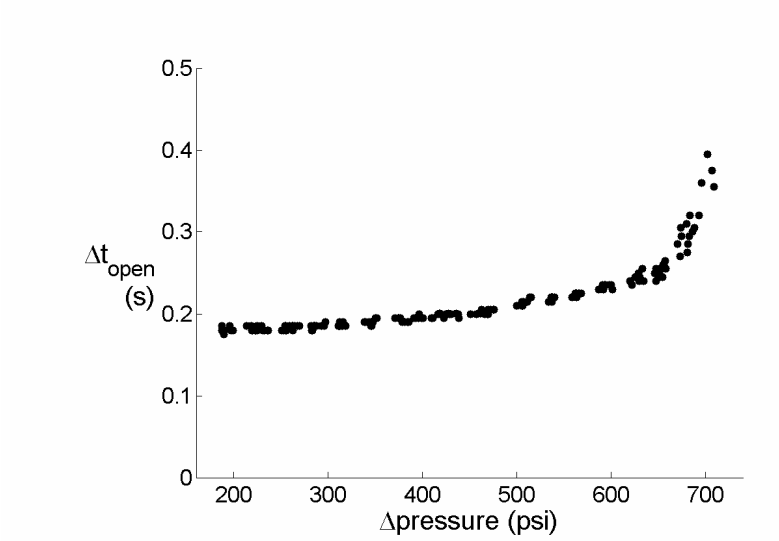

Figure 2.8. Duration to open the DSKM valve with respect to the pressure differential across the valve.

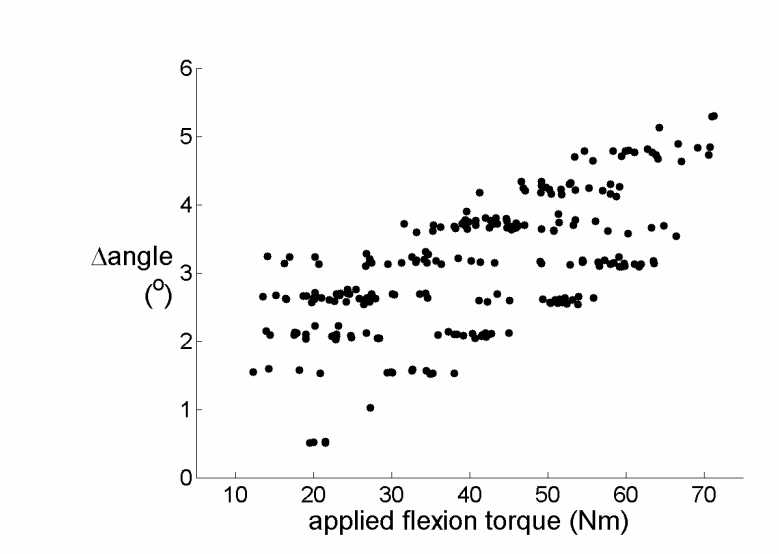

Figure 2.9. Change in angle into flexion when the DSKM is locked (compliance) with respect to applied flexion torque.

Figure 2.9 shows the knee compliance (Δangle) with respect to the applied flexion torque. The compliance was calculated relative to the full extension angle threshold of **Rule 1** of the FSKC. Note that the measured compliance in the locked mechanism is a contribution of both the hydraulics and mechanical structure of the device (i.e., machining tolerance of the mounting components). At the minimum design locking torque of 50 Nm, 2.5^{o} to 4.5^{o} of compliance was observed.

2.6 MECHANISM VALIDATION WITH ABLE-BODIED INDIVIDUALS

The DSKM was evaluated with three able-bodied individuals to test if the FSKC can change state of the DSKM responsively and consistently during normal gait. All able-bodied individuals recruited to participate in this research signed a consent form approved by an institutional review board.

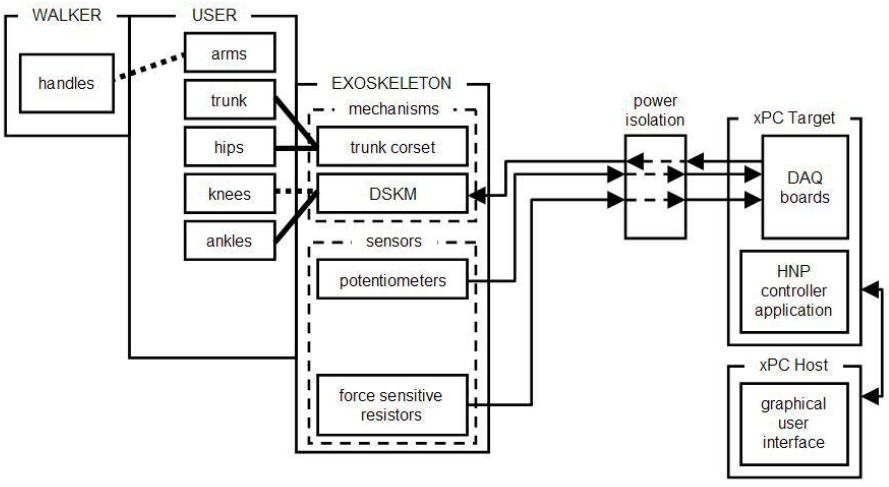

Figure 2.10. Experimental setup for testing the DSKM with able-bodied individuals.

Figure 2.10 shows the experimental setup. Since no FNS was used, only **Rules 1** and **2** of the knee mechanism control module were implemented to control the DSKM. A pair of DSKMs was installed on a trunk corset with hip joints that restricted motion to the sagittal plane. The solid lines connecting the trunk corset to the trunk and hips indicate a fixed constraint imposed by the exoskeleton, while the dotted line between the DSKM and knees indicate a variable constraint. The size of exoskeleton was adjustable to fit each subject. The ankle joints of the DSKM were unlocked in the sagittal plane. The target and host computers were used to implement the FSKC and collect data. Twenty meters of shielded multi-conductor cabling was used to connect the exoskeleton to the controller. Subjects were instructed to walk at their preferred speed along an eight meter walkway while wearing the prototype exoskeleton. The subjects used a walker for additional support. Approximately 50 strides of data was collected and analyzed for each subject. The able-bodied subjects walked at an average gait speed of 0.78 ± 0.07 m/s.

Figure 2.11a, **2.11b**, and **2.11c** respectively shows the average knee angle, force sensitive resistor activity, and the percentage of samples that the DSKM was unlocked (± 1 standard deviation) with respect to percentage gait cycle of all three subjects. The vertical lines delineate the gait events (loading response (LR), mid stance (MSt), terminal stance (TSt), pre-swing (PSw), initial swing (ISw), and late swing (LSw)) as defined in [14]. During the LR and MSt phases, the knee is almost always locked. The transition from locked to unlocked begins in TSt with the majority occurring during PSw. The DSKM is almost always unlocked during the swing phases. Occasional locking during the swing phases is due to inadequate foot-to-ground clearance as illustrated by FSR

activity of **Figure 2.11c**. As discussed in **Section 2.4.2**, this shortcoming is addressed by **Rule 3** of the FSKC.

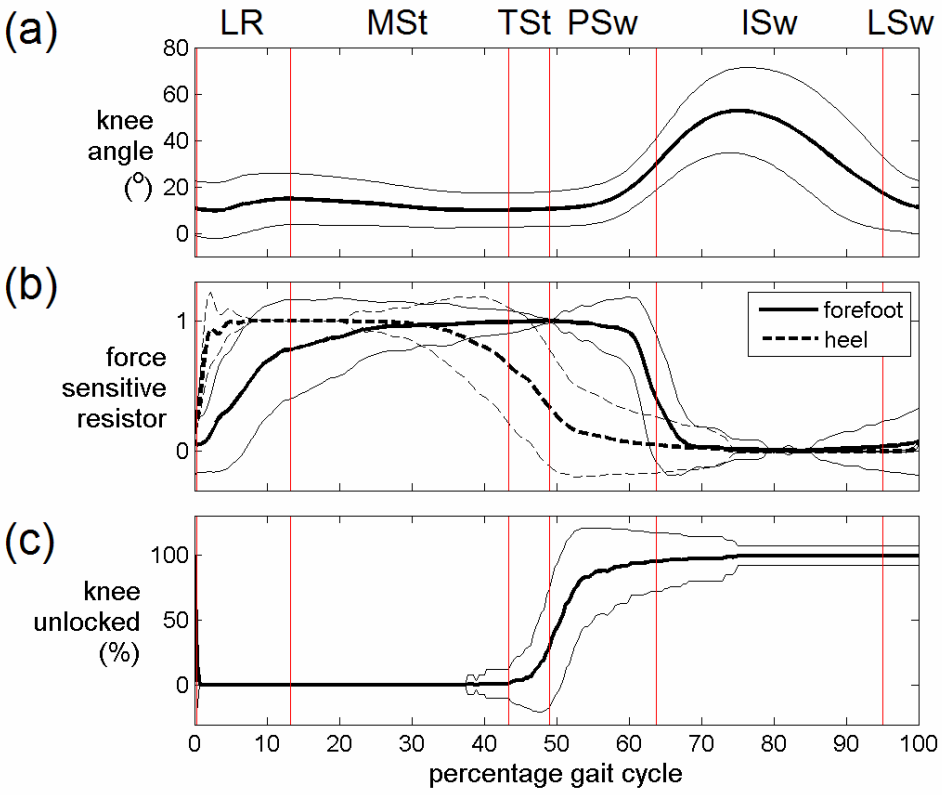

Figure 2.11. Response of the DSKM during normal gait (LR = loading response, MSt = mid stance, TSt = terminal stance, PSw = pre-swing, ISw = initial swing, LSw = late swing).

2.7 CONCLUSIONS

The current work shows the feasibility of utilizing a hydraulic approach in developing a controllable knee constraint to assist in restoring gait after SCI. This new hydraulic DSKM has improved upon existing designs in that it is capable of consistently unlocking under an applied flexion torque of up to 49 Nm (at full knee extension).

The development of the hydraulic knee mechanism from conception to implementation was expedited by using a simplified transmission solution. This

compromise reduced the ROM in which the mechanism can effectively support the user. Thus, future work may center on choosing an optimal transmission type. A rack-and-pinion solution will facilitate a constant moment arm with respect to knee angle. Thus, the constraint can support against a high torque at any angle in which the knee is locked. However, the gears may increase the size and weight of the device. Another solution may be to use a more complex linkage or a cam design to optimize the profile of the moment arm with respect to the knee angle. Similar to the current design, larger moment arms will occur at knee angles that require high impedance while smaller moment arms will occur at knee angles coincident with high angular velocities during gait to minimize mechanism passive resistance. With this approach, a larger cylinder bore can be used to increase the maximum operating torque without substantially increasing passive resistance.

2.8 REFERENCES

1. J. F. Lehmann and J. B. Stonebridge, "Knee lock device for knee ankle orthoses for spinal cord injured patients: an evaluation," *Arch. Phys. Med. Rehabil*., vol. 59, no. 5, pp. 207-211, 1978.

2. H. Kagaya, Y. Shimada, K. Sato, M. Sato, K. Iizuka, and G. Obinata, "An electrical knee lock system for functional electrical stimulation," *Arch. Phys. Med. Rehabil*., vol. 77, pp. 870-873, 1996.

3. R. Harrison, E. Lemaire, Y. Jeffreys, and L. Goudreau, "Design and pilot testing of an orthotic stance-phase control knee joint, *Orthopadie Technik,* pp. 2-4, 2001.

4. G. Kim, S. Kang, J. Ryu, M. Mun, and K. Kim, "Unlockable Knee Joint Mechanism for Powered Gait Orthosis," *Int, J. Precision Eng & Manufacturing*, vol. 10, no. 3, pp. 83-89, July 2009.

5. N. G. Van Leederdam, and E. E. Kunst, "New UTX-swing orthosis: Normal gait and safe standing," *Orthopadie Technik*, vol. 50, pp. 506-515, 1999.

6. G. Nijenbanning, J. A. Goudsmit, "Gravity operated locking hinge," United States patent US 20030153854. Aug 14, 2003.

7. B. J. Hatton, D. L. Hatton, and Z. G. Wallace, "Articulating knee supports," United States patent US 6635024. Oct 21, 2003.

8. T. Yakimovich, J. Kofman, and E. D. Lemaire, "Design and evaluation of a stance-control knee-ankle-foot orthosis knee joint," *IEEE Trans. Neur. Sys. Rehab. Eng.*, vol. 14, no. 3, pp. 361-369, Sept. 2006.

9. R. B. McGhee, R. Tomovic, Y. Yang, and I. C. MacLean, "An experimental study of a sensor-controlled external knee locking system," *IEEE Trans. Biomed. Eng.*, vol. 25, pp. 195-199, 1978.

10. S. E. Irby, K. R. Kaufman, R. W. Wirta, and D. H. Sutherland, "Optimization and application of a wrap-spring clutch to a dynamic knee-ankle-foot orthosis," *IEEE Trans. Rehab. Eng.*, vol. 7, pp. 130-134, 1999.

11. N. Sclater, and N. P. Chironis, Mechanisms and Mechanical Devices Sourcebook. New York, NY: McGraw-Hill, 2001.

12. J. C. Moreno, F. Brunetti, E. Rocon, and J. L. Pons, "Immediate effects of a controllable knee ankle foot orthosis for functional compensation of gait in patients with proximal leg weakness," *Med. Biol. Eng. Comp.*, vol. 46, no. 1, pp. 43-53, 2007.

13. T Yakimovich, E. D. Lemaire, and J. K. Kofman, "Engineering design review of stance-control knee-ankle-foot orthoses," *J. Rehabil. Res. & Dev.*, vol. 46, no. 2, pp. 257-268, 2009.

14. J. Perry, Gait Analysis: Normal and Pathological Function, Thorofare, NJ: SLACK Incorporated, pp. 92, 94, 1992.

15. S. K. Ng and H. J. Chizeck, "Fuzzy model identification for classification of gait events in paraplegics," *IEEE Trans. Fuzzy Syst.*, vol. 5, pp. 536–544, Nov. 1997.

16. M. M. Skelly and H. J. Chizeck, "Real-time gait event detection for paraplegic FES walking," *IEEE Trans. Neural Systems Rehab. Eng.*, vol. 9, no. 1, pp. 59-68, March 2001.

17. R. Kobetic and E. B. Marsolais, "Synthesis of paraplegic gait with multichannel functional neuromuscular stimulation," *IEEE Trans. Rehabil. Eng.*, vol. 2, no. 2, pp. 66–79, Jun. 1994.

CHAPTER 3

DESIGN OF A VARIABLE CONSTRAINT HIP MECHANISM FOR A HYBRID NEUROPROSTHESIS FOR POSTURAL SUPPORT AND FREE STEPPING

The content in this chapter is partially based on the following published manuscripts:

C. S. To, R. Kobetic, J. R. Schnellenberger, M. L. Audu, and R. J. Triolo. "Design of a variable constraint hip mechanism for a hybrid neuroprosthesis to restore gait after spinal cord injury," *IEEE/ASME Trans. Mechatronics*, vol. 13, no. 2, pp. 197-205, 2008

R. Kobetic C. S. To, J. R. Schnellenberger, M. L. Audu, T. C. Bulea, R. Gaudio, G. Pinault, S. Tashman, and R. J. Triolo. "Development of a hybrid orthosis for stand, walking, and stair climbing after spinal cord injury," *Journal of Rehabilitation Research & Development*, vol. 46, no. 3, pp. 447-462, 2009.

M. L. Audu, C. S. To, R. Kobetic, and R. J. Triolo, "Gait evaluation of a novel hip constraint orthosis with implication for walking in paraplegia," *IEEE Trans. Neural Syst. Rehab. Eng*. Submitted Oct. 27, 2009; Accepted Feb. 2, 2010.

3.1 INTRODUCTION

THKAFO for gait restoration have universally coupled trunk stabilization with hip immobilization. For instance, the HGO [1] constrains all hip joint motion to the sagittal plane, thus providing full coronal trunk support. However, the range of hip flexion is limited with stops to maintain trunk support in the sagittal plane [2]. The RGO [3], similar to the HGO, fully constrains trunk and hip motion in the coronal plan, but incorporates a mechanism that reciprocally couples hip extension with contralateral flexion and vice versa. During stance, the RGO provides full sagittal trunk support and at the same time facilitates reciprocal stepping, initiated by contralateral hip extension. However, because sagittal hip motion is linked to trunk motion through a rigid corset, contralateral hip extension requires posterior sagittal trunk motion [4], which is unintuitive and may be disconcerting for the user. Furthermore, reciprocal coupling between the hips is fixed at a 1:1 HFECR, limiting step length. These compromises, however, have not precluded continued development to improve the functional performance of the RGO since its conception.

Initial advancements of the RGO focused on simplifying the hip reciprocation mechanism, which evolved from utilizing Bowden cables [3, 5] for torque transfer to a simple pivoting bar/tie rod design known as the Isocentric RGO (IRGO) [6]. A recent innovation includes a modified RGO, the R^2GO [7], that facilitates the pelvic rotation characteristic of normal gait by coupling hip flexion with external hip rotation and hip extension with internal hip rotation in addition to reciprocal coupling of the hips in the sagittal plane. The gait of an individual impaired by SCI with the R^2GO showed a reduction in the vertical moment of the body relative to that of an RGO, which may

increase the efficiency of gait. Other innovations involve the application of external power assistance to the RGO. These efforts include the use of DC motors [8, 4] and pneumatic artificial muscles [9] to help drive the reciprocal motion of the RGO. Such power-assisted RGOs have been reported to decrease gait effort by the users with SCI relative to RGO gait, and have been shown to reduce the lateral and vertical compensatory motions involved in RGO gait [4]. However, no significant improvements in gait speed were observed among any of these new enhancements to the standard RGO. This may be due to the fact that the constraints imposed on the sagittal kinematics by the 1:1 HFECR of the RGO were not addressed in any of the designs. The evaluation of a RGO with a 2:1 HFECR showed increases in stride length, with appreciable increases in gait speed when hip flexion was assisted by FNS [10].

Consequently, this work focuses on the development of a mechanism that would optimally modulate the reciprocal coupling of the hips. Hip reciprocation would only be active during instances of trunk instability; otherwise the hip, mobilized by FNS, would be free to allow for variable step lengths.

3.2 Concept of the Variable Constraint Hip Mechanism

The objective of the prototype hip mechanism is to maintain trunk postural stability throughout the entire gait cycle while allowing unimpeded functional sagittal hip movement. Accordingly, the hip mechanism must maintain a state of high impedance when trunk support is needed, but transition to a state of low impedance to allow for mobility. In order to design this variable constraint hip mechanism (VCHM), it is

important to identify the extent of postural support required by the user with respect to specific phases of the gait cycle. Dall *et al.* [11] measured the tension in the two cables of a Louisiana State University RGO responsible for the reciprocal coupling of the hips during gait in individuals with paraplegia. The study concluded that hip extension during stance does not nominally function to drive contralateral hip flexion during swing as commonly assumed. Instead, the reciprocator was primarily stressed during the double support phases of gait to prevent bilateral hip flexion. Dall *et al.* also surmised that the hip reciprocator acts to restrict hip flexion during the later half of the swing phase. The proposed operation of the VCHM is based on these principles.

3.2.1 Conceptual Operation

Figure 3.1 illustrates the intended operation of the VCHM in conjunction with the controllable locking knee mechanism detailed in **Chapter 2**. The assumption is that the FNS of target lower extremity muscles are capable of driving the lower extremity joint angles while trunk and hip stability are maintained by the VCHM. During the double support phases of gait, the hip will be reciprocally coupled to prevent bilateral hip flexion. During single support, the hip will be freed to extend. Any stance hip flexion (forward trunk tilt) will be prevented by the unidirectional locking of the hip joint against further hip flexion. However, failure of the single stance hip to extend will result in bilateral hip flexion (forward trunk tilt). **Figure 3.2** shows that if the relative angle between the trunk and the ipsilateral limb is maintained throughout stance, then the orientation of the trunk will gradually increase anteriorly beginning at heel strike and continuing through the step (from left to right). Thus, in the event that the single stance

hip is not extending due to insufficient hip extensor strength, the hips will be reciprocally coupled so that the flexing swing hip will assist in extending the stance hip.

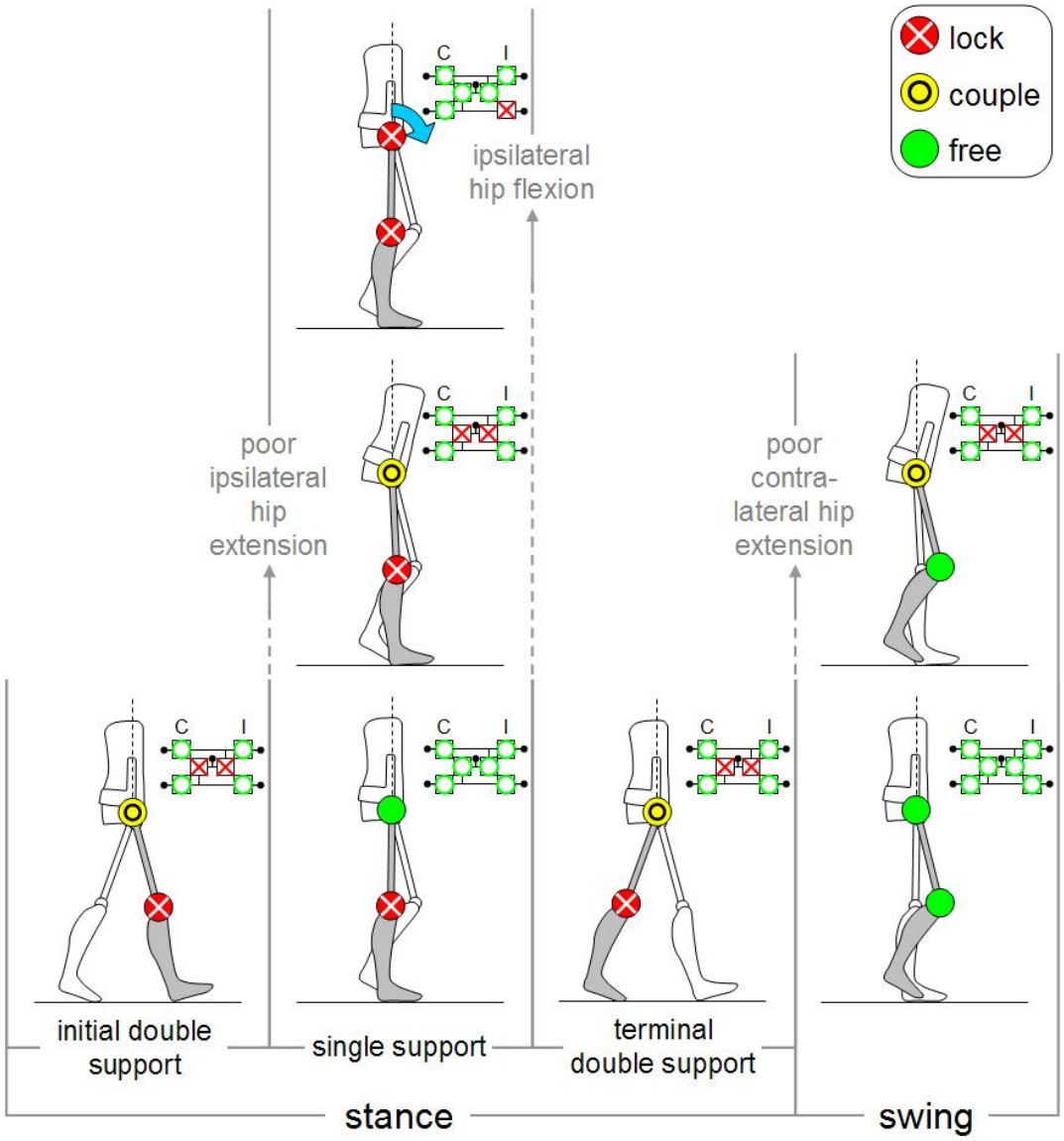

Figure 3.1. Conceptual operation of the VCHM. The small schematic on the top right corner of each figure is a simplified representation of the states of each hydraulic valve of the VCHM: O = opened; X = closed. Refer to **Figure 3.3** for a detailed schematic of the hydraulic system.

Note that locking the single stance hip against flexion was chosen to be the initial response for the lack of single stance hip extension over reciprocally coupling the hips because reciprocally coupling the hips would impede hip flexion and hence reduce step

length. Whether through locking or reciprocal coupling, hip flexion is impeded during single stance to minimize anterior trunk tilt. The hip will be freed throughout the swing phase allowing the VCHM to accommodate any stride length achievable by the user. However, if the contralateral stance hip is unable to extend efficiently, the hips will be reciprocally coupled during swing. Thus, this control scheme facilitates free hip flexion during swing for extended step length with the provision that the FNS of target hip extensor muscles can drive the contralateral limb into extension.

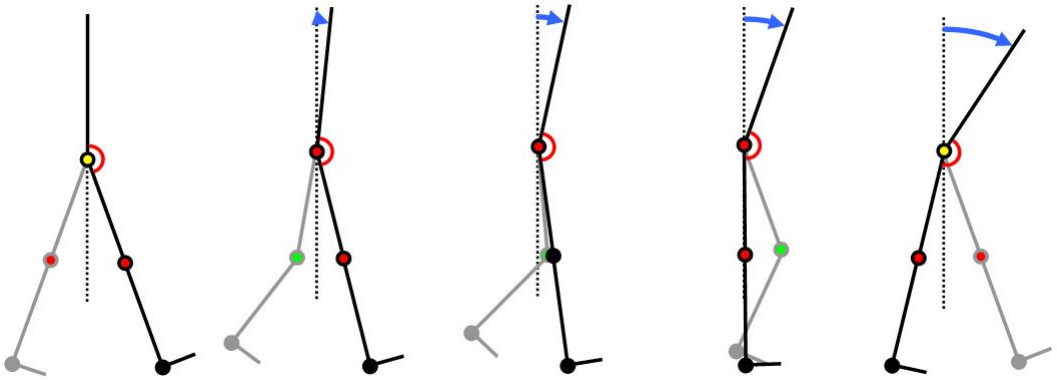

Figure 3.2. The lack of hip extension during single stance will result in forward trunk tilt at the end of the step.

3.2.2 Design Description

This VCHM was designed as a hydraulic system (**Figure 3.3a**). A fluid power system was selected for its control versatility and power economy. A hydraulic system was chosen over a pneumatic system, since 1) the relative incompressibility of a liquid provides high impedance when flow is restricted and 2) the portability of the system requires small components resulting in high system internal pressures. A double acting hydraulic cylinder was linked via a mechanical transmission to each hip joint of the orthosis. The corresponding ports of the opposing cylinders were connected to produce a

closed hydraulic circuit. A 2-way, 2-position normally open (open to flow when de-energized) solenoid valve was positioned at each port of the cylinders.

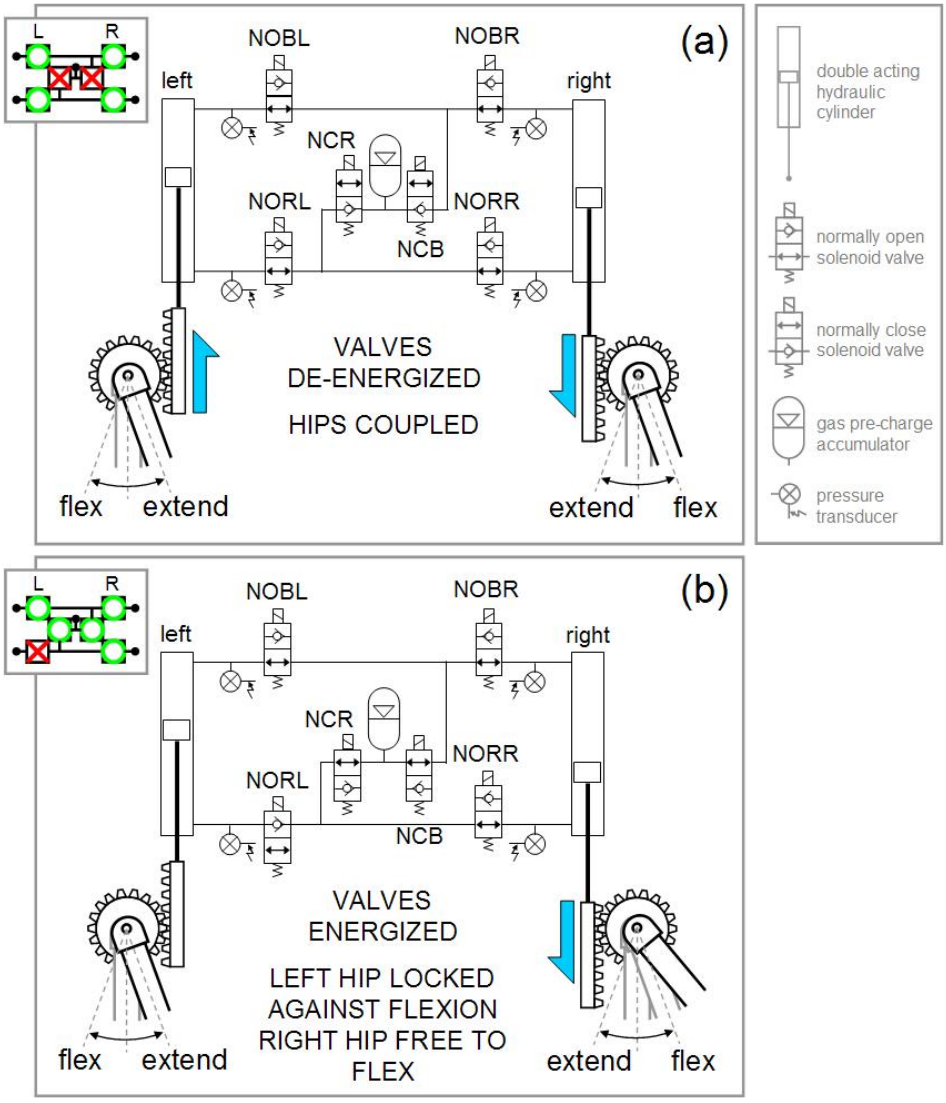

Figure 3.3. Hydraulic schematic of the VCHM. (a) Default (unpowered) state of the VCHM has the hips reciprocally coupled. (b) Opening or closing specific solenoid valves can independently lock (left) or free (right) a hip joint. The small schematic on the top left corner of each figure is a simplified representation of the states of each solenoid valve: O = opened; X = closed.

Two 2-way, 2-position normally closed (closed to flow when de-energized) solenoid valves serve to modulate the flow of fluid between the blind and rod ends of the hydraulic circuit and into an accumulator.

The hydraulic circuit was designed so that the pistons are reciprocally coupled to each other when all the valves are de-energized (**Figure 3.3a**). When one piston of a cylinder is forced to extend, the rod end of the piston of the contralateral cylinder is pressurized and thus forced to retract. As a result, without power, the VCHM defaults to a standard RGO. By energizing specific solenoid valves, the pistons of the hydraulic cylinders can be individually locked and/or freed to move in one or both directions (**Figure 3.3b**). For example, to bidirectionally lock a piston both normally open (NO) valves at the two ports of the corresponding cylinder must be energized (closed), thus preventing flow from both ends of the cylinder. Bidirectional free piston motion can be achieved by energizing (opening) both normally closed (NC) valves (right cylinder of **Figure 3.3b**). Fluid is now allowed to flow freely from one end of the cylinder to the other and into the accumulator.

The accumulator is required when flow is transferred between ends of the cylinder. Since the piston rod partially occupies the volume in the rod end of a double acting cylinder and the fluid is essentially incompressible, the output flow volume per unit piston displacement of the blind end is larger than the input flow volume per unit piston displacement of the rod end. The volume differential between cylinder ends is accounted for by the accumulator. When flow moves from the cylinder blind side to the rod side, a volume equal to that of the rod *enters* the accumulator, causing the accumulator pressure to increase. Conversely, when flow moves from the cylinder rod side to the blind side, a volume equal to that of the rod *exits* the accumulator and enters the cylinder blind side, causing the accumulator pressure to decrease. In this case, the pressurized accumulator prevents the system pressure from decreasing to vacuum.

Unidirectional piston locking/freeing requires the activation of the NO valve at the rod end to lock against piston extension (left cylinder of **Figure 3.3b**) or blind end to lock against piston retraction and the contralateral NC valve. The rod end NO and blind end NC valves would be energized to prevent piston extension (hip flexion) and allow piston retraction (hip extension) and the blind end NO and rod end NC valves would be energized to prevent piston retraction (hip extension) and allow piston extension (hip flexion). However, when the piston is moved in the direction of the free cylinder end, vacuum formation in the locked cylinder end will resist the free motion. Thus, unidirectional piston control necessitates a feedback signal, such as force applied to the piston or cylinder end pressure, to de-energize the closed NO valve.

3.3 MECHANISM COMPONENT SELECTION, OPTIMIZATION, AND FABRICATION

The following factors were considered when selecting the hydraulic components and designing/fabricating auxiliary components (i.e., exoskeleton uprights/structure, mounting brackets for hydraulics and sensors) for the VCHM. 1) In order to minimize the cost of the system, an effort was made to use commercially available off-the-shelf components. Modifications were made to the off-the-shelf components when necessary. 2) The device must be adjustable and modular to accommodate different user sizes and simplify maintenance. 3) The portability of the system requires that all components are as compact and light weight as possible. Essentially, the goal was to minimize the system size so that the system could fit in the user's wheelchair for convenient donning/doffing. 4) The power requirements must be minimal, allowing the system to be

used for a reasonable duration before the power supply is needed to be recharged/replaced. Hydraulic oil, ISO VG 46, with a moderate kinematic viscosity was selected for the hydraulic system to minimize leakage and turbulent flow. In general, the maximum operating pressure and flow rate of the hydraulic system were minimized to accommodate the system requirements and facilitate a broad mechanical impedance range.

3.3.1 Hydraulic Rotary Actuator

Before pressure and flow rate were specified, the transmission linking the piston rod of the cylinder to the hip joint of the THKAFO was first characterized. A simple rack-and-pinion (**Figure 3.3**) was chosen to convert rotary motion (sagittal hip motion) into linear translation (cylinder extension/retraction). The cylinder coupled to the revolute hip joint via a mechanical transmission is a type of hydraulic rotary actuator (HRA). A custom HRA for the hip mechanism was developed since 1) most commercially available HRAs do not provide an adequate transmission ratio for gait and sit-to-stand motions and 2) off-the-shelf HRAs that conform to the torque requirements during gait generally have a geometry unacceptable on a wearable system. Since the system should easily be donned while the user is seated in a wheelchair, the HRA must be small enough so that when mounted to the orthosis, the entire system can fit in the wheelchair.

The component specifications of the HRA were subjected to constrained nonlinear optimization. The flow coefficient (C_V) of the valves was selected as the objective function to be minimized. The C_V ($\mathrm{gpm}/\sqrt{\mathrm{psi}}$) is a measure of valve flow

capacity that describes the relationship between the pressure drop (psi) and the flow rate (gpm) through the valve. Thus, the magnitude of the valve C_V is proportional to the physical size and power requirements of the valve. The C_V is calculated from empirically determined flow rate and pressure drop measurements across the valve by **Equation 3.1**.

$$C_V = Q\sqrt{\frac{S_g}{\Delta p}}, \frac{\text{gpm}}{\sqrt{\text{psi}}}. \tag{3.1}$$

Where Q (gpm) is the flow rate through the valve, Δp (psi) is the pressure drop through valve at the corresponding Q, and S_g is the specific gravity of the fluid (≈ 0.88 @ 20°C for ISO VG 46). The HRA was characterized by five parameters: 1) number of pinion gear teeth, 2) gear module, 3) gear face width, 4) cylinder bore size, and 5) cylinder stroke length. Gear face width and cylinder stroke length were constrained to keep the HRA size relatively small. The C_V was expressed as a function of the number of pinion gear teeth (z), gear module (m, mm), and cylinder bore size (D, in) as shown in **Equation 3.2**. These unknowns were bounded by commercially available specifications of each measure. A mixture of metric and imperial units was used in **Equation 3.2** to readily accommodate industry standards.

$$C_V(z,m,D) = 0.00128\pi\omega_{\max} zmD^2\sqrt{\frac{S_g}{\Delta p}}, \frac{\text{gpm}}{\sqrt{\text{psi}}}. \tag{3.2}$$

A maximum hip angular velocity ($\omega_{\max}$) of approximately 90°/s was estimated from a computer model of the HNP [12]. A maximum allowable pressure drop of 0.34 bar (5 psi) through a valve was assigned at the flow rate generated by $\omega_{\max}$. The following factors were established as the nonlinear inequality constraints for optimizing the HRA components. 1) The maximum operating pressure of the cylinder must be within

commercially available specifications. 2) The HRA must accommodate the range of hip motion involved in both gait and sit-to-stand. 3) The number of pinion gear teeth must be greater than a standardized minimum [13] to avoid undercutting. 4) The gear-to-rack contact ratio must be greater than a standardized minimum to facilitate smooth continuous tooth dynamics. 5) The maximum gear tooth bending stress during operation must be less than an established maximum to guard against gear tooth breakage. 6) The maximum gear tooth-surface durability during operation must be less than an established maximum to prevent surface pitting and wear of the gear tooth. In determining the operational maximum gear tooth bending stress and surface durability, a maximum torque of 35 Nm [11] with a safety factor of two was assumed to be applied to the hip mechanism during gait.

Conservative estimates of the geometry factor and derating factors (i.e., application, load distribution, size, and dynamic load factor) for gear tooth bending stress and surface durability were used [13]. Since the transmission will be backdriven in both flexion and extension directions during operation, the allowable tooth bending stress was reduced by 30 %, as commonly done in practice, to account for reverse tooth bending. To minimize cost for the initial prototype, a 1144 steel, 14.5^{o} pressure angle spur gear-set (McMaster-Carr, Elmhurst, IL, USA) with a pinion of 0.75" face width, 2.5" pitch diameter, and 12 pitch (≈ 2 module) was used. A 14.5^{o} pressure angle gear set was selected to maximize contact ratio for minimal backlash. A 7/8" bore, 3" stroke hydraulic cylinder (Clippard Minimatic, Cincinnati, OH, USA) with a maximum operating pressure of 138 bar (2000 psi) was selected. **Table 3.1** shows a summary of the specifications of the custom HRA (**Figure 3.3**) for the VCHM (Note, the unit load and K

factor are indices of gear tooth loading that measure the load intensity being carried per unit size in the gear mesh for tooth bending strength and tooth surface durability respectively).

Table 3.1
Hydraulic Rotary Actuator

type	spur rack-&-pinion
torque per unit pressure	1.13 Nm/bar
displacement	0.215 $cm^3/^o$
unit load	57.87 N/mm^2
K	1.82 N/mm^2
linear/rotary transmission ratio	0.55 $mm/^o$
contact ratio	1.76
range of motion	137^o

In the first prototype HRA design (**Figure 3.4a**) the cylinders were positioned vertically on each side of the thoracic corset with the rack translating up and down relative to the hip joint as the hip rotated into extension and flexion, respectively. This configuration of the HRA resulted in two problems. 1) In a seated position (for system donning/doffing), when the actuators are flexed, the fully extended cylinders position the ends of the racks far below the hip joint, which impinge on the chair. 2) Preliminary experiments of individuals with paraplegia walking with the VCHM revealed that the placement of the cylinders impede the user's backward arm motion during the single stance/swing phases of gait. These two difficulties have lead to a redesign of the HRA as shown in **Figure 3.4b** (Refer to **Appendix C** for CAD drawings). In the new design, the cylinder is fixed to the thigh upright of the KAFO via a clevis. The pinion is fixed rigidly to the thoracic corset via a custom slotted mounting plate and bracket. The rack is connected to the rod via a clevis and meshed to the pinion posteriorly relative to the hip joint. Sagittal hip movement causes the rack to rotate around the pinion, with hip flexion resulting in cylinder extension and hip extension resulting in cylinder retraction. The

clevis connections made between the cylinder and thigh upright and between the cylinder rod and the rack allow the rotary actuator to be manually unlocked (via the translation of a spring return collar) to move into abduction.

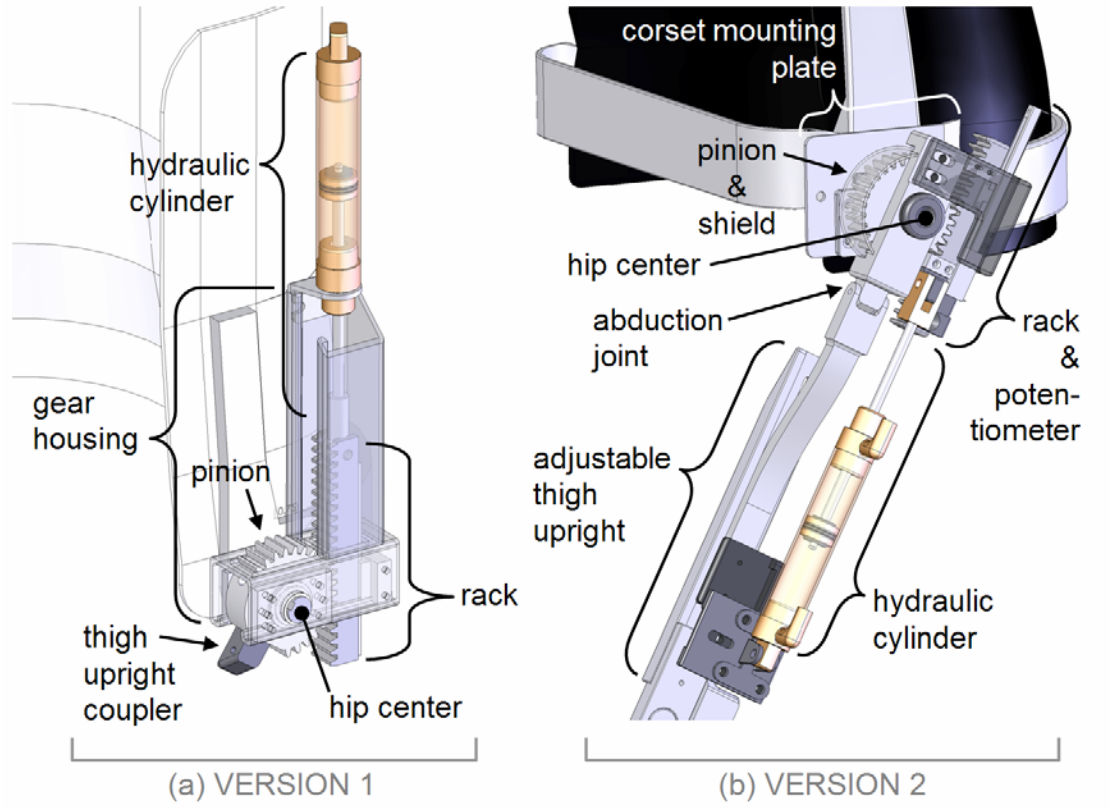

Figure 3.4. (a) Version 1 and (b) version 2 of the hydraulic rotary actuator for the VCHM.

A polycarbonate shield around the pinion protects the user from the gear teeth. This redesign also simplifies system maintenance by allowing for easy system disassembly/reassembly. Mounting points were relocated for easy accessibility. Quick release pins were used for fixing the cylinder clevises to the rack-and-pinion transmission. The entire transmission can be quickly unslotted from the thoracic corset. The structural components of the HRA were fabricated from a combination of 2024, 6061, 6063 aluminum alloy, and 1045, 4140, 4142, and galvanized low-carbon steel

alloys (Refer to **Appendix C** for the material of each component). The final HRA weighs 3.2 kg (≈ 7 lbs) with the rack-and-pinion transmission components of the HRA weighing approximately 1.8 kg (≈ 4 lbs).

3.3.2 Solenoid Valves

Four parameters were considered when specifying the solenoid valves: 1) C_V, 2) cracking pressure, 3) power consumption, and 4) response time.

The required C_V of the solenoid valves was 0.13 from the optimization of the HRA. Off-the-shelf poppet type NO and NC solenoid valves (Allenair Corp., Mineola, NY, USA) were selected with a C_V of 0.195. **Figure 3.5** diagrams the interior geometry and flow direction of the NO and NC valves. Note that the valves will only maintain a closed state when pressure is applied to port B. Pressure above a threshold (cracking pressure) applied to port C (for the NO valves) or port A (for the NC valves) will force open the respective valve. Thus, the valves must be oriented as specified in **Figure 3.3**.

Hydraulic flow tests (**Figure 3.6a**) were conducted to validate the C_V of the stock valves. These flow experiments consisted of connecting an opened valve to a fixed displacement pump and measuring the duration of time to fill a specified volume, from which flow was calculated. Flow from the pump was modulated with a flow control valve positioned at the output of the pump. The pressure on each side of the valve was measured with a digital pressure transducer. Both flow directions for each valve type were tested. **Figure 3.7a** shows the relationship of the valve pressure differential and flow for both valve flow directions. The C_V of the stock NO valves was determined to be approximately 0.1.

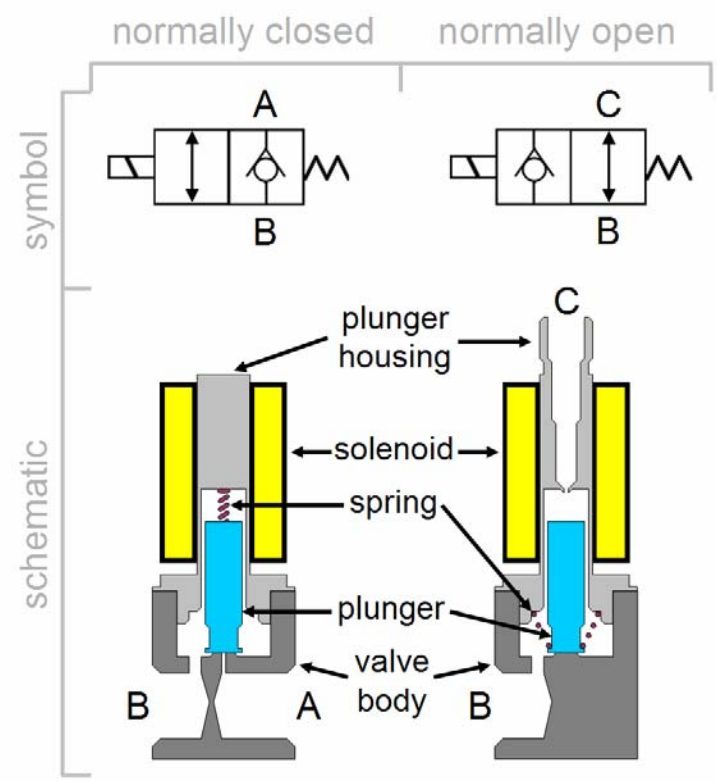

Figure 3.5. Hydraulic symbol and interior schematic of the 2-way, 2-position normally open (NO) and normally closed (NC) solenoid valve (Allenair Corp., Mineola, NY, USA).

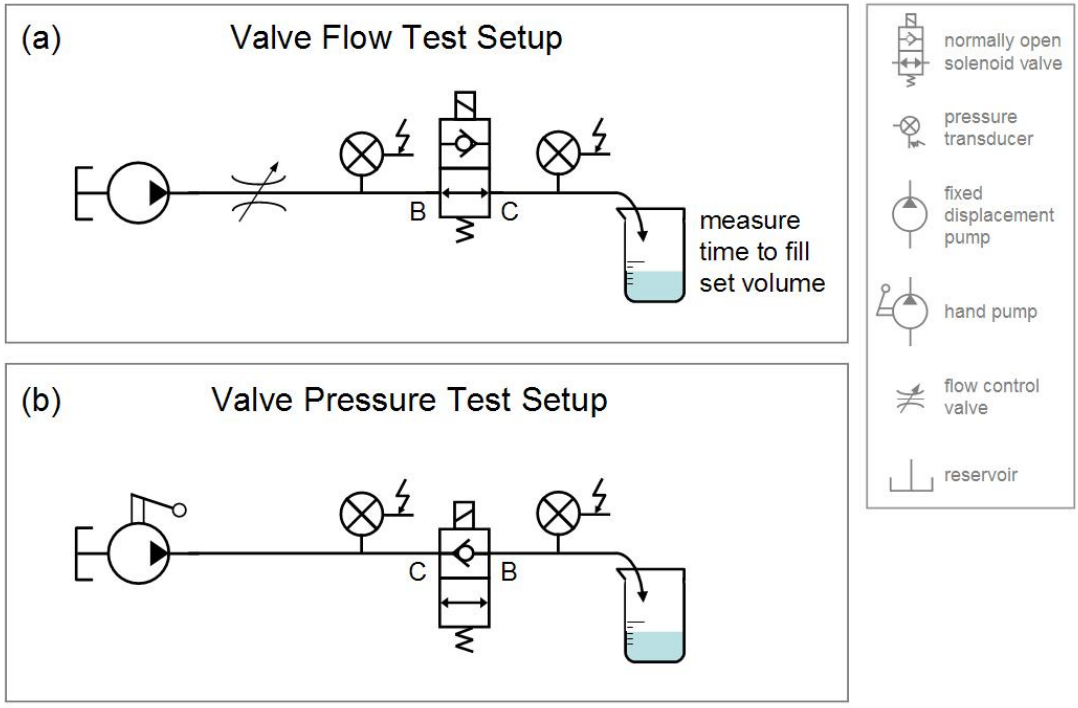

Figure 3.6. Experimental setups for (a) flow and (b) pressure testing the stock NO solenoid valve.

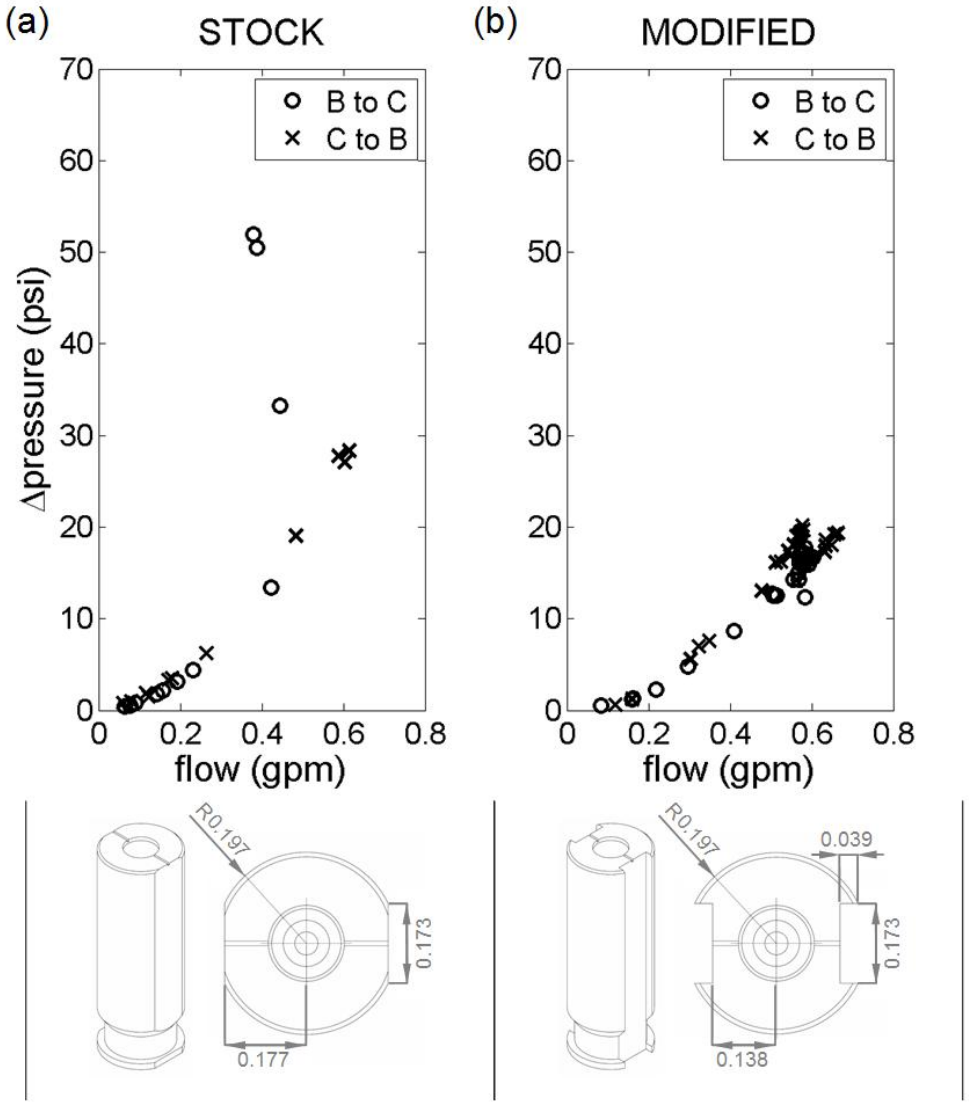

Figure 3.7. Change in pressure (psi) versus flow (gpm) characteristics and plunger geometry of the (a) stock and (b) modified NO solenoid valves.

When flow is passed from port B to C of the NO valve, the pressure differential increased dramatically when flow increased above 0.4 gpm. This can be explained as follows. When flow is introduced from port B to C, pressure is built up under the plunger due to the relatively small flow area between the plunger and housing. As the flow rate increases, this built up pressure is eventual large enough to compress the spring holding the plunger in place and elevate the plunger, which acts to reduce flow area. The reduced

flow area results in an increase in differential pressure to maintain a constant flow rate. Modifications were made to the geometry of the NO valve plunger with the intent of increasing the C_V. Valve pressure differential versus flow for both valve flow directions and the modifications to the stock NO valve plunger are diagrammed in **Figure 3.7b**. The NO valve plunger modifications increased the flow area between the plunger and housing by 117 %. The C_V of the modified NO valve and stock NC valves were tested to be approximately 0.14 and 0.17 respectively. Both of these C_V values are compatible with the HRA optimization (> 0.13). With a valve orifice of 2.38 mm and at an estimated maximum fluid velocity of 5.78 m/s, the Reynolds number was calculated to be 299 (less than 2000, indicating laminar flow).

As introduced earlier, the cracking pressure is the minimum differential pressure imposed on the valve that induces internal leakage when the valve is in a closed state. The chosen solenoid valves can be forcibly opened unidirectionally by a differential pressure. Since the valve plunger is held in its unpowered position by a spring, a high pressure at port C relative to port B can induce leakage in the NO valve, while a high pressure at port A relative to port B can induce leakage in the NC valve. The NO valves with the modified plungers were pressure tested to determine if the modifications to the plunger influenced the holding strength of the magnetic field induced by the solenoid, which would alter the cracking pressure of the valve (**Figure 3.6b**). In addition, the effect of inconsistencies in the machining of the plungers on the cracking pressure was tested. In these tests the valve was initially closed. Pressure was applied to port C of the NO valve using a manual hand pump. The pressure was gradually increased until internal leakage of the valve occurred, indicated by a pressure drop. The cracking

pressures of three modified plungers and one stock plunger were evaluated (**Figure 3.8**) using a single stock solenoid. To assure that the magnetic field was consistent over the stock solenoids, three separate solenoids were also tested over a single modified plunger. This test showed a small (4 % change in cracking pressure) yet significant difference ($p = 0.0003$) over individual stock solenoids. Modifications to the plunger of the NO valve to increase the C_V did not alter the original cracking pressure ($p = 0.1199$). The average cracking pressure of the modified NO was determined to be 2.2 bar (32 psi). The cracking pressure of an NC solenoid valve was also tested and determined to be 3.2 bar (46 psi). In testing the NC valve, pressure was applied to port A.

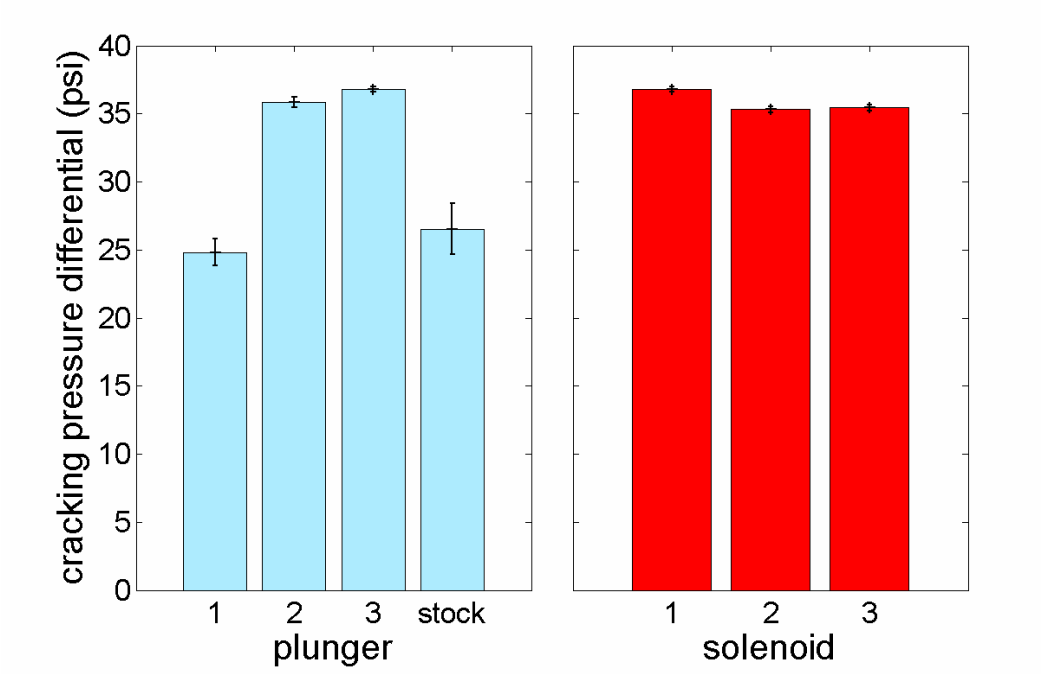

Figure 3.8. Influence of the NO valve modifications and solenoid on the cracking pressure.

The power requirement for the solenoid of each valve was 7 W at 12 VDC. Maximum valve activation in the gait cycle occurs during single support (**Figure 3.1**). During single support, one NO valve may be energized to prevent hip flexion and two

NC valves will be energized to allow free hip flexion during contralateral swing. Thus, a maximum of three valves will be energized at one time requiring a total instantaneous power of 21 W for valve operation during gait. This corresponds to a total instantaneous current of roughly 1.75 A. In-house custom circuitry (**Figure 2.7**), developed to drive the solenoid valves, was powered by a 12 VDC supply from a Sony NP-F970 lithium ion rechargeable battery pack (Sony Corp., Tokyo, Japan). The voltage of the battery was rated at 7.2-8.4 V with a storage capacity of 6600 mAh. A boost converter circuit was used to increase battery voltage to 12 V. Note that the power supply for the VCHM valves is separate from the power supply for the dual-state knee mechanism described in **Chapter 2**.

The response times for the complete transition of the valve state from opened to closed and vice versa must be small relative to the time course of a stride length (≈ 2 s [14]) for individuals with paraplegia walking with a HNP. Specifically, it is critical for the valve response times to be small so that unstable trunk activity (i.e., sagittal hip motion) is minimal between the onset time of the valve state transition initiated by signal feedback and the completed valve state transition time in which the VCHM can then effectively stabilize the trunk. The no load pulse on and off times were tested to be approximately 12 ms and 32 ms respectively for the NO valve and 12 ms and 43 ms respectively for the NC valve. At an estimated maximum hip angular velocity of 90^{o}/s, the maximum hip rotation during the valve transition period will be less than 4^{o}. **Table 3.2** summarizes the specifications of the solenoid valves.

Table 3.2
Solenoid Valves

manufacturer	Allenair (modified NO valve)
type	2-way, 2-position
voltage	12 VDC
power consumption	7 W
orifice	2.38 mm
$C_V\ (\text{gpm}/\sqrt{\text{psi}})$	$NO_{B\rightarrow C}$: 0.144, $NO_{C\rightarrow B}$: 0.136 $NC_{B\rightarrow A}$: 0.176, $NC_{A\rightarrow B}$: 0.166
response time	NO: 12 ms (on), 32 ms (off) NC: 12 ms (on), 43 ms (off)
cracking pressure	$NO_{C\rightarrow B}$: 2.2 ± 0.4 bar $NC_{A\rightarrow B}$: 3.2 ± 0.5 bar

3.3.3 Accumulator

Since the primary purpose of the accumulator is to take up the difference in volume between the blind and rod ends of the cylinder, the capacity of the accumulator is small. A 0.075 L capacity welded diaphragm accumulator (Hydac, Bethlehem, PA, USA) with a gas precharge pressure of 4 bar (58 psi) and maximum operating pressure of 250 bar (3600 psi) was selected. Diaphragm accumulators offer the smallest volumes that are commercially available, are compact, relatively lightweight, and cost effective. The precharge pressure of the accumulator was determined based on the intended resting pressure of the hydraulic system. The system was pressurized to approximately 5 bar (70 psi) to minimize the compliance (when the VCHM is constraining hip flexion) induced from any remaining internal air bubbles and prevent the instantaneous pressure in any part of the system from dropping below the vapor pressure (< 1 mmHg @ 20^{o}C for ISO VG 46) of the hydraulic fluid which would result in further cavitation. **Table 3.3** summarizes the specifications of the accumulator.

Table 3.3
Accumulator

manufacturer	Hydac
type	diaphragm
size	0.075 L
gas precharge	4 bar
max operating pressure	250 bar

3.3.4 Assembly

The hydraulic system was connected by accessory hose and fittings (Parker Hannifin Corp., Cleveland, OH, USA). The pressure losses through the hose and fittings were tested to be less than 0.06 bar (0.9 psi) at a flow rate of approximately 4.28 lpm (1.13 gpm). During gait, the estimated maximum flow rate in the system was 1.17 lpm (0.31 gpm). The solenoid valves were oriented so that port B of each valve would resist the pressure generated from the ipsilateral cylinder (**Figure 3.2** and **Figure 3.4**). In this way, leakage through the valve due to the valve differential pressure exceeding the cracking pressure was eliminated. A hydraulic line with a manual needle valve was set in parallel with each NC solenoid valve, allowing the VCHM to be uncoupled without power. Hydraulic quick-release nipples were installed at each cylinder port and several key locations throughout the hydraulic system to facilitate pressure measurements or serve as system fluid priming points (Refer to **Chapter 4** for details on system priming).

Figure 3.9 shows a prototype of the VCHM. The VCHM alone weighs approximately 9 kg (≈ 20 lbs). It is a modular mechanism that can be installed on thoracic corsets of different sizes. Custom knee-ankle-foot orthoses (KAFOs) were designed and fabricated to be adjustable to accommodate different users. Abduction of the hips, to simplify donning/doffing, is achieved by releasing a manual spring return collar.

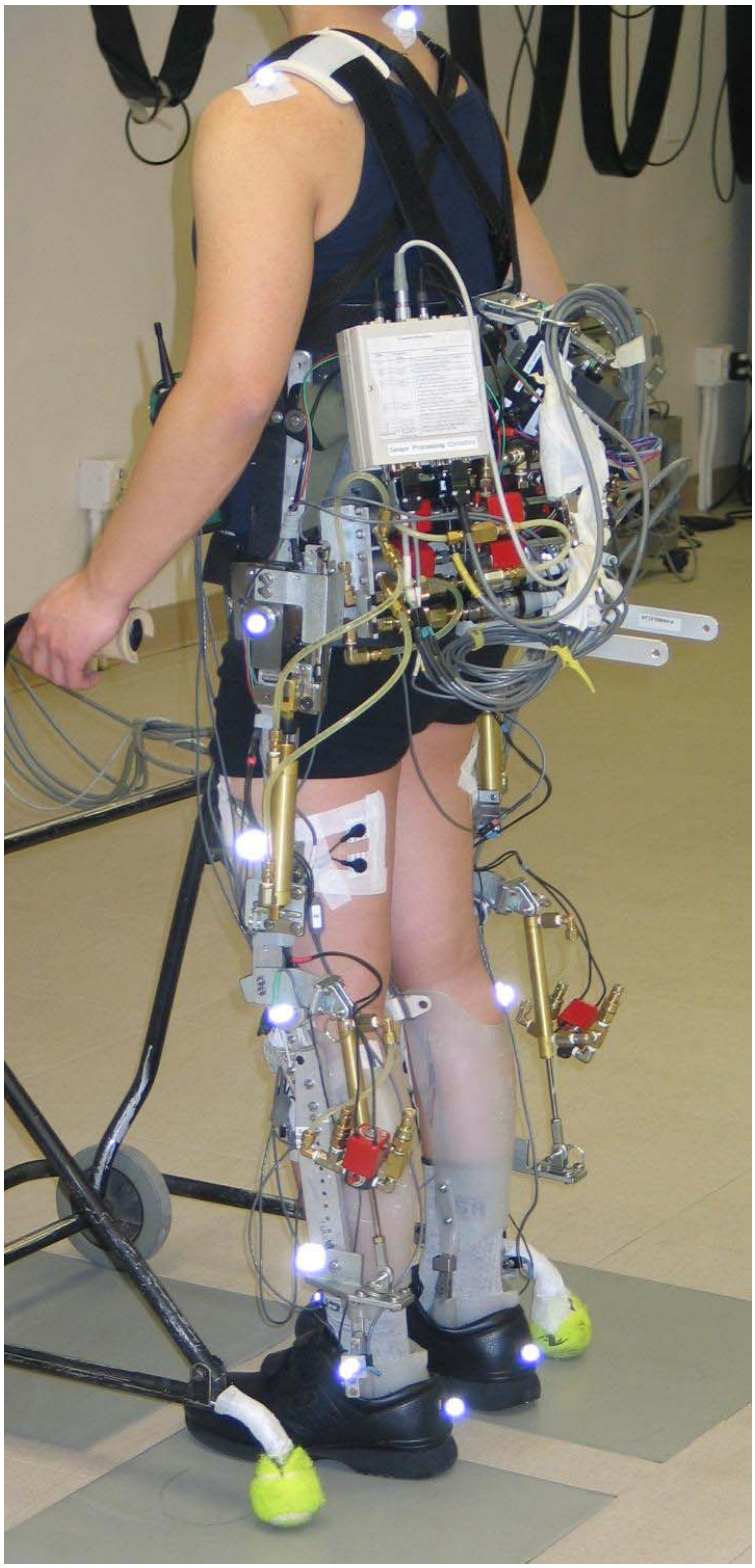

Figure 3.9. Prototype of the VCHM adjustable to fit different individuals. The hydraulic dual-state knee mechanisms (**Chapter 2**) are also shown.

3.4 SYSTEM CHARACTERIZATION

Bench testing has been conducted to evaluate the 1) locking torque, 2) locking compliance, 3) passive resistance, and 4) mechanical efficiency of the VCHM. In all the experiments, the Biodex Pro System 3 robotic dynamometer (Biodex Medical Systems, Shirley, NY, USA) was used to actuate the right HRA of the VCHM (**Figure 3.10**).

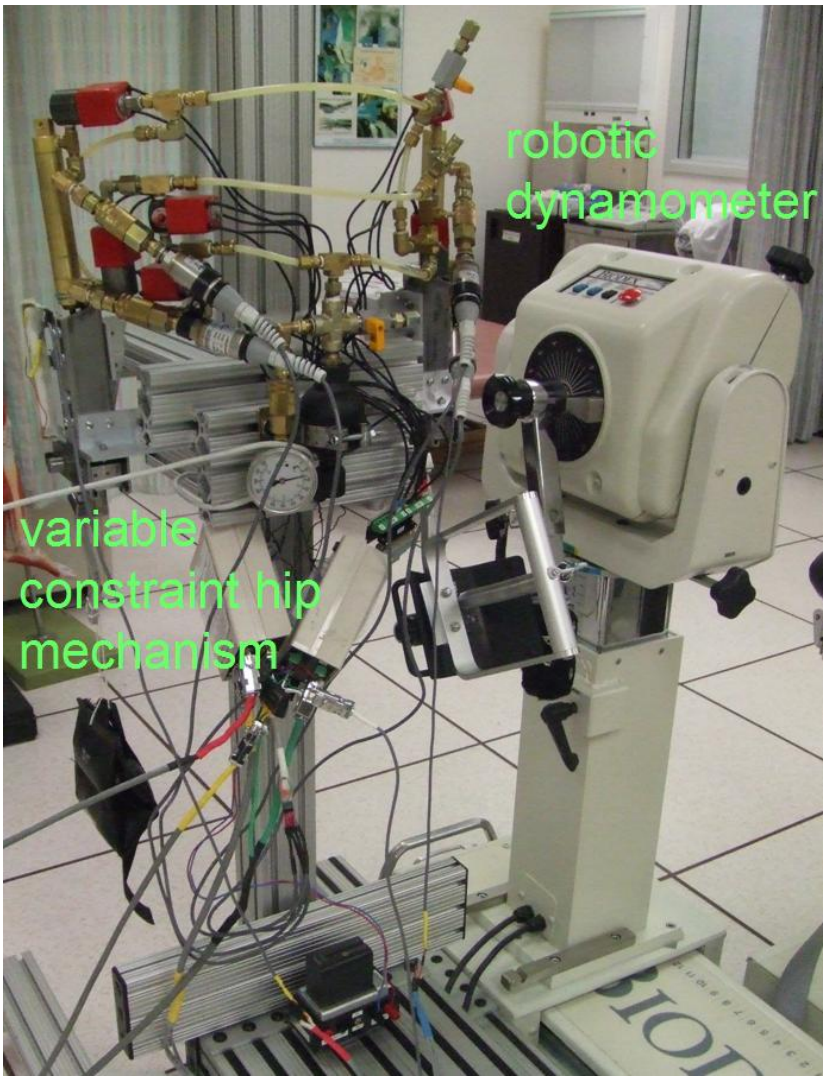

Figure 3.10. Bench testing setup of the VCHM. The right HRA of the VCHM is driven by a robotic dynamometer (Biodex Medical Systems, Shirley, NY, USA).

The solenoid valves of the VCHM were controlled with software developed in the Simulink®/xPC Target (The MathWorks, Inc., Natick, MA, USA) real-time

environment. The rack of the HRA transmission was instrumented with a slide potentiometer (Alps Electric Co., Tokyo, Japan) to measure cylinder movement (**Figure 3.3b**). HRA angle was calculated from the linear cylinder movement. Digital pressure transducers (Gems Sensors Inc., Plainville, CT, USA) were attached to each port of each cylinder via hydraulic quick-release couplers to measure cylinder pressure.

Angle and pressure data were collected at 200 Hz using custom data acquisition software developed in Matlab®. The analog signals corresponding to the applied torque and angular velocity of the dynamometer were sampled at 240 Hz with a Vicon 370 Motion Analysis System (Vicon, Oxford, UK). Only the data coincident with the preset angular velocities were used in the analyses of the passive resistance and mechanical efficiency studies. In other words, transients corresponding to the system accelerating to or decelerating from constant velocity at transitions in movement direction were not included in the analysis. The angle and dynamometer data were filtered online with a 5^{th}-order low-pass digital Butterworth filter with a cutoff frequency of 10 Hz. The dynamometer torque data were filtered again offline with a 3^{rd}-order low-pass digital Butterworth filter with a cutoff frequency of 3 Hz. The pressure data were filtered online with a 7^{th}-order low-pass digital Butterworth filter with a cutoff frequency of 20 Hz.

3.4.1 Locking Torque & Compliance

In a study by Dall *et al*. [11], where the hip torque applied to a RGO was determined during gait with individuals with paraplegia, a maximum torque of 35 Nm was obtained (subject body weight ranged between 54 kg and 84 kg). Thus, if the VCHM is able to resist at least 35 Nm of applied hip torque, it was considered able to

support a user with paraplegia during gait. To verify the system locking torque and compliance, the dynamometer was set to apply a flexion torque on the HRA while the HRA was locked against flexion. The maximum applied torque was manually increased from 10 Nm to 60 Nm.

The VCHM was able to withstand a maximum applied flexion torque of 60 Nm, verifying that it should be capable of supporting against bilateral hip flexion. **Figure 3.11** shows the locking compliance of the VCHM relative to applied torque.

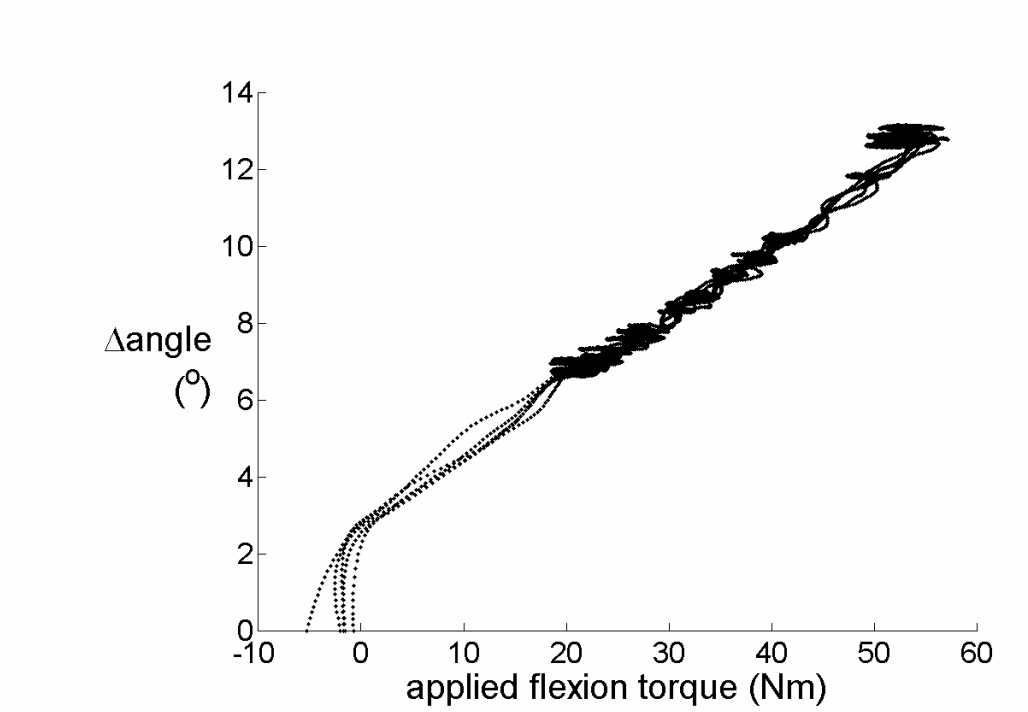

Figure 3.11. Locking compliance (change in angle into flexion when the VCHM is locked against flexion) versus applied flexion torque.

The locking compliance is the variation in hip angle into flexion while the HRA is locked against flexion by the closure of the NO rod side valve. The initial, approximately 3°, increase in compliance at low torque magnitude indicates minor amounts of play in the mechanical transmission components. Afterwards, compliance increases proportionally

with the magnitude of the applied torque due to the compression of any air bubbles remaining in the closed hydraulic circuit. Roughly 8^o to 9^o of compliance was observed at the target maximum locking torque of 35 Nm. In general, any locking compliance is undesirable as it would compromise the ability of the VCHM to support against trunk tilt responsively. However, the locking compliance observed in the VCHM is comparable to anterior trunk tilt observed in the IRGO [14].

3.4.2 Passive Resistance

The passive resistance of the VCHM is the torque necessary to drive the system at a particular angular velocity when the HRAs of the VCHM are in a freed or coupled state. To ascertain the passive resistance of the mechanism, the right HRA was actuated at a constant angular velocity while the left HRA was unloaded. A range of angular velocities characteristic in gait from 5^o/s to 120^o/s was applied to the right HRA. Separate tests were performed when the HRAs of the VCHM were in the uncoupled and coupled states. The inertial component of the measured torque, necessary to accelerate the mass of the dynamometer attachment and mechanism was subtracted from the total measured torque to obtain the passive resistance torque.

Figure 3.12 shows the range of torques applied to the right HRA with respect to angular velocity of the dynamometer. The plot is divided by direction of sagittal hip motion (flexion/extension) and state of the HRAs (coupled/uncoupled). A three-way analysis of variance (ANOVA) with 95 % confidence ($p < 0.05$) showed that the magnitude of torque applied to the HRA is significantly influenced by angular velocity, direction of rotation, and HRA coupling state ($p = 0.0000$ for all three factors). For each

plot, the median torque values increased with angular velocity. Also, the torques were higher when the HRAs are coupled. When the HRAs were decoupled the median resistive torque was typically below 2 Nm at low speeds and did not exceed 4 Nm even at high angular velocities in the flexion direction.

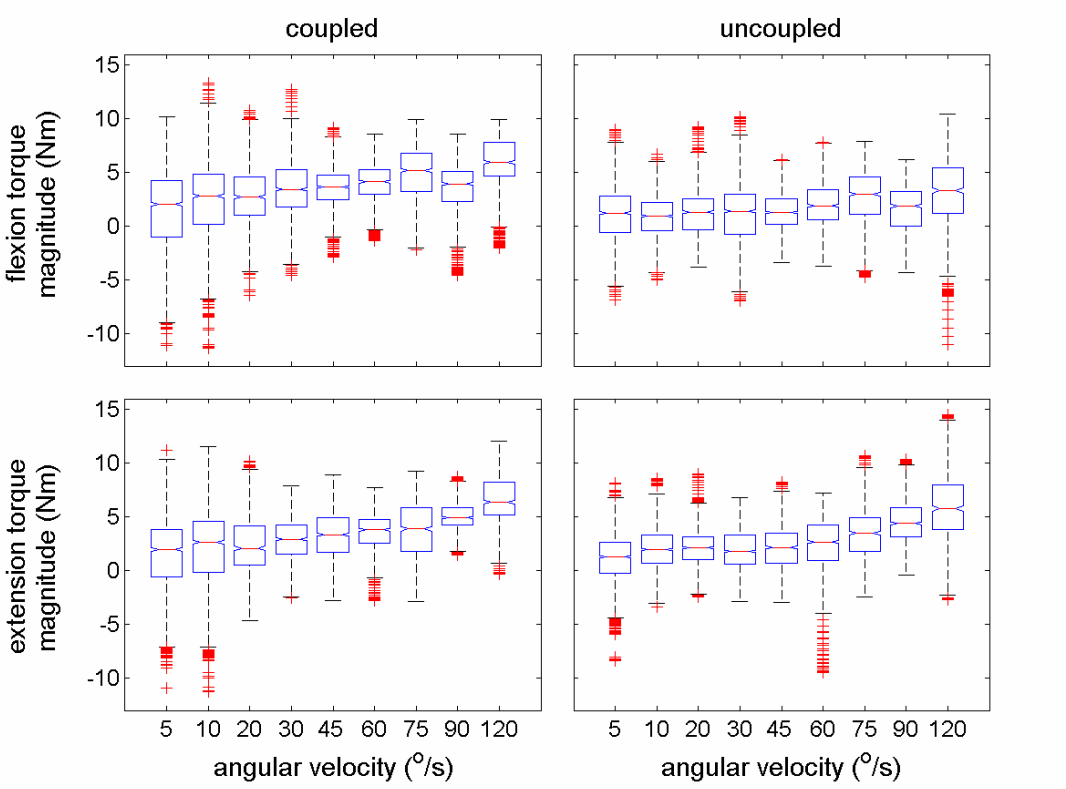

Figure 3.12. VCHM passive resistance. The torque magnitude applied to the right HRA was measured for the HRAs coupled and uncoupled for nine discrete angular velocities.

As anticipated, the resistive torques in the extension direction were generally higher than those in flexion. This is due to the volume differential between cylinder ends. In the design of the HRA, hip flexion was coupled to hydraulic cylinder extension and hip extension was coupled to hydraulic cylinder retraction. This decision was made to minimize the passive resistance in the flexion direction since it is difficult to acquire strong hip flexors for FNS [15]. Hip extension requires fluid to be transferred from the

blind side to the rod side. Since the fluid media is relatively incompressible, this volume reduction is compensated for by the accumulator. Extension torque is necessary to pressurize and expand the diaphragm of the accumulator. When the HRAs were coupled, the median resistive torques of the VCHM were below 4 Nm at low hip angular velocities and did not exceed 6 Nm at the higher angular velocities during gait (60-90^{o}/s).

Kobetic and Marsolais [16] measured the average isometric hip flexion and extension moments produced by FNS in 23 subjects with paraplegia to be 60 Nm (0^{o}) and 63 Nm (45^{o} flexion) respectively. A combination of percutaneous intramuscular, subfascial, and surface electrodes were used to activate primary hip flexor (iliopsoas, sartorius, gracilis, and tensor faciae latae) and extensor (posterior abductor magnus and hamstrings) muscles. High hip angular velocities occur during single support and swing. At these phases of gait, the HRAs of the VCHM are decoupled. For high angular velocities, only about 7 % of the achievable hip flexion torque generated by FNS is required to overcome mechanism passive resistance. Likewise, mechanism passive resistance in the extension direction at high angular velocities can be overcome by 10 % of the achievable hip extension torque generated by FNS. The resistive torques of the coupled HRAs being higher than that of the uncoupled HRAs is expected because of the accumulated stiction and viscous effects of two cylinders in the coupled system. The coupling of the HRAs of the VCHM is most prevalent during double stance. During double stance the hip angular velocities are generally low and thus the system resistive torques will be low (< 4 Nm) and should not significantly impede user motion.

3.4.3 Mechanical Efficiency

With the HRAs coupled, a mass was placed on the lever arm (thigh upright) of the left HRA while the right HRA was rotated by the dynamometer at an angular velocity of 5 ^{o}/s, 10 ^{o}/s, and 20^{o}/s. The angular velocity of the right HRA was kept low to minimize the inertial effects of the left HRA. This is justified since the HRAs are predominantly coupled during double support, which generally is associated with relatively low hip angular velocities. The torque applied to the left HRA by each mass was calculated. The mechanical efficiency of the hip mechanism was defined as the ratio of the output torque versus the input torque.

Figure 3.13a shows the linear regression curves with 95 % confidence intervals of the output torque magnitude versus the input torque for three angular velocities in the flexion and extension directions of the right HRA. A two-way ANOVA was performed to test the influence of angular velocity and direction of rotation on the slope magnitude and intercept (passive resistance) of system output versus input torque curves. For the slope magnitudes, no significant difference was seen for different angular velocities ($p = 0.1342$) and rotation directions ($p = 0.2094$). For the intercepts, no statistical difference was seen for angular velocity ($p = 0.8093$), but there was a 95 % statistical significance among different rotation directions ($p = 0.0301$). **Figure 3.13b** shows the system average mechanical efficiency (η_M) as a function of input flexion and extension torque. System mechanical efficiency plateaued at approximately 0.7 with the mechanical efficiency being slightly higher in flexion than extension.

A high mechanical efficiency is not critical to the intended operation of the hip mechanism. The main purpose of coupling the HRAs is not to transfer torque between

the hips (Each hip will be independently driven by muscle contractions elicited by FNS.), but to inhibit bilateral hip rotation in the same direction. Since no work is involved in preventing bilateral hip rotation, a low mechanical efficiency would not compromise the efficacy of the VCHM. In the case where the HRAs are coupled during single stance or swing so that the flexing swing hip is assisting the single stance hip to extend, due to weak hip extensors or fatigue, a high mechanical efficiency would be beneficial.

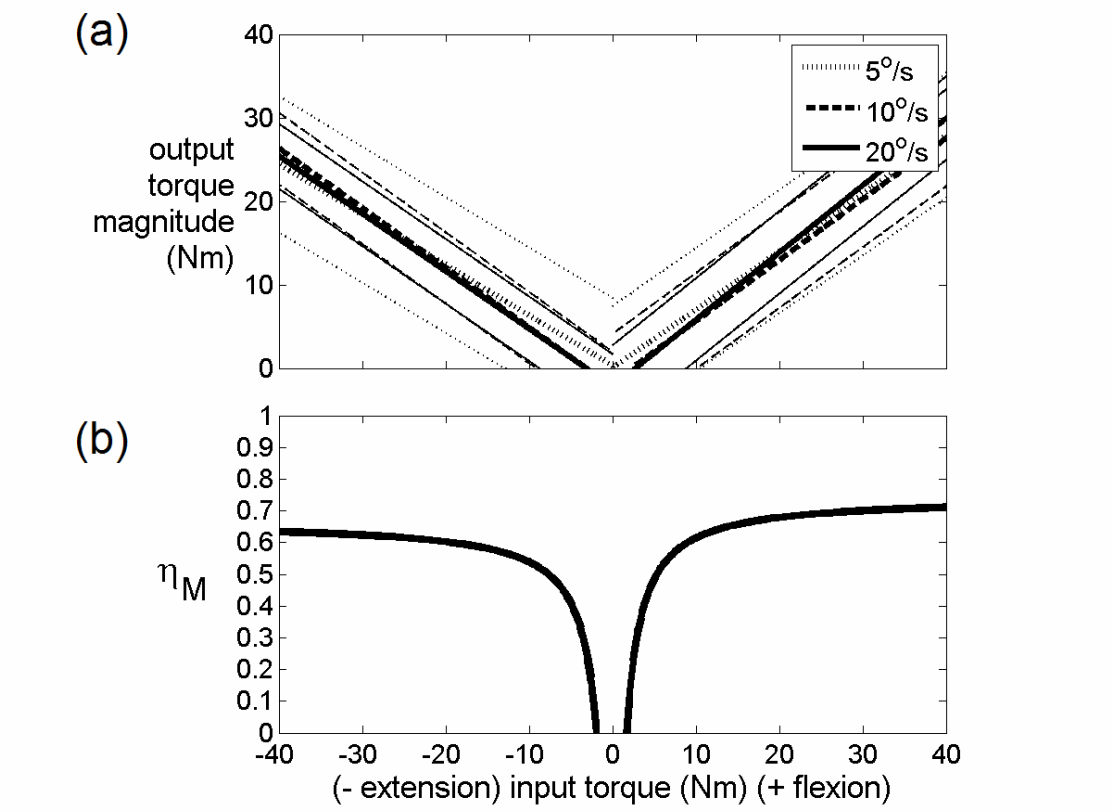

Figure 3.13. (a) VCHM output torque versus input torque. The input torque is the torque necessary to drive the right HRA at 5, 10, and 20°/s for the HRAs coupled. The output torque was calculated from the influence of a mass fixed to the left HRA. (b) VCHM mechanical efficiency (η_M) as a function of input torque for hip flexion and extension rotation directions.

3.5 CLOSED-LOOP CONTROL

A finite state machine (**Figure 3.14**) was designed to control the states of the VCHM according to **Section 3.2.1**. This finite state postural controller (FSPC) uses feedback signals, which include 1) foot-ground contact, 2) hip angular velocities, and 3) cylinder pressures.

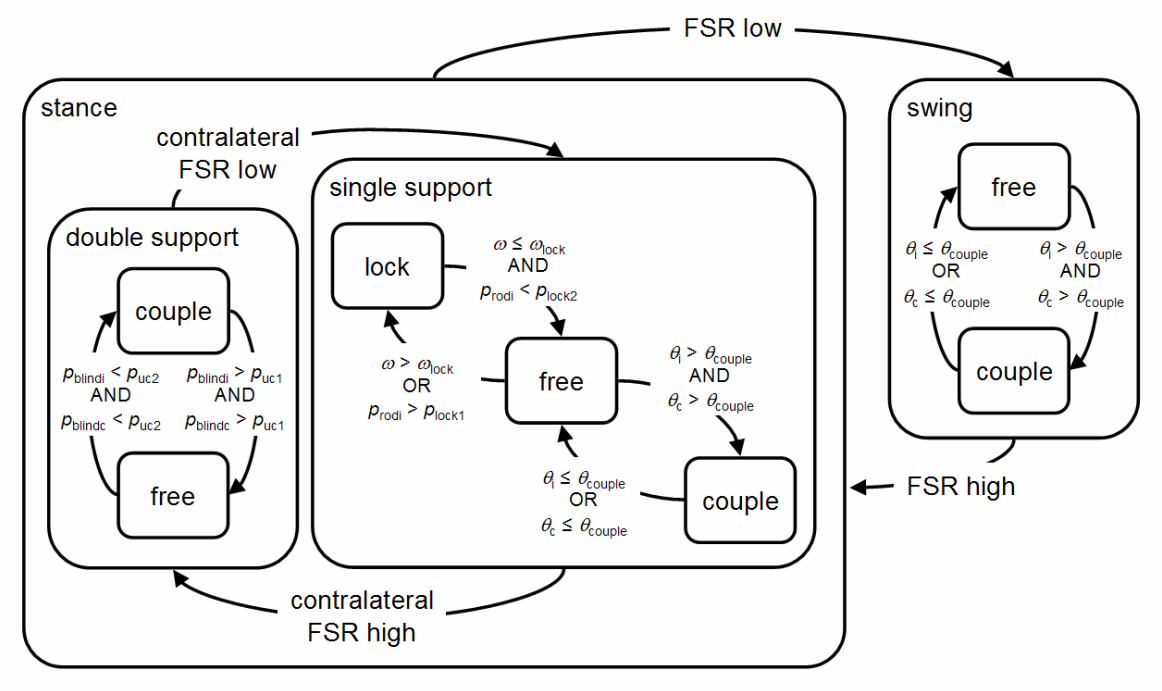

Figure 3.14. Finite state postural controller (FSPC) for the VCHM.

3.5.1 Sensors for Signal Feedback

The exoskeleton was instrumented with the following sensors to acquire the above feedback signals: 1) FSRs (B & L Engineering, Tustin, CA, USA), embedded in the soles of the shoes, were used to measure foot-ground contact instances. One FSR was positioned under the 1st metatarsal, 1st phalange, 5th metatarsal, and heel of each foot. For the purposes of the current controller, the only information required from the FSRs is whether or not the heel or forefoot is in contact with the ground. The recordings of the

FSRs under the forefoot (1st metatarsal, 1st phalange, and 5th metatarsal) of impaired gait have been observed to be fairly inconsistent relative to normal gait. Thus, to increase robustness, the 1st metatarsal, 1st phalange, and 5th metatarsal FSRs were summed into a single forefoot FSR signal with a saturation value equal to one. 2) The rack of each HRA was instrumented with a slide potentiometer (Alps Electric Co., Tokyo, Japan) to measure cylinder movement. Hip joint angle was calculated from the linear position of the rack. The hip joint angles were differentiated to determine the instantaneous hip angular velocities. 3) Digital pressure transducers (Gems Sensors Inc., Plainville, CT, USA) were attached to each port of each cylinder via hydraulic quick-release couplers to measure cylinder pressure. All sensors were powered through the same supply that was sourced by the solenoid valves of the VCHM. All the sensors were permanently attached to the exoskeleton and do not require realignment after donning for different users.

3.5.2 Finite State Postural Controller

Real-time detection of double stance, single stance, and swing phases of the gait cycle is required for the operation of the FSPC. The rules to transition the VCHM from one state to another are based on an event detector that discriminates among the aforementioned gait phases using foot-ground contact instances. A high signal from either heel or forefoot FSR indicates that the corresponding foot is in contact with the ground, whereas the foot is designated as off the ground only if both the heel and forefoot FSR are low. To increase response time, the designation of whether a FSR signal was high or low was determined by hysteresis thresholding – an input must exceed a first

threshold for an output to be high and a second threshold (greater than the first in the case of FSRs) must be subceeded for an output to be low.

Double stance occurs when both ipsilateral and contralateral FSRs are high resulting in the reciprocal coupling of the hips through the de-energization of all valves. The FSPC allows users to bilaterally extend their hips (through upper extremity exertion on the walking aid) if they feel they have excessive anterior trunk tilt (bilateral hip flexion). To allow for bilateral hip extension, the hips are uncoupled (both NC valves opened) based on feedback from the blind end cylinder pressures. A hysteresis thresholding scheme was also employed for the cylinder pressures, with the first pressure threshold (p_{uc1}) being relatively high to ensure user intention and the second pressure threshold (p_{uc2}) being lower than the first to allow for free bilateral hip extension. Both ipsilateral and contralateral blind end cylinder pressures (p_{blindi} and p_{blindc}) must exceed the thresholds for the system to uncouple.

When the ipsilateral FSRs are high and the contralateral FSRs are low the subject is in the single support phase of gait and the hip is freed by opening both NC valves. The hip angular velocities (ω) are used along with the ipsilateral rod end cylinder pressures (p_{rodi}) to lock/unlock the VCHM to prevent forward trunk tilt during single limb stance. Hysteresis thresholding was again employed for the rod end cylinder pressure feedback signal. Hip flexion velocity above an assigned threshold, ω_{lock}, will cause the FSPC to lock the hip against flexion by energizing the ipsilateral rod side NO valve. Once the NO valve is closed, the pressure at the rod end of the corresponding cylinder will exceed a pressure threshold, p_{lock1}, due to the hip flexion torque imposed by the user. The rod side NO valve will remain closed as long as the cylinder rod end pressure (p_{rodi}) is greater than

p_{lock1}. Once the cylinder rod end pressure drops below a second threshold, p_{lock2}, due to the reduction of user hip flexion torque, the rod side NO valve will be de-energized and opened to allow unrestricted hip extension.

The reduction in cylinder rod end pressure may be due to either an increase in the stimulation of ipsilateral hip extensors (**Chapter 4**) or user intervention by upper extremity exertion on the walking aid. The value of p_{lock2} must be greater than p_{lock1} to minimize the hip extension torque necessary to unlock the hip. Thus, the purpose of p_{lock1} is to maintain the locked state of the hip between the instant when hip angular velocity is reduced to zero (once the hip is locked from exceeding ω_{lock}) to when the cylinder pressure is increased above p_{lock2}. In the event that the pressure exceeds p_{lock1} but never exceeds p_{lock2}, the hip will be unlocked once the pressure drops below p_{lock1}.

During single stance the hips are coupled if the angle of both ipsilateral and contralateral hips (θ_i and $\theta_{c,}$ respectively) exceed a threshold (θ_{couple}) (i.e., both hips are bilaterally flexed). The hips will be uncoupled (independently free) once either θ_i or θ_c is less than θ_{couple}.

Swing occurs when the ipsilateral FSRs are low resulting in the hip being freed by opening both NC valves. As in the case of single stance, the hips are coupled if θ_i and θ_c exceed θ_{couple}. The hips will be uncoupled once either θ_i or θ_c is less than θ_{couple}.

3.5.3 Controller Threshold Determination

The thresholds of the FSPC involved in locking the hip against flexion to prevent anterior trunk tilt during single stance (ω_{lock}, p_{lock1}, and p_{lock2}) were empirically determined through bench testing of the VCHM. This was necessary to optimize the

locking/unlocking characteristics of the VCHM. The FSPC was implemented in the Simulink®/xPC Target real-time programming environment. In the following two experiments hip angle, hip angular velocity, cylinder pressure and applied torque were collected and filtered with low-pass digital Butterworth filters. The angle and pressure data were sampled at 250 Hz. The angle data were filtered in real-time with a 5^{th}-order Butterworth low-pass filter at a cutoff frequency of 10 Hz. Angular velocity was calculated from angle data. The pressure data were filtered in real-time with a 7^{th}-order Butterworth low-pass filter at a cutoff frequency of 20 Hz. Torque data were sampled at 600 Hz and filtered offline with a Butterworth low-pass filter at a cutoff frequency of 3 Hz.

The first experiment focused on establishing values for ω_{lock} and p_{lock2} through the following two approaches: 1) Minimize the duration from the onset of hip flexion, during single stance, to when the FSPC outputs a signal to close the rod side NO valve. 2) Minimize the hip extension moment required by the user to unlock the VCHM. The FSPC was evaluated by driving the right HRA of the VCHM with a robotic dynamometer. The objective was to simulate the dynamics of hip flexion during single stance. The dynamometer has an angular acceleration of approximately $115^o/s^2$ up to a maximum angular velocity of $60^o/s$ for flexion and extension of the hip. The dynamometer has limited programmability and must complete its preset ROM in one direction before changing direction. However, the preset ROM can be scaled, but must be done manually and during operation. The dynamometer was attached to the right HRA via a 5 lb/in spring. A typical trial (**Figure 3.15**) consisted of the right HRA being driven into 1) *extension*, at the beginning of the stance phase, 2) *flexion*, to simulate hip

flexion during single stance, and 3) *extension*, to represent the recovery from stance hip flexion as a result of increased hip extensor stimulation or upper extremity effort on a walking aid. **Figure 3.16** shows the signals measured from a typical trial.

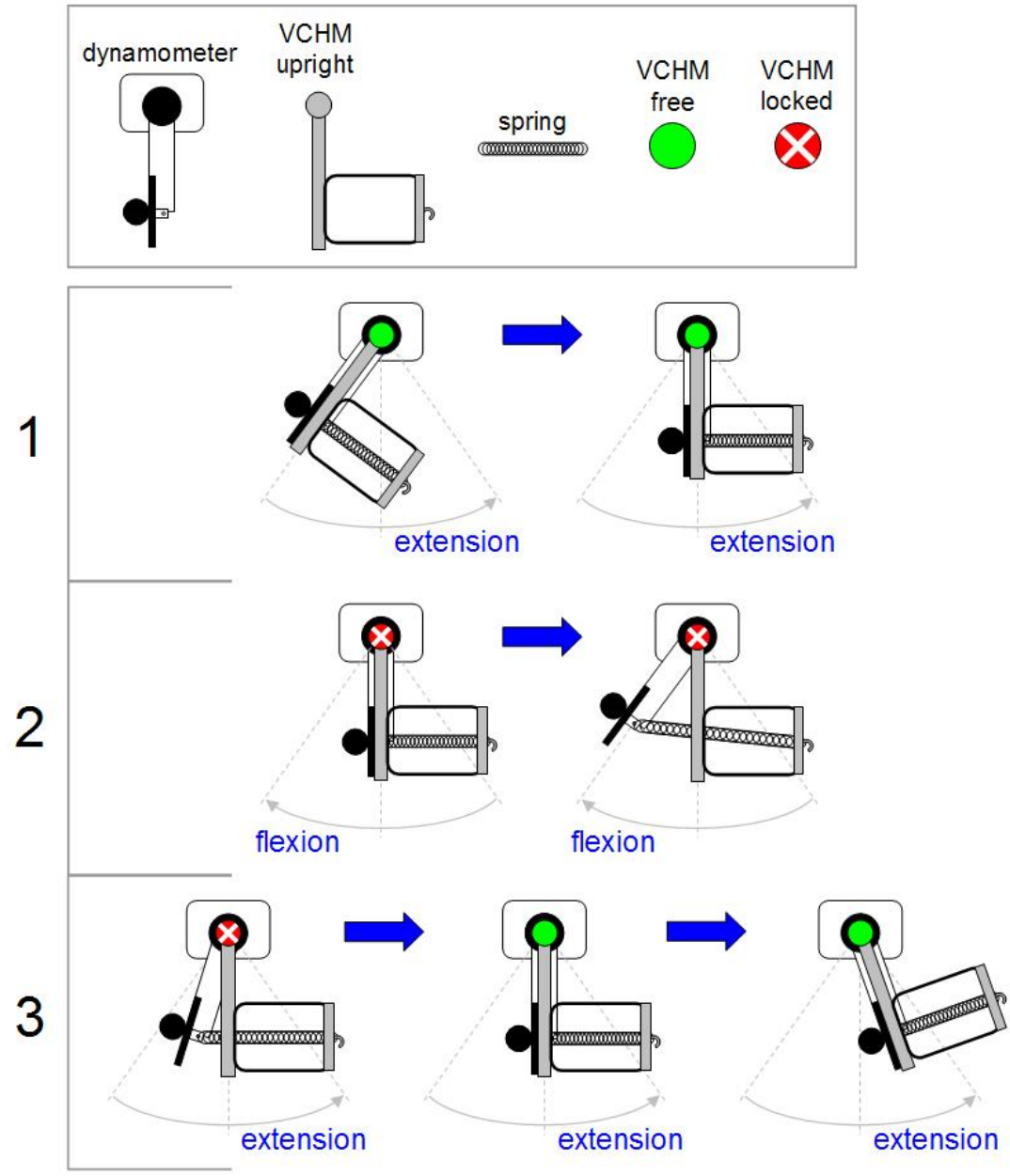

Figure 3.15. Simulation of hip flexion during single stance using a robotic dynamometer.

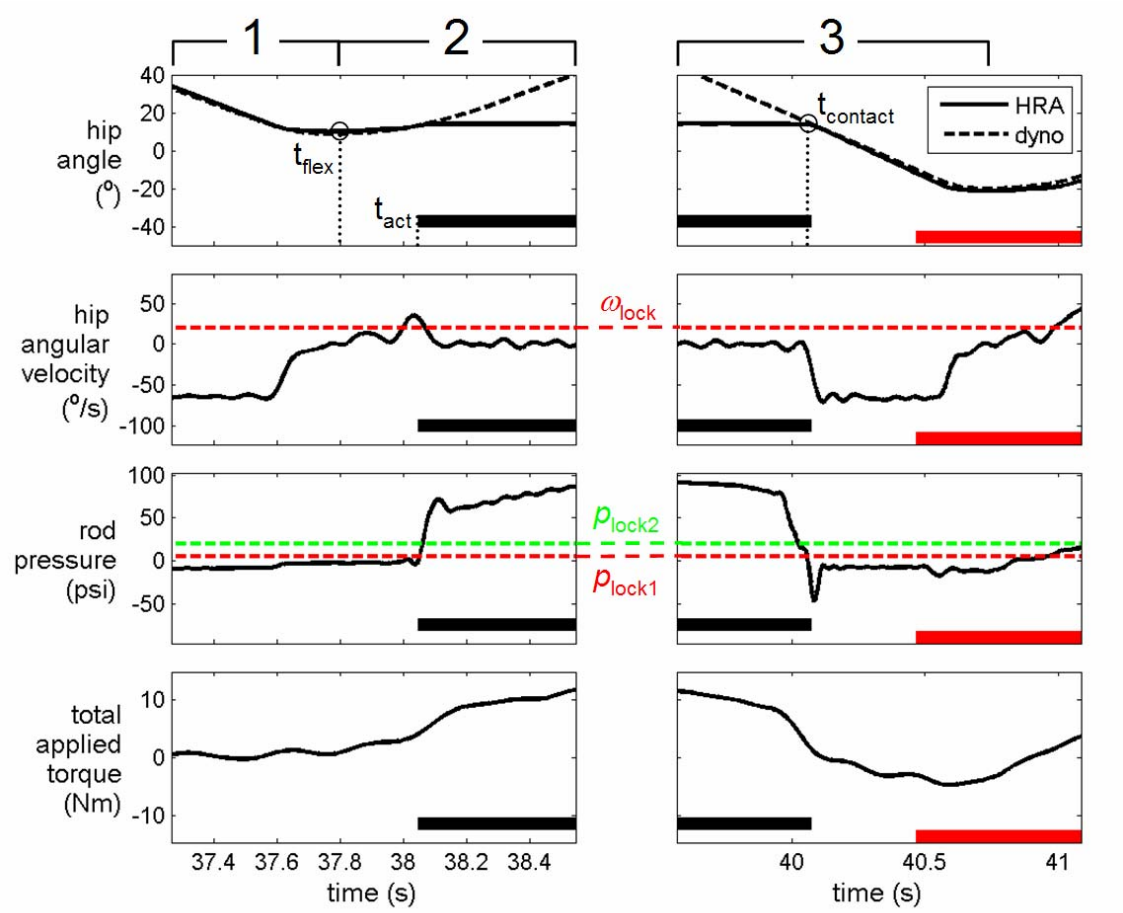

Figure 3.16. Signals collected from a typical trial to determine optimal threshold values for the FSPC. The dark horizontal bar under each curve indicates the period when the VCHM is locked against hip flexion. Phases 1, 2, and 3 correspond to those depicted in **Figure 3.15**.

During **Phase 1**, the HRA is free and in contact with the dynamometer and is being pushed into extension by the dynamometer. In **Phase 2**, the dynamometer extension ROM was scaled down to force the dynamometer to move into flexion.

The dynamometer pulls the HRA into flexion via the spring. Once the HRA angular velocity increases above ω_{lock}, the FSPC locks the HRA against flexion while the dynamometer was still allowed to move into flexion while stretching the spring. When the HRA is locked against flexion, the spring continuously applies a flexion torque on the HRA, thereby pressurizing the rod side of the cylinder above p_{lock1}. In **Phase 3**, the

dynamometer extension ROM was scaled back up to allow for full extension. The dynamometer extends and eventually contacts and unlocks the HRA (due to the rod side cylinder pressure drop below p_{lock2}), allowing the HRA to be pushed into full extension.

Multiple trials were done with different values of each threshold (ω_{lock}, p_{lock1}, and p_{lock2}). Note, for trials testing for ω_{lock}, a large enough p_{lock1} value was chosen such that the HRA locked due to the angular velocity exceeding ω_{lock} as opposed to the rod side cylinder pressure exceeding p_{lock1}. A free swing trial was taken to measure the torque contribution from the passive resistance of the right HRA and the inertial component required to move the dynamometer attachment. This torque was subtracted from the test trials to determine the torque needed to unlock the HRA.

The second experiment dealt with defining a value for p_{lock1}. Even if the VCHM is uncoupled (both hips are independently free), movement of one HRA can influence the pressure measured on the contralateral HRA since the VCHM is a closed system. As a result, flexion of the contralateral swing hip can cause in accidental locking of the stance hip. The value of p_{lock1} must be chosen to prevent this effect. In this experiment, with the VCHM uncoupled, the right hip joint was actuated at various flexion angular velocities by the dynamometer, while the pressure of the left cylinder was measured.

Figure 3.17a shows the duration between the onset of hip flexion (t_{flex}) and the valve activation (t_{act}) to lock the HRA against flexion for each ω_{lock} value tested. The median durations between hip flexion onset and valve activity for ω_{lock} values between 0^o/s and 10^o/s are less than 0.13 s. The maximum noise inherent in the hip angular velocity signal used for feedback in the FSPC was measured to be $\pm 3^o$/s. To prevent the hip from accidentally locking at 0^o/s, it is necessary to define a threshold that exceeds the

maximum noise amplitude. The hip flexion angles for ω_{lock} values between 3°/s and 10°/s are not statistically different (p = 0.3002). Thus, a ω_{lock} value between 3°/s and 10°/s is acceptable for the FSPC. **Figure 3.17b** shows the extension torque applied to the HRA for each p_{lock2} tested. This extension torque is the average torque measured by the dynamometer from the instant the dynamometer attachment extends into contact with the HRA ($t_{contact}$) to the end of the pulse off time of the NO valve (32 ms after the valve has been de-energized).

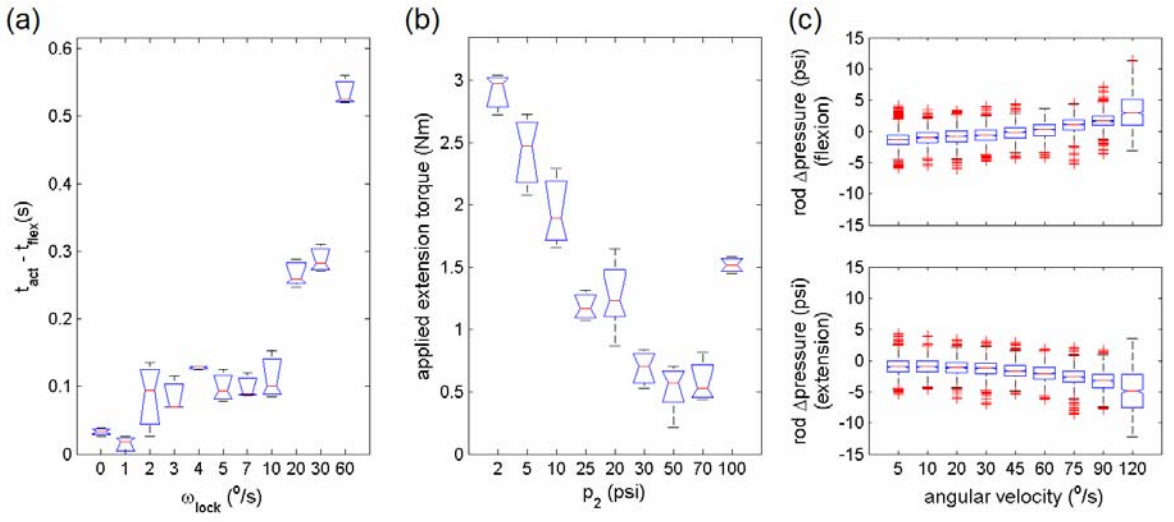

Figure 3.17. FSPC single stance locking threshold determinants.

An extension torque greater than 1 Nm is required to unlock the VCHM for p_{lock2} values less than 30 psi. This suggests that a p_{lock2} value greater than 30 psi is acceptable for the FSPC. However, p_{lock2} should not be set too high so that the cylinder pressure does not exceed the threshold when the hip is locked. In this case, the hip will unlock when the cylinder pressure of the locked hip drops below p_{lock1}, which will require the user to exert unnecessary moment to unlock the hip. **Figure 3.17c** shows the change in cylinder pressure while the contralateral cylinder is actuated at different flexion angular

velocities. The hip flexion angular velocity of individuals with paraplegia generally do not exceed 60^{o}/s [17]. The changes in cylinder pressure are less than 5 psi at angular velocities up to 75^{o}/s. Thus, p_{lock1} values greater than 5 psi are suitable for the FSPC. Optimal threshold values for the FSPC that would provide robust and repeatable operation are summarized in **Table 3.4**. Thresholds, p_{uc1}, p_{uc2}, and θ_{couple}, were determined heuristically during human subject experiments.

Table 3.4
FSPC Threshold Values

threshold	value
FSR 1	0.1
FSR 2	0.2
p_{uc1}	50 psi
p_{uc2}	10 psi
p_{lock1}	10 psi
p_{lock2}	50 psi
θ_{couple}	0^{o}
ω_{lock}	6^{o}/s

3.6 MECHANISM VALIDATION WITH ABLE-BODIED INDIVIDUALS

The VCHM and FSPC were tested with able-bodied individuals to 1) verify that the FSPC changes the states of the constraints of the VCHM as intended and 2) determine how the VCHM influences sagittal hip gait kinematics relative to RGO and normal gait. **Figure 3.18** summarizes the experimental setup. All able-bodied individuals were recruited through signed consent approved by an institutional review board. An exoskeleton equipped with the VCHM and adjustable KAFOs was fitted to each subject. Hip angle, hip angular velocity, cylinder pressure, FSR, and VCHM valve activity were collected. The potentiometers and pressure transducer signals were zero calibrated during quiet standing with the HRAs of the VCHM uncoupled. All data were sampled at

200 Hz. The angle data were filtered in real-time with a 5th-order Butterworth low-pass filter at a cutoff frequency of 10 Hz. The pressure and FSR data were filtered in real-time with a 7th-order Butterworth low-pass filter at a cutoff frequency of 20 Hz.

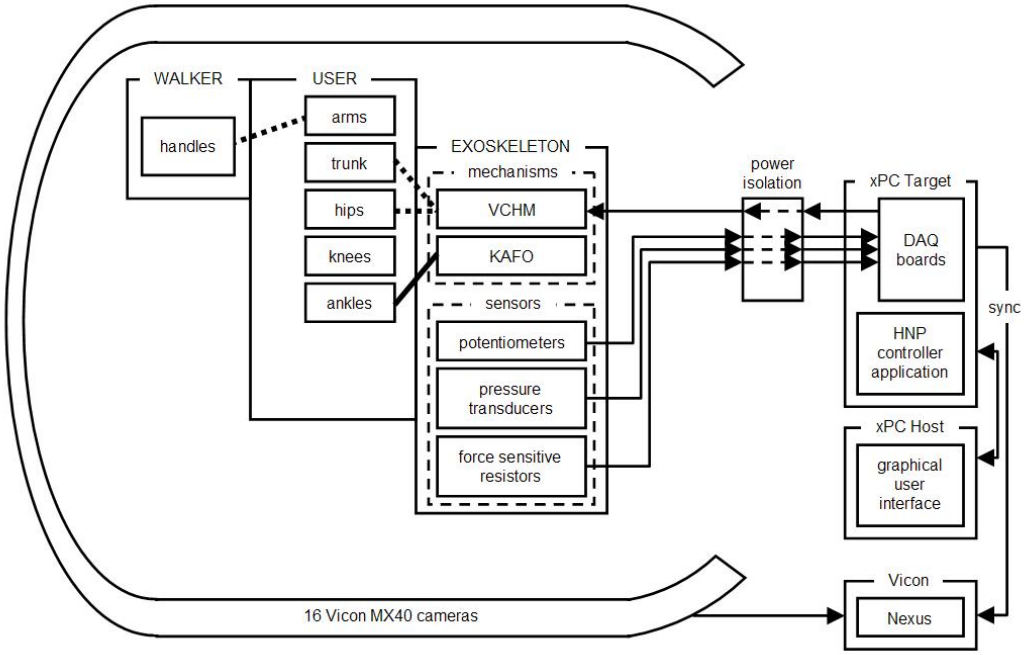

Figure 3.18. Experimental setup for testing the VCHM with able-bodied individuals.

3.6.1 Operation During Gait

To evaluate whether the FSPC will reliably modulate the constraints of the VCHM as intended without accidental locking, the able-bodied subjects were instructed to walk at their preferred speed along an eight meter walkway while wearing the prototype exoskeleton. Three able-bodied individuals were recruited for this experiment. The subjects walked with knees and ankles free in the sagittal plane. A rolling walker was used by the subjects for safety. Since able-bodied gait is approximately periodic, the measured signals should be invariant with respect to the same gait phases among

subsequent gait cycles. Subjects 1, 2, and 3 walked at an average speed of 0.85 m/s, 0.70 m/s, and 0.81 m/s, respectively.

Figure 3.19 shows the average ipsilateral and contralateral hip angle, percentage of samples that the hip is locked against flexion, and percentage of samples that the hips are uncoupled for each subject (± 1 standard deviation) with respect to percentage gait cycle. The vertical lines delineate the gait events (loading response (LR), mid stance (MSt), terminal stance (TSt), pre-swing (PSw), initial swing (ISw), and late swing (LSw)) as defined in [18].

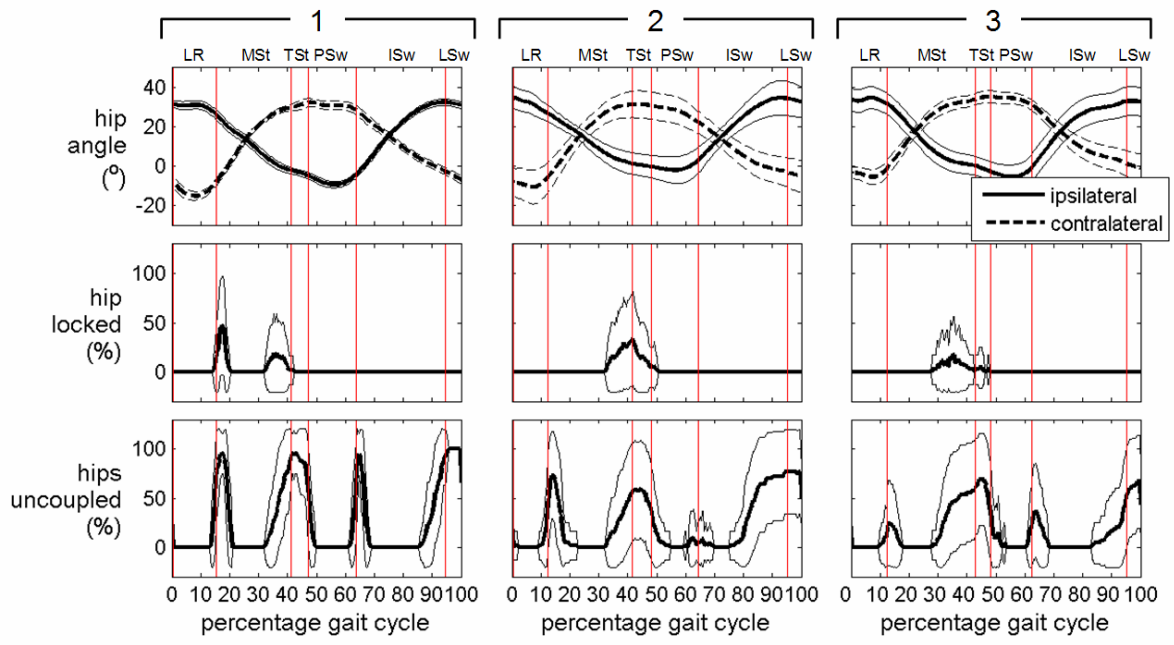

Figure 3.19. Average hip angle, hip locking, and hip uncoupling instances (± 1 standard deviation) with respect to percentage gait cycle for each able-bodied subject walking with the VCHM.

For all three subjects, hip locking against flexion occurred minimally and for short bursts primarily during MSt. The low percentage of samples in which the stance hip was locked against flexion is because the able-bodied subjects do not require trunk support from the orthosis. The hips were predominantly coupled during the double

stance phases of gait (i.e., LR and PSw). The pattern of hip uncoupling over the gait cycle seems to be similar among all three subjects, with the average instances of hip uncoupling being greatest for subject 1. The hips are uncoupled at the onset of MSt, coupled in the middle of MSt, and uncoupled again at the end of MSt. The hips remain uncoupled through the end of TSt, which allows for unimpeded contralateral swing. This pattern of hip uncoupling is fairly symmetric between limbs as ipsilateral ISw and LSw correspond with contralateral MSt and TSt, respectively.

Coupling of the hips during the single stance phase (MSt and TSt) and swing phases (ISw and LSw), indicate that both hips are flexed beyond the threshold angle, θ_{couple}, which is relative to the subject's standing posture during the initial zero calibration of the hip angle sensors. The more time the hips are bilaterally flexed relative to θ_{couple}, the more time the hips will be coupled, reducing the time for free hip flexion for swing over the gait cycle and ultimately defaulting to the full hip coupling of a RGO. Thus, unimpeded swing is marginalized by the efficiency of stance hip extension. Increasing the value of θ_{couple} may not be the solution for users with paraplegia, as the tendency for the user would be to increase bilateral hip flexion along with θ_{couple}, resulting in an overall increased anterior trunk tilt.

3.6.2 Influence of Constraint Modulation on Hip Kinematics

The effect of walking with the VCHM on sagittal hip angle was evaluated by having the subjects walk at their preferred velocity with a standard Isocentric RGO (IRGO) and normally, without a device. As with the VCHM, the IRGO was made adjustable and custom fit to each subject. The knees and ankles were freed when the

subjects walked with the IRGO. The able-bodied subjects also walked with the VCHM unpowered to evaluate how well the reciprocal coupling of the VCHM approximated that of an IRGO. For consistency, the subjects used a walker for all test cases. During IRGO gait and normal gait, hip angle was determined from the locations of reflective markers, placed at key locations on the IRGO and/or bony landmarks of the body (refer to **Chapter 4** for details). The locations of the reflective markers were tracked by a 16-camera Vicon MX40 (Vicon, Inc., Oxford, UK) motion analysis system (sampling at 100 Hz). The hip angles while walking with the VCHM was compared to those of IRGO gait and normal gait.

During VCHM operation, the coupling/uncoupling of the hips occur during continuous hip motion. **Figure 3.20** illustrates the influence of these constraint state changes on the kinematics of the hip during gait. **Figure 3.20** shows the hip angle and the torque calculated from the cylinder pressure (**Appendix A**) 100 ms before and after hip uncoupling and coupling. Ten curves, randomized over the three subjects, were plotted for each signal and constraint state transition. The horizontal bars under the each set of curves indicate when the hips are uncoupled. All curves have a smooth profile during the instant of the constraint state transition.

Figure 3.21a shows the average hip angle trajectories (± 1 standard deviation) of gait with an unpowered VCHM (hips coupled continuously) and gait with an IRGO with respect to percentage gait cycle. **Figure 3.21b** shows the average hip angle trajectory (± 1 standard deviation) of gait with a VCHM controlled by the FSPC plotted with that of normal gait with respect to percentage gait cycle. **Table 3.5** lists the normalized root mean square deviation (NRMSD) values between each tested case.

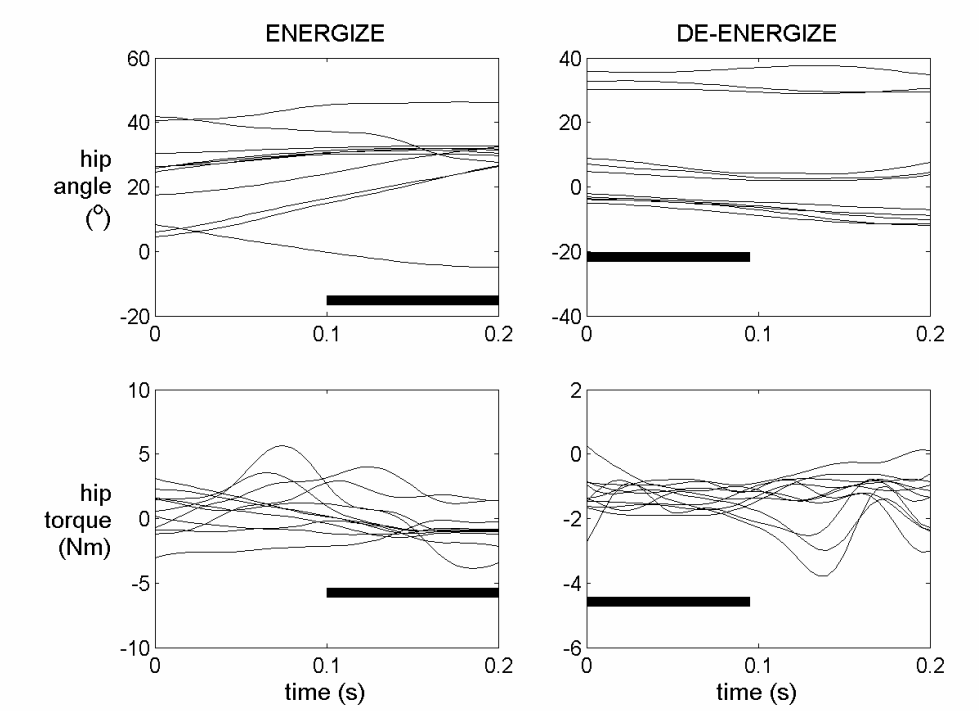

Figure 3.20. Response of hip angle and HRA torque with valve activity of uncoupling (energize NC valves) and coupling (de-energize NC valves) the hips.

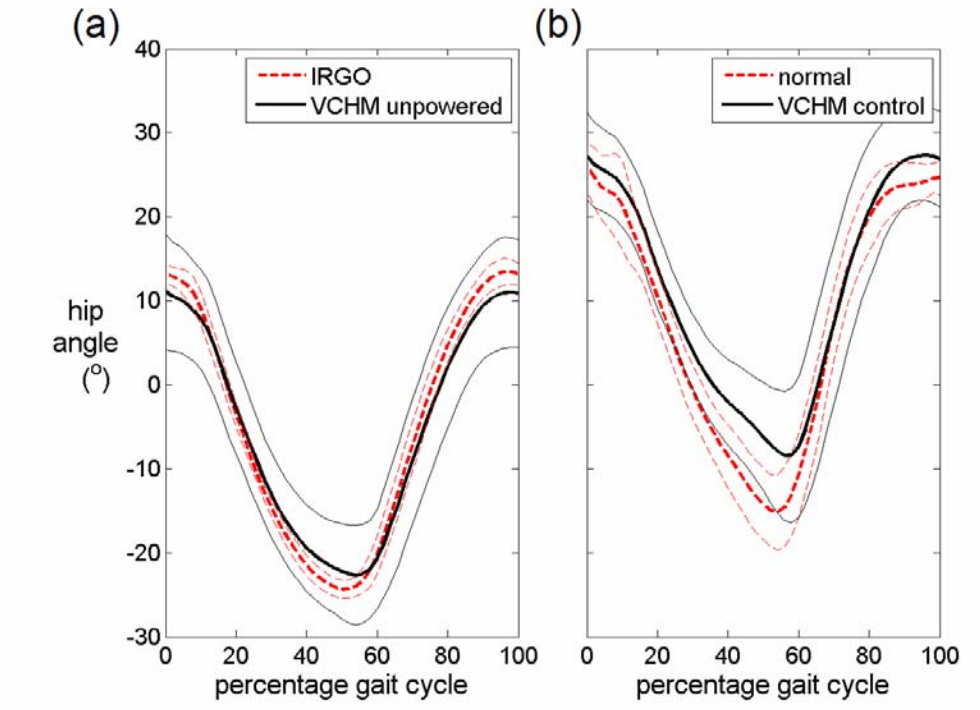

Figure 3.21. Average hip angle (± 1 standard deviation) with respect to percentage gait cycle for (a) IRGO, unpowered VCHM, (b) normal, and VCHM controlled by the FSPC.

The NRMSD values show that the hip trajectory of the controlled VCHM is closer to normal gait than the unpowered VCHM and IRGO. Also of note is that the hip trajectory of the unpowered VCHM is very similar to that of the IRGO (NRMSD = 0.0566), verifying the effectiveness of the VCHM coupling. These results indicate that controlled VCHM constrains the user less than the IRGO, allowing for more instances of free mobility.

Table 3.5
Able-bodied Gait with VCHM
Normalized Root Mean Squared Deviation

Control → Experimental ↓	**IRGO**	**normal**
IRGO	0	0.3355
VCHM unpowered	0.0566	0.3939
VCHM control	0.4508	0.1167

3.7 CONCLUSIONS

The goal of the VCHM is to provide trunk support to the user on an as needed basis such that exoskeleton operation does not interfere with limb mobility. This should reduce the upper extremity exertion on an assistive device relative to FNS-only and brace-only gait while simultaneously allowing for unconstrained unilateral swing to vary stride length with the demand to achieve variations in walking speed. Alternatively, when integrated with the dual state knee mechanism (**Chapter 2**), the VCHM should be able to entirely support the user without activation of the lower extremity muscles during double stance. As a result, the user should be able to rest periodically while standing to compensate for lower extremity muscle fatigue after prolonged periods of gait without the need to sit.

Similar to existing mechanical orthoses, the VCHM is passive in that the device does not inject energy into the user during operation. Thus, there are no safety concerns in which the user must resist or adapt to perturbations generated from the device. Furthermore, there are no additional physical impairments that would preclude an individual from using the VCHM that have not already been specified for use of either bracing or FNS systems.

This work has shown that a portable hydraulic system developed for the purpose of controlling postural stability can accommodate the hip dynamics of an individual with paraplegia walking with a FNS system. The use of hydraulics in wearable/minimal power systems holds multiple design challenges, some of which have been dealt with in this chapter and **Chapter 2**. The portable nature of the device prohibits the use of a large power source. Consequently, the decision was to design a passive device that would serve to support and redirect forces (i.e., reciprocal hip coupling) as opposed to an active device that would inject energy into the system. However, a passive device must be driven by the user, as opposed to an active device which would be self-driven. Thus, minimizing the passive resistance of the device was paramount. In the design of the VCHM, flow and pressure were optimized according to the specific load capacities of the user population. In doing so, the flow during system operation was minimized, resulting in relatively minimal passive resistance torque magnitudes. Another necessity of portability is that the mass of the device must be small. A difficulty with miniaturizing hydraulics is that the liquid-to-air ratio decreases along with the size of the system. Complete priming a hydraulic system is not feasible due to trapped air bubbles (within fittings or cylinder heads) and minute system leakage through seals. For large hydraulic

systems, incomplete priming is not an issue due to the high liquid-to-air ratio. For miniature hydraulic systems, any internal air may significantly affect system impedance against a load. A solution to this problem has been to actively increase actuator pressure against the load to compensate for any compliance. This would however require converting the passive system into an active system. In the design of the VCHM, the resting pressure of the entire system was increased 5 bar above atmospheric to minimize the volume of internal air bubbles. However, the amount of pressure that can be increased is limited by both the maximum operating pressure and operating pressure range of the system. Since the maximum operating pressure is invariable (without respecifying the hydraulic components), increasing the system resting pressure effectively reduces the operating pressure range of the hydraulics.

3.8 REFERENCES

1. G. K. Rose, "The principles and practice of hip guidance articulations," *Prosth. & Orth. Intnl.*, vol. 3, pp. 37-43, 1979.

2. R. E. Major, J. Stallard, and G. K. Rose, "The dynamics of walking using the hip guidance orthosis (hgo) with crutches," *Prosth. & Orth. Intnl.*, vol. 5, pp. 19-22, 1981.

3. R. Douglas, P. F. Larson, R. D'Ambrosia, R. E. McCall, "The LSU reciprocating gait orthosis," *Orthopedics*, vol. 6, pp. 834-839, 1983.

4. Y. Ohta, H. Yano, R. Suzuki, M. Yoshida, N. Kawashima, and K. Nakazawa, "A two-degree-of-freedom motor-powered gait orthosis for spinal cord injury patients," *Proc. IMechE Part H: J. Engineering in Medicine*, vol. 221, no. 6, pp. 629-639, 2007.

5. R. J. Jefferson, M. W. Whittle, "Performance of three walking orthosis for the paralyzed: a case study using gait analysis," *Prosth. & Orth. Intnl.*, vol. 14, pp. 103-110, 1990.

6. W. M. Motloch, "Principles of orthotic management for child and adult paraplegia and clinical experience with the isocentric RGO," *Proc. 7th World Congress of the International Society for Prosthetics and Orthotics*, Chicago, pp. 28, Jun 28 - July 3, 1992.

7. A. Pedotti, M. Ferrarin, J. Quintern, and R. Riener, *Neuroprosthetics: from Basic Research to Clinical Application*, Germany: Springer-Verlag Berlin Heidelberg, pp. 493-502, 1996.

8. B. M. Y. Nouri and A. Zaidan, "Computer control of a powered two degree freedom reciprocating gait orthosis," *ISA Transactions*, vol. 45, no. 2, pp. 249-258, 2006.

9. G. Kim, S. Kang, S. Kang, J. Ryu, M. Mun, and K. Kim, "Unlockable knee joint mechanism for powered gait orthosis," *Int. J. Precision Engineering and Manufacturing*, vol. 10, no. 3, pp. 83-89, July 2009.

10. L. Yang, M. H. Granat, J. P. Paul, D. N. Condie, and D. I. Rowley, "Further development of hybrid functional electrical stimulation orthoses," *Spinal Cord*, vol. 34, no. 10, pp. 611-614, Oct. 1996.

11. P. M. Dall, B. Muller, I. Stallard, J. Edwards, and M. H. Granat, "The functional use of the reciprocal hip mechanism during gait for paraplegic patients walking in the Louisiana State University reciprocating gait orthosis," *Prosth. & Orth. Intnl*., vol. 23, pp. 152-162, 1999.

12. C. S. To, R. F. Kirsch, R. Kobetic, and R. J. Triolo, "Simulation of a functional neuromuscular stimulation powered mechanical gait orthosis with coordinated joint locking," *IEEE Trans. Neural Syst. Rehab. Eng*., vol. 13, no. 2, pp. 227-235, 2005.

13. D. W. Dudley, *Handbook of Practical Gear Design*, Boca Raton, FL: CRC Press LLC, pp. 3.74–3.115, 1994.

14. E. B. Marsolais, R. Kobetic, G. Polando, K. Ferguson, S. Tashman, R. Gaudio, S. Nandurkar, and H. R. Lehneis, "The Case Western Reserve University hybrid gait orthosis," *J. Spinal Cord Med.*, vol. 23, no. 2, pp. 100-108, 2000.

15. R. Kobetic, E. B. Marsolais, and P. C. Miller, "Function and strength of electrically stimulated hip flexor muscles in paraplegia," *IEEE Trans.Rehab. Eng*., vol. 2, no. 1, pp. 11-17, Mar. 1994.

16. R. Kobetic and E. B. Marsolais, "Synthesis of paraplegic gait with multichannel functional neuromuscular stimulation," *IEEE Trans. Rehab. Eng.*, vol. 2, no. 2, pp. 66-79, June 1994.

17. P. Krawetz and P. Nance, "Gait analysis of spinal cord injured subjects: Effects of injury level and spasticity," *Arch. Phys. Med. Rehabil.*, vol. 77, pp. 635-638, July 1996.

18. J. Perry, *Gait Analysis: Normal and Pathological Function*, Thorofare, NJ: SLACK Incorporated, pp. 10-16, 1992.

CHAPTER 4

DEVELOPMENT AND IMPLEMETATION OF A CLOSED-LOOP CONTROLLER FOR THE REAL-TIME MODULATION OF ELECTRICAL STIMULATION AND JOINT CONSTRAINTS OF A PROTOTYPE HYBRID NEUROPROSTHESIS FOR RESTORING GAIT

4.1 INTRODUCTION

A HNP is the merger of two different rehabilitation techniques, exoskeletal orthoses and FNS, for restoring bipedal locomotion to individuals paralyzed by SCI. The focus of traditional passive exoskeleton systems is to keep the user upright and on both feet. Lower extremity movements that bring about forward progression are strictly a product of the reactionary kinetics on the exoskeleton induced by the coordinated upper extremity actions on a walking aid. Alternatively, with FNS systems the lower extremities are actively driven to directly provide forward progression as well as to

support the weight of the user. Upper extremity effort on the walking aid is relegated to stabilizing trunk posture.

In this research, the hybridization of an exoskeleton and FNS was intended to achieve two main objectives. First, to employ the exoskeleton for all supportive tasks to reduce the role of stimulated muscle to exclusively driving limb movements and relieve the voluntary upper extremity exertion on the walking aid. These supportive tasks include bearing both the weight of the user and exoskeleton statically as wells as dynamically, maintaining trunk posture, and guiding limb trajectories. The reduction of stimulation duty cycle should delay the onset of fatigue of the paralyzed muscles targeted for stimulation [1], while the lessening upper extremity exertion should delay the onset of fatigue on the voluntary muscles. Second, when selected constraints of the exoskeleton are removed, the FNS of target muscles will produce functional joint dynamics for ambulation. The successful combined implementation of both objectives should result in fatigue resistant gait with mobility unaltered from a FNS-only gait system. The success of these objectives is corollary to the validation of the hypotheses proposed in **Chapter 1**.

4.2 CLOSED-LOOP CONTROL OF FNS

Chapters 2 and **3** described the development of the exoskeletal component of the HNP. With this prototype exoskeleton consisting of passive mechanisms, the function of the exoskeleton will be to support the user when necessary. Knowledge of each exoskeleton constraint state will allow for the deactivation of the FNS to the target muscles of the constrained joint when no mobility is required. Furthermore, with

feedback from sensors signals of the instrumented exoskeleton, the stimulus intensities to target muscles can be increased such that the desired endpoints of the joint trajectories, when constrained by the exoskeleton, will functionally stabilize the user but not impede the motion of other joints. The stimulus to the extensor muscles of the hip and knee joints were exclusively targeted by the controller for modulation since these extensor muscles are responsible for supporting body weight and maintaining posture.

The proceeding work focused on the real-time modulation of FNS by synchronizing exoskeletal operation with FNS activity. The goal was to minimize the duty cycle of target extensor muscles and promote upright posture that would allow for efficient forward progression. FNS modulation to each muscle was done relative to baseline stimulus parameters. These baseline FNS patterns were tuned specifically for the study participant to achieve gait with FNS alone. Since only controllable hip and knee constraints were developed, the ankle joints were constrained by AFOs at all times and FNS to ankle target muscles was not modulated.

The maximum allowable stimulus pulse width (PW) on all channels was limited to 250 μs, while the minimum stimulus inter-pulse interval (IPI) was limited to 30 ms for a maximum frequency of 33.33 Hz in order to minimize muscle fatigue [2]. The maximum stimulus PW of individual channels was further limited to prevent tissue damage [51] and the recruitment of adjacent muscles [4]. The constant current amplitude of 20 mA was used throughout all system development and testing.

Because the controller is designed to deactivate stimulation during periods of constrained joint motion, the stimulus duty cycle to the target hip and knee extensors could be smaller for a HNP as compared to a FNS-only system. Thus, the effects of

fatigue due to prolonged electrical stimulation can be reduced in the HNP relative to a FNS-only system with an equivalent number of stimulus channels.

4.2.1 Software

The FNS controller consists of three separate modules. 1) A set of output signals from the controller containing the timing of specific phases of the gait cycle are used for feedback to synchronize exoskeletal constraint operation with FNS activity. 2) The knee FNS control module and 3) hip FNS control module are respectively responsible for the real-time modulation of the stimulation to the target knee and hip extensors based on exoskeleton kinematics and constraint states. All software for the FNS controller was developed and implemented in the Matlab®/Simulink® (The MathWorks, Inc., Natick, MA, USA).

4.2.1.1 Gait Phase Output Signals

The FNS controller sends out individual signals which indicate the occurrence of specific phases in the gait cycle for each leg. These gait phases can be considered as versions of pre-swing, initial swing, and mid swing phases [5] specifically modified for control purposes. Furthermore, for the purposes of this controller initial swing and mid swing were combined into a single phase referred to as early swing. The two resulting phases of gait (pre-swing and early swing) are critical for the responsive operation of the DSKM described in **Chapter 2**. Knowledge of the pre-swing phase will allow for knee extensor stimulation by the knee FNS control module to unload the DSKM, facilitating responsive unlocking. Information from early swing phase will be needed to prevent DSKM locking during swing. Without this feedback signal, the DSKM will lock upon

foot contact on the ground, based on feedback from FSRs installed under the soles of the feet. Foot-to-ground contact can readily happen with insufficient foot-to-ground clearance during swing. According to the finite state machine of the DSKM, the knee joint will remain unlocked as long as the limb is in early swing, thus preventing locking of the DSKM during premature foot-to-ground contact.

The output signals are derived from the stimulation activity of the target knee flexors and extensors. The period of pre-swing was set to begin 210 ms before the onset of knee flexor stimulation and set to end at the onset of knee flexor stimulation. The period of early swing was set to begin 120 ms prior to the onset of knee flexor stimulation and set to end 210 ms after the onset of knee extensor stimulation. The onset time of early swing was made a set time before knee flexor activation to allow the DSKM to unlock before knee flexion occurs. This is to 1) prevent an applied flexion moment on the DSKM which would prolong the unlocking duration and 2) account for the response time of the DSKM solenoid valve such that the knee does not flex against a locked DSKM which would impair the joint trajectory and result in poor foot-to-ground clearance. The end of early swing was made a set time after knee extensor stimulation onset to allow time for the swing limb to clear the ground before DSKM locking occurs.

4.2.1.2 Knee FNS Control Module

The knee FNS control module will respectively coordinate the unlocking/locking of the knee constraint with the activation/deactivation of knee extensor muscles. As a result, all knee extensor muscles will be deactivated during the stance phases of gait, significantly reducing the duty cycle of the muscle stimulation [70, 69, 7].

Table 4.1 shows the complete finite state machine of the FNS controller for modulating the stimulus parameters. For each rule, all the IF conditions must be satisfied in order for the THEN clause to be executed.

Table 4.1
HNP FNS Controller Finite State Machine

module	rule	IF	THEN
knee	1	ipsilateral DSKM valve state is closed	deactivate knee extensor stimulation
		ipsilateral knee angle has crossed below knee threshold 1	
		ipsilateral knee angle < knee threshold 2	
		gait phase ≠ pre-swing	
	2	ipsilateral DSKM valve state transitioned from opened to closed	decrease knee extensor stimulation IPI to 30 ms
		ipsilateral knee angle has not crossed below knee threshold 1 or ≥ knee threshold 2	
hip	3	contralateral DSKM valve state is opened	increase hip extensor stimulation PW to maximum levels and decrease stimulation IPI to 30 ms
		ipsilateral DSKM valve state is closed	
		both VCHM NC valve states are closed	
	4	ipsilateral VCHM rod NO valve state is closed	increase hip extensor stimulation PW to maximum levels and decrease stimulation IPI to 30 ms
	5*	ipsilateral DSKM valve state is closed	deactivate hip extensor stimulation
		ipsilateral hip angle has crossed below hip threshold 1	
		ipsilateral hip angle < hip threshold 2	
* **Rule 5** takes precedence over **Rule 4**			

Modulation of the PW to the knee extensors consists of only the deactivation of stimulus activity from baseline levels by the following rule.

Rule 1: *When the knee is fully extended, locked against flexion, and not in the pre-swing phase of gait, stimulation to the stance knee extensors is deactivated.* The knee is considered to be fully extended when the knee angle has extended beyond knee

angle threshold 1 and remains less than knee angle threshold 2 (knee flexion angle is positive). A rotary potentiometer (Vishay, Malvern, PA, USA) on each DSKM was used measure sagittal knee joint movement.

Hysteresis thresholding accommodates the compliance observed in the DKSM. Thus, the compliance of the DSKM which causes the knee angle to be greater than the knee angle threshold 1 will not reactivate preset stimulation levels. If the knee angle exceeds knee angle threshold 2, the baseline stimulation PW levels will be resumed. Knee angle threshold 2 is the acceptable change in knee angle into flexion relative to knee angle threshold 1 while the DSKM is in a locked state. The threshold values used for the FNS controller are shown in **Table 4.2**. The knee being locked against flexion is determined from the signal which controls the state of the DSKM valve. When the valve is closed, the knee is locked against flexion. The knee being both fully extended and locked against flexion indicates that the limb is in stance and can fully support the user, and that the body's center of mass is at its highest to allow for proper foot-to-ground clearance of contralateral swinging limb. The pre-swing phase of gait is determined from the FNS controller output signal (*Section 4.2.1.1*). Stimulation is applied to the knee extensors to reduce the flexion torque applied to the DSKM prior to the DSKM unlocking. This is to assure that the DSKM will unlock responsively.

Table 4.2
FNS Controller Threshold Values

threshold		**value (^{o})**
knee angle	1	3
	2	13
hip angle	1	0
	2	-8

Due to software restrictions, IPI modulation is limited to switching between 60 ms and 30 ms corresponding to a stimulus frequency of 16.67 Hz and 33.33 Hz respectively. In actuality, the stimulation frequency is at a constant 33.33 Hz. Reduction of the frequency to 16.67 Hz was done by zeroing the PW of every other period. The following rule decreases the stimulus IPI of target knee extensors to 30 ms.

Rule 2: *When the knee transitions to a locked state but has not reached full extension, knee extensor stimulation IPI is decreased to 30 ms and remains so until the knee has fully extended*. DSKM locking indicates that the foot has contacted the ground (**Chapter 2**). However, since the knee is still flexed, the body's center of mass may not be high enough to allow for proper foot-to-ground clearance during contralateral swing. As described in **Chapter 2**, a knee extension velocity (permitted by an accumulator) will automatically open the valve of the DSKM assuring functional locking once the knee is fully extended. Note, that PW was not increased along with frequency to prevent over stimulation of the quadriceps muscles.

4.2.1.3 Hip FNS Control Module

The hip FNS control module serves to maintain functional hip extension motion throughout the single stance phase. The stimulus PW can be increased or deactivated depending on the state of the exoskeleton constraints and hip kinematics. There are two rules that dictate whether the PW is increased. Stimulus frequency of the hip extensors is increased simultaneously with PW.

Rule 3: *When the hips are coupled during single stance, stimulation PW and frequency of the stance limb hip extensors are maximally increased*. Hip coupling occurs when both normally closed valves of the VCHM (**Chapter 3**) are closed, designated by

the valves state signals. Single stance is designated when the ipsilateral DSKM locked (valve closed) and contralateral DSKM is unlocked (valve opened). As described in **Chapter 3**, reciprocal coupling during single stance occurs when there is bilateral hip flexion. The intention of the reciprocally coupling the hips is for contralateral hip flexion to assist ipsilateral hip extension. In order to maximize hip extension and minimize the hindrance that the coupling constraint imposes on the contralateral flexion ROM, the extension motion of the ipsilateral hip was maximized with increased muscle stimulation. A limiter was encoded into the FNS controller to ensure that the stimulus parameters do not exceed safety limits.

Rule 4: *When the hip is locked against flexion during single stance, stimulation PW and frequency of the stance limb hip extensors are maximally increased*. The hip being locked against flexion and single stance is detected when ipsilateral rod valve of the VCHM is signaled to close. This rule was designed to ensure continuous hip extension during single stance to facilitate continuous forward propulsion and prevent anterior trunk tilt.

Rule 5: *When the stance hip is fully extended, the stimulation to the stance hip extensors is deactivated*. Stance is detected with the DSKM is locked (valve is closed). Similar to **Rule 1** of the knee FNS control module, hysteresis thresholding is used to determine if the hip is fully extended. The hip is fully extended once the hip angle crosses below hip angle threshold 1 (hip extension is negative) and is considered fully extended until the hip angle is greater than hip angle threshold 2 (**Table 4.2**). The magnitude of the difference between hip angle thresholds 1 and 2 is the acceptable compliance of the VCHM while the VCHM is constraining the hip against flexion. A

slide potentiometer (Alps Electric Co., Tokyo, Japan) at each hydraulic cylinder of the VCHM was used to measure piston position which was then used to calculate hip angle. **Rule 5** takes precedence over **Rule 4**. Thus, once the stance hip is fully extended, stimulation to target extensors is deactivated. Any stance hip flexion will be prevented by the VCHM locking the hip against flexion.

4.2.2 Hardware

The FNS controller was prototyped and implemented using three primary pieces of equipment (**Figure 4.1**): 1) a target computer 2) a host computer, and 3) a muscle stimulator unit. Custom power isolation circuitry (Advanced Platform Technology Center, Cleveland, OH, USA) was used to reduce leakage current at the user's end.

The target PC runs an xPC target (The MathWorks, Inc., Natick, MA, USA) kernel that facilitates the real-time implementation of custom applications. The target PC is responsible for the implementation of the entire controller for the HNP and all data acquisition. The HNP controller consists of the finite state machines for controlling the DSKM (**Chapter 2**), VCHM (**Chapter 3**), and FNS modulation as well as the zero calibration and low pass filtering of sensor signals. The target PC was equipped with a Pentium Dual-Core microprocessor (Intel Corporation, Santa Clara, CA, USA) at 3 GHz and 2 GB of RAM. A NI PCI-6025E and NI PCI-6071E data acquisition board (National Instruments, Austin, TX, USA), with multiple analog inputs and digital input/output channels, were installed in the target PC for sensor signal acquisition and the output of control states to the exoskeleton. Approximately 20 meters of shielded multi-conductor cabling connect the exoskeleton to the target PC. All communication between the target

PC and exoskeleton was at a frequency of 200 Hz during laboratory experiments with research volunteers.

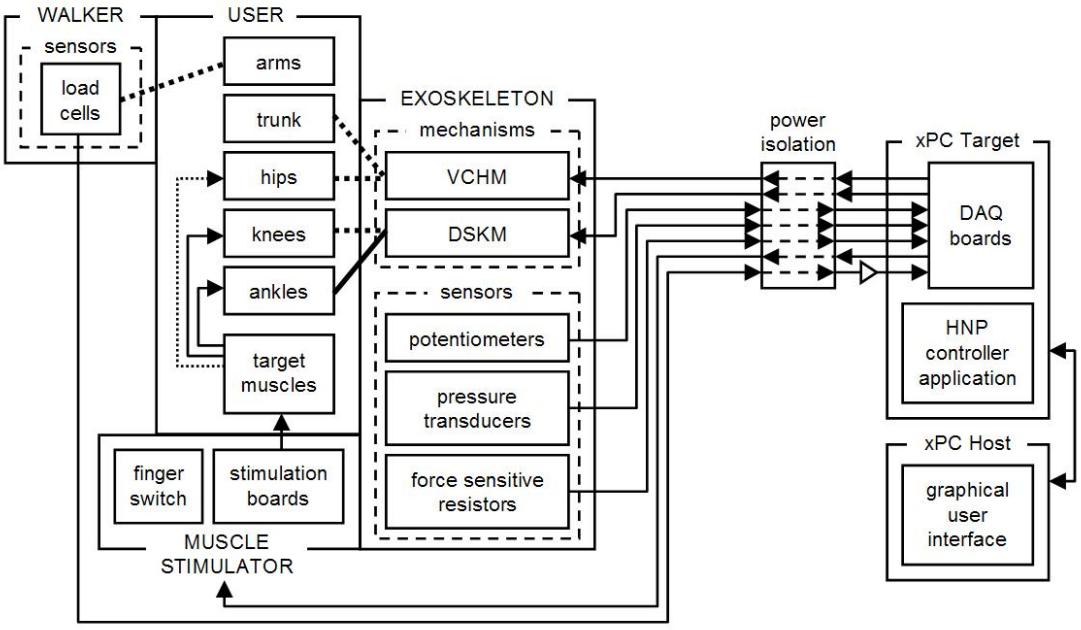

Figure 4.1. Hardware for controller of the HNP consists of xPC target computer, xPC host computer, and the muscle stimulator (Universal External Control Unit).

The host PC is a Windows® (Microsoft Corporation, Redmond, WA, USA) based machine that runs Matlab®/Simulink® and is responsible for building the target application into the target PC and controlling the target application during operation. The host and target computers communicate via the TCP/IP protocol. The host PC runs a graphical user interface (GUI) which was developed to simplify the building, calibration, implementation, and testing of the HNP controller. The GUI (**Figure 4.2**) acts to send commands to and acquire signals from the target PC during real-time implementation. Operation of the HNP is achieved by first pushing the *start* button (which functions as a *stop* button when the application has started) on the GUI. The activity of the user can then be selected in the *Activity* panel. The function of the two buttons in the *Activity*

panel is dependent on the user's current activity. For instance, when the *Sit* button is pushed, the same button changes to a *Stand* button. Thus, once standing, the user only has the option to either sit or walk.

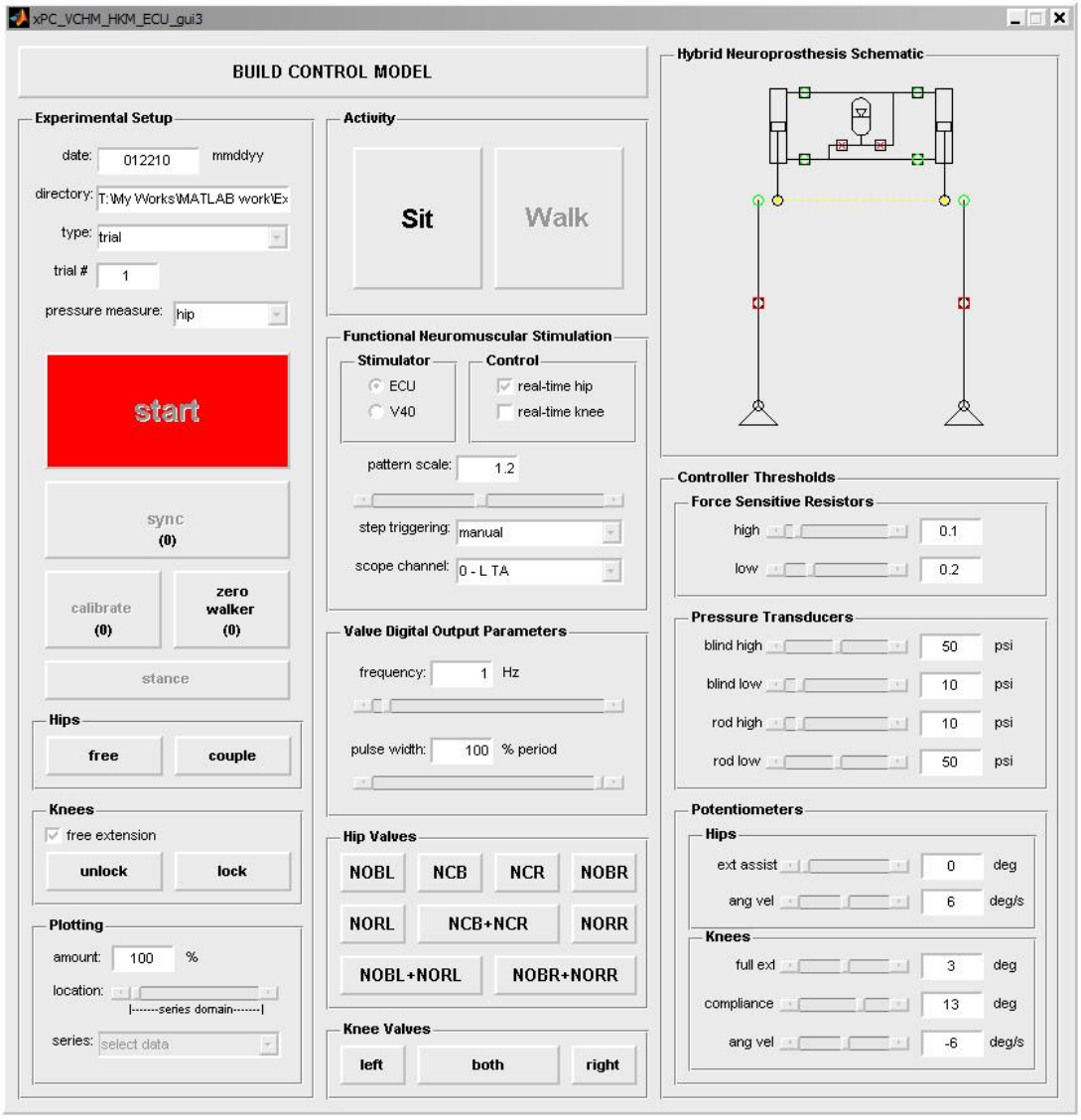

Figure 4.2. Graphical user interface for the HNP controller that runs on the xPC host machine.

Zero calibration of the sensor signals is done by toggling the *calibrate* (for exoskeleton sensors) and *zero walker* (for instrumented walker sensors) buttons. The zero calibration of specific sensor signals is dependent on whether the user is sitting or standing which is

consistent with the selected activity in the *Activity* panel of the GUI. During operation, the *Hybrid Neuroprosthesis Schematic* shows the exoskeleton constraints and solenoid valve states in real-time. The controller thresholds relating to the exoskeleton finite state machines can be tuned during operation. Data are sent from the target PC to the host PC and saved in host PC on a trial-by-trial basis with the GUI by pushing the *stop* button. After each trial is taken, selected data can be immediately plotted with the plot pull down menu in the *Experimental Setup* button panel.

The muscle stimulator unit (**Figure 4.3**), known as the Universal External Control Unit (UECU) was responsible for delivering the functional electrical stimulation to target muscles to drive limb motion. The UECU contains a communication board (5 MHz HC12A4 processor, 1 MB NVRAM, 2 MB flash memory), system board (8 MHz HC12B32 processor, 768 EEPROM, 1 KB RAM, 32 KB flash memory), and two percutaneous stimulation output boards (8 MHz HC12B32 processor, 768 EEPROM, 1 KB RAM, 32 KB flash memory). Each stimulation board is populated with 12 cathodic channels and a single anode. The stimuli from each channel consist of biphasic charge-balanced asymmetric pulses characterized by the PW, IPI, and current amplitude parameters. Since each stimulation board only has one anode, only one channel can output stimulus from each board at any one time. A one millisecond delay was set between the outputs of each channel within each stimulation board. The individual stimulation boards were synchronized with customized software toolkit (Cleveland FES Center Technical Development Laboratory, Cleveland, OH, USA) developed in Simulink® for the UECU. A 20 m Cat-6, 550 MHz patch cable (Black Box Corporation, Lawrence, PA, USA) was used to connect the UECU to the target PC.

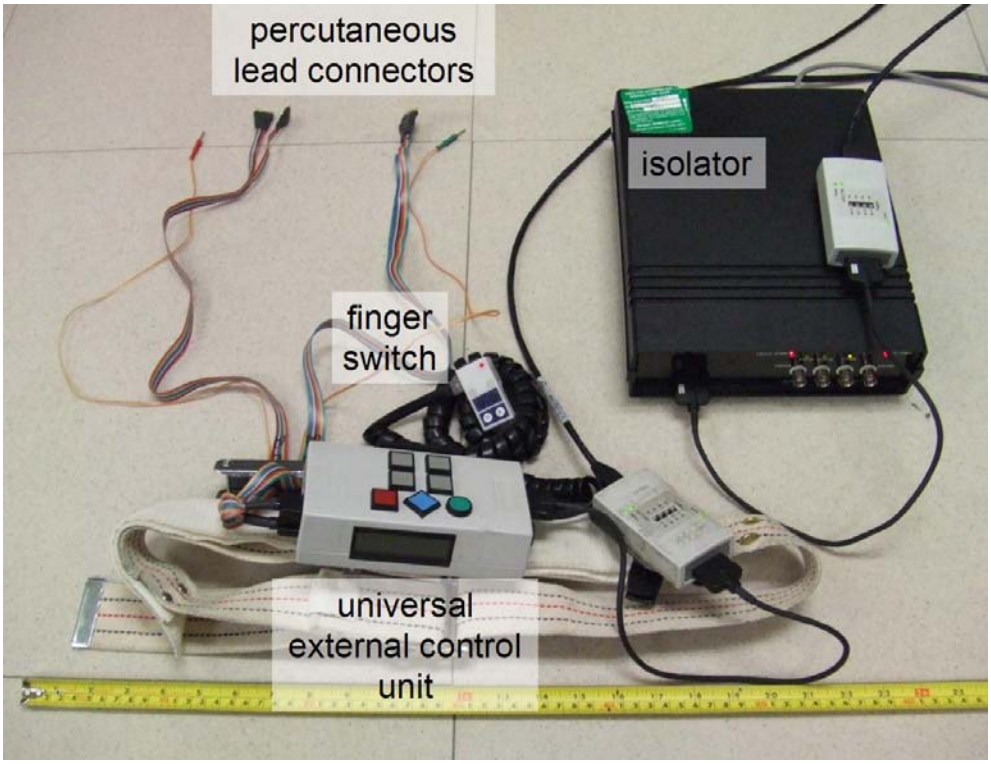

Figure 4.3. Universal External Control Unit (UECU) (Cleveland FES Center Technical Development Laboratory, Cleveland, OH, USA) to deliver stimulus to target muscles.

The target PC sends the instantaneous stimulus parameters (i.e., PW, IPI, and current amplitude) to the UECU via serial communication at 33.33 Hz. The UECU is powered by an internal Sony NP-F570 7.2V – 8.4V lithium ion rechargeable battery pack. With a fully charged battery, the UECU is capable of running continuously for six hours.

4.2.3 User Interface & Operation

The activity states are selected through button polling with a finger switch (**Figure 4.3**) by the user. The finger switch has a GO and a STOP button. A button debounce algorithm incorporated into the controller prevents the switching of activity states from accidental button presses. For a button press to be recognized, a button must

be pressed for at least 60 ms and the time between consecutive button presses must be at least 90 ms. The current stimulation activity state was displayed on the liquid crystal display of the UECU. From a seated position, the user could stand by pressing GO. Once in stance position, the user could choose to either sit back down by pressing STOP or walk by pressing GO. If STOP was pressed to sit, the user will be prompted to press STOP again to initiate the sitting stimulation pattern. If GO was pressed to walk, the stimulation was output to facilitate a left step. The stimulus at the end of the step was maintained until the GO button was pressed again to execute a right step. Subsequent steps were executed by polling GO for each step (manually triggered stepping). The GO button poll was accepted and buffered near the end of each step (> half the step duration) to allow the user to input the command for the next step before the current step had ended. If this was done, the next step was executed immediately after the current step had ended. This was done to facilitate increased cadence at the user's command. Automated stepping, in which succeeding steps were triggered automatically instead of by button poll, could also be performed by selecting this option on the host GUI (**Figure 4.2**). When STOP was pressed during walking, the stimulation pattern would transition into the standing stimulation pattern at the end of the step in which STOP was triggered.

4.3 FNS CONTROLLER VALIDATION PRIOR TO EVALUATION WITH HUMANS

Validation of the FNS controller was conducted prior to the evaluation with individuals paralyzed by SCI to verify the intended operation and that the output stimulus was within safety limits. The output response of the FNS controller was simulated using

the kinematic and exoskeleton constraint data collected from an able-bodied subject walking with the DSKM and VCHM as the inputs to the controller. The baseline stimulation patterns used for the simulation were profiled specifically for an existing participant with paraplegia walking with a 16-channel percutaneous intramuscular FNS-only system. As such, the stimulation patterns have been verified to be capable of producing FNS-only gait dynamics. The able-bodied data were averaged and scaled to the stride duration of the stimulation pattern. The maximum stimulus parameters for each channel were set to the user safety limits. Button polling to trigger each step was programmed to occur automatically, immediately after the completion of each step.

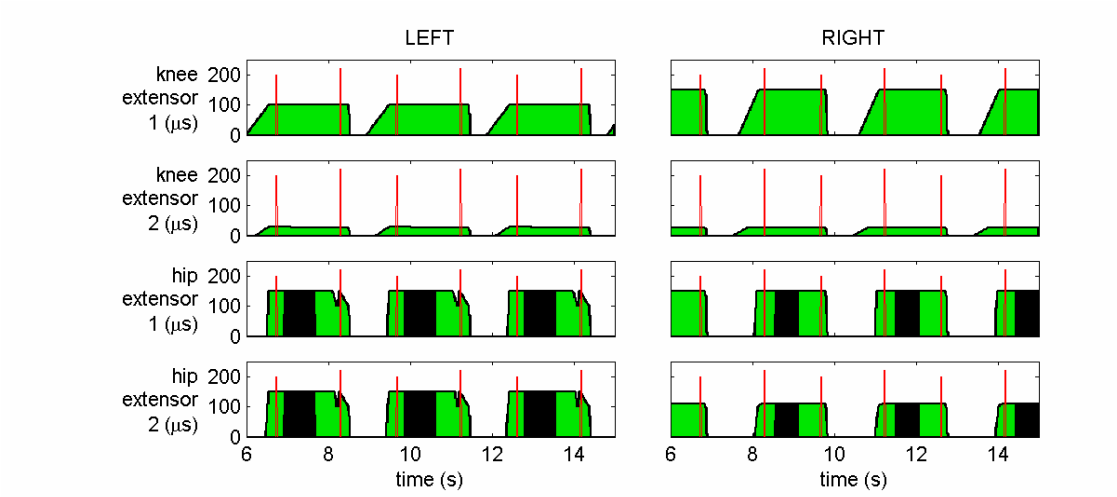

Figure 4.4. Baseline stimulus PW patterns for simulating the FNS controller output. The dark bands are coincident with a stimulus IPI of 30 ms, otherwise the IPI is 60 ms.

Figure 4.4 shows the baseline stimulation patterns for the target hip and knee extensors for the left and right legs with respect to time. Knee extensor 1 and 2 are respectively the vastus medialis and lateralis for the left leg and the vastus intermedius, and lateralis for the right leg. Hip extensors 1 and 2 are respectively the posterior part of the adductor magnus and the gluteus maximus for both legs. The magnitude of the

stimulation patterns is the PW magnitude in μs. The dark bands indicate instances when the stimulus IPI was set to 30 ms, otherwise the IPI was a constant 60 ms. The periodic spikes indicate the automated button poll instances with the higher spike being the poll to trigger a left step.

Figure 4.5 shows all the inputs and outputs of the FNS controller for the left and right legs with respect to time. The inputs of the FNS controller are the exoskeleton constraint states and the hip and knee angles. For the constraint states, the horizontal bars indicate when a joint is either locked against flexion or coupled.

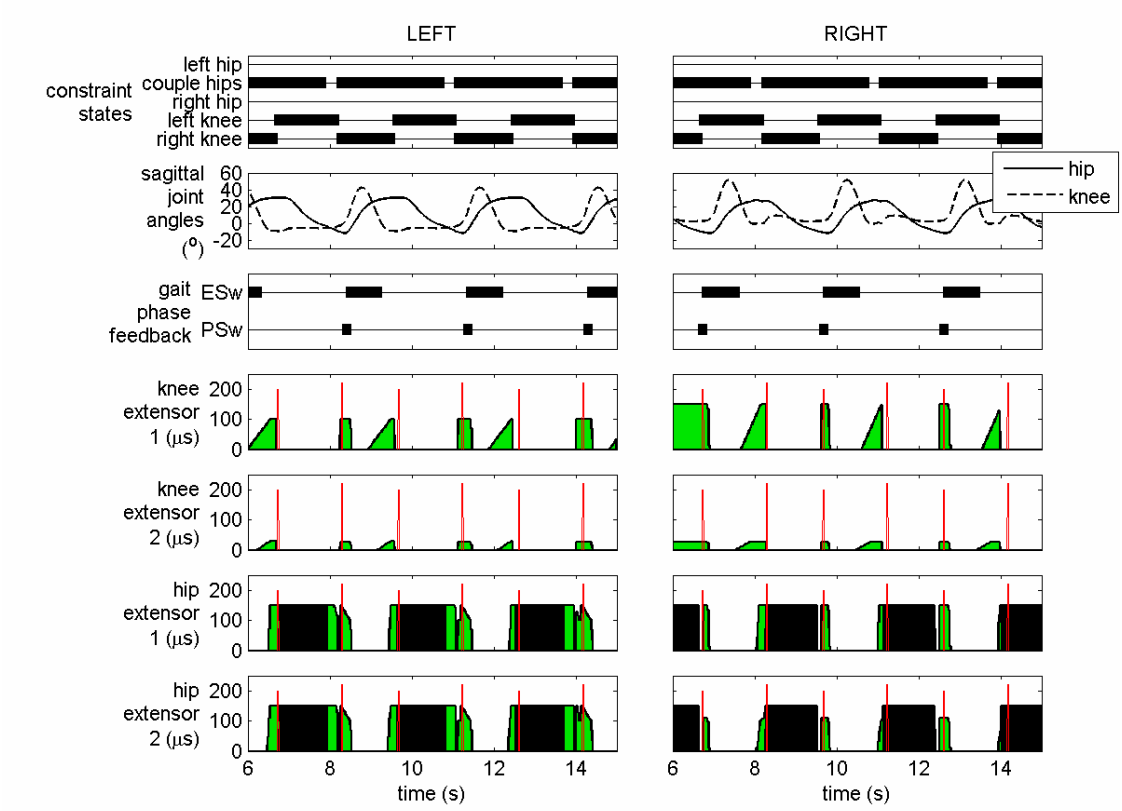

Figure 4.5. Simulated inputs (exoskeleton constraint states and joint angles) and outputs (gait phase feedback and muscle stimulus) of the FNS controller.

The outputs of the FNS controller are the gait phase feedback signals and the knee and hip extensor stimulus parameter patterns. The gait phase feedback signals consist of the

pre-swing (PSw) phase signal and the early swing (ESw) phase signal. Notice that the PSw signal is high (horizontal bar) just before knee flexion, allowing for knee extension to unload the DSKM. The ESw signal is high throughout swing to prevent accidental DSKM locking. Comparing the baseline stimulus patterns in **Figure 4.4** with **Figure 4.5**, the knee extensor stimulus for each knee is deactivated when the corresponding DSKM is locked. In the case of the hip extensors, the stimulus PW for hip extensor 1 and 2 for the left leg and hip extensor 1 for the right leg are already at the maximum PW limit of 150 ms, thus no increase in PW magnitude was observed. However, for these hip extensors the IPI was decreased to 30 ms for a longer duration relative to the baseline IPI. For right hip extensor 2, both PW and IPI were modulated relative to baseline levels. The increase in hip extensor stimulus levels was in response to bilateral hip flexion during single stance when the ipsilateral DSKM was locked. For all the hip extensors a short period of stimulus deactivation occurs just prior to the triggering of the ipsilateral step. Deactivation of the hip extensors is coincident with full hip extension.

4.4 EVALUATION OF THE HNP WITH AN INDIVIDUAL PARALYZED BY SCI

4.4.1 Study participant

One individual with paraplegia was recruited to evaluate the prototype HNP and consented as approved by the institutional review board of the Louis Stokes Cleveland Department of Veterans Affairs Medical Center. The participant was a male, 1.57 m in height, and weighed 70 kg. The participant has a thoracic level SCI at the 9th thoracic vertebrae and was categorized through the American Spinal Injury Association as an

ASIA A class injury, denoting that no motor or sensory function is preserved in the sacral segments. The participant was implanted with 24 percutaneous intramuscular stimulating electrodes which included stimulation channels to target muscles for the hip flexors (tensor fasciae latae, sartorius, and iliopsoas), hip extensors (adductor magnus (posterior), hamstrings, and gluteus maximus) and knee flexors (gracilis and sartorius), knee extensors (vastus medialis, lateralis, and intermedius) and ankle dorsiflexion (tibialis anterior), and ankle plantar flexion (gastrocnemius and soleus). The participant has had over 24 years of experience with this multichannel lower extremity FNS system for exercise and level ground walking [50].

4.4.2 Experimental Control Cases

The objective of this work is to show that an HNP with controllable constraints and closed-loop control incorporates the advantages of both existing brace-only and FNS-only gait systems. Thus, the postural support of the HNP was evaluated relative to that of a standard IRGO. Meanwhile the ability of the HNP to provide for joint mobility was evaluated against that of a FNS-only system.

Figure 4.6 summarizes the experimental setup for testing the participant during IRGO-only gait. Six-axis load cells (AMTI, Inc., Watertown, MA, USA), instrumented to each handle of a walker (**Figure 4.7**), was used to measure the vertical component of the force applied to the walker by the upper extremities during gait. The xPC target and host system was used solely for the data acquisition of the walker load cells. The load cell signals were low-pass filtered online (7^{th}-order Butterworth) at a cut-off frequency of 20 Hz. The load cells were zeroed with the accompanying amplifiers and through the

host GUI periodically throughout the experiment to minimize the contribution of drift in the recorded signals. The solid lines between the exoskeleton mechanisms and the user body/joints indicate fixed constraints, while the dashed line between the uses arms and walker indicate a variable constraint.

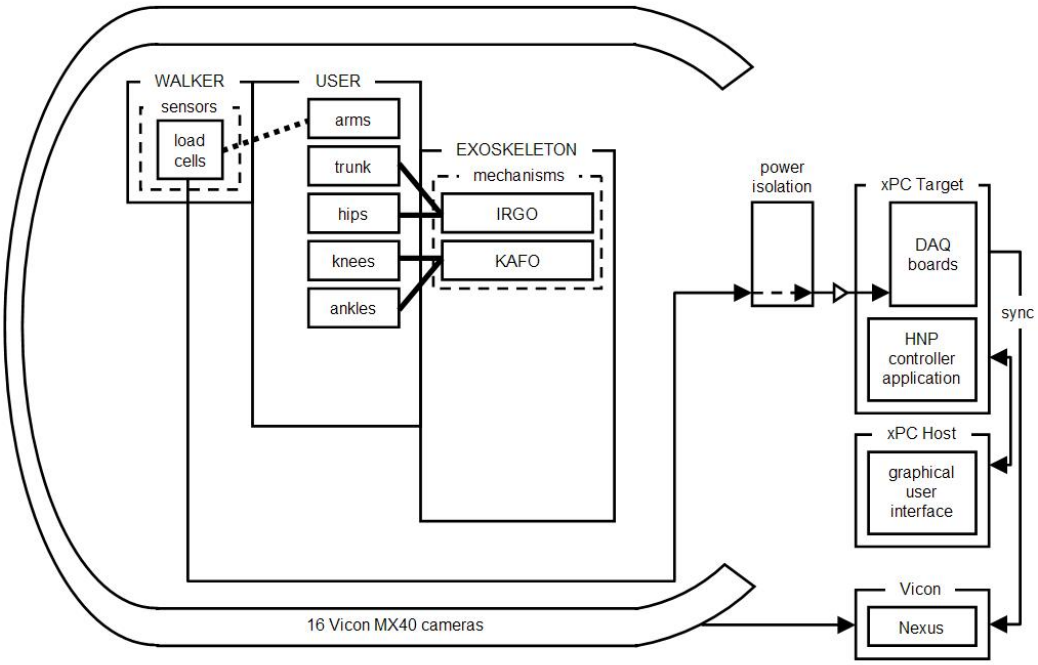

Figure 4.6. Experimental setup for evaluating the IRGO-only gait system with an individual paralyzed by SCI.

To don the custom fitted IRGO, the IRGO was seated on a chair with the hip uprights abducted and the knees flexed. The participant would transfer from his wheelchair to the chair with the proper assistance. Donning of the IRGO consisted of fastening a strap across the lower torso, pelvis, and just below the knee, and wearing the shoes (with the FSRs embedded under the soles of the shoes) over the AFO of the IRGO. A 16-camera Vicon MX40 (Vicon, Inc., Oxford, UK) motion analysis system (sampling at 100 Hz) encompass an eight by three meter work volume. This system recorded the locations of reflective markers placed at key locations on the exoskeleton and/or bony landmarks of

the body. Vicon Nexus software was used for the calibration of the cameras and capture of the marker coordinates. Nineteen markers were placed on the lower extremities and four on the trunk, based on the recommendations specified in [9], but modified to accommodate the presence of the exoskeleton (**Table 4.3**).

Figure 4.7. Instrumented walker with load cells to measure vertical upper extremity forces.

All the markers on the lower extremities were attached to the exoskeleton while markers on the trunk were attached to bony landmarks of the body. These marker locations were used to calculate the trunk and joint kinematics. The offsets to the marker coordinates imposed by the exoskeleton were factored into the kinematic calculations. A digital pulse was sent from the target PC to the Vicon workstation to synchronize the data collected by the separate data acquisition systems.

Table 4.3
Vicon Marker Locations for Experimental Cases

FNS-only	exoskeleton
jugular notch	jugular notch
spinous process of C7 vertebrae	spinous process of C7 vertebrae
left acromio-clavicular joint	left acromio-clavicular joint
right acromio-clavicular joint	right acromio-clavicular joint
posterior superior iliac spine	corset above posterior superior iliac spine
left anterior superior iliac spine	left hip center of rotation
right anterior superior iliac spine	right hip center of rotation
upper lateral 1/3 surface of right thigh	upper lateral 1/3 surface of right thigh upright
lower lateral 1/3 surface of left thigh	lower lateral 1/3 surface of left thigh upright
left lateral epicondyle	left knee center of rotation
right lateral epicondyle	right knee center of rotation
upper lateral 1/3 surface of right shank	upper lateral 1/3 surface of right AFO
lower lateral 1/3 surface of left shank	lower lateral 1/3 surface of left AFO
left lateral malleolus	left ankle center of rotation
right lateral malleolus	right ankle center of rotation
left calcaneous	left calcaneous
right calcaneous	right calcaneous
left 2nd metatarsal head	left 2nd metatarsal head
right 2nd metatarsal head	right 2nd metatarsal head

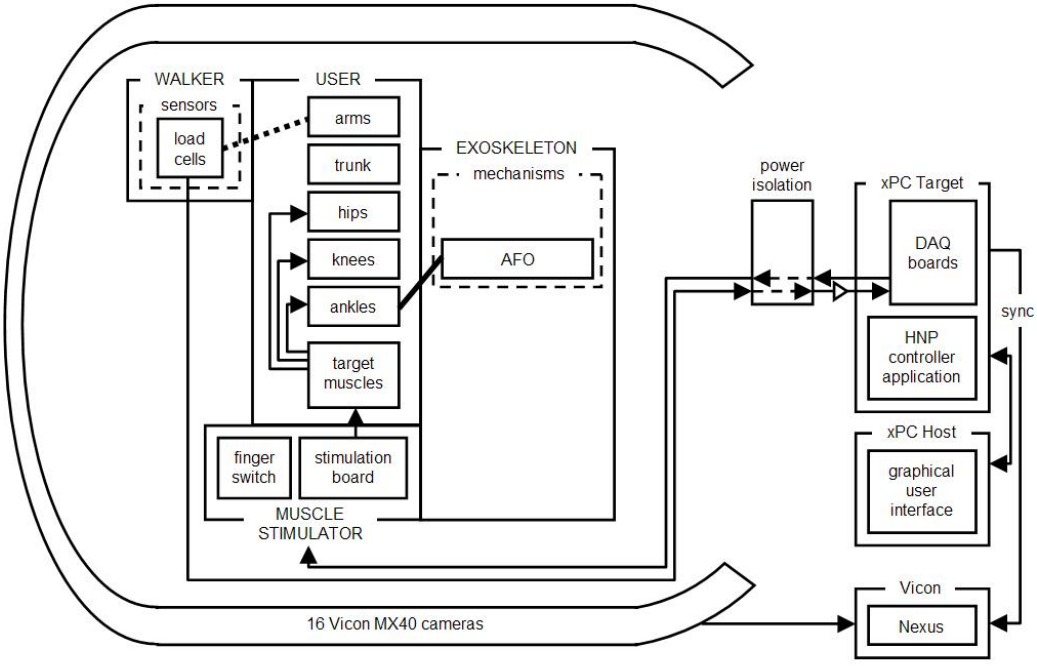

Figure 4.8. Experimental setup for evaluating the FNS-only gait system with an individual paralyzed by SCI.

Figure 4.8 summarizes the experimental setup for testing the participant during FNS-only gait. User-specific muscle stimulation patterns for walking were profiled through rules for generating FNS walking [4]. Stimulation patterns for sitting and standing were profiled heuristically through user feedback. These baseline stimulation patterns were profiled using the VORTEX Stimulation Pattern Editor© (version 3.1b, 1990, by Gregory Borges) and assessed with the participant using the prototype V40 muscle stimulator. The baseline stimulus PW and IPI for walking are respectively shown in **Figure 4.9a** and **4.9b**. These baseline stimulation parameters were then ported over to the HNP controller using custom application (**Figure 4.10**) developed in Matlab®.

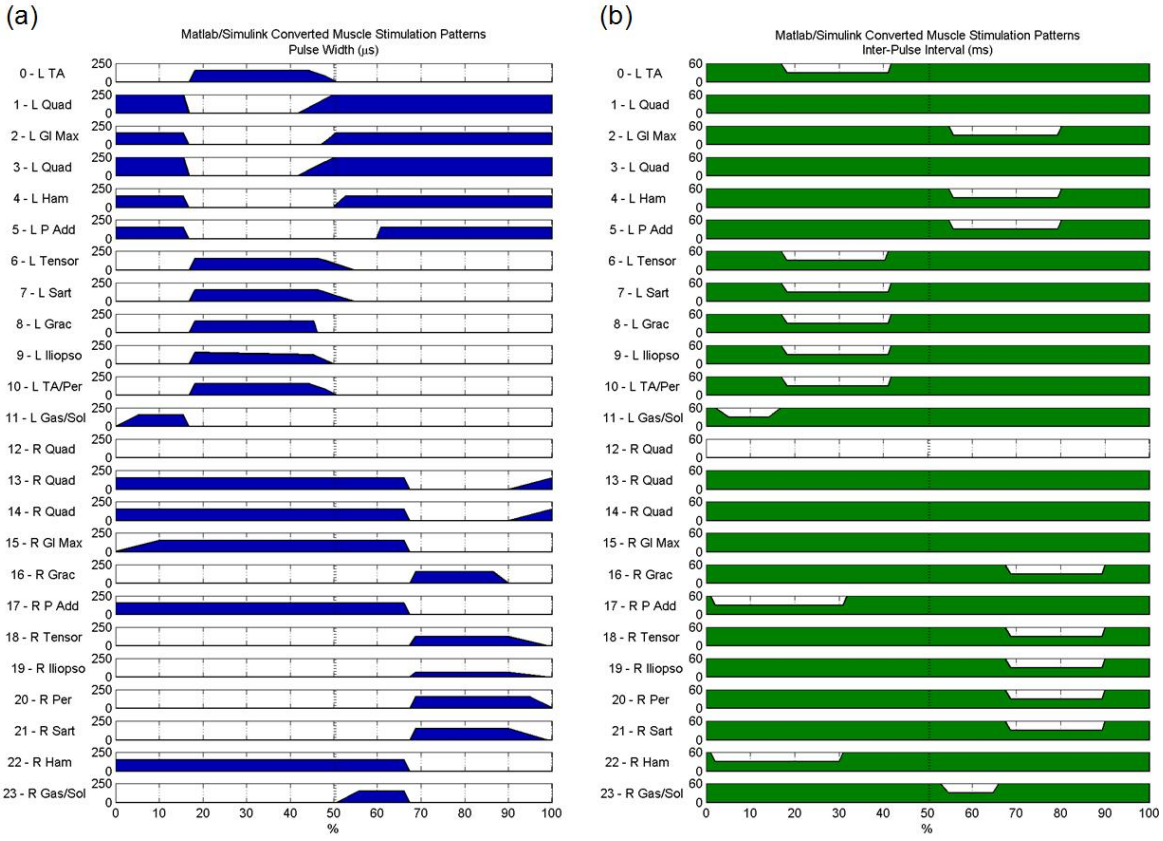

Figure 4.9. User-specific stimulus (a) PW and (b) IPI patterns for the study participant paralyzed by SCI.

The xPC target and host system collected upper extremity force measurements from the walker load cells and sent the baseline stimulation parameters to the UECU which output the open-loop stimulus to target muscles for driving the lower extremity joints. For FNS-only walking, automated stepping was preferred by the participant. The entire stimulation pattern was also scaled by a factor of 1.1 in accordance with the preference of the user.

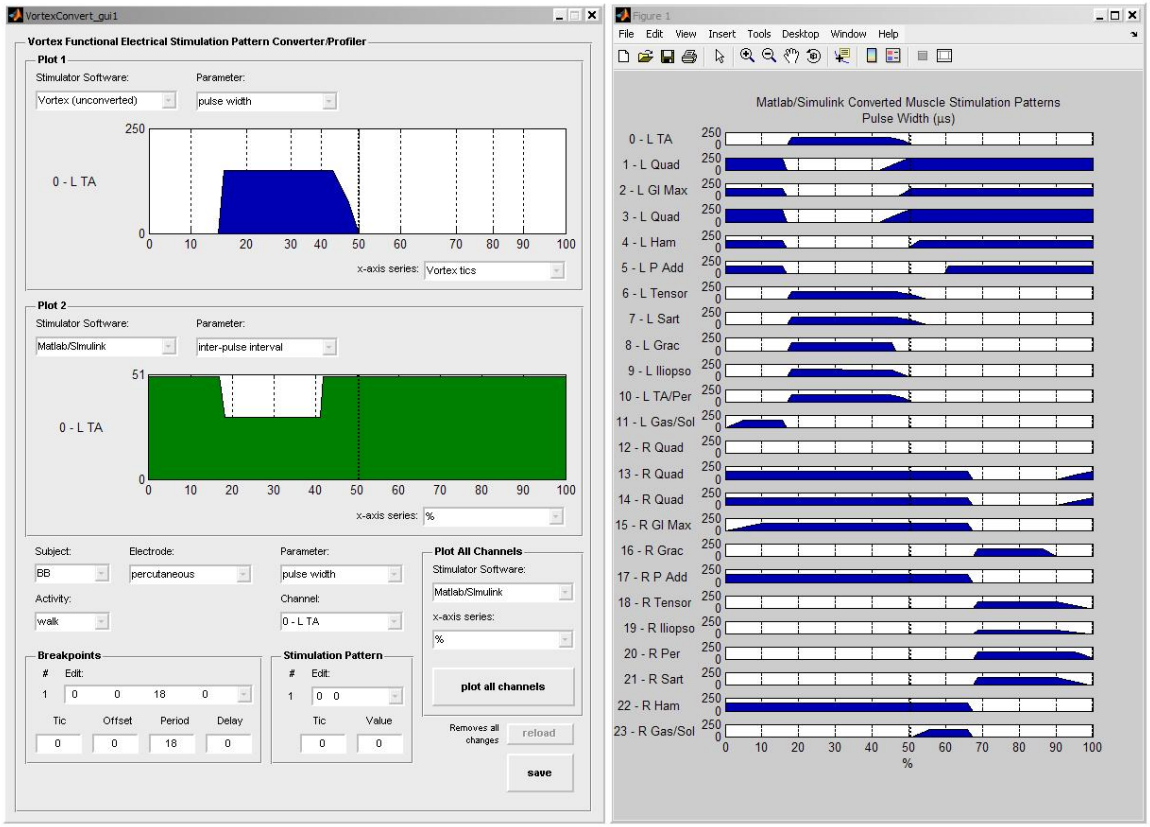

Figure 4.10. Custom software for porting stimulation patterns into FNS controller.

The participant walked with a pair of AFOs to constrained ankle motion to the sagittal plane. The Vicon MX40 system was used to record marker positions on the user as defined by [9] (**Table 4.3**).

For the control cases and subsequent experiments, the participant was instructed to walk a distance of approximately eight meters at his preferred speed for each of six trials. During the experimental trials, spotters remained close to the participant at all times for safety. All data were analyzed and averaged with respect to percentage gait cycle with ± 1 standard deviation. The gait cycle was resolved from heel strike instances which were determined from the local minima of the calcaneous marker coordinates in the vertical axis of the Vicon work volume. Furthermore, the dynamics of each leg were analyzed independently due to the variations between legs in joint passive properties and muscle response to stimulation (i.e., due to differences in muscle fiber types and the exact location of implanted electrode within each muscle). Approximately 25 strides were analyzed for each control case.

4.4.3 Evaluation of the DSKM and Knee FNS Control Module

The objective of the following experiment was to determine if the DSKM can adequately support the user during stance without stimulus to the knee extensors (**Hypothesis 5**). **Figure 4.11** diagrams the experimental setup for evaluating the FNS controller in combination with the DSKM. A pair of DSKMs was installed on an IRGO, custom fitted to the participant, to provide continuous reciprocal hip coupling during the walking trials. Henceforth, this configuration of the HNP will be referred to as HNP-knee. The exoskeleton of the HNP-knee weighed approximately 14.1 kg. The solid lines between the IRGO and the trunk and hip joint in **Figure 4.11** indicate a fixed constraint whereas the dashed line between the DSKM and knee joint indicate a variable constraint. The AFO of the DSKM constrained the ankle joint to neutral in all planes of motion. The

donning procedure of this exoskeleton was identical to that of the IRGO-only. Since the VCHM was not used in this experiment, only the knee FNS control module of the FNS controller was implemented. A solid line between the target muscles and the hip and ankle joints indicate only baseline stimulus patterns were used to activate the muscles for the hip and ankle joints. A dashed line between the target muscles and knee joint indicate that the stimulus to the knee extensors could be modulated from baseline by the FNS controller. When walking with this system, the participant preferred manually triggered stepping, with the baseline stimulation pattern scaled by a factor of 1.5.

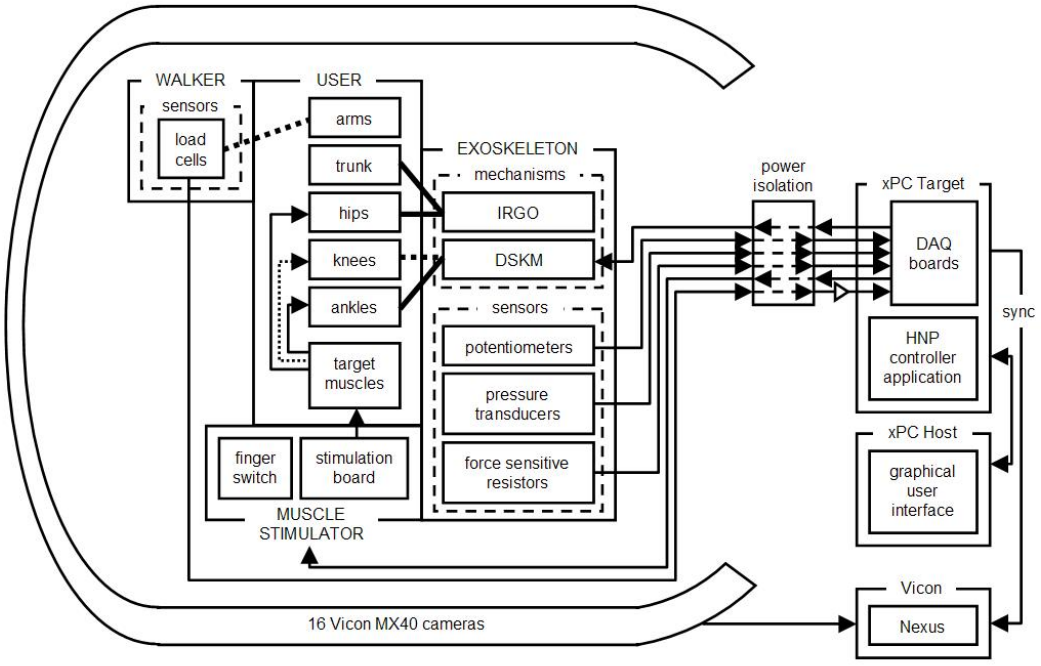

Figure 4.11. Experimental setup for evaluating the HNP-knee, consisting of the IRGO hip reciprocator, a pair of DSKMs, and knee FNS control module, with an individual paralyzed by SCI.

A pressure transducer (Gems Sensors Inc., Plainville, CT, USA) positioned at each side of the valve of the DSKM measured the pressure differential across the valve from which the applied torque on the DSKM was calculated (**Appendix A**). The pressure transducers were low-pass filtered at a cut-off frequency of 20 Hz (7^{th}-order

Butterworth). FSRs (B & L Engineering, Tustin, CA, USA) were placed in the insole to measure foot-to-ground contact information and rotary potentiometers (Vishay Spectrol, Malvern, PA, USA) to measure knee angles were low-pass filtered at a cut-off frequency of 20 Hz (7^{th}-order Butterworth) and 10 Hz (5^{th}-order Butterworth) respectively. The FSRs were zero calibrated by unloading the feet while the participant was in a seated position. The potentiometers and pressure transducers were zero calibrated while the participant was in a quiet standing position, held by FNS, with the DSKMs unlocked. Zero calibration of the sensors lasted for a period of five seconds. Vicon reflective markers were placed on the upper torso and exoskeleton as shown in **Table 4.3**.

To evaluate the supportive abilities of the DSKM, random walking trials were conducted with the knee FNS control module either enabled (HNP-knee1) or disabled (HNP-knee2). In the trials with the disabled FNS controller, the baseline stimuli to the knee extensors were not modulated. Approximately 25 strides were analyzed for each experimental case. The mean, minimum, and maximum of each recorded signal were determined for within each stride. Analysis of variance with 95 % confidence ($p < 0.05$) determined statistical significance between experimental and control cases.

4.4.3.1 Validation of the DSKM

Hyporthesis 5: *The DSKM can adequately support the user during gait, such that the gait dynamics observed with stimulation to the knee extensors deactivated is comparable to those observed with baseline knee extensor stimulation*. **Figure 4.12** shows the average knee angle, percentage of samples that the knee extensor stimulus deactivated and DSKM unlocked, and calculated flexion torque applied the DSKM with respect to percentage gait cycle for the left (L) and right (R) limbs of the participant

impaired by SCI. The solid and dashed curves for each signal are respectively from HNP-knee1 and HNP-knee2.

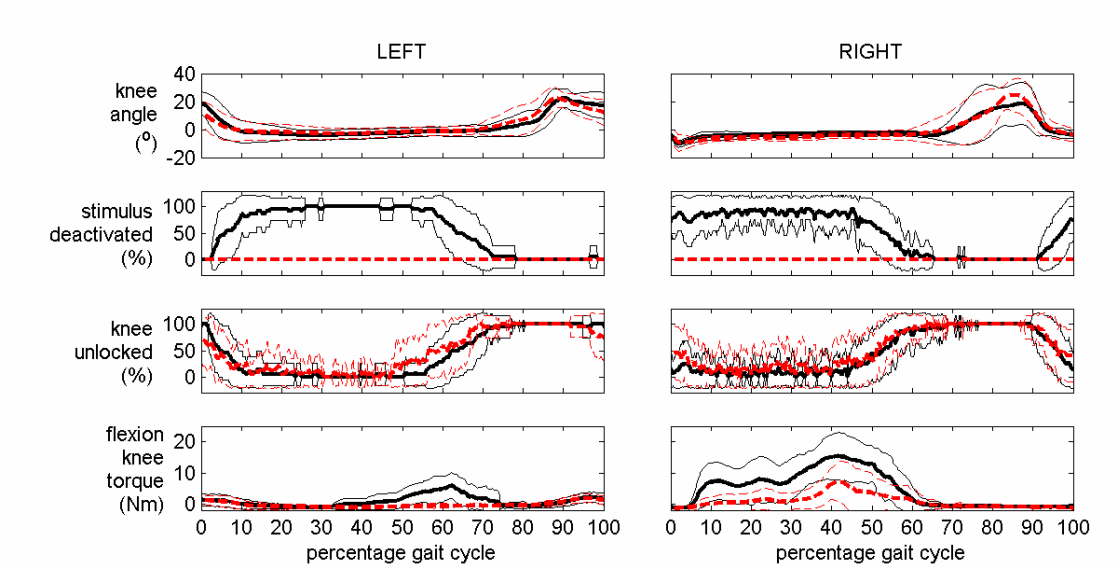

Figure 4.12. The average knee angle, percentage of samples of knee extensor stimulus deactivation and DSKM unlocking, and calculated flexion torque applied to the DSKM with respect to percentage gait cycle for the left and right limbs for HNP-knee1 (solid) and HNP-knee2 (dashed).

With the FNS controller enabled the stimulus to the knee extensors was deactivated whenever the DSKM locked the knee against flexion. Note that no IPI modulation from the FNS controller was observed. This means that FNS was consistently able to drive the knee into full extension at the end of swing before foot contact onto the ground, further implying that the passive resistance and the weight of the DSKM did not significantly interfere with ability of the FNS to extend the knee.

The stimulation activity applied to the target knee extensors was further assessed by quantifying the average number of pulses, electrical charge injected, and muscle duty cycle with respect to a stride for the cases of baseline stimulation and stimulation modulated by the knee module of the FNS controller (**Table 4.4**). In **Table 4.4**, channels 1 and 3 correspond to electrodes stimulating the left quadriceps, while channels 13 and

14 correspond to electrodes stimulating the right quadriceps. The muscle duty cycle is the duration of time in which the target muscle is activated by the electrical stimulation relative to the total duration of the stride.

Table 4.4
Effect of Knee Module of the FNS Controller
on Baseline Stimulus Activity of the Knee Extensors

muscle channel→ parameter↓		**1 and 3**	**13 and 14**
number of pulses per stride	baseline	130 (23)	136 (19)
	controller	38 (4)	47 (17)
	C/B (%)	29.83 (5.05)	34.17 (8.03)
	p-value	0.0000	0.0000
electric charge (μC/stride)	baseline	625.18 (113.78)	391.28 (57.04)
	controller	168.04 (20.59)	127.74 (52.03)
	C/B (%)	27.51 (4.97)	31.81 (8.61)
	p-value	0.0000	0.0000
muscle duty cycle (%)	baseline	84.34 (2.05)	86.19 (1.80)
	controller	25.10 (3.92)	29.53 (7.39)
	C/B (%)	29.83 (5.05)	34.17 (8.03)
	p-value	0.0000	0.0000

- Refer to **Figure 4.9** for the target muscle corresponding to the listed channel number.
- C/B = percentage of stimulation modulated by FNS controller relative to baseline stimulation
- The number indicated in parentheses is one standard deviation.
- The p-value was determined using ANOVA between the baseline and controller for each parameter.

The muscle duty cycle was calculated by summing the durations of individual stimulus pulse trains within the stride and dividing this sum by the total duration of the stride. The charge injected to the muscle per stride was calculated by summing the pulse widths of individual pulses within the stride and multiplying this sum by the stimulus current amplitude (20 mA). In this regard, the duty cycle is invariant to changes in

stimulus frequency, whereas the electrical charge is sensitive to changes in stimulus frequency since it is a function of the number of stimulus pulses. The percentage of stimulation activity of the FNS controller (C) relative to baseline (B) for each parameter in **Table 4.4** is represented as C/B. For instance, with the FNS controller, an average of 38 pulses was counted per stride for muscle channels 1 and 3, while for baseline stimulation, an average of 130 pulses were counted for the same channels. The C/B was determined to be 29.83 %. This means that the number of pulses per stride of the FNS controller was 29.83 % of the baseline stimulation. With the knee FNS control module (HNP-knee1), the number of pulses, injected charge to the target knee extensors, and stimulation duty cycle per stride and was reduced to 27 % to 34 % of the baseline stimulation. For each parameter in **Table 4.4**, the difference between the FNS controller and baseline were statistically significant as indicated by the listed p-values.

Table 4.5 shows the absolute duration of the duty cycle for each muscle group. The average duration of the strides with the HNP-knee1 was 4.586 seconds. Thus, with the FNS controller, stimulation was applied to the both muscle groups for an average duration of less than 1.5 s/stride, allowing over 3 s/stride for the muscles to rest. Accordingly, with the FNS controller, the percentage of stimulation activity relative to inactivity (ON/OFF) was between 34 % and 43 %. If baseline stimulation was used, the average duration of stimulation activity would be approximately 4 s/stride for both the left and right quadriceps. With baseline stimulation, the ON/OFF was between 548 % and 635 %. These results indicate that with a knee mechanism that is capable of constraining the knee in full extension during stance, the stimulation activity to target knee extensors could be significantly reduced relative to baseline levels. This reduction

in stimulation activity has the potential of delaying the onset of fatigue in the target muscle.

Table 4.5
Effect of Knee Module of the FNS Controller
on Absolute Duty Cycle Durations of the Knee Extensors

muscle channel→ parameter↓		1 and 3	13 and 14
duration stimulation ON (s)	baseline	3.899 (0.692)	4.081 (0.576)
	controller	1.138 (0.130)	1.424 (0.520)
duration stimulation OFF (s)	baseline	0.710 (0.049)	0.643 (0.017)
	controller	3.471 (0.690)	3.300 (0.271)
ON/OFF (%)	baseline	548.29 (84.14)	635.52 (96.18)
	controller	33.83 (6.99)	43.45 (16.04)

- Refer to **Figure 4.9** for the target muscle corresponding to the listed channel number.
- The number indicated in parentheses is one standard deviation.

Between the two experimental cases, the flexion torque applied to the DSKM was consistently larger (L: p = 0.0000; R: p = 0.0000) when the FNS controller was enabled since the knee extensor FNS was deactivated. The average maximum torque for HNP-knee1 was observed to be 9.0 Nm at 60 % gait cycle and 19.8 Nm at 38 % gait cycle respectively for the left and right knee. Even though knee extensor stimulation was deactivated for the majority of stance, the compliance measured in the DSKM during instances when the DSKM locked the knee against flexion was not statistically different between HNP-knee1 and HNP-knee2 (L: p = 0.2916; R: p = 0.3563), with the average DSKM compliance being less than 1^{o} for both sides in both cases (**Table 4.6**). The ROMs of the knee angles were statistically similar between experimental cases (L: p = 0.8321; R: p = 0.2390), with the average maximum knee flexion being approximately 28^{o} (L) and 36^{o} (R) when the FNS controller was enabled. **Table 4.7** lists the average sagittal

ROMs of the trunk, hips, and knees for both experimental cases with the control cases. A single standard deviation taken among all strides analyzed is indicated in the parentheses.

Table 4.6
DSKM Locking Compliance

case	average (°) (1 SD)		maximum (°)	
	L	R	L	R
HNP-knee1	0.34 (0.84)	0.89 (1.55)	4.89	8.15
HNP-knee2	0.49 (0.66)	0.78 (1.16)	3.67	8.16

Table 4.7
HNP-Knee Sagittal Ranges of Motion

case		minimum (°) (1 SD)		maximum (°) (1 SD)		ROM (°) (1 SD)	
		L	R	L	R	L	R
HNP-knee1	trunk	-4.32 (1.34)		10.28 (2.39)		14.60 (2.59)	
	hip	-16.47 (2.50)	-12.61 (2.61)	17.76 (2.74)	22.97 (2.98)	34.22 (3.21)	35.58 (3.67)
	knee	-5.96 (3.54)	-11.05 (2.21)	28.12 (3.98)	35.94 (5.29)	34.08 (2.72)	46.98 (5.93)
HNP-knee2	trunk	-2.42 (2.88)		11.38 (2.49)		13.80 (2.85)	
	hip	-13.23 (2.92)	-12.08 (2.91)	18.64 (3.46)	21.58 (3.32)	31.87 (3.76)	33.66 (3.72)
	knee	-5.52 (2.14)	-11.02 (2.29)	28.11 (5.06)	33.32 (6.16)	33.63 (4.27)	44.34 (6.77)
IRGO-only	trunk	-9.04 (3.00)		9.46 (2.64)		18.51 (3.96)	
	hip	-17.97 (4.92)	-19.66 (3.53)	18.92 (6.67)	16.91 (3.63)	36.89 (7.25)	36.58 (4.24)
	knee	8.86 (2.42)	0.53 (1.61)	16.50 (1.63)	7.75 (1.72)	7.64 (2.81)	7.22 (1.67)
FNS-only	trunk	12.80 (3.29)		24.33 (1.44)		11.52 (4.06)	
	hip	-3.63 (4.06)	3.08 (5.34)	74.15 (11.33)	73.40 (4.25)	77.78 (12.73)	70.32 (7.56)
	knee	-8.40 (3.65)	-4.52 (4.42)	63.86 (5.29)	83.09 (4.10)	72.26 (5.31)	87.61 (6.29)

Figure 4.13 shows the trunk orientation and total vertical force exerted by the upper extremities on the walker, represented as percentage body weight (% BW) plotted

relative to right gait cycle. The exoskeleton of the HNP was designed to be self supportive. To show the absolute contribution of the HNP to the overall reduction of the upper extremity effort, the weight of the exoskeleton was not added to the participant's body weight when normalizing the upper extremity forces. The average maximum trunk orientation ($p = 0.1302$) and upper extremity effort ($p = 0.2452$) were similar between both cases, with the average maximum trunk tilt and upper extremity force for HNP-knee1 being 10^{o} and 54 % BW respectively.

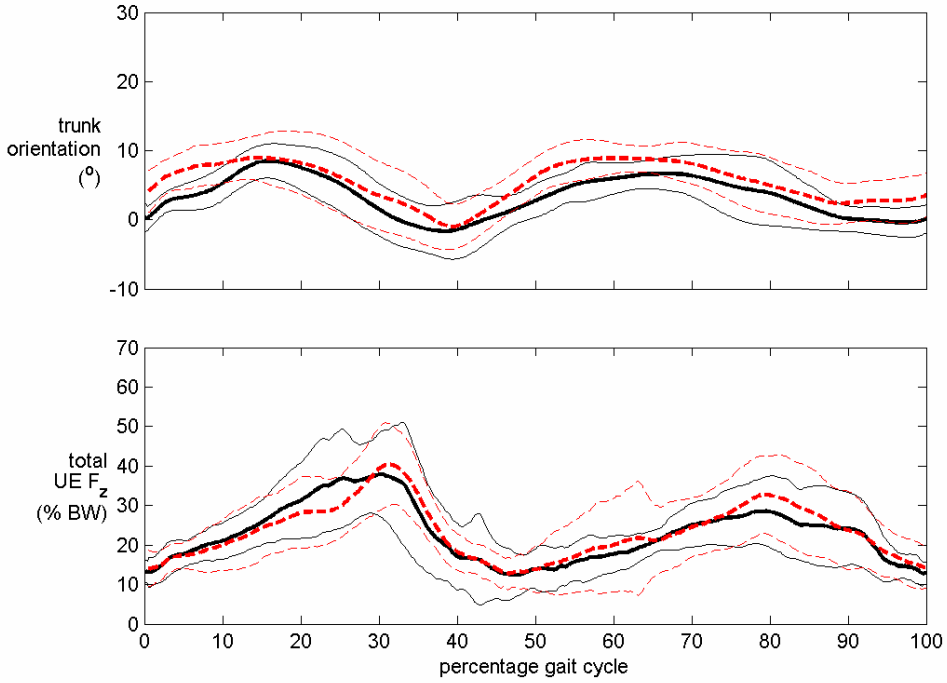

Figure 4.13. The average trunk orientation and upper extremity forces on the walker represented as percentage body weight (% BW) plotted relative to right gait cycle for HNP-knee1 (solid) and HNP-knee2 (dashed).

Table 4.8 shows the gait parameters for both HNP-knee cases compared to the IRGO and FNS-only controls. Between HNP-knee1 and HNP-knee2, there were no differences ($p > 0.05$) observed between individual gait parameters. These results

support **Hypothesis 5** by showing that there were no significant differences in the gait dynamics between the cases when the stimuli to the knee extensors were either deactivated or continuously applied during the stance phase of gait. This indicates that the DSKM can adequately support the user during stance without knee extensor stimulation.

Table 4.8
HNP-Knee Gait Parameters

case	**speed (m/s) (1 SD)**	**cadence (steps/s) (1 SD)**		**step length (m) (1 SD)**	
		L	R	L	R
HNP-knee1	0.142 (0.131)	0.408 (0.259)	0.536 (0.153)	0.228 (0.089)	0.364 (0.089)
HNP-knee2	0.125 (0.192)	0.525 (0.188)	0.614 (0.97)	0.240 (0.094)	0.343 (0.090)
IRGO-only	0.117 (0.241)	0.515 (0.283)	0.606 (0.148)	0.238 (0.103)	0.305 (0.122)
FNS-only	0.425 (0.266)	0.913 (0.263)	0.816 (0.508)	0.410 (0.074)	0.417 (0.124)

4.4.3.2 Gait with the HNP versus Control Cases

The following examines the differences in gait dynamics between the HNP-knee1, consisting of the combined use of the IRGO, DSKM, and knee FNS control module, and the FNS-only and IRGO-only control cases. **Figure 4.14** show the average trunk orientation and upper extremity forces of the HNP-knee1 (solid) plotted with IRGO-only (dashed-dotted) and FNS-only (dashed). As expected, the average maximum forward trunk tilt was similar between the HNP-knee1 and IRGO-only cases ($p = 0.2146$). However, the sagittal trunk ROM of the HNP-knee1 was 21 % ($p = 0.0001$) less than that of the IRGO-only. A smaller trunk ROM indicates less upper extremity motion necessary to stabilize the trunk which further indicates that less work was being done by the upper extremities. Accordingly, the average upper extremity forces were different between these two cases ($p = 0.0000$), with average and average maximum forces for the

HNP-knee1 being 17 % and 30 % less than those of the IRGO-only case, respectively. The average trunk orientation for the HNP-knee1 was 3^{o} relative to 19^{o} for FNS-only ($p = 0.0000$). The average upper extremity forces for the HNP-knee1 were 36 % less than the FNS-only ($p = 0.0000$), however, average maximum forces were similar ($p = 0.5016$). These results indicate that the HNP-knee1 reduces upper extremity load on the walking aid observed in both IRGO-only and FNS-only gait.

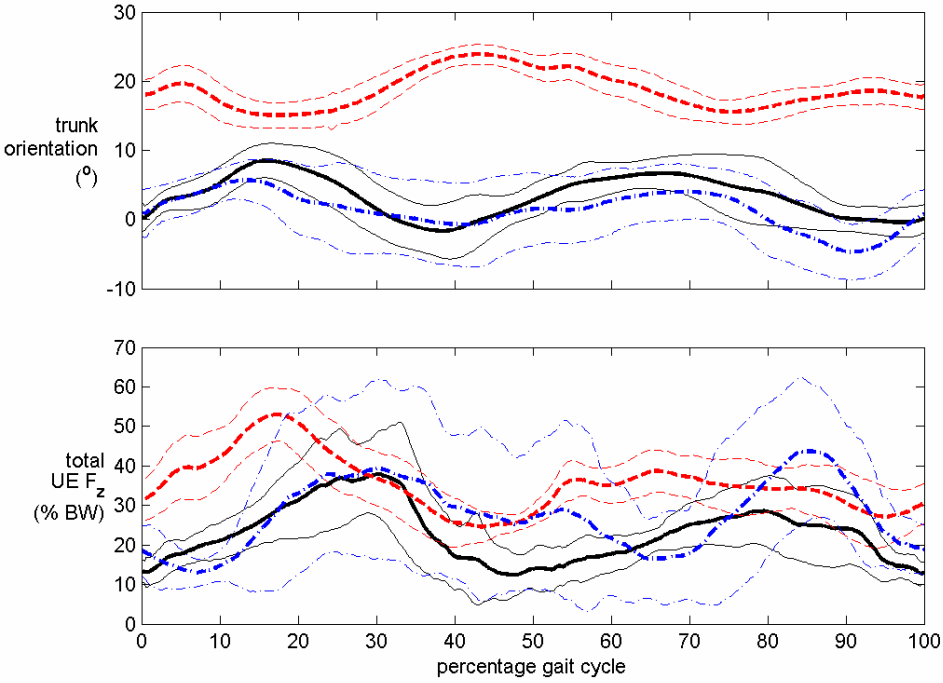

Figure 4.14. The average trunk orientation and upper extremity forces on the walker represented as percentage body weight (% BW) plotted relative to right gait cycle for the HNP-knee1 (solid) and FNS-only (dashed) and IRGO-only (dashed-dotted).

When walking with an IRGO-only system there is a tendency to apply high impulsive loads on the walking aid to allow for foot-to-ground clearance. The HNP-knee1 reduces the need for these impulse loads by allowing for knee flexion during swing. Conversely, when walking with a FNS-only system a more continuous load was

applied to the walking aid to stabilize the trunk. The HNP-knee1 reduces this continuous loading of the walking aid through the action of the hip reciprocator of the IRGO, which provides anterior/posterior as well as medial-lateral trunk support.

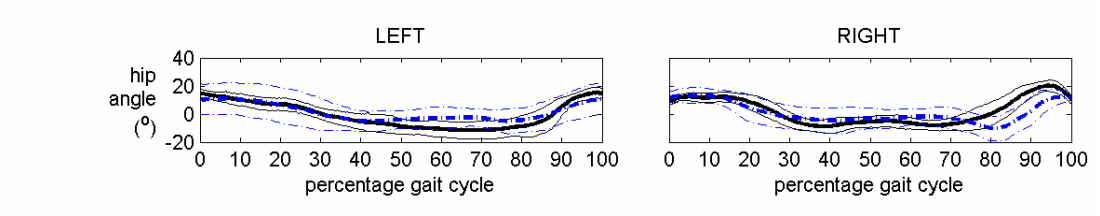

Figure 4.15. The average hip angles for HNP-knee1 (solid) and IRGO-only (dashed-dotted).

Figure 4.15 shows the average hip angles of the HNP-knee1 (solid) plotted with the IRGO-only case (dashed-dotted). The average maximum achievable hip flexion for the HNP-knee1 was approximately 18^{o} (L) and 23^{o} (R). For the IRGO-only, the average maximum hip flexion was 19^{o} (L) and 17^{o} (R), with the right side being statistically different than that of the HNP-knee1 ($p = 0.0000$). Since an IRGO was used in the HNP-knee1, this would suggest that the combination of FNS and knee flexion during swing was beneficial in increasing right side hip flexion. This increase in hip flexion lead to slight but insignificant increases in cadence (L: $p = 0.7889$; R: $p = 0.0874$), step length (L: $p = 0.2250$; R: $p = 0.2261$), and stride length ($p = 0.2737$), however a significant increase in gait speed ($p = 0.0172$) was found.

Figure 4.16 shows the average hip and knee angles of the HNP-knee1 (solid) plotted with the FNS-only case (dashed). Recall that for the HNP-knee1 the participant preferred to walk with manually triggered stepping, whereas in the FNS-only experiments the user preferred automatically triggered stepping. For automatically triggered stepping, the durations of the stance and swing phases are defined by the pre-programmed stimulation pattern. With manually triggered stepping there was generally a delay

between steps. This delay has the effect of increasing the duration of the stance phase of gait relative to the swing phase.

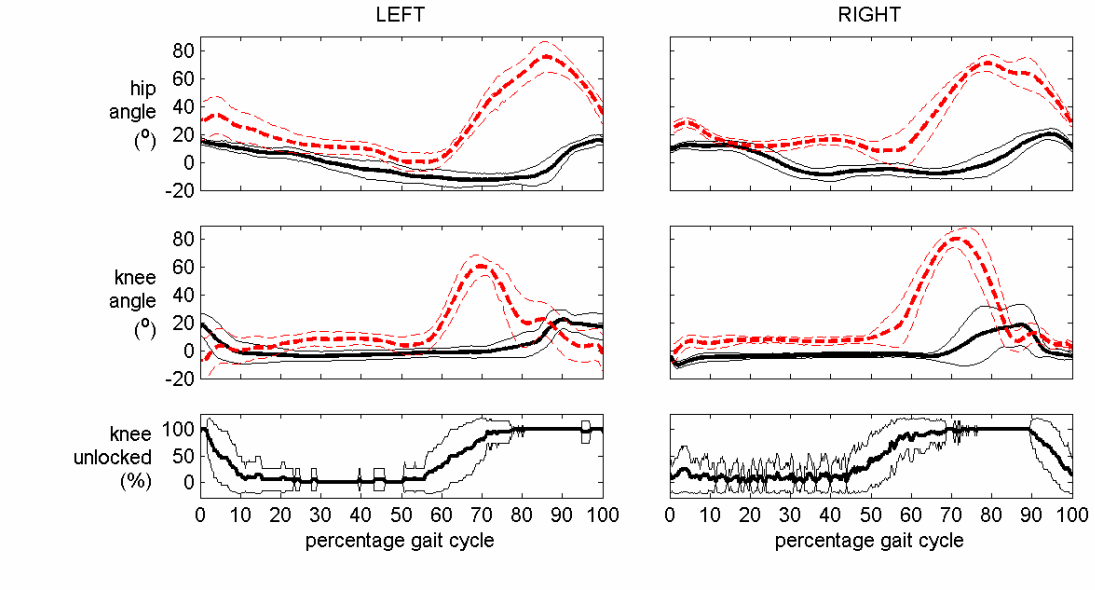

Figure 4.16. The average hip and knee angles for HNP-knee1 (solid) and FNS-only (dashed).

Thus, in **Figure 4.16** there is the appearance that the swing phase of the HNP-knee1 case is shorter and delayed relative to the FNS-only case since the joint trajectories are plotted relative to percentage gait cycle. The swing phase durations between cases are in fact identical, as defined by the pre-programmed stimulation pattern. The stance phase duration for the HNP-knee1 case is longer than that of the FNS-only case and thus ends later in the gait cycle. At 74^{o} (L) and 73^{o} (R), the average maximum hip flexion angles of the FNS-only case are significantly greater than those of the HNP-knee1 (L: $p = 0.0000$; R: $p = 0.0000$) since the HNP-knee1 the used a hip reciprocator. Similarly, the average maximum knee flexion during FNS-only walking (L: 64^{o}; R: 83^{o}) is significantly greater than that of the HNP. The limited hip flexion of the HNP-knee1 in combination with the use of a larger stimulation pattern scaling factor (i.e., slower progression through the

pattern) and manually triggered stepping resulted in the significantly reduced gait parameters relative to the FNS-only case (**Table 4.8**).

4.4.4 Evaluation of the VCHM and Hip FNS Control Module

The results presented in **Section 4.4.3** indicate that an HNP-knee1 utilizing the DSKM, knee FNS control module, and a hip reciprocator from an IRGO, can significantly reduce the vertical upper extremity force applied to the walker relative to the IRGO-only and FNS-only systems. However, the IRGO hip reciprocator had a 1:1 HFECR, which limited hip flexion and resulted in low gait parameters relative to FNS-only gait. In this section, the fixed hip reciprocator of the HNP was replaced with the VCHM and combined with the hip FNS control module and DSKM. This configuration of the HNP will be referred to as the HNP-hip. The exoskeleton of the HNP-hip weighed approximately 22.2 kg. The objectives were 1) to evaluate if the VCHM can stabilize the trunk (**Hypothesis 1**), resulting in reduced upper extremity exertion on the walking aid relative to the IRGO-only (**Hypothesis 2**) and FNS-only systems, 2) while simultaneously allowing for functional stepping dynamics (**Hypothesis 3** and **4**), and 3) to determine if the hip FNS control module can facilitate comparable gait dynamics to baseline FNS levels (**Hypothesis 6**).

Figure 4.17 diagrams the experimental setup for testing a HNP-hip. This setup is identical to that for testing the DSKM and knee FNS control module (**Figure 4.11**) except for the following. First, the VCHM variably constrains the trunk and hip joints instead of the fixed constraint of the IRGO. Second, stimulation to target hip extensors can be modulated from baseline. In the following experiment, the knee FNS control

module was not implemented. The VCHM utilized slide potentiometers for position control and pressure transducers and FSRs for force control. Signal filtering and zero calibration procedures were identical to those described in **Section 4.4.3**. In the case of zero calibrating the potentiometers and pressure transducers of the VCHM, both hydraulic rotary actuators of the VCHM were freed to unload the mechanism prior to sensor calibration. Thus, during sensor zeroing, the participant was held in quiet standing by FNS and upper extremity loading on the walker. The participant preferred manual triggered stepping, with the baseline stimulation pattern scaled by a factor of 1.2. Walking trials were randomized between an HNP with the hip FNS controller enabled (HNP-hip1) and disabled (HNP-hip2: baseline stimulus). Approximately 25 strides were analyzed for each test case.

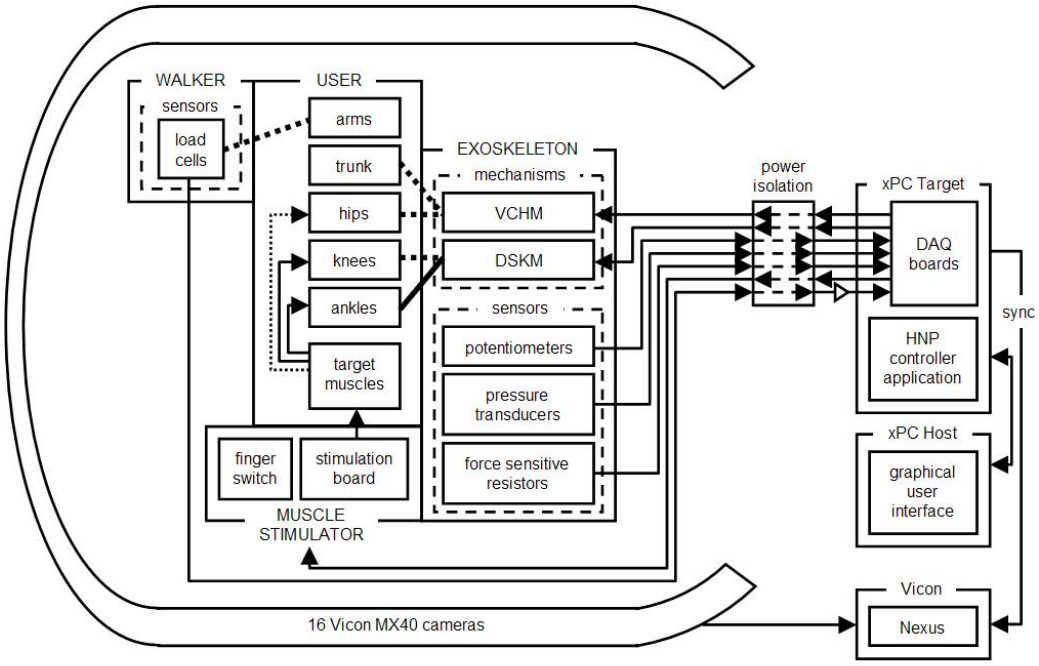

Figure 4.17. Experimental setup for evaluating the HNP-hip, consisting of the VCHM, a pair of DSKMs, and hip FNS control module, with an individual paralyzed by SCI.

4.4.4.1 Validation of the VCHM and Hip FNS Control Module

Hyporthesis 6: *The synchronous implementation of the VCHM and closed-loop control of FNS to target hip extensors will provide improved gait dynamics relative to the utilization of baseline hip extensor stimulation*. **Figure 4.18** shows the average hip angle, percentage of samples that the hip extensor stimulus deactivated, IPI modulation occurred, hip locked, hips uncoupled, and the calculated torque applied the VCHM with respect to percentage gait cycle. The solid and dashed curves for each signal are from the HNP-hip1 and HNP-hip2 trials, respectively.

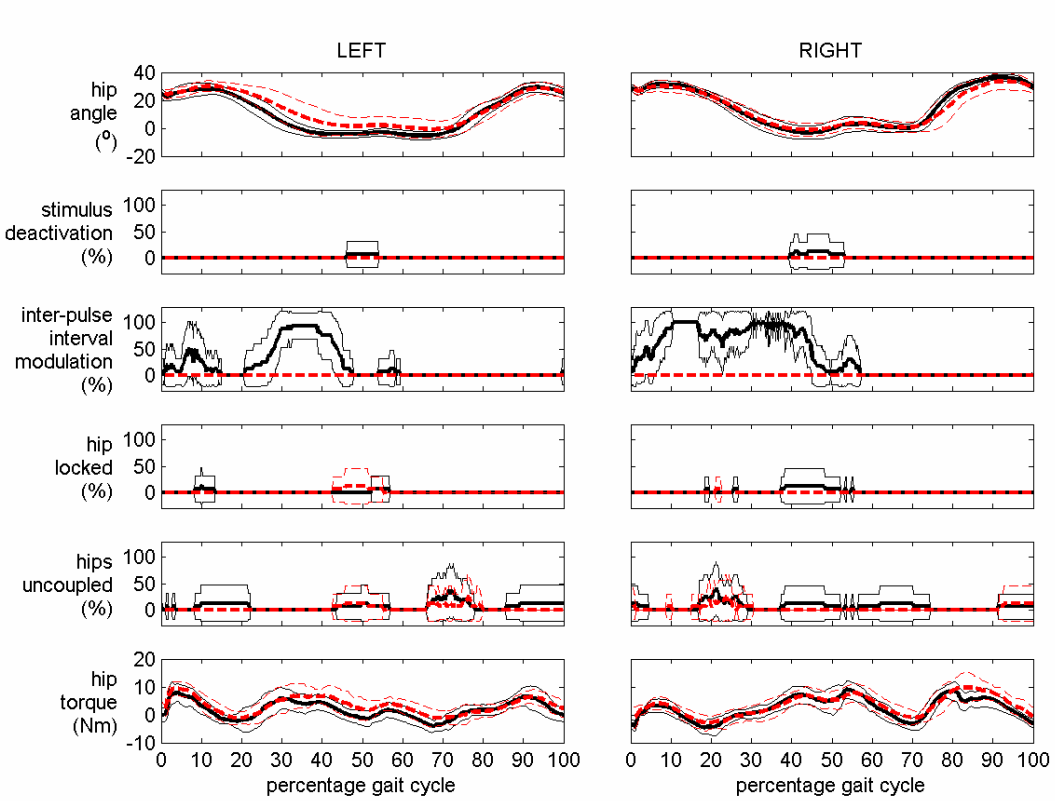

Figure 4.18. The average hip angle, percentage of samples of hip extensor stimulus deactivation, IPI modulation, hip locking, hip uncoupling, and calculated torque applied to the VCHM with respect to percentage gait cycle for HNP-hip1 (solid) and HNP-hip2 (dashed).

For HNP-hip1, hip extensor stimulation was deactivated between 40 % and 60 % of the gait cycle at end of the stance phase when the hip was fully extended for both sides. The

percentage of samples that the stimulation deactivated was relatively low. The hip FNS control module deactivated the hip extensors at most 6 % of the time on the left and 12 % of the time on the right. IPI modulation, which constituted the net increase of stimulation frequency from 16.67 Hz (IPI = 60 ms) to 33.33 Hz (IPI = 30 ms), occurred during stance for both sides of HNP-hip1. IPI modulation occurred more often on the right side, peaking at 100 % from 11 % to 17 % of the gait cycle. This was due to the fact that the baseline stimulus IPI for the right gluteus maximus was set at a constant 60 ms allowing for modulation to take place (**Figure 4.9**). The baseline stimulus IPIs for other hip extensors such as the adductor magnus, hamstrings, and left gluteus maximus were already set for the lower limit of 30 ms for half the duration of the stance phase. Similarly, no stimulus PW modulation occurred due to the fact that the baseline stimulus PW for all hip extensors were already profiled to their maximum safety limits.

In order to further examine the effects that the hip FNS control module has on the stimulation activity of the target hip extensor muscles relative to baseline stimulation levels, the number of pulses per stride, electrical charge injected into each muscle, and the muscle duty cycle were determined (**Table 4.9**). Due to the low prevalence of stimulation deactivation coupled with the increases in stimulus frequency during stance, the number of pulses per stride and charge injected to the target hip extensors (refer to **Figure 4.9** for the corresponding muscle for each channel), with the hip FNS control module (HNP-hip1), were significantly larger than baseline levels. With exception to channel 15, the number of pulses and injected charge with the FNS controller was approximately 20 % greater than baseline levels. For channel 15 (right gluteus maximus), the number of pulses and injected charge were almost 50 % greater than

baseline. This was because the baseline stimulus frequency for channel 15 was pre-programmed at a constant 16.67 Hz. When more hip extension torque was needed as determined from the hip kinematics and VCHM constraint state, the stimulation frequency of channel 15 could be increased to 33.33 Hz. For the other hip extensors, increases in stimulus frequency occurred less due to the maximum baseline levels. Thus, increases in the number of pulses and injected charge of channel 15 relative to baseline was greater than that experienced in the other hip extensors ($p = 0.0000$) since there was more opportunity for the FNS controller to increase the stimulus frequency of channel 15.

Table 4.9
Effect of Hip Module of the FNS Controller
on Baseline Stimulus Activity of the Hip Extensors

muscle channel→ parameter↓		**2**	**4**	**5**	**15**	**17**	**22**
number of pulses per stride	baseline	45 (6)	45 (6)	37 (5)	30 (2)	47 (3)	47 (3)
	controller	53 (6)	53 (6)	41 (6)	44 (4)	56 (5)	56 (5)
	C/B (%)	117.86 (2.72)	118.34 (2.89)	121.27 (2.85)	149.54 (10.63)	118.21 (5.91)	120.27 (5.86)
	p-value	0.0005	0.0004	0.0010	0.0000	0.0000	0.0000
electric charge (μC/stride)	baseline	134.44 (16.91)	117.21 (15.89)	99.71 (16.00)	82.75 (5.00)	138.89 (8.38)	137.37 (8.87)
	controller	158.58 (18.17)	140.70 (16.71)	120.80 (16.42)	122.40 (9.99)	164.75 (14.79)	165.83 (14.93)
	C/B (%)	118.09 (2.77)	120.24 (2.01)	121.48 (2.90)	148.06 (10.70)	118.53 (6.00)	120.65 (5.96)
	p-value	0.0005	0.0003	0.0009	0.0000	0.0000	0.0000
muscle duty cycle (%)	baseline	74.21 (2.79)	72.60 (2.86)	53.90 (4.31)	60.50 (2.93)	76.21 (2.41)	76.16 (2.57)
	controller	72.99 (3.80)	71.47 (3.77)	52.99 (5.34)	57.53 (4.00)	74.65 (4.39)	75.11 (4.34)
	C/B (%)	98.33 (2.81)	98.44 (2.83)	98.19 (4.15)	95.16 (5.87)	97.95 (4.56)	98.62 (4.53)
	p-value	0.3070	0.3509	0.5975	0.1900	0.2102	0.3967

- Refer to **Figure 4.9** for the target muscle corresponding to the listed channel number.
- C/B = percentage of stimulation modulated by FNS controller relative to baseline stimulation
- The number indicated in parentheses is one standard deviation.
- The p-value was determined using ANOVA between the baseline and controller for each parameter.

In **Table 4.9**, the C/B of muscle duty cycle for all the muscles indicate a slight yet insignificant reduction in duty cycle of the FNS controller relative to baseline. This is

due to the low instances of hip extensor deactivation during the end of stance when the hip FNS control module was implemented. The similarities in the duty cycle between controller and baseline are also reflected in the average absolute durations of stimulus activity and inactivity (**Table 4.10**). The average stride duration for HNP-hip1 was 3.005 seconds. Depending on muscle channel, the average duration of stimulation activity for both controller and baseline range from 1.6 to 2.2 s/stride. The average duration of stimulation inactivity for both controller and baseline range from 0.7 to 1.4 s/stride. Since there was minimal deactivation of the hip extensor stimulation by the FNS controller, these variations in the duration of stimulation activity and inactivity are more apparent among channels (due to the differences in the profiled baseline pattern of each channel) than between the FNS controller and baseline. Accordingly, the percentage of stimulation activity relative to stimulation inactivity, ON/OFF, ranged broadly between 115 % and 320 %.

Table 4.10
Effect of Hip Module of the FNS Controller
on Absolute Duty Cycle Durations of the Hip Extensors

muscle channel→ parameter↓		**2**	**4**	**5**	**15**	**17**	**22**
duration stimulation ON (s)	baseline	2.243 (0.343)	2.195 (0.340)	1.635 (0.324)	1.777 (0.103)	2.242 (0.173)	2.241 (0.182)
	controller	2.208 (0.359)	2.163 (0.355)	1.608 (0.340)	1.690 (0.143)	2.197 (0.212)	2.211 (0.213)
duration stimulation OFF (s)	baseline	0.770 (0.049)	0.818 (0.049)	1.379 (0.093)	1.163 (0.133)	0.698 (0.068)	0.699 (0.068)
	controller	0.805 (0.075)	0.8506 (0.072)	1.405 (0.117)	1.249 (0.147)	0.743 (0.121)	0.729 (0.119)
ON/OFF (%)	baseline	292.63 (48.96)	269.14 (43.86)	119.03 (24.14)	154.45 (18.26)	323.88 (37.83)	323.65 (41.42)
	controller	277.24 (55.35)	256.51 (49.23)	115.45 (26.32)	137.25 (20.25)	303.86 (57.83)	311.49 (59.92)

- Refer to **Figure 4.9** for the target muscle corresponding to the listed channel number.
- The number indicated in parentheses is one standard deviation.

The results indicate that increases in stimulation frequency to the target hip extensors through the hip FNS control module significantly increased the charge injected to the muscle relative to baseline levels. This increase in charge is not expected to cause tissue damage due to the prescribed safety limits in the stimulation frequency [4]. Furthermore, the minimally observed stimulation deactivation did not significantly decrease the duty cycle of the hip extensors.

Hip locking against flexion occurred infrequently throughout stance for both cases. However, for HNP-hip1, hip locking tends to be coincident with stimulus deactivation. This was expected as hip flexion may result when there is no hip extension moment to support the user due to hip extensor inactivity. The VCHM would lock to prevent any hip flexion during stance. Hip uncoupling tended to occur more often for HNP-hip1 than HNP-hip2. For HNP-hip2, hip uncoupling occurred mostly during late stance and early swing of the left side, corresponding to late swing and early stance of the right side. For HNP-hip1, hip uncoupling occurred infrequently throughout the entire gait cycle, peaking between 30 % to 40 % at 70 % of the left gait cycle and 20 % of the right gait cycle. Hip uncoupling during swing reduces the resistance contributed by the contralateral limb and passive resistance of the VCHM (refer to **Chapter 3**), thus allowing for a larger hip flexion ROM.

The hip torque was calculated from the recorded pressure data and VCHM transmission geometry (**Appendix A**). The average torques (**Figure 4.19**) with the FNS controller active were between 37 % (L) and 28 % (R) smaller than those with pre-programmed stimulation patterns (L: $p = 0.0166$; R: $p = 0.0465$). At 10 Nm the average maximum torque for HNP-hip1 was 17 % lower on the left side ($p = 0.0333$) than HNP-

hip2. However, at 12 Nm, the average maximum torque between HNP-hip1 and HNP-hip2 were similar on the right side (p = 0.3736). A positive flexion hip torque was coincident with either a hip being locked against flexion or the hips being coupled. Thus, a flexion torque indicates that the VCHM is acting to support the user. Since there were more instances of hip uncoupling for HNP-hip1, the VCHM was resisting the user less and thus, there was less torque applied to the VCHM than HNP-hip2.

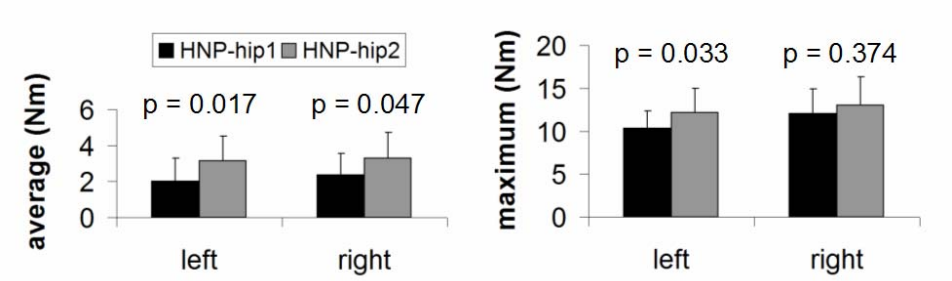

Figure 4.19. The average and average maximum calculated torque applied to the VCHM.

Table 4.11 lists the ROMs for the trunk, hip, and knee joints for both cases. The average ROM for the hip angle for HNP-hip1 (L: 37°; R: 41°) is 10 % larger than that of HNP-hip2 for both sides (L: p = 0.0448; R: p = 0.0385). This is attributed primarily to increased hip extension (L: p = 0.0091; R: p = 0.1937). **Table 4.12** shows the gait parameters for both cases. The average gait speed of HNP-hip1 is faster than HNP-hip2 (p = 0.0246), due to increased right side step length (p = 0.0486).

Figure 4.20 shows the trunk orientation and total vertical forces exerted by the upper extremities on the walker, represented as percentage body weight (% BW) with respect to the right gait cycle. As in **Section 4.4.3**, the weight of the exoskeleton was not added to the user's weight when normalizing the upper extremity forces. No differences were observed in the average trunk orientation (p = 0.4596) and average maximum trunk orientation (p = 0.4678) between cases. For the average upper extremity forces, HNP-

hip1 was 6 % greater than HNP-hip2 (p = 0.0058). However, no statistical difference (p = 0.0965) was found for the average maximum upper extremity forces.

Table 4.11
HNP-Hip Sagittal Ranges of Motion

case		minimum (°) (1 SD)		maximum (°) (1 SD)		ROM (°) (1 SD)	
		L	R	L	R	L	R
HNP-hip1	trunk	4.27 (2.03)		19.49 (1.98)		15.22 (2.32)	
	hip	-6.86 (2.85)	-3.95 (4.05)	30.18 (3.69)	36.62 (2.10)	37.04 (4.17)	40.58 (4.18)
	knee	-5.59 (2.85)	-10.69 (5.77)	42.46 (6.34)	45.71 (9.61)	48.05 (4.64)	56.40 (6.41)
HNP-hip2	trunk	5.29 (2.62)		18.89 (2.72)		13.60 (3.22)	
	hip	-2.38 (6.02)	-2.22 (3.52)	31.30 (3.27)	34.55 (5.22)	33.68 (5.18)	36.77 (5.94)
	knee	-5.06 (3.95)	-3.78 (7.70)	39.74 (5.50)	49.88 (5.32)	44.80 (7.29)	53.66 (7.10)
IRGO-only	trunk	-9.04 (3.00)		9.46 (2.64)		18.51 (3.96)	
	hip	-17.97 (4.92)	-19.66 (3.53)	18.92 (6.67)	16.91 (3.63)	36.89 (7.25)	36.58 (4.24)
	knee	8.86 (2.42)	0.53 (1.61)	16.50 (1.63)	7.75 (1.72)	7.64 (2.81)	7.22 (1.67)
FNS-only	trunk	12.80 (3.29)		24.33 (1.44)		11.52 (4.06)	
	hip	-3.63 (4.06)	3.08 (5.34)	74.15 (11.33)	73.40 (4.25)	77.78 (12.73)	70.32 (7.56)
	knee	-8.40 (3.65)	-4.52 (4.42)	63.86 (5.29)	83.09 (4.10)	72.26 (5.31)	87.61 (6.29)

Table 4.12
HNP-Hip Gait Parameters

case	speed (m/s) (1 SD)	cadence (steps/s) (1 SD)		step length (m) (1 SD)	
		L	R	L	R
HNP-hip1	0.291 (0.161)	0.681 (0.072)	0.702 (0.060)	0.394 (0.057)	0.437 (0.079)
HNP-hip2	0.252 (0.155)	0.601 (0.134)	0.700 (0.106)	0.394 (0.043)	0.348 (0.135)
IRGO-only	0.117 (0.241)	0.515 (0.283)	0.606 (0.148)	0.238 (0.103)	0.305 (0.122)
FNS-only	0.425 (0.266)	0.913 (0.263)	0.816 (0.508)	0.410 (0.074)	0.417 (0.124)

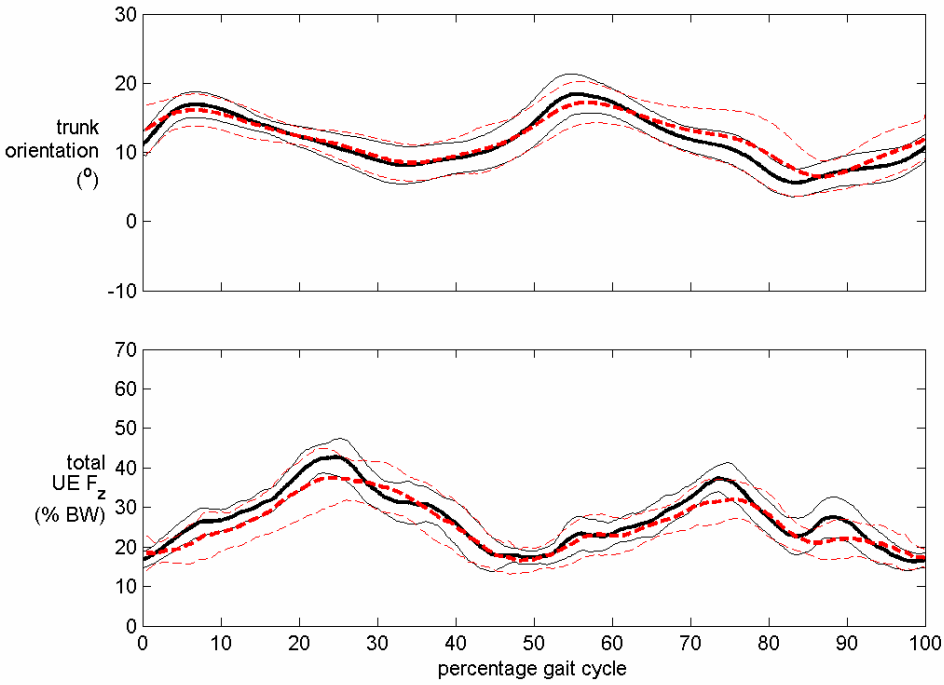

Figure 4.20. The average trunk orientation and upper extremity forces on the walker represented as percentage body weight (% BW) plotted relative to right gait cycle for case HNP-hip1 (solid) and case HNP-hip2 (dashed).

The above results can be summarized as follows. The VCHM does assist in preventing anterior trunk tilt as observed from the applied flexion torque on the system. Hip uncoupling instances were more prevalent for HNP-hip1 relative to HNP-hip2. This may be due to the decrease in stimulus IPI to the hip extensors in HNP-hip1, which would drive the hips further into extension. However, decreasing the stimulus IPI (i.e., increasing stimulus frequency) may expedite the onset of muscle fatigue [4]. The VCHM responds to full stance limb hip extension by uncoupling the hips. This would allow the contralateral swing hip to flex more. This can be justified from the fact that the flexion torque applied to the VCHM for HNP-hip1 was significantly less than HNP-hip2. As a result, the hip ROM for HNP-hip1 was found to be significantly greater than that for

HNP-hip2. Accordingly, the gait speed of HNP-hip1 was higher relative to HNP-hip2. Thus, HNP-hip1 provided improved gait kinematics over HNP-hip2 despite small increases to the upper extremity kinetics.

4.4.4.2 Gait with the HNP versus Control Cases

This section examines **Hypotheses 1**, **2**, **3**, and **4** proposed in **Chapter 1**. Accordingly, the gait dynamics of the HNP-hip1 were compared to those observed in IRGO-only and FNS-only gait. Once again, HNP-hip1 consists of the VCHM, DKSM, and hip FNS control module, whereas the HNP-knee1, evaluated in **Section 4.4.3**, combined the DSKM, knee FNS control module, and 1:1 hip reciprocator. **Figure 4.21** shows the study participant taking a complete stride for each experimental case.

Hypothesis 1: *The trunk orientation of individuals with SCI walking with the prototype HNP is comparable to walking with a RGO*. **Figure 4.22** show the average trunk orientation and upper extremity forces of the HNP-hip1 (solid) plotted with IRGO-only (dashed-dotted) and FNS-only (dashed). **Figure 4.23** summarizes the average and average maximum trunk orientation for the IRGO-only, FNS-only, HNP-knee1, and HNP-hip1 cases. The trunk orientation for the HNP-hip1 was on average 10^{o} ($p = 0.0000$) more anterior than the IRGO-only case. This additional amount of forward trunk tilt may be due to a combination of VCHM compliance and the existence of minimal forward trunk tilt during sensor zero calibration. However, a modest amount of forward trunk tilt does no mean that the VCHM is not supporting the user's posture. As shown in **Figure 4.18**, a flexion torque is applied on the VCHM throughout gait indicating that the VCHM is resisting against the forward trunk tilt. For the IRGO-only, an average trunk

orientation of 1.3^{o} is due to the posterior movement of the trunk to force the stance hip into extension. On average, the trunk tilted up to 9.0^{o} posteriorly.

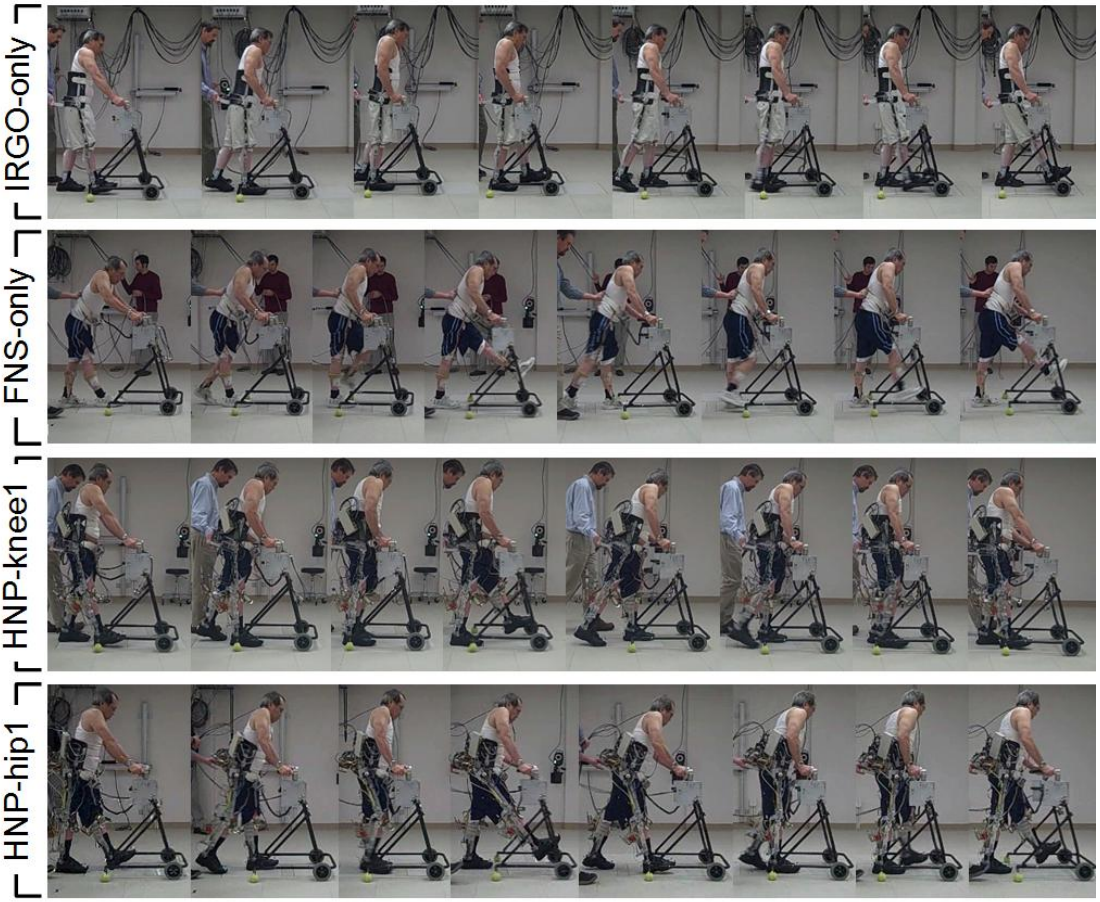

Figure 4.21. A representative stride taken by the study participant for each experimental case.

With an average maximum trunk anterior trunk tilt of 9.5^{o}, the average ROM of the trunk during IRGO-only gait is 18.5^{o}. Since the upper extremities are responsible for the dynamic stabilization of the trunk, the amount of motion of the trunk is related to the amount of work performed by the upper extremities. The average ROM in the HNP-hip1 case is approximately 15.2^{o}, 18% less than the IRGO-only case ($p = 0.0004$). This was also consistent with what was observed in the HNP-knee1 case.

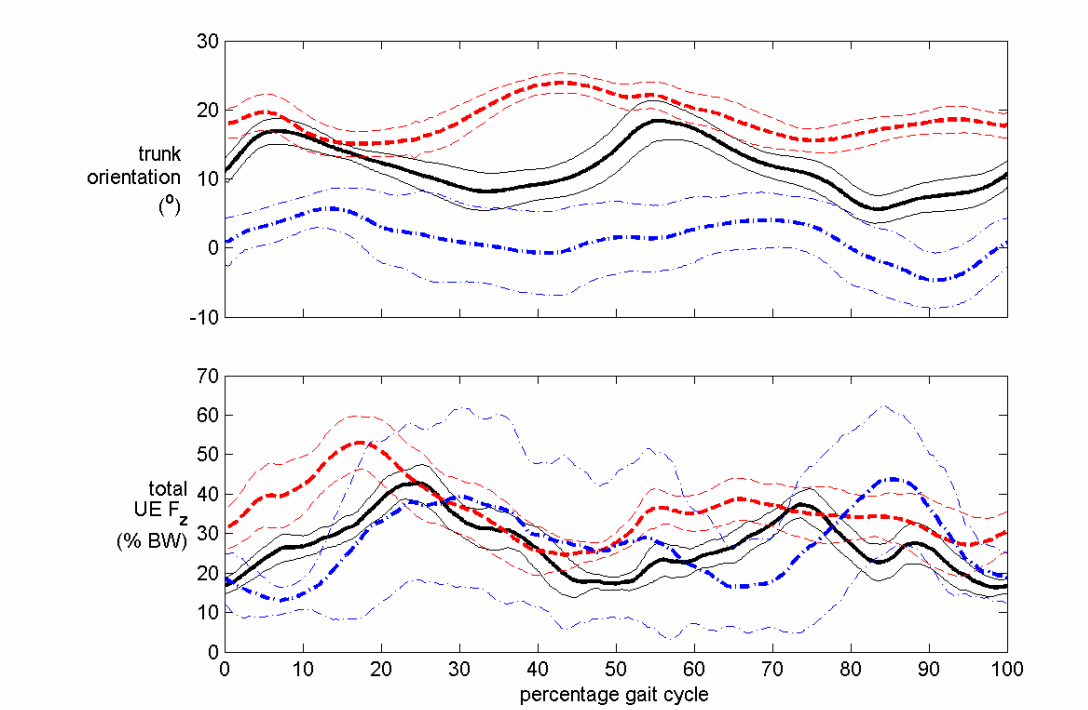

Figure 4.22. The average trunk orientation and upper extremity forces on the walker represented as percentage body weight (% BW) plotted relative to right gait cycle for the HNP-hip (solid) and FNS-only (dashed) and IRGO-only (dashed-dotted).

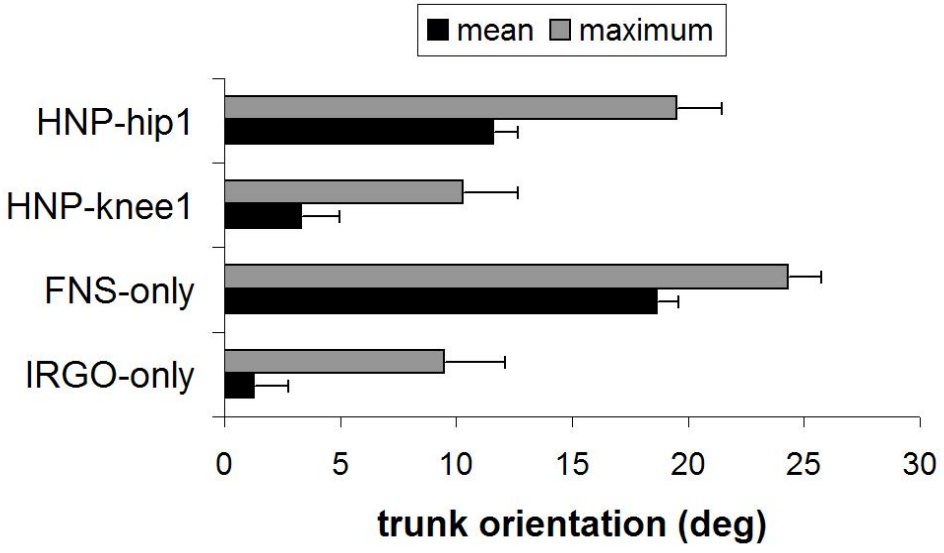

Figure 4.23. Mean and maximum trunk orientation for all test cases.

The average and average maximum trunk orientation of the HNP-hip1 are, respectively, 38 % ($p = 0.0000$) and 20 % ($p = 0.0000$) less than FNS-only. However, the average sagittal trunk ROM of the HNP-hip1 is 32 % greater than the FNS-only case ($p = 0.0198$). This may be due to the fact that whenever the hips are constrained to be reciprocally coupled there is a need for posterior sagittal trunk motion which increases the necessary ROM in the trunk. When the hips are reciprocally coupled, hip extension is coupled to posterior trunk motion. For IRGO-only gait, hip flexion is exclusively driven by posterior trunk tilt to facilitate contralateral hip extension, whereas for FNS-only gait hip flexion is driven independently by FNS of target muscle and not coupled to the trunk. For the HNP-hip1 and HNP-knee1 cases, hip flexion and extension are driven by FNS, but if the hips are coupled, hip extension will force posterior trunk motion. These results are contrary to **Hypothesis 1**, but do show that the VCHM does help to maintain trunk posture significantly better than the actions of the upper extremities in FNS-only gait.

Hypothesis 2: *The maximum upper extremity effort applied to a walking aid while an individual with paraplegia ambulates with the prototype HNP is less than walking with a RGO alone*. **Figure 4.24** summarizes the average and average maximum upper extremity forces for the IRGO-only, FNS-only, HNP-knee1, and HNP-hip1 cases. Note, that for all experimental cases, the upper extremity forces were normalized with respect to participant's body weight, without the weight of the exoskeleton. The average upper extremity forces applied to the walker for the HNP-hip1 and IRGO-only cases were similar ($p = 0.3129$), whereas the average maximum upper extremity force of the HNP-hip1 was observed to be 40 % ($p = 0.0000$) less than that of the IRGO-only case. Furthermore, the average and average maximum upper extremity forces for the HNP-hip1

were, respectively, 24 % ($p = 0.0000$) and 16 % ($p = 0.0001$) less than those of the FNS-only case. Between the HNP cases, the average upper extremity force for the HNP-hip1 was 19 % higher than the HNP-knee1 case ($p = 0.0000$). However, the average maximum upper extremity force for the HNP-hip1 was 14 % ($p = 0.0069$) lower than the HNP-knee1 case. Thus, for the HNP-knee1, even with knee flexion to allow for foot-to-floor clearance during swing, higher impulsive forces relative to the HNP-hip1 may still have been necessary to facilitate a step.

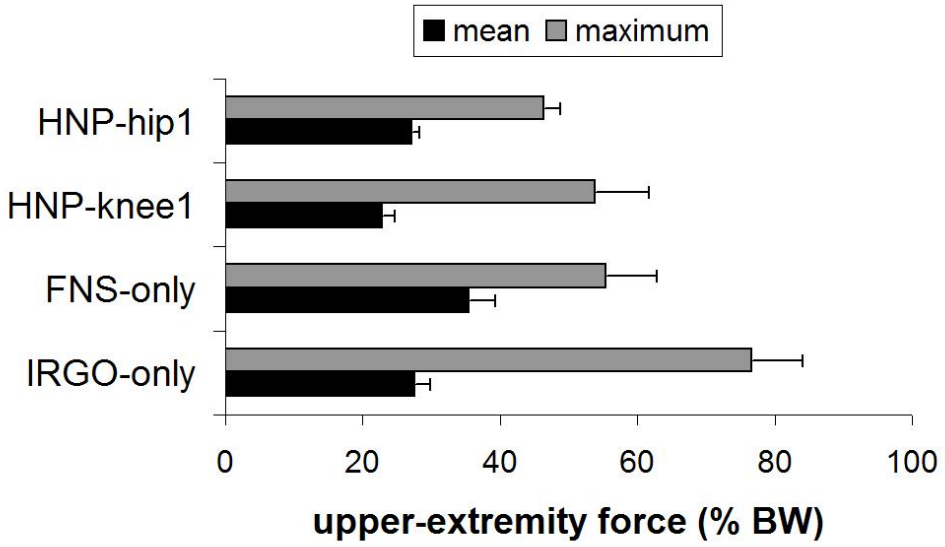

Figure 4.24. Mean and maximum upper extremity forces in percentage body weight for all test cases

These results support **Hypothesis 2** and also show that the HNP-hip1 decreased the upper extremity loads relative to FNS-only gait and is instrumental in dampening impulsive load which is concurrent with used of a hip reciprocator. These reductions in upper extremity forces were apparent even with the weight of the exoskeleton, indicating that the exoskeleton was self-supporting.

Hypothesis 3: *The sagittal hip ROM allowed by the HNP during gait is comparable to FNS-only gait*. **Figure 4.25** summarizes the hip ROM for the IRGO-only, FNS-only, HNP-knee1, HNP-hip1, and normal gait.

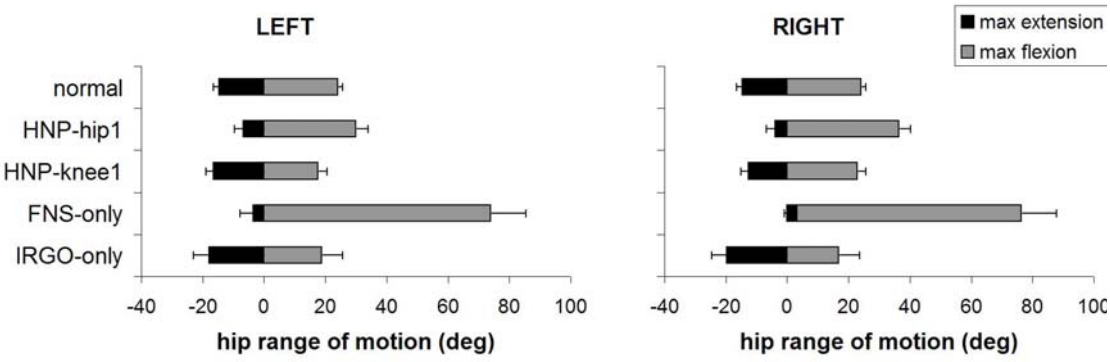

Figure 4.25. Average maximum hip flexion and extension all test cases versus normal gait.

The HNP-hip1 was able to achieve degrees of hip flexion that were from 60 % (L) to 117 % (R) greater than the IRGO-only case (L: p = 0.0000; R: p = 0.0000), while hip extension was 62 % (L) to 80 % (L) less than the IRGO-only. The total hip ROM for the HNP-hip1 was 0.4 % (L) to 11 % (R) larger than that of the IRGO-only (L: p = 0.2586; R: p = 0.0026). Similar results were observed when comparing the HNP-hip1 and HNP-knee1, in which the HNP-hip1 had significantly greater hip flexion and less hip extension (L: p = 0.0000; R: p = 0.0000 for both directions), but an overall increased hip ROM (L: p = 0.0132; R: p = 0.0004). **Figure 4.26** shows the average hip and knee angles of the HNP-hip1 (solid) plotted with those of the FNS-only control case (dashed). Since manual triggered stepping was used in the HNP-hip1 case, while automatically triggered stepping was used in the FNS-only case, the duration of stance relative to swing is larger for HNP-hip1 than FNS-only (as previously described for HNP-knee1). As a result, when plotted together and normalized with respect to percentage gait cycle, the swing phase appears shorter in duration and delayed for the HNP-hip1 case relative to the FNS-

only case. The average hip ROM for the HNP-hip1 was 42 % (R) to 52 % (L) less than that of the FNS-only case (L: p = 0.0000; R: p = 0.0000). However, a hip ROM of approximately 40^{o} is consistent with normal gait [5]. Furthermore, the large hip flexion ROM observed in FNS-only are generally atypical and may be unique to the study participant [10].

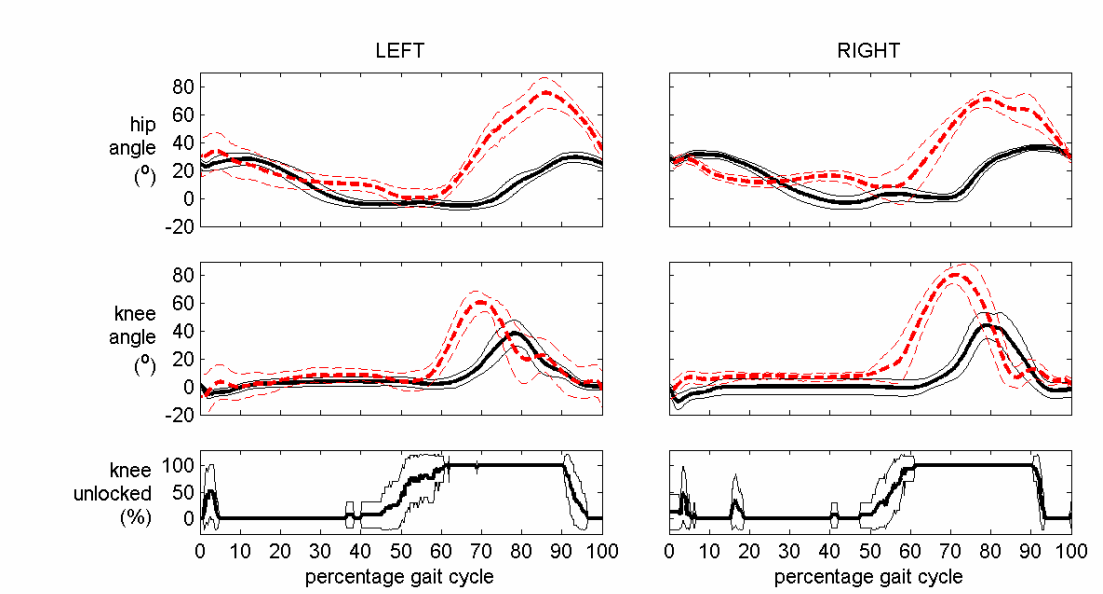

Figure 4.26. The average hip and knee angles for HNP-hip1 (solid) and FNS-only (dashed).

While the average maximum hip flexion angles with the HNP-hip1 were 50 % (R) to 59 % (L) less than those exhibited with FNS-only (L: p = 0.0000; R: p = 0.0000), the hips of the HNP-hip1 extended 89 % (L) to 228 % (R) more than those of FNS-only (L: p = 0.0025; R: p = 0.0000). The reduced hip flexion produced by the HNP-hip1 may be due to the intermediate reciprocal hip coupling of the VCHM, as evidenced from the calculated flexion hip torque of **Figure 4.18**. However, the hip coupling and increased stimulation frequency of the HNP-hip1 case seems instrumental in increasing hip extension relative to FNS-only. Full extension of the stance hip is particularly important

for forward propulsion and defining upright trunk posture. The above results do not support **Hypothesis 3**, but do suggest that the HNP-hip1 primarily facilitates the extension of the contralateral hip which may compromise swing phase flexion as described in **Chapter 3**. This feature was built into the controller of the VCHM because full hip extension at the end of stance is critical for the maintenance of upright trunk posture.

The average maximum knee flexion for the HNP-hip1 is approximately 44% (L: 39 %; R: 49 %) less than that of the FNS-only case (L: $p = 0.0000$; R: $p = 0.0000$). However, the average maximum knee flexion for the HNP-hip1 was up to 51 % (L: 51 %; R: 27 %) greater than that of the HNP-knee1 case (L: $p = 0.0000$; R: $p = 0.0005$). Similarly, the average maximum hip flexion for the HNP-hip1 was about 65 % greater (L: 70 %; R: 59 %) greater than that of the HNP-knee1 case (L: $p = 0.0000$; R: $p = 0.0000$). This suggests that the minimal knee flexion observed in the HNP-knee1 case was less attributable to any unresponsiveness of the DSKM, but more related to the degree of achievable hip flexion. **Figure 4.27** shows the relationship between thigh orientation and knee angle for HNP-hip1, HNP-knee1, FNS-only, and normal gait (**Chapter 3**). The ratio between the maximum thigh orientation and knee angle achieved in each case was determined. For each HNP case, the trunk orientation to knee angle ratio was within a standard deviation to that obtained for normal gait. This indicates that the amount of knee flexion achievable in the HNP cases was not diminished by DSKM operation.

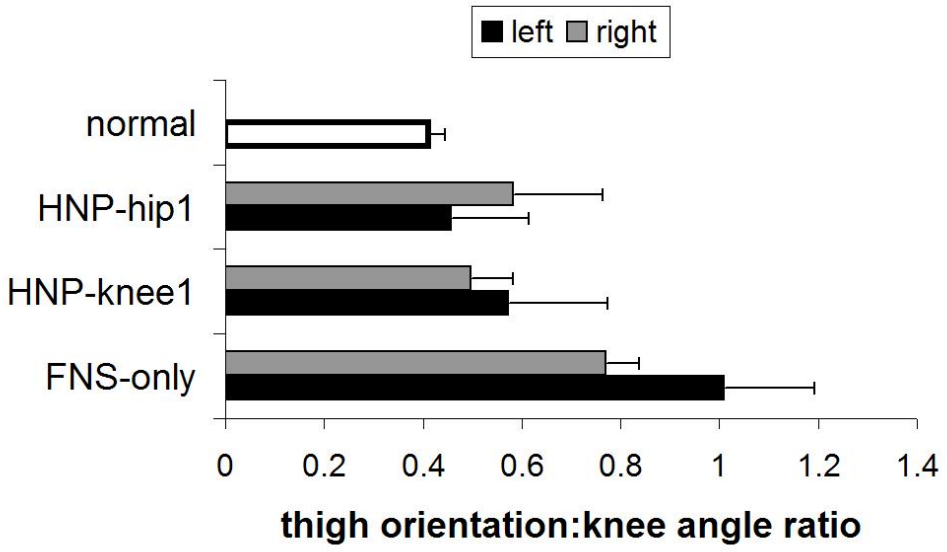

Figure 4.27. Ratio between the maximum thigh orientation and maximum knee angle during gait for normal, HNP-hip1, HNP-knee1, and FNS-only.

Hypothesis 4: *An individual with SCI walking with the prototype HNP will achieve a stride length comparable to walking with a FNS-only gait system*. **Figure 4.28** summaries the step lengths for the IRGO-only, FNS-only, HNP-knee1, and HNP-hip1 cases. The step lengths between the HNP-hip1 and FNS-only cases were not statistically different (L: p = 0.8538; R: p = 0.2601), even though the hip ROM for FNS-only was determined to the statistically greater than that of the HNP-hip1. As seen in **Figure 4.26**, average FNS-only hip angle peaks at approximately 83 % of the gait cycle (L: 86 % ; R: 79 %) and proceeds to fall to approximately 44 % (L: 47 % ; R: 40 %) of the peak value at heel strike. Conversely, hip flexion at heel strike is reduced to only approximately 83% of peak hip flexion (L: 85 %; R: 81 %) with HNP-hip1. Thus, the hip kinematics of the HNP-hip1 for making a step is more efficient than FNS-only, supporting **Hypothesis 4**. The speed and cadence of the HNP-hip1 are 32 % (p = 0.0000) and approximately 20 % (L: 25 %; R: 14 %) less than FES-only walking (L: p = 0.0218; R: p = 0.6741). This is

attributed to the participant's preferred use of automatically triggered stepping and smaller scaling factor for the baseline stimulation patterns for FNS-only walking versus manually triggered stepping and prolonged stimulation pattern for the HNP-hip1.

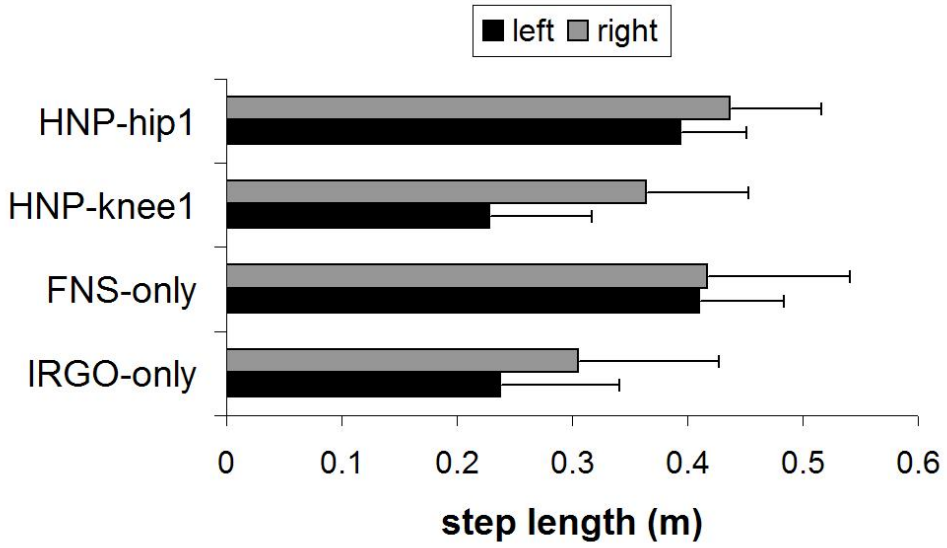

Figure 4.28. Average step length for all test cases.

4.5 CONCLUSIONS

The objective of the prototype HNP was to provide functional stepping to individuals paralyzed by SCI. The concept was to minimize both the voluntary (i.e., upper extremity actions) and involuntary (i.e., FNS activated muscle) work performed by the user. This was implemented with an exoskeleton with controllable constraints that could support the user. In doing so, stimulation to load bearing muscles could be deactivated and less upper extremity exertion on the walking aid was needed.

The results in this chapter validate the feasibility of this system in the following ways. 1) The prototype knee mechanism was able to support the user without stimulation

and lock/unlock responsibly through gait. This knee mechanism allowed for the deactivation of the stimulation to the knee extensors during stance resulting in a decrease in muscle duty cycle to 30 % of baseline levels. These reductions in knee extensor activity relative to FES-only gait may serve to delay fatigue of the knee extensors and thus prolong walking durations. 2) The prototype hip mechanism was shown to be able to support the user, reducing the amount of anterior trunk tilt relative to FNS-only walking and the amount of upper extremity force on the walking aid relative to both IRGO-only and FNS-only walking. The latter was true even with the exoskeleton component of the HNP-hip1 being approximately a third of the user's body weight indicating that the exoskeleton was self-supporting. 3) Closed-loop modulation of the HNP-hip1 hip constraints allowed for improved hip flexion and ROM relative to walking with a hip reciprocator with a fixed 1:1 HFECR. 4) The synchronized operation of the exoskeleton with closed-loop control of FNS allowed for the deactivation of stimulation to target extensors without producing adverse effects on the gait dynamics. 5) The closed-loop control of FNS allowed for real-time increases in stimulation frequency to the hip extensors which provided increased hip extension and further improved hip ROM. 6) The increases in the hip ROM resulted in step lengths that were comparable to FNS-only walking. Collectively, these results show that the exoskeleton component of HNP-hip1 was able to provide functional support to the user without compromising the stepping kinematics facilitated by the FNS component of HNP-hip1.

Even though the HNP-hip1 proved to reduce the upper extremity forces on the walker relative to the IRGO-only and FNS-only cases, the inability of the HNP-hip1 to maintain the user's posture comparable to the HNP-knee1 or IRGO-only may still

contribute to the upper extremity forces. This is supported by the fact that the average upper extremity force of the HNP-hip1 was significantly higher than that of the HNP-knee1. As noted earlier, the sagittal orientation of the trunk posture depends on whether the hip can reach full extension at the end of stance. With maximal stimulation and the help of reciprocal hip coupling, full hip extension was rarely achieved as indicated by minimal instances in which the hip extensors were deactivated (**Figure 4.18**) during HNP-hip1 walking. The modulation of the stimulus frequency of the hip extensors to maximal levels may significantly fatigue the muscles faster. Furthermore, the use of hip coupling during single stance to assist hip extension impedes contralateral hip flexion. This may be the primary reason that the achievable hip flexion of the HNP-hip1 during gait was significantly smaller than that of FNS-only.

Future work that may improve the postural control of the HNP-hip1 should focus on the following. First, increasing the mechanical efficiency of the VCHM would reduce system compliance and provide more efficient reciprocal coupling, making the VCHM more rigid against bilateral hip flexion. Second, hip coupling alone may not be sufficient in assisting hip extension. Thus, the incorporation of an active component to the exoskeleton may be necessary to augment hip extension and to reduce the high stimulus parameter levels that may contribute to muscle fatigue. With improved hip extension it is reasonable to expect that deactivation of stimulation to the hip extensor via the hip FNS control module will be more prevalent. This may lead to significant reductions in hip extensor duty cycle that would be beneficial in minimizing fatigue.

4.6 REFERENCES

1. M. Goldfarb, K. Korkowski, B. Harrold, and W. Durfee, "Preliminary evaluation of a controlled-brake orthosis for FES-aided gait," *IEEE Trans. Neur. Sys. Rehab. Eng.*, vol. 11, no. 3, pp. 241-248, Sept. 2003.

2. S. G. Caroll, R. J. Triolo, H. J. Chizeck, R. Kobetic, and E. B. Marsolais, "Tetanic response of electrically stimulated paralyzed muscle at varying interpulse intervals," *IEEE Trans. Biomed. Eng.*, vol. 36, no. 7, pp. 644-653, 1989.

3. J. T. Mortimer, D. Kaufman, and U. Roessmann, "Intramuscular electrical stimulation: Tissue damage," *Ann. Biomed. Eng*., vol. 8, pp. 235-244, 1980.

4. R. Kobetic and E. B. Marsolais, "Synthesis of paraplegic gait with multichannel functional neuromuscular stimulation," *IEEE Trans. Rehab. Eng*., vol. 2, no. 2, pp. 66-79, June 1994.

5. J. Perry, *Gait Analysis: Normal and Pathological Function*, Thorofare, NJ: SLACK Incorporated, pp. 10-16, 1992.

6. M. Goldfarb and W. Durfee, "Design of a controlled-brake orthosis for FES-added gait," *IEEE Trans. Rehab. Eng.*, vol 4, no. 1, pp. 13-24, Mar. 1996.

7. H. Kagaya, Y. Shimada, K. Sato, M. Sato, K. Iizuka, and G. Obinata, "An electrical knee lock system for functional electrical stimulation," *Arch. Phys. Med. Rehabil*., vol. 77, pp. 870-873, Sept. 1996.

8. S. Nandurkar, E. B. Marsolais, and R. Kobetic, "Percutaneous implantation of iliopsoas for functional neuromuscular stimulation," *Clin. Orthop.*, vol. 389, pp. 210-217, 2001.

9. R. B. Davis III, A. Ounpuu, D. Tybursji, and J. R. Gage, "A gait analysis data collection and reduction technique," *Human Movement Science*, vol. 10, pp. 575-587, 1991.

10. R. Kobetic, E. B. Marsolais, and P. C. Miller, "Function and strength of electrically stimulated hip flexor muscles in paraplegia," *IEEE Trans.Rehab. Eng*., vol. 2, no. 1, pp. 11-17, Mar. 1994.

CHAPTER 5

THE HYBRID NEUROPROSTHESIS: CONSTRAINTS WITHOUT LIMITATIONS

5.1 INTRODUCTION: SUMMARY OF THE RESEARCH

The preceding chapters described the design and implementation of 1) an exoskeleton consisting of two controllable passive hydraulic mechanisms and 2) a finite state controller which combined the operation of the exoskeleton with the real-time modulation of electrical stimulation to target muscles to facilitate assistive gait. Six hypotheses were examined to test the feasibility of this prototype HNP.

Hypothesis 1: *The trunk orientation of individuals with SCI walking with the prototype HNP is comparable to walking with a RGO.* The trunk orientation of the complete HNP was shown to be on average 10^{o} greater than that of a RGO, but 7^{o} less than that of FNS-only. These results do not support **Hypothesis 1,** although they do show that the HNP can maintain a better user posture than that of FNS-only which exclusively relies on upper extremity actions on the walking aid to support trunk posture.

Thus, the HNP achieves an intermediate posture which delivers a positive change towards the advantages offered by the IRGO-only.

Hypothesis 2: *The maximum upper extremity effort applied to a walking aid while an individual with paraplegia ambulates with the prototype HNP is less than walking with a RGO alone*. It was shown that the maximum upper extremity effort during gait with an HNP was respectively 40 % and 16 % less than that of IRGO-only and FNS-only gait. This was despite that fact that the HNP maintained a forward trunk orientation greater than that of the IRGO-only and that the weight of the exoskeleton component of the HNP was approximately 30 % of the user's body weight (which was not included in the normalization of the upper extremity forces exerted on the walker to % BW). These results support **Hypothesis 2** and show that the HNP can effect a positive reduction in upper extremity effort when compared to conventional bracing, and imply that such a system may be more comfortable and less demanding on the user.

Hypothesis 3: *The sagittal hip ROM allowed by the HNP during gait is comparable to FNS-only gait*. It was shown that the hip ROM of the HNP was up to 50 % less than that of the FNS-only as a result of less hip flexion observed during HNP gait. The priority of the controller of the HNP is to minimize bilateral hip flexion by reciprocally coupling the hip such that the contralateral swing hip assists the stance hip into extension. This reciprocal coupling can act to restrain the hip flexion of the swing limb. Although these results do not support **Hyporthesis 3**, it was observed that the hip flexion ROM of normal gait was more similar to that of HNP gait than that of FNS-only gait. In addition, the relatively large hip flexion ROM observed in FNS-only gait may be unique to the study participant [1]. The exaggerated swing limb hip flexion exhibited by

this subject actually resulted in the leg extending far past the point of ground contact as evidenced by the similarities between the stride lengths for FNS-only and HNP walking.

Hypothesis 4: *An individual with SCI walking with the prototype HNP will achieve a stride length comparable to walking with a FNS-only gait system*. Even though the hip ROM for the FNS-only was substantially larger than that of the HNP, the step lengths between HNP and FNS-only gait were similar. This was because the larger hip flexion ROM of FNS-only was not functional to facilitating stepping. For FNS-only, the swinging limb would pass the point of eventual initial contact and retract due to the effects of gravity. This "pass-retract" gait deficit exhibited by the subject effectively eliminated the contribution of the greater hip flexion ROM, observed in FNS-only gait to step length. Because the step lengths between FNS-only and HNP walking were statistically indistinguishable, in spite of the increase in hip ROM with FNS-only, these results support **Hypothesis 4**.

Hyporthesis 5: *The DSKM can adequately support the user during gait, such that the gait dynamics observed with stimulation to the knee extensors deactivated is comparable to those observed with baseline knee extensor stimulation*. The dynamics of walking with the DSKM combined with the knee FNS control module were comparable to those of walking with the DSKM combined with baseline stimulation. These dynamic parameters include knee ROM, mechanical compliance, trunk orientation, upper extremity forces, gait speed, cadence, and step length. The similarities between the gait with the knee FNS control module and baseline stimulation provide strong evidence to support **Hypothesis 5**, suggesting that stimulation to the knee extensors can be decreased significantly with the DSKM without adversely affecting overall walking performance.

Hyporthesis 6: *The synchronous implementation of the VCHM and closed-loop control of FNS to target hip extensors will provide improved gait dynamics relative to the utilization of baseline hip extensor stimulation*. Significant improvements in the hip ROM and gait speed were observed with the implementation of the hip module of the FNS controller without compromising trunk orientation and upper extremity forces relative to baseline stimulation. These results show that the real-time closed-loop control of stimulation to target hip extensors can feasibly improve the step length and gait speed relative to open-loop methods, thus providing evidence to support **Hypothesis 6**.

In summary, the prototype HNP was compared with two existing assistive gait systems, IRGO-only and FNS-only, each being a modality which was collectively implemented in the HNP. It was shown that the exoskeleton of the HNP could completely support the user without the assistance of the FNS. Gait with the HNP was found to have reduced upper extremity effort applied to the walking aid relative to both IRGO-only and FNS-only, yet allow for step lengths comparable to FNS-only. Thus, these results indicated that the functional support provided by the exoskeleton of the HNP did not adversely affect the stepping kinematics provided by the FNS of the HNP. This was despite the fact the weight of the prototype exoskeleton was a third of the user's body weight, further implying that the HNP not only stabilized the user but was also self-supporting.

During HNP gait, it was observed that the trunk was oriented more anteriorly than that during gait with continuous 1:1 hip reciprocating coupling (i.e., IRGO). The HNP had a greater forward trunk tilt due to the minimal hip extension and relatively low mechanical efficiency of the VCHM. The weight of the VCHM may also be a

contributing factor to the forward trunk tilt. The majority of the mass of the VCHM was positioned posteriorly at the lumbar level of the user. This would shift the combined center of mass of the user and exoskeleton posteriorly. The forward trunk tilt may be the user's reaction to the offset in center of mass. Recall from **Chapter 3** that forward trunk tilt can be achieved with the VCHM if there is insufficient stance hip extension (**Figure 3.2**). Thus, a forward trunk tilt was maintained to correct for the offset in center of mass in order to prevent from falling backwards. Nevertheless, the HNP does provide trunk support, as indicated by the recorded torques applied to the VCHM in **Figure 4.18,** and provides reduced upper extremity effort relative to the IRGO-only. This indicates the amount of upper extremity activity is not necessarily indicative of the amount of trunk tilt. This chapter further elaborates on this topic while exploring the implications to the developed technology of this work and the future directions that might be taken.

5.2 IMPLICATIONS

5.2.1 The Potential for the Viable Implementation of the New HNP

The viability of this new HNP assistive gait system to the user population hinges on the fact that the system can be practical in the user's life activities. The obvious parameters for the functional and practical implementation of this HNP are speed and maximal ambulation distance and duration.

Gait speed is related to the achievable step length of the user. In this research, a novel hip mechanism was designed and shown to be capable of controllably locking, freeing, or reciprocally coupling the hips depending on the posture of the user. The

intermittent switching between hips being freed and reciprocally coupled during gait partially relieves the constraint that the extending stance hip imposes on the flexing swing hip when the hips are reciprocally coupled. Thus, this variable reciprocal coupling of the hips facilitated by the VCHM allows for hip flexion ROMs that at significantly larger than those observed in a standard RGO with a fixed 1:1 HFECR, thus allowing for larger step lengths. Accordingly, the HNP was shown to provide step lengths comparable to those of a FNS-only system. Assuming that the stance hip can achieve adequate extension to maintain upright trunk posture such that reciprocal hip coupling is no longer necessary to support the trunk, the VCHM should be capable of accommodating any hip flexion ROM that is drivable by the user's hip flexors and within the designed ROM of the device. In this way, variable gait speeds can be achieved with the VCHM through modulating step length in addition to walking cadence.

The variable step lengths allowed by the VCHM may be able to extend ambulation with the HNP beyond level over-ground to enable negotiating over uneven terrain or ascending ramps, curbs, or stairs. For instance, in stair ascent, the VCHM would provide trunk support during the double support periods and accommodate the high stepping motions necessary to climb a stair step.

Achieving functional long distance walking is related to both speed and energy efficiency. The goal of this new HNP was to reduce the overall muscle activity during the assistive gait of individuals with paraplegia. It has been shown that the majority of the energy consumption in FNS-only gait is due to upper extremity exertion [2]. The results of this research showed that the forces generated from the voluntary upper extremity actions on the walking aid during HNP gait were significantly reduced relative

to existing assistive gait systems. With the combined implementation of both the DSKM and the knee FNS control module, the stimulation duty cycle of the knee extensors was reduced to 30 % of the baseline stimulation. This reduction in stimulation duty cycle was characterized as a sustained deactivation of the target muscles during stance, approximately two seconds in duration. This length of resting time for the muscles has been shown to be effective in limiting the drop in knee extension torque as a result of fatigue [3].

The combined implementation of the VCHM and the hip FNS control module resulted in an increase in stimulation frequency of the hip extensors relative to baseline stimulation in order to maximize hip extension to maintain trunk posture and forward progression. These results may be merely indicative of the fact that the torque generated by the hip extensors of the study participant was rarely able to fully extend the hip during stance, which was the criterion for the deactivation of the hip extensors in the FNS controller. Even so, the VCHM and FNS controller were able to successfully deactivate the hip extensors without compromising the dynamics of gait during a number of strides during experimental testing, showing that a reduction stimulation duty cycle is feasible. With sufficient stimulated hip extension, it is reasonable to expect that the hip extensor stimulation would be consistently deactivated at the end of stance, thus reducing the stimulation duty cycle to the hip extensors. Accordingly, with reduced upper extremity effort and lower extremity muscle activity, this HNP has the potential of providing gait that is more energy efficient than existing assistive gait systems.

With future improvements, as described later in this chapter, this HNP may also have the potential in providing assistive gait such that the gait speed and walking distances and durations are functional to activities of daily living.

5.2.2 Alternate Applications for the Prototype Exoskeleton

This work directly applies to the health, well-being, and functional independence of individuals with paraplegia. In addition to being a debilitating and costly condition, SCI significantly restricts access to life opportunities and compromises the ability to work, engage in social or leisure activities, pursue an education, or assume other roles associated with an independent and productive lifestyle. This technology can be applied to restore functional gait to individuals with neurological conditions other than SCI who have impaired lower extremity motor function such as stroke, traumatic brain injury, or multiple sclerosis. The principal determinants of the user population will be the excitability of the peripheral motor nerves for the FNS component of the system (typically SCI at the lower thoracic level or above), adequate upper extremity strength to balance with a walker or crutches (typically SCI at upper thoracic levels or below), and adequate joint ROM for reciprocal ambulation.

Although the prototype exoskeleton was specified as an integral component of a HNP, the exoskeleton can be used independently, serving as a therapeutic device for individuals recovering from neurological impairments, orthopaedic conditions, or other physical injuries or illnesses that have prohibited an individual from walking for an extended period of time. The Lokomat® (Hocoma, Zurich, Switzerland) is a treadmill based lower extremity robotic orthosis developed to for the purposes of relearning the

coordination involved in gait and restore muscle mass after such disabilities. Once the controller has been made portable, the prototype exoskeleton would give patients the option to leave the hospital and move their limbs in a more realistic and functional manner. The sensor signals used for closed-loop control could be recorded and used for gait assessment. The conclusions drawn from this work facilitates a better understanding of control methods that may be useful in restoring gait. With further work, gait assistance provided by this control system should extend walking duration and distance leading to improved overall health and wellbeing.

5.2.3 Passive Portable Hydraulics

In this work, the hydraulic mechanisms of the exoskeleton were miniaturized sufficiently through optimization to successfully evaluate the feasibility of the HNP. As briefly discussed in **Chapter 3**, the use of miniature hydraulics in a passive mode posed many design challenges, mechanically as well as in terms of controllability. The exoskeleton must resist high forces to support of the user. Within the hydraulic systems, these forces are seen as applied pressures. As pressure is inversely proportional to area, the smaller the bore size of the hydraulic cylinder, the larger the internal pressures will be with a given applied force. For instance, if the VCHM and DSKM are each resisting 70 Nm of applied joint flexion torque, the maximum internal pressures of each mechanism would be approximately 900 psi for the VCHM (offset by internal resting pressure) and 1000 psi for the DSKM. The miniaturization of hydraulic components is not only necessary to maintain system portability but also to minimize the allowable flow rates in the system. The maximum system flow rate is restricted by the flow coefficients of the

hydraulic valves which describe the flow versus pressure drop relationships. Maximizing the valve flow coefficient will minimize head losses for a given flow rate. Thus, utilizing valves with sufficiently large flow coefficients keeps the resistance of the hydraulic mechanisms low, allowing the mechanisms to be backdrivable by the actions of the user. However, the power requirement of a valve generally increases with flow coefficient.

Since the primary objective of the exoskeleton is to support the user, any mechanical compliance during constrained activity is undesirable. The interface between exoskeleton and human should provide enough compliance to prevent dynamic loads from causing system failure. With active hydraulics, compliance can be countered by actively pressurizing the hydraulic system, whereas in passive hydraulics, the only preventative measure that can be taken is to make the liquid-to-air ratio as large as possible. This is especially critical for miniature hydraulics implemented in this work due to the small volume of the hydraulics itself, which is further compounded by a small linear-to-rotary transmission ratio between the hydraulic cylinder and hip joint. The transmission ratios for the VCHM and DSKM were defined to achieve optimum pressure and flow characteristics. The task of priming a hydraulic system is to maximize the liquid-to-air ratio. The building of each hydraulic circuit of the exoskeleton was done such that air bubbles could almost always rise to a bleed port and the likelihood of air bubbles being trapped was low. The valve manifold of the VCHM consisted of one inlet valve to inject fluid into the system and six separate bleed ports, strategically positioned such that air would tend to gather at these ports while the system was at rest. The hydraulic cylinders were positioned distal relative to the valve manifold to allow air bubbles to rise from the cylinders to the bleed ports of the valve manifold. Furthermore,

when installing ancillary hydraulics such as the pressure transducers at the ports of each mechanism it was necessary to prime the cavity of each pressure transducer individually before installation. Otherwise, any air from the transducer would be transferred into the rest of the hydraulic system. Even with all these precautions, however, it was not feasible to purge all the air from the hydraulic systems due to air bubbles being trapped within the heads of the cylinders and within area fluctuations in the fittings and tubings, as well as leakage through the seals. This was more apparent in the VCHM than the DSKM since the hydraulic circuit of the VCHM was much more complex. To account for this, the VCHM was pressurized to reduce the size of remaining air bubbles. As noted in **Chapter 3**, the amount that the resting pressure of the VCHM could be raised was limited, since doing so reduces the operating pressure range of the hydraulics.

The above discussion should be considered if full optimization of the VCHM or DSKM is intended for the future or for any technology that involves the high loading of passive miniature hydraulics.

5.2.4 Influence of Sagittal Trunk Kinematics on Forward Progression

Upon examining the trajectory of the trunk orientation for each of the test cases involving an exoskeleton in **Chapter 4**, it can be generalized that local maxima occur at the end of the double stance phases of gait (i.e., loading response and pre-swing) for all cases. This was also observed in To *et al.* [4] and can be explained by **Figure 5.1**.

In all cases, the knee and ankle are respectively constrained in full extension and neutral by the exoskeleton for the entire duration of the single stance phase. During single stance, the user is supported by the stance limb and upper extremity actions on the

walking aid. Since the recorded average upper extremity force is always less than 30 % body weight, the majority of the user's body weight was supported by the stance limb. Thus, the stance foot is directly under the body's center of mass and the stance limb is approximately vertical in orientation (**Event 1**). This means that the body is elevated as high as possible by the stance limb. The trunk orientation reaches a local minimum at the end of single stance, as a result of the posterior movement of the trunk due to upper extremities pushing against the walker to facilitate hip extension and contralateral hip flexion (if hips are reciprocally coupled).

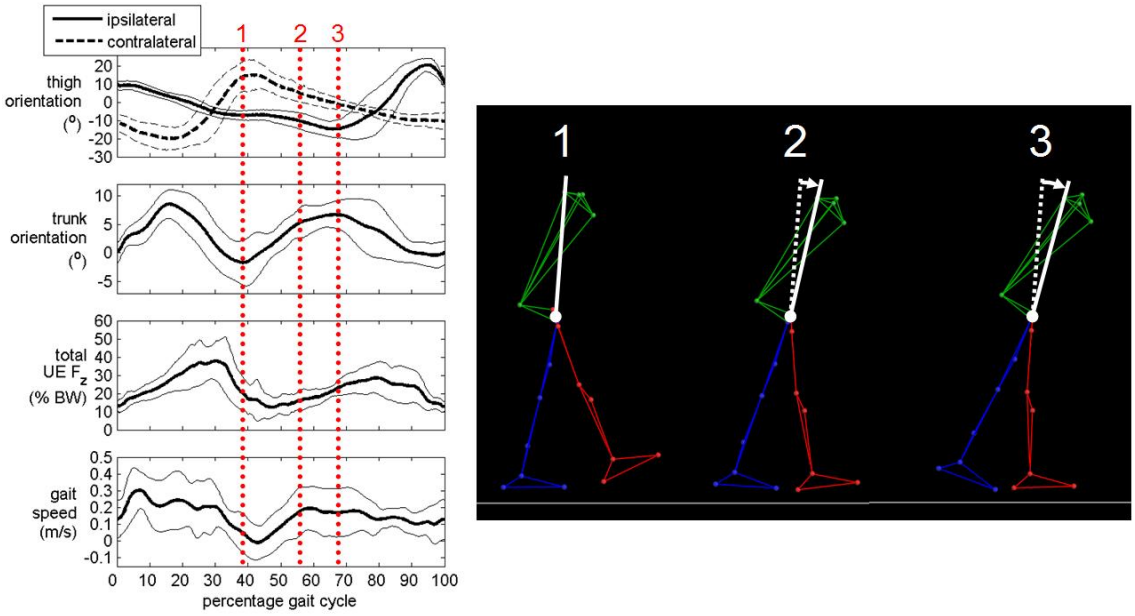

Figure 5.1. Influence of the exoskeleton constraint on the trunk orientation. Walking with a 1:1 hip reciprocator and a pair of DSKMs.

This assistance from the upper extremities is indicated by the local maximum in the upper extremity forces just prior to **Event 1**. Also, notice at this point, that the instantaneous forward velocity is near zero since the trunk has to move backwards to extend the stance hip. In order for forward progression to continue and the contralateral swing limb to contact the ground for heel strike, the orientation of the body must rotate forward over the

stance foot, orienting the trunk anteriorly to force the orientation of the stance thigh to extend as much as the swing thigh is flexed (**Event 2**). Here, the anterior orientation of the trunk is not due to thigh flexion relative to the pelvis and trunk, but associated with the anterior orientation of the entire body which can be analogized to an inverted pendulum. This inverted pendulum effect is necessary because there is no stance knee flexion or ankle dorsiflexion to shorten the stance limb to lower the body onto the flexed contralateral swing limb. Furthermore, forward orientation of the trunk could be prevented if stance hip extension occurred coincidently as the body oriented forward. However, this was not observed to have taken place.

In this work, the hips are reciprocally coupled, the knees are locked against flexion at full extension, and the ankles are locked at neutral by the exoskeleton during double stance. During double stance, forward trunk orientation continues to increase to transfer the body's center of mass on the leading stance limb and unload the trailing stance limb to prepare for swing (**Event 3**). Sagittal hip movement is linked to the trunk by the exoskeleton constraints. Thus, in order to maintain upright trunk posture during weight transfer, the hips must bilaterally extend. This is not possible with IRGO since the hips are reciprocally coupled. The VCHM allows for bilateral hip extension during double stance, however, no bilateral hip extension was observed. This could be due to the fact that to achieve bilateral hip extension it may be necessary to push against the walker with the upper extremities which will impede weight transfer and forward progression.

Consequently, forward progression necessitates the forward orientation of the trunk despite continuous reciprocal hip coupling. An anteriorly oriented trunk facilitates

1) forward progression at the end of single stance in addition to 2) weight transfer during double stance. This was consistent in all study cases involving an exoskeleton, since the knees and ankles were constrained in full extension and neutral respectively during stance. There was approximately 10^{o}-20^{o} increase in forward trunk orientation from the end of single stance (when forward trunk orientation is at its smallest) to the end of double stance (when forward trunk orientation is at its largest). In order to restore the trunk posture (to that at the end of single stance) the upper extremities needed to apply approximately 40 % of the user's body weight on the walker for all cases.

The forward trunk orientation observed at heel strike can be minimized through controlled dorsiflexion of the trailing ankle. However, a more complex approach will be needed to prevent the forward trunk orientation that occurs progressively throughout double stance. In normal gait, the weight transfer from trailing to leading limb is primarily accomplished through the preservation of forward momentum via mechanics of the heel rocker upon heel strike of the leading limb [5]. This heel rocker action provides shock absorption via the eccentric contractions of the quadriceps and ankle dorsiflexors allowing for controlled knee flexion and ankle plantar flexion, respectively. This complex interplay among the joint actions of the leading limb functions to roll the mass of the body over the heel, thus preserving forward progression. To achieve this form of control new constraint mechanisms must be developed to facilitate variable impedance control of the knee and ankle joints.

5.3 FUTURE DIRECTIONS

Immediate future work would include the evaluation of the HNP with more participants with paraplegia to confirm the findings of the current work. In these experiments, all components of the HNP (i.e., VCHM, DSKM, and hip and knee FNS control modules) should be implemented simultaneously. To enhance participant performance, further evaluations may be preceded by the full customization of the exoskeleton to reduce system size and weight and improve mechanical efficiency of the VCHM.

Many of the structural members of the exoskeleton, such as the leg uprights and the components for mounting the cylinders, valves, ancillary hydraulics, gearing, and sensors, were designed and fabricated to be highly modular and adjustable to facilitate design flexibility, variable subject size, and ease of maintenance in the prototyping process. Accordingly, many of the components can be simplified to contain fewer individual pieces to minimize the amount of material used. Structural components such as the lateral uprights of the exoskeleton and the mounting pieces for the hydraulic cylinders and cylinder-to-hip rack-&-pinion transmission of the VCHM are currently constructed out of steel and aluminum alloys. Materials with higher specific strength could be used such as titanium alloys and carbon fiber to minimize size and weight. Modifications to the hydraulic components of the VCHM can further reduce the weight of the exoskeleton. The solenoid valves are currently connected with standard fittings and tubing. The number of heavy brass hydraulic fittings can be minimized by repositioning the valves in a more compact configuration with a custom valve manifold made from hard coated aluminum. The purpose of the accumulator in the VCHM is to

take up the difference in volume between the blind and rod ends of the cylinders (total volume of all the cylinders < 0.03 L) during joint motion. The capacity of the current accumulator (0.075 L) used can be decreased significantly. Finally, the power supply and processing and control circuitry can be condensed into a single unit. The mechanical efficiency of the VCHM can be increased by designing the valve manifold such that air can more easily be bled out of the system. This is done by reducing fluctuates in the inner diameter of pipe/tubing where air bubbles can be trapped and ensuring that air bubbles can rise to a bleed port/valve. Furthermore, helical gears and higher tolerance clevises and pins can be used in the hydraulic rotary actuators of the VCHM to reduce backlash. These steps to optimizing the exoskeleton may 1) improve gait speed and limb coordination by reducing the mass that needs to be accelerated forward, 2) reduce the forward trunk tilt experience when walking with the VCHM, and 3) be beneficial in making the sit-to-stand transitions easier for the user.

If future evaluations of HNP consistently show the reduction in upper extremity forces and comparable step length relative to FNS-only, gait experiments should be undertaken to evaluate energy consumption through measuring oxygen consumption or physiological cost index. In addition, the maximum walking duration and distance achievable with the HNP and FNS-only gait could be assessed. Accordingly, these experiments must be conducted outside the laboratory where there is sufficient space for the participant to walk to fatigue. The HNP control system (target and host PC) can be temporarily mobilized with the use of an external power source such as an uninterruptible power supply (UPS).

The current work showed that the upright posture during gait with a VCHM improved relative to FNS-only, but was still not comparable to gait with an IRGO. Improvements in posture will have a directly impact in increasing step length. First and foremost, the VCHM focuses on maintaining trunk posture by reciprocally coupling the hips until bilateral hip flexion is eliminated. Since the 1:1 reciprocal hip coupling will act to impede the flexion motion of the swing limb and thus reduce step length, it is important to reduce the amount of time that the hips are reciprocally coupled. This can be done by minimizing instances of bilateral hip flexion through maintaining upright trunk posture. A simple solution to improving posture may be to use surface electrodes to recruit the erector spinae muscles of the lumbar region of the back to extend the spine. However, this approach requires that more muscles be activated under FNS, resulting in a higher demand on the user. Increasing the stimulus intensity of hip flexors, through the FNS controller may also help in driving contralateral hip extension when the hips were reciprocally coupling. However, the increases in stimulus PW and frequency to the hip flexors are limited due to the already high baseline levels. The following considers two methods for improving joint kinematics with the HNP: 1) the application of a FNS controller that performs modifications to the stimulation patterns for next stride to optimize the coordination between lower extremity muscles (i.e., "next stride correction") and 2) the incorporation of an active mechanism to help power limb movement in addition to FNS of paralyzed muscle.

5.3.1 Considerations for Improving Joint Coordination

With the additional weight and constraints of the exoskeleton, the baseline stimulation patterns defined for FNS-only gait may not be adequate for facilitating

optimal joint coordination with the HNP. As a result, forward progression may be compromised. The current FNS controller modulates the stimulus in real-time based on the state of the instantaneous exoskeleton constraints. Originally, a second control algorithm was considered to run in parallel with the real-time controller. This parallel controller would change the stimulation parameters of the entire stride based on sensor information collected in past strides. Assuming that the dynamics of the next stride would be fairly close to the previous stride, the idea was to make corrections to the gait kinematics, observed to be necessary in the previous strides, by altering the stimulation patterns for the next stride. Thus, the stimulation patterns for all target muscles would be automatically re-profiled for each subsequent stride. The primary benefits to this type of "next stride correction" control scheme would be the potential to optimize the onset/offset of muscle activity online, as opposed to relying on the pre-programmed baseline stimulation patterns, which are identified through heuristical means for the open-loop case and may not be robust for HNP gait and over the entire duration of gait. The duration from the onset of stimulation to the attainment of the desired force is on the order of 100 ms. Because of the relatively long response times of paralyzed muscle, it is currently impractical to correct for gait deviations with FNS as they occur. It is however feasible to perform corrections to the gait cycle on a cycle-to-cycle basis [6-8]. Gait corrections by FNS necessitate the application of stimulation to target muscles before the desired muscle action is required. By allowing for the modulation of stimulus onset/offset times, this FNS controller design lends itself to account for the muscle recruitment duration necessary to achieve the desired force output and may allow for improved coordination among the joint kinematics. Furthermore, in order to maintain the

synergy between certain muscles, the stimulation patterns of these muscles must be changed together. The muscles can be synergistically grouped via principal component analysis based on the normal electromyography measurements of the target muscles.

To execute this type of online stimulation pattern optimization, a method of assessing gait kinematics was necessary. Since the range of the force output for stimulated muscle is limited and the force output of stimulated muscle is not necessarily consistent over time, the use of PID control of instantaneous joint trajectories through the definition of a state-space model of the HNP system was deemed impractical. A more discrete approach was taken such that a particular joint angle must be within a specific ROM during a particular phase of gait. To achieve this form of control, a gait event detector (GED) was developed. Gait events are instances in the gait cycle in which the phase of gait changes. These sequential transitions among key gait phases are points in the gait cycle where muscle force must be applied to facilitate the dynamical transitions of the lower extremities. By knowing the gait events, the exact timing of the gait phases are known and thus, the average joint trajectories of each gait phase can be assessed and, if necessary, modified in the next gait cycle by altering the muscle stimulation patterns appropriately.

5.3.1.1 Gait Event Detection

Gait event detection is a means of predicting specific gait events in real-time as the individual is walking by utilizing some form of sensory input. Extensive work has gone into developing GEDs for controlling FNS walking systems. Heuristic approaches, machining learning, and soft computing techniques have been employed to define the rule base for state machines used in gait event detection. Initial GEDs have utilized

handcrafted rules to some success [9-12]. However, with a handcrafted rule base, it is difficult to include the aspects of the gait that might be unique to a particular user [13]. Automatic rule determination can be performed via a class of machine learning algorithms known as supervisory controllers by mapping inputs to known outputs of the modeled system. Inductive learning algorithms [13-16] and adaptive logic networks [15-17] have been applied to gait event detection. Kirkwood and Andrews [13] utilized crutch force and foot pressure recordings to train an inductive learning algorithm to replicate the times when the user triggered a switch to deliver electrical stimulation to the peroneal nerve. The controller yielded a prediction accuracy of 97.9 %. When compared to a controller with handcrafted rules for the same user, the inductive learning controller produced increased walking speeds. This was explained by the fact that the anticipatory actions of the user were encoded into the rules derived from inductive learning. Control systems that use fuzzy sets as opposed to the classic crisp sets have been introduced into gait event detection by Ng and Chizeck [18]. Fuzzy inference systems (FIS) are less sensitive than thresholding methods to sensor noise and small variations in the input signals that are prevalent from stride to stride in paraplegic gait. Ng and Chizeck [18, 19] developed a FIS-based GED utilizing hip, knee, and ankle joint sensory feedback that achieved a prediction accuracy of 94 % for five gait events.

Improvements in gait event detection accuracy have been made by augmenting gait event predictions from machine learning and soft computing techniques with a heuristically defined supervisory rule set [16, 20]. The signals that have been used to discriminate among individual gait events include foot-to-ground contact pressure [12, 13, 15, 20] electromyogram of upper extremity muscles [21], electroneurogram of

peripheral lower extremity nerves [17], upper extremity force on a walking aid [12], and lower extremity joint angles [15, 18, 19], angular velocity [12, 19], and acceleration [11, 16]. A current limitation to gait event detection is the selection of a practical sensor set. The inconvenience of donning/doffing individual sensors and the difficulties in consistent sensor alignment make existing GEDs impractical for daily clinical use [22]. The exoskeleton in the current work already provides a convenient structure to instrument a variety of sensors.

5.3.1.2 Fuzzy Inference System GED

In this study, the controllers developed for the VCHM (i.e., FSPC), DSKM (i.e., FSKC), and FNS modulation are essentially GEDs. Unlike the FIS GED, the threholds for detecting the gait events for these controllers were determined through a combination of empirical and heuristical means. The FSPC and FSKC only detected three (i.e., double stance, single stance, and swing) and two (i.e., stance and swing) phases of gait, respectively, and used feedback from foot-to-ground contact instances. The FNS controller only detected two gait phases (i.e., pre-swing and early-swing), which were derived from the pre-programmed stimulation pattern. The above methods cannot be utilized for the gait event detection of this proposed FNS controller for "next stride correction". The gait cycle must be divided into phases which are short enough in duration such that the inputs to the controller can be generalized into a simple change in stimulation activation time and/or stimulus parameter (i.e., PW and IPI).

A GED was developed for the HNP that incorporates a dual layer control algorithm, consisting of a 1) fuzzy inference system and 2) supervisory rule set. Sensors measuring the sagittal hip, knee, and ankle angle and the foot-to-ground contact pressure

of the forefoot and heel of each foot are used as the sensory information for gait event detection. Both joint angle and foot-ground contact pressure have been shown to provide adequate information for gait event detection [19, 20]. The gait cycle was divided into six gait phases with respect to the right limb – loading response, midstance, terminal stance, pre-swing, initial swing, and late swing [5].

The following briefly describes the FIS component of the GED. For a complete description of the FIS refer to **Appendix B**. The first control layer of the GED is a FIS that serves to estimate the gait events. The FIS involves the mapping of ten input variables (six joint angles and four foot pressure sensors) to a single output variable (gait event). Six input membership functions, one for each fuzzy set (i.e., gait phase), occupies the range of the sensor input during the entire gait cycle. The shape of each input membership function is the Gaussian probability density function of the input during a particular gait event. In this way, the degrees of overlap between membership functions were automatically prescribed. One IF-THEN rule was used to govern each gait event. Singletons were used as output membership functions.

The second control layer is a set of supervisory rules structured in the form of a finite state machine, which serve to refine the gait event estimates output from the FIS [19]. There are two basic supervisory rules. The first rule limits the minimum duration of a gait phase. Essentially, the duration of each gait phase must be at least 50 % of the running average duration of that gait phase. The second rule guarantees that the gait events are predicted in a sequential order. If the FIS estimates a gait event that has already occurred, the supervisory control layer disregards the estimate and maintains the

current gait phase. However, if the FIS prematurely skips a gait event, the supervisory layer will only advance one gait phase from the previous gait phase before the change.

The input membership functions are continuously modified after every gait cycle to update the initial membership function parameters obtained from the training data. A running mean and standard deviation of each GED input within each gait phase are continuously calculated during gait.

The accuracy of the FIS GED was tested with two able-bodied subjects walking with the prototype exoskeleton. The sensitivity of the GED to gait speed was tested by having the subjects walk at three different gait speeds (i.e., preferred, slow, and fast speed). The fast and slow speeds were set at approximately ±20 % of the preferred speed. Each speed was maintained using a metronome. The knees and the ankles of the mechanical orthosis were unlocked in the sagittal plane. Sagittal lower extremity joint angles were collected from the potentiometers at each joint. Foot-to-ground contact information was measured with FSRs placed under the soles of each foot. Gait events were determined for each trial from the FSR data. These predetermined gait events were used as the standard to which the gait events estimated by the FIS GED were compared. The GED was trained using the predetermined gait events, joint angles, and FSR data of a single trial of the subjects walking at their preferred speed. The trained GED was then used to determine the gait events for the remaining test trials with the subjects walking at three different gait speeds. The GED predicted gait events were then compared to the gait events predetermined from FSR data (**Figure 5.2**).

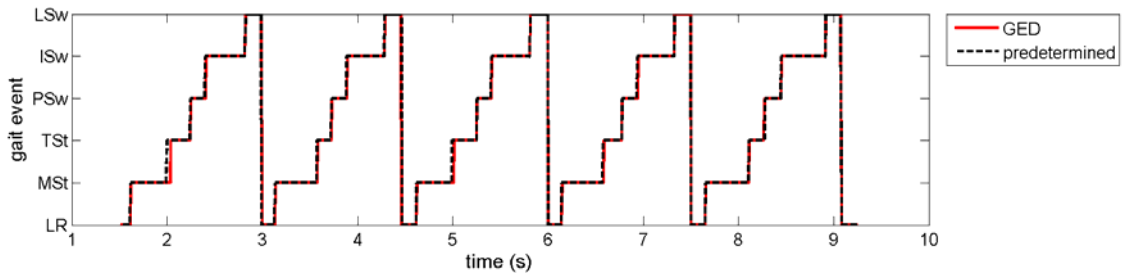

Figure 5.2. Offline output for the FIS GED to detect six gait events. LR = loading response, MSt = mid stance, TSt = terminal stance, PSw = pre-swing, ISw = initial swing, LSw = late swing.

Figure 5.3 shows the accuracy of the GED for determining the gait events for the preferred, slow, and fast speeds for each subject.

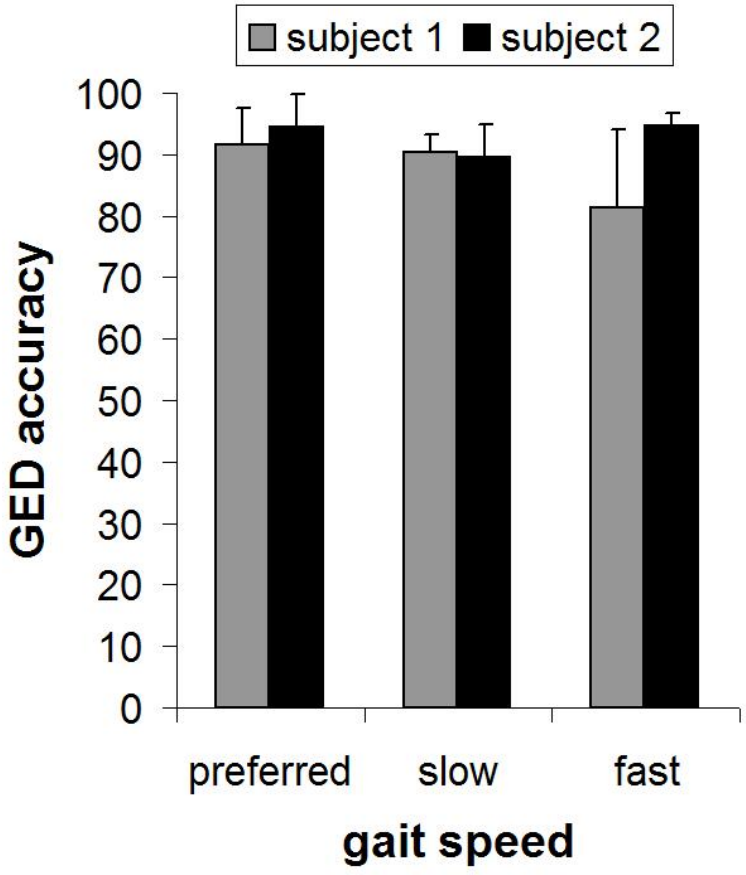

Figure 5.3. Accuracy of the fuzzy inference system gait event detector for two able-bodied subjects and three gait speeds.

Future work should focus on the development of this "next stride correction" FNS controller based on the output of the FIS GED. The goal is to optimize the stimulation patterns of all muscles targeted for FNS control for each successive stride such that forward progression is increased through improvements in joint coordination. In general, the following design which utilizes two sets of parameters, 1) the average duration of each gait phase and 2) the mean sagittal joint angles within each gait phase, may be feasible for this new FNS controller. This FNS controller compares the changes between a respective set of desired parameters and set of current parameters predicted by the FIS GED to determine if the stimulation patterns require modification for the next stride. The assumption is that the dynamics of the next stride will be fairly close to the previous stride. Changes in the average gait event duration will proportionally alter onset/offset stimulation times while changes in mean sagittal joint angle will proportionally alter the stimulus PW and/or IPI of the target muscles for the next stride to drive the system closer to the desired gait pattern.

5.3.2 Considerations for an Active Mechanism for the Exoskeleton

In this work a 24-channel FNS system was used with three primary hip extensors recruited for each limb. Even with all three primary hip extensors activated maximally it was difficult to fully extend the hip at the end of the stance phase. Insufficient hip extension compromises forward propulsion as well as gives rise to anterior trunk tilt. Exoskeletons of HNPs have traditionally been principally passive devices so that the power consumption of the exoskeleton component would be minimal. The underlying assumption in the hybrid approach is that the paralyzed muscles driven by FNS can

adequately serve as the active component of the HNP. With insufficient hip extension, it may be necessary to incorporate an active component to the exoskeleton to provide additional hip extension torque. The amount of torque provided by this active mechanism only has to be enough to augment that achievable by the hip extensors targeted for FNS. **Figure 4.18** indicates that the maximum applied flexion torque on the VCHM as approximately 12 Nm. Thus, the maximum extension torque provided by the proposed active component of the exoskeleton should be at least 12 Nm.

Multiple design challenges come along with the development of this active mechanism. Many of these design challenges are associated with the selection, specification, and optimization of the components of the device which include the prime mover, transmission (i.e., the coupling of the prime mover to the hip), and power supply. With the selection of a particular prime mover comes with the decision to select specific auxiliary components that must be chosen appropriately as well.

For instance, the selection of an electric motor as the prime mover will necessitate the selection of a gearbox to provide the speed and torque conversion. Since a high gear reduction ratio will be required to reduce the speed and increase the torque to accommodate the required hip dynamics, a harmonic drive gearing mechanism such as those used in the strength augmentation exoskeletons, Berkeley lower extremity exoskeleton (BLEEX) [23] and the Hybrid Assistive Leg (HAL-5) [24], may be the best choice for performing the gear reduction. Harmonic drives offer a compact solution to high gear reductions with minimal backlash. One distinct difference between augmentation exoskeletons (i.e., BLEEX and HAL-5) and restorative exoskeletons used in a HNP is that for the restorative exoskeletons, the mobile joints must be backdrivable

by the muscles targeted for FNS. With high gear reduction ratios (on the order of 100), a large amount of applied torque from the user will be necessary to turn the output shaft of the motor due to the inherent friction in the gears. The harmonic drives can be made artificially backdrivable by driving the motor in the desired direction using torque [25] or velocity [26] control. However, this method requires the motor to be run continuously throughout the entire motion of the joint (even when no torque assistance is needed). It would be necessary to develop a mechanism that either acts to decouple the motor from the high gear reduction transmission (i.e., clutch) or reduce the gear reduction ratio of the transmission such that the motor could be backdriven whenever the torque assistance from the motor is not necessary.

An alternative might be selecting a hydraulic motor as the prime mover. In this case, the hydraulic rotary actuators of the VCHM would be the hydraulic motors. With the original hydraulic rotary actuators of the VCHM, backdrivability would not be an issue. A pump must then be selected to drive the hydraulic motor and an accompanying electric motor selected to drive the pump. Access to pump pressure might be controlled via a directional control valve. To achieve a rapid pressure response to the hydraulic rotary actuators of the VCHM without using a large and costly pressure-compensated variable displacement pump, an accumulator charged by a simple fixed displacement pump can be implemented as a pressure source. Feedback from a pump side pressure transducer could be used to recharge accumulator pressure. Components are commercially available to prototype and assess the feasibility of this active hydraulic mechanism.

5.4 CONSTRAINTS WITHOUT LIMITATIONS

This chapter speculated on the significance of the research beyond its intended scope and explored future steps that could be taken to make functional assistive gait realizable. In summary, immediate future work should include the 1) mechanical optimization in the exoskeleton component of the HNP, in both form (i.e., size and weight) and function (i.e., mechanical efficiency), 2) assessment of additional participants, 3) online optimization of muscle stimulation patterns for improved joint coordination, and 4) integration of an active component to the exoskeleton to assist hip extension by FNS. Since the HNP is directly interfaced with the user, the optimization is critical for achieving the best performance from the user. Evaluation of the system with additional participants is important to confirm the results in the current study. Also, walk to fatigue experiments would determine if the statistically relevant improvements translate into clinically relevant improvements. The last two considerations for future work focus on improving upon the active component of the HNP. These proposed methods have the potential of improving trunk posture and forward progression. Optimizing the stimulation patterns is necessary to assess the peak performance of the FNS system when used with the HNP. If it is found that FNS alone is not sufficient to provide adequate hip extension through the new "next stride correction" FNS controller, the results could be used to determined the maximum torque required from the an active mechanism of the exoskeleton. It is important to minimize the required output torque of this active mechanism in order to minimize mass and power requirements such that the system mass does not place an even higher demand on muscles driving joints that are not augmented by the active mechanism.

The general premise for coupling the motion of two joints is to augment the deficient motion of a joint with torque supplied from the dynamics of a second joint that possesses sufficient kinetics to provide augmentation to the first joint. In this study, the stance hip was reciprocally coupled to the contralateral swing hip such that the flexing swing hip would assist stance hip extension. FNS was used as the driving mechanism for the lower extremity joints. However, the muscles activated by FNS were not able to supply enough torque to prevent the joint coupling from compromising the flexion motion of the swing hip. Increases in stimulus intensity through the FNS controller were limited since the baseline stimulation levels for most of the muscles targeted for FNS modulation were already set to maximum safety limits. Thus, the main benefit of joint coupling was in the prevention of the relative motion among the hips and the trunk during double stance when FNS was not required to drive motion. However, dynamic advantages of joint coupling can be realized with the feasibility of the active mechanism. The active mechanism would increase the net torque (i.e., generated by both FNS and active mechanism) achievable by the joint. Conceivably, joints that originally receive no assistance from the active mechanism can be actively driven as well by coupling the respective joint to the joint directly powered by the active mechanism. This design for an active system minimizes the number of prime movers necessary to mobilize multiple joints. Since the relative lower extremity joint kinematics is known and periodic during gait, this distributed power assist system may be ideal for gait. For instance, consider that the active mechanism was designed to power only hip extension as proposed in **Section 5.3.2**. Provided that the active mechanism is capable of generating the require torque, the active mechanism could augment contralateral hip flexion by reciprocally coupling the

hips. Furthermore, with appropriate modifications to the hydraulics, the active mechanism could be extended to augment contralateral knee flexion through the reciprocal coupling of the hips and coupling of contralateral hip flexion with contralateral knee flexion. The coupling ratio between hip flexion and knee flexion may be defined to that determined in **Figure 4.27** by respecifying the cylinder bore sizes of the VCHM and DSKM. With this type of system, the HNP may be capable of facilitating stair ascent which involves larger joint ROMs and moments with a less margin of error in limb trajectory relative to level ground walking. While FNS-only systems has been demonstrated to be feasible in facilitating stair ascent dynamics [27], these factors place a high demand on the consistency and strength of muscles elicited by electrical stimulation. As a result, FES-only stair ascent is exclusive to FES systems equipped with a high number of stimulation channel. The proposed active exoskeleton for the HNP should reduce the demands on FNS for driving joint mobility.

Since the conception of gait assistive systems there has been a strict compromise between stability and mobility. The implementation of the prototype HNP has shown that this compromise can be relaxed through optimally defining the constraints of the system by considering the importance of both stability and mobility at each instant in the gait cycle.

5.5 REFERENCES

1. R. Kobetic, E. B. Marsolais, and P. C. Miller, "Function and strength of electrically stimulated hip flexor muscles in paraplegia," *IEEE Trans.Rehab. Eng*., vol. 2, no. 1, pp. 11-17, Mar. 1994.

2. E. B. Marsolais and B. G. Edwards, "Energy costs of walking and standing with functional neuromuscular stimulation and long leg braces," *Arch. Phys. Med. Rehabil*., vol. 69, pp. 243-249, April 1988.

3. R. Kobetic and E. B. Marsolais, "Synthesis of paraplegic gait with multichannel functional neuromuscular stimulation," *IEEE Trans. Rehab. Eng*., vol. 2, no. 2, pp. 66-79, June 1994.

4. C. S. To, R. F. Kirsch, R. Kobetic, and R. J. Triolo, "Simulation of a functional neuromuscular stimulation powered mechanical gait orthosis with coordinated joint locking," *IEEE Trans. Neural Syst. Rehab. Eng*., vol. 13, no. 2, pp. 227-235, 2005.

5. J. Perry, *Gait Analysis: Normal and Pathological Function.* Thorofare, NJ: SLACK Inc., 1992, pp. 61, 100, 120, 247.

6. H. M. Franken, P. H. Veltink, G. Baardman, R. A. Redmeyer, and H. B. K. Boom, "Cycle-to-cycle control of swing phase of paraplegic gait induced by surface electrical stimulation," *Med. Biol. Eng. Comp.*, vol. 33, pp. 440-451, 1995.

7. P. H. Veltink, "Control of FES-induced cyclical movements of the lower leg," *Med. Biol. Eng. Comp.*, vol. 29, pp. NS8-NS12, 1991.

8. H. M. Franken, P. H. Veltink, G. Baardman, R. A. Redmeijer, and H. B. K. Boom, "Experimental on/off control of the swing phase of paraplegic gait induced by surface electrical stimulation," *Proc. 15th IEEE EMBS Conf.*, San Diego, CA, USA, pp. 1324-1325, 1993.

9. H. M. Franken, W. de Vries, P. H. Veltink, G. Baardman, and H. B. K. Boom, "State detection during paraplegic gait as part of a finite state based controller," *Proc. 15th IEEE EMBS Conf.*, San Diego, CA, USA, pp. 1322-1323, 1993.

10. B. J. Andrews, R. W. Barnett, G. F. Phillips, C. A. Kirkwood, N. Donaldson, D. N. Rushton, and D. A. Perkins, "Rule-based control of a hybrid FES orthosis for assisting paraplegic locomotion," *Automedica*, vol. 11, pp. 175-199, 1989.

11. A. T. M. Willemsen, F. Bloemhof, and H. B. K. Boom, "Automatic stance-swing phase detection from accelerometer data for peroneal nerve stimulation," *IEEE Trans. Biomed. Eng.*, vol. 37, no. 12, pp. 1201-1208, Dec. 1990.

12. I. P. I. Pappas, M. Popovic, T. Keller, V. Dietz, and M. Morari, "A reliable gait phase detection system," *IEEE Trans. Neural Systems Rehab. Eng.*, vol. 9, no. 2, pp. 113-125, June 2001.

13. C. A. Kirkwood and B. J. Andrews, "Finite state control of FES systems: Application of AI inductive learning techniques," *Proc. 11th IEEE EMBS Conf.*, Seattle, WA, USA, pp. 1020-1021, 1989.

14. Z. M. Nikolic and D. B. Popovic, "Automatic rule determination for finite state model of locomotion," *Proc. 16th IEEE EMBS Conf.*, Baltimore, MD, USA, pp. 1382-1383, 1994.

15. A. Kostov, B. J. Andrews, D. B. Popovic, R. B. Stein, and W. Armstrong, "Machine learning in control of functional electrical stimulation systems for locomotion," *IEEE Trans. Biomed. Eng.*, vol. 42, pp. 541–551, June 1995.

16. R. Williamson and B. J. Andrews, "Gait event detection for FES using accelerometers and supervised machine learning," *IEEE Trans. Rehab. Eng.*, vol. 8, no. 3, pp. 312-319, Sept. 2000.

17. M. Hansen, M. K. Haugland, and T. Sinkjaer, "Evaluating robustness of gait event detection based on machine learning and natural sensors," *IEEE Trans. Neural Systems Rehab. Eng.*, vol. 12, no. 1, pp. 81-88, March 2004.

18. S. K. Ng and H. J. Chizeck, "A fuzzy logic gait event detector for FES paraplegic gait," *Proc. 15th IEEE EMBS Conf.*, San Diego, CA, USA, pp. 1238-1239, 1993.

19. S. K. Ng and H. J. Chizeck, "Fuzzy model identification for classification of gait events in paraplegics," *IEEE Trans. Fuzzy Syst.*, vol. 5, pp. 536–544, Nov. 1997.

20. M. M. Skelly and H. J. Chizeck, "Real-time gait event detection for paraplegic FES walking," *IEEE Trans. Neural Systems Rehab. Eng.*, vol. 9, no. 1, pp. 59-68, March 2001.

21. D. Graupe, K. H. Kohn, A. Kralj, and S. Basseas, "Patient controlled electrical stimulation via EMG signature discrimination for providing certain paraplegics with primitive walking functions," *J. Biomed. Eng.*, vol. 5, no. 3, pp. 220-226, July 1983.

22. B. J. Andrews, A. Kostov, and R. B. Stein, "Gait event and user intention detection for FES-control: Selecting sensors," *Proc. 17th IEEE EMBS Conf.*, Montreal, Que., Canada, vol. 2, pp. 1153-1154, 1995.

23. A. Zoss and H. Kazerooni, "Design of an electrically actuated lower extremity exoskeleton," *Advanced Robotics*, vol.20, no. 9, pp. 967-988, 2006.

24. H. Kawamoto, S. Kanbe, and Y. Sankai, " Power assist method for HAL-3 estimating operator's intention based on motion information," *Proc. IEEE International Workshop on Robot and Human Interactive Communication*, Millbrae, CA, USA, pp. 67-72, Oct. 2003.

25. H. Kazerooni, "Dynamics and control of instrumented harmonic drives," *ASME Trans. J. Dynamic Systems, Measurements, and Control*, vol. 117, pp. 15-19, Mar. 1995.

26. T. Nef and P. Lum, "Improving backdrivability in geared rehabilitation robots," *Med. Biol. Eng. Comput.*, DOI 10.1007/s11517-009-0437-0, Jan. 2009.

27. R. Kobetic, S. G. Carrol, and E. B. Marsolais, "Paraplegic stair climbing assisted by electrical stimulation," 39*th* *Annual Conference on Engineering in Medicine and Biology*. pp. 265, 1986.

APPENDIX A

PRESSURE TO TORQUE CALIBRATIONS

A way to estimate the applied torque is to calculate the torque from the mechanism geometry and pressure transducer measurements. However, the geometry of the cylinder heads and the flow area reduction through the cylinder ports give rise to pressure losses. These cylinder head losses are not measured by the pressure transducers which only measure the pressure outside the cylinder ports. In order to accurately calculate the applied hip torque from the cylinder pressure, a calibration curve of measured torque, τ_m (applied by a robotic dynamometer), versus calculated torque, τ_c (calculated from the pressure transducers and transmission geometry), was individually determined for the DSKM and VCHM. The measured torque and pressure data was acquired from the respective system characterization of each mechanism described in **Section 2.5.2** and **Section 3.4.1**. The moment arm of the VCHM is the pinion radius of the hydraulic rotary actuator while the instantaneous moment arm of the DSKM linkage mechanism was determined from the measured knee angle. **Figure A.1a** and **Figure A.2a** show respectively the actual torque measured (τ_m) by the dynamometer plotted against the estimated torque calculated from pressure (τ_c) for the DSKM and VCHM. First-order least squares regressions with 95 % confidence intervals was fitted to each data set. **Equation A.1** and **Equation A.2** are the least squares regressions for calibrating τ_c to τ_m for pressure measured from the DSKM and VCHM, respectively.

$$\tau_m = 1.314\tau_c - 0.915 \text{ (Nm)} \quad \textbf{(A.1)}$$

$$\tau_m = 1.127\tau_c - 0.856 \text{ (Nm)} \quad \textbf{(A.2)}$$

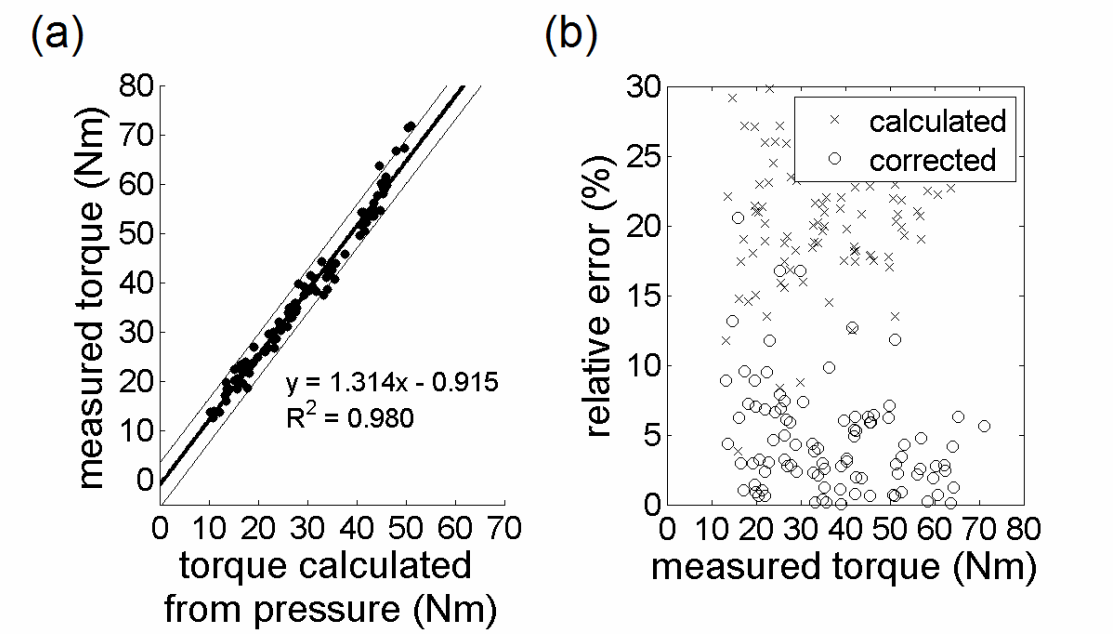

Figure A.1. Calibration of the torque applied to the DSKM calculated from the joint angle and pressure.

Figure A.1b shows the relative error with respect to torque magnitude from additional validation data when **Equation A.1** was applied to torque estimates calculated from pressure for the DSKM.

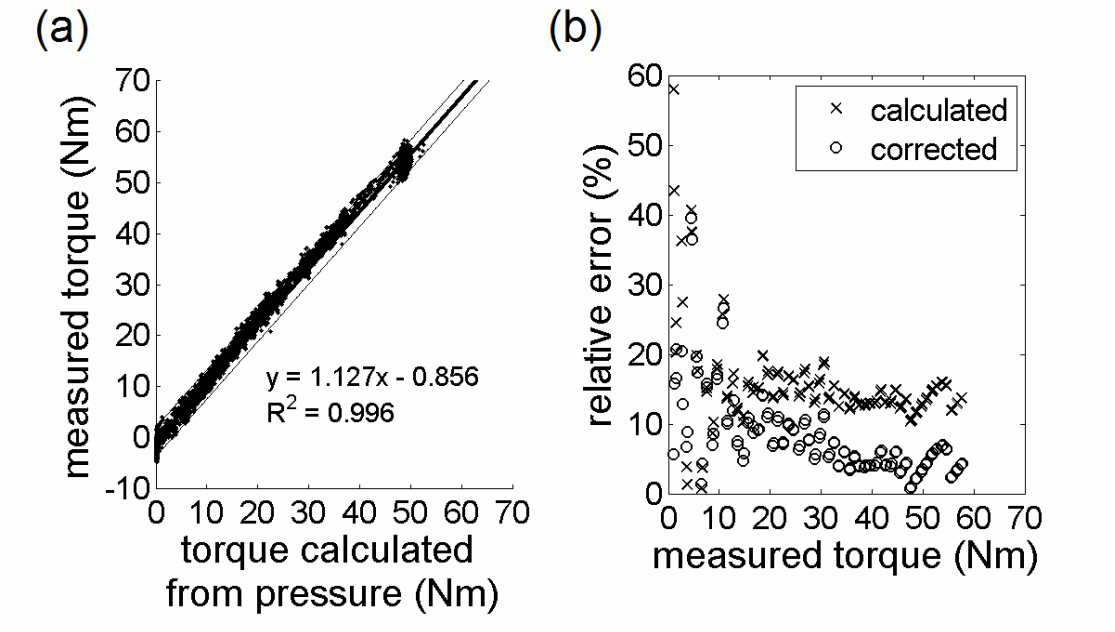

Figure A.2. Calibration of the torque applied to the VCHM calculated from pressure.

Similarly, **Figure A.2b** shows the relative error in validation torque data calculated using pressure data from the VCHM and corrected using **Equation A.2**. The corrected torque was generally within 10 % of the measured torque data which is sufficient for obtaining estimates of the user applied torques on each mechanism.

APPENDIX B

FUZZY INFERENCE SYSTEM GAIT EVENT DETECTOR

The following describes how the FIS component of the GED (**Chapter 5**) determines the gait events. This first control layer is a zero-order Takagi-Sugeno-Kang FIS that serves to estimate the gait events. The gait cycle was divided into six gait phases with respect to the right limb – loading response (LR), midstance (MSt), terminal stance (TSt), pre-swing (PSw), initial swing (ISw), and late swing (LSw). The FIS involves the mapping of ten input variables (i.e., six joint angles and four foot pressure sensors) to a single output variable (i.e., gait event). A fuzzy set, characterizing each gait event, is a set of ordered pairs defined in **Equation B.1**.

$$GE_{ij} = \{(x_i, \mu_{GE_{ij}}(x_i)) \mid x_i \in X_i\}. \quad \textbf{(B.1)}$$

In **Equation B.1**, x_i is the instantaneous input of a sensor (i = 1, 2, . . . , 10), X_i is the universe of discourse or continuous range of the sensor input during the entire gait cycle, and $\mu_{GE_{ij}}(x_i)$ is the membership function representing the fuzzy set for each gait event (j = 1, 2, . . . , 6). Thus, six input membership functions occupy the universe of discourse of each of the ten inputs. The shape of the input membership functions is the Gaussian probability density function of the input during a particular gait event (**Figure B.1**). This method eliminates the subjectivity and heuristics normally involved in defining membership functions. The sensor signals are fuzzified by the input membership functions which assign a degree of belonging (between 0 and 1) of a particular input to each gait event. One IF-THEN rule was used to govern each gait event. The antecedent (IF variables) of the each rule, a_j, is resolved by an intersection or T-norm operator,

algebraic product, to obtain a single value representing the degree of support for each rule as shown in **Equation B.2**.

$$a_j = \bigcap_{i=1}^{10} \mu_{GE_{ij}}(x_i) = \prod_{i=1}^{10} \mu_{GE_{ij}}(x_i). \quad \textbf{(B.2)}$$

The output of the antecedent (degree of support) of each rule is weighted and applied in the implication method by the algebraic product operator to modify the fuzzy set of the consequent (THEN variable) of the rule.

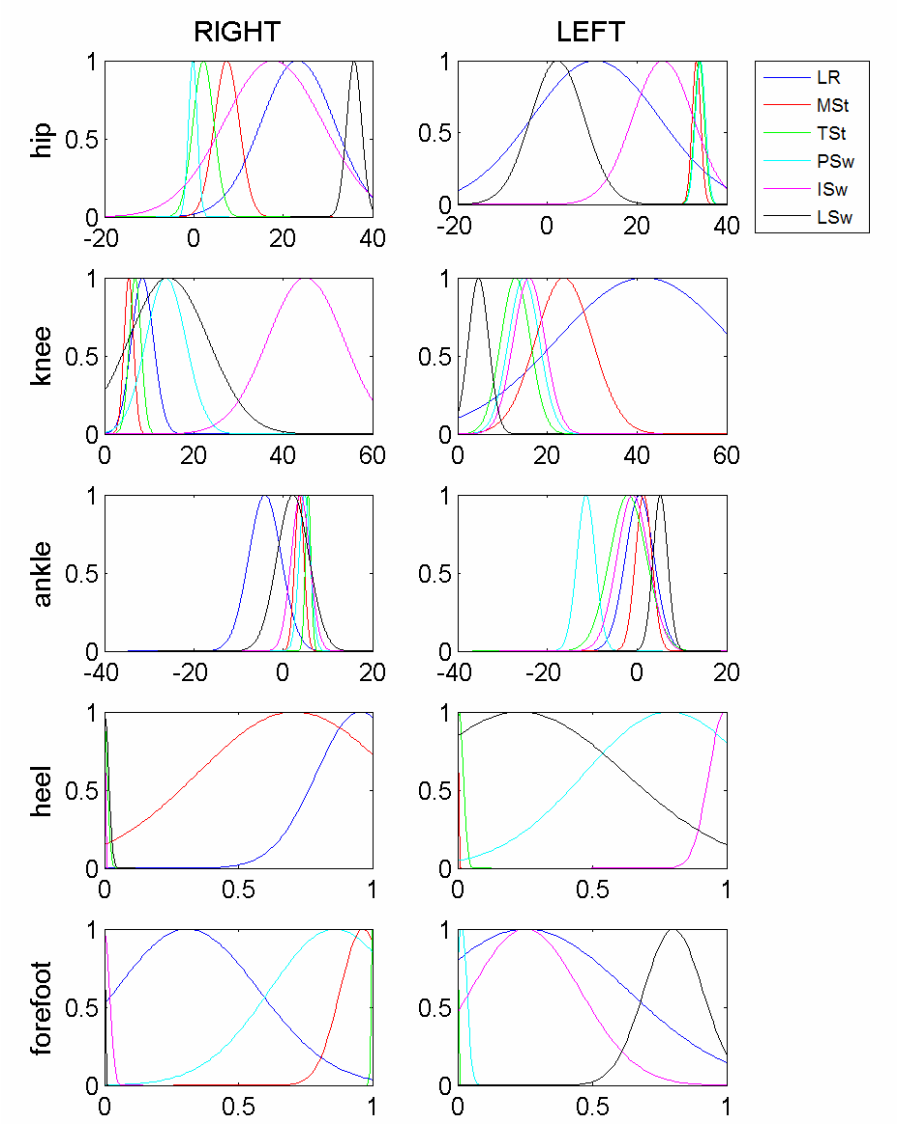

Figure B.1. Input membership functions trained from an able-bodied subject walking at preferred speed.

Each output membership function is represented as a singleton with each gait event denoted as a single value in the output universe of discourse. The modified output membership functions, representing the output of each rule, are then aggregated by summation into a single fuzzy set. The fuzzy set is defuzzified into a single output value representing the predicted gait event by calculating the center of area of the singletons. The aggregation and defuzzification methods are executed by **Equation B.3**:

$$\text{gait event} = \frac{\sum_{j=1}^{6} \mu'_{GE_j}(a_j, w_j) f_j}{\sum_{j=1}^{6} \mu'_{GE_j}(a_j, w_j)}. \qquad \textbf{(B.3)}$$

In **Equation B.3**, $\mu'_{GE_j}(a_j, w_j)$ is the implicated output membership function of each consequent, w_j is the weight applied to the antecedent, a_j, and f_j is the output of each rule (i.e., scalar value assigned to each gait event).

APPENDIX C

CUSTOM COMPONENTS DESIGNED FOR THE PROTOTYPE EXOSKELETON OF THE HYBRID NEUROPROSTHESIS

The following parts were designed using SolidWorks 3-D CAD Design Software (Dassault Systèmes SolidWorks Corp., Concord, MA) and machined on a Smithy® Midas 1220 LTD lathe-mill-drill (Smithy Company, Ann Arbor, MI, USA) or Sherline 5400/5410 tabletop mill (Sherline Products, Inc., Vista, CA, USA).

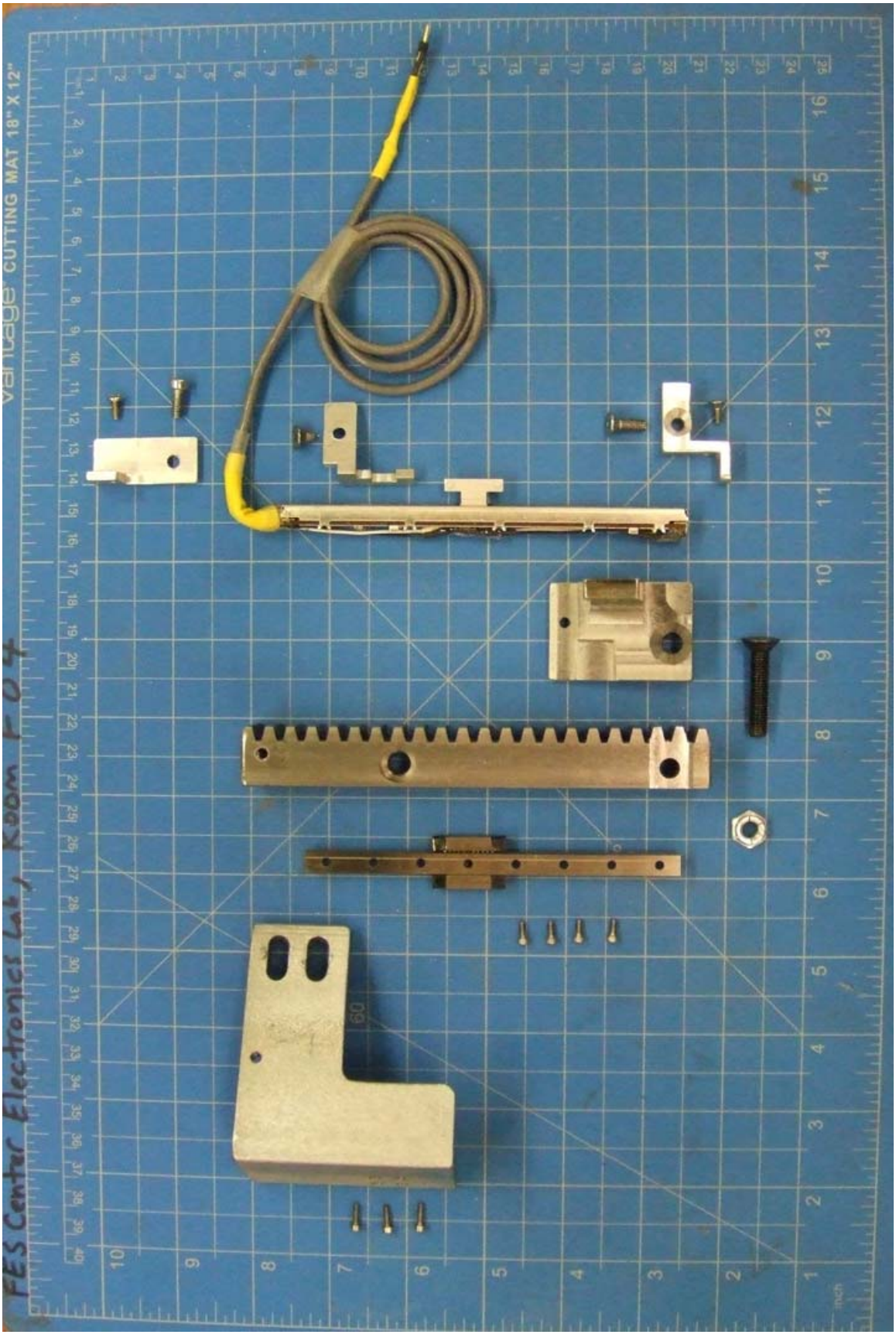
CUTTING MAT 18" X 12"
FES Center Electronics Lab, Room 204

Vantage CUTTING MAT 18" X 12"
FES Center Electronics Lab, Room F04
60°
45°

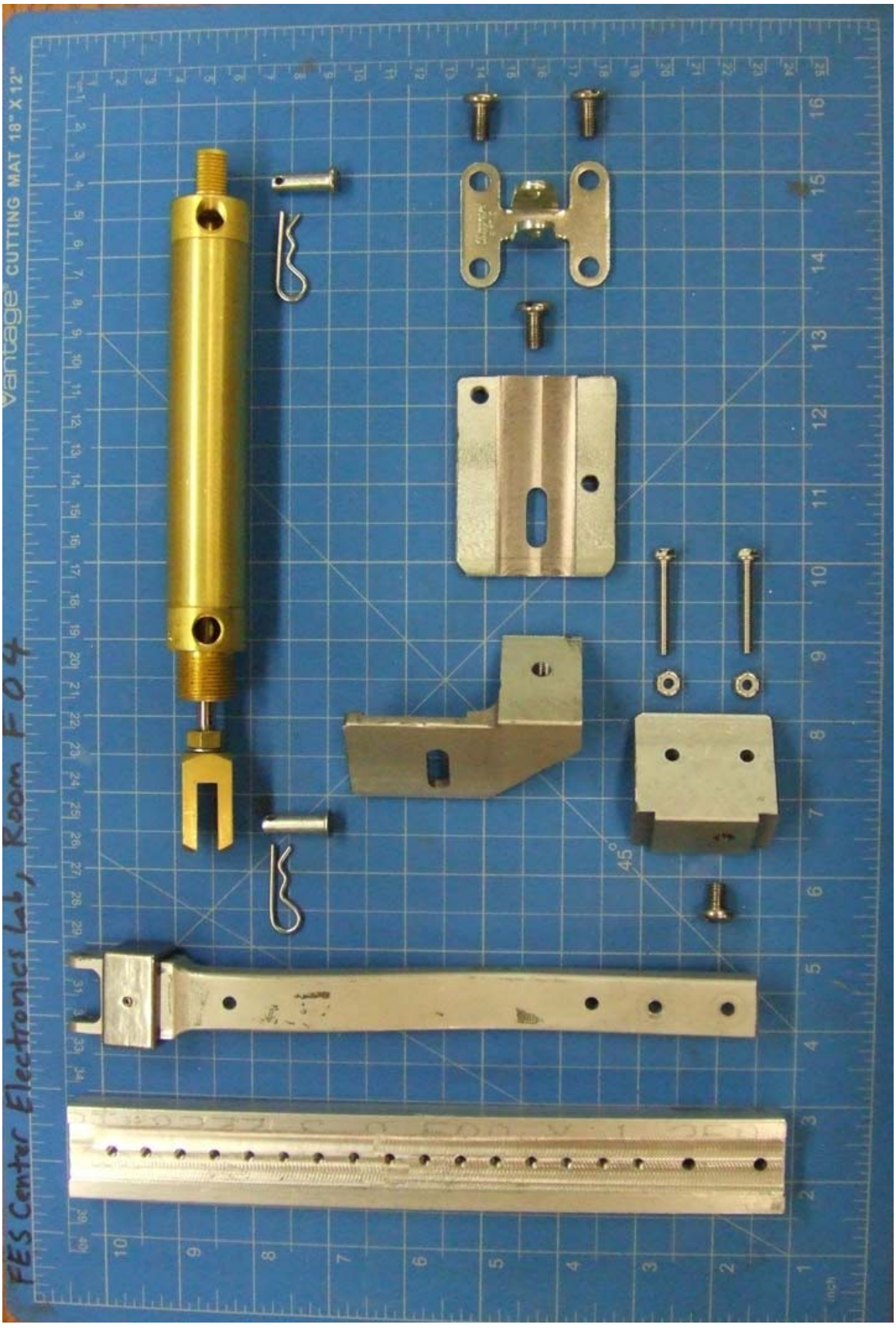
Vantage CUTTING MAT 18" X 12"
FES Center Electronics Lab, Room F04
45°


Vantage CUTTING MAT 18" X 12"
FES Center Electron
Room F04


Vantage CUTTING MAT 18" X 12"
FES Center Electronics Room F04
45°

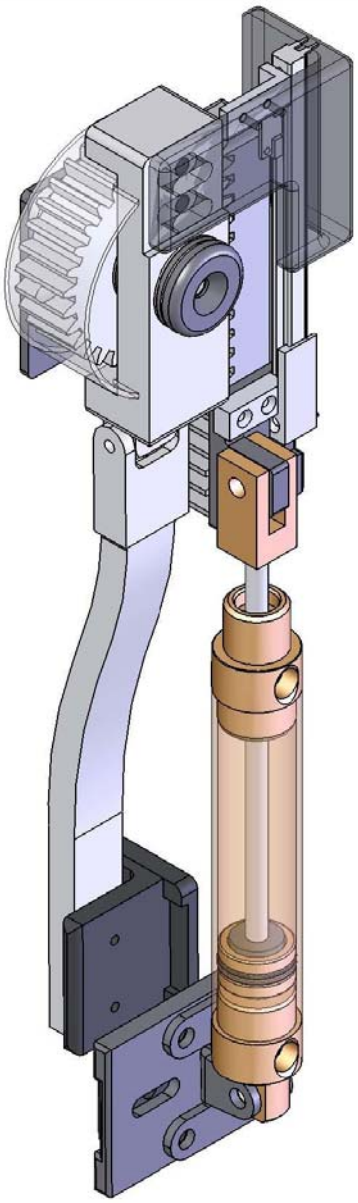

		DIMENSIONS ARE IN INCHES TOLERANCES: FRACTIONAL ± ANGULAR: MACH ± BEND ± TWO PLACE DECIMAL ± THREE PLACE DECIMAL ±		NAME	DATE
			DRAWN		
			CHECKED		
			ENG APPR.		
			MFG APPR.		
			Q.A.		
		MATERIAL	COMMENTS:		
NEXT ASSY	USED ON	FINISH	Designed by Curtis S. To on Dec. 2007 for the Variable Constraint Hip Mechanism for the Hybrid Neuroprosthesis		
APPLICATION		DO NOT SCALE DRAWING			

Cleveland FES Center

Hydraulic Rotary Actuator Concept 03 (left)

SIZE	DWG. NO.	REV.
A	HydraulicRotaryActuator_concept03_3D	
SCALE:1:1.5	WEIGHT:	SHEET 1 OF 1

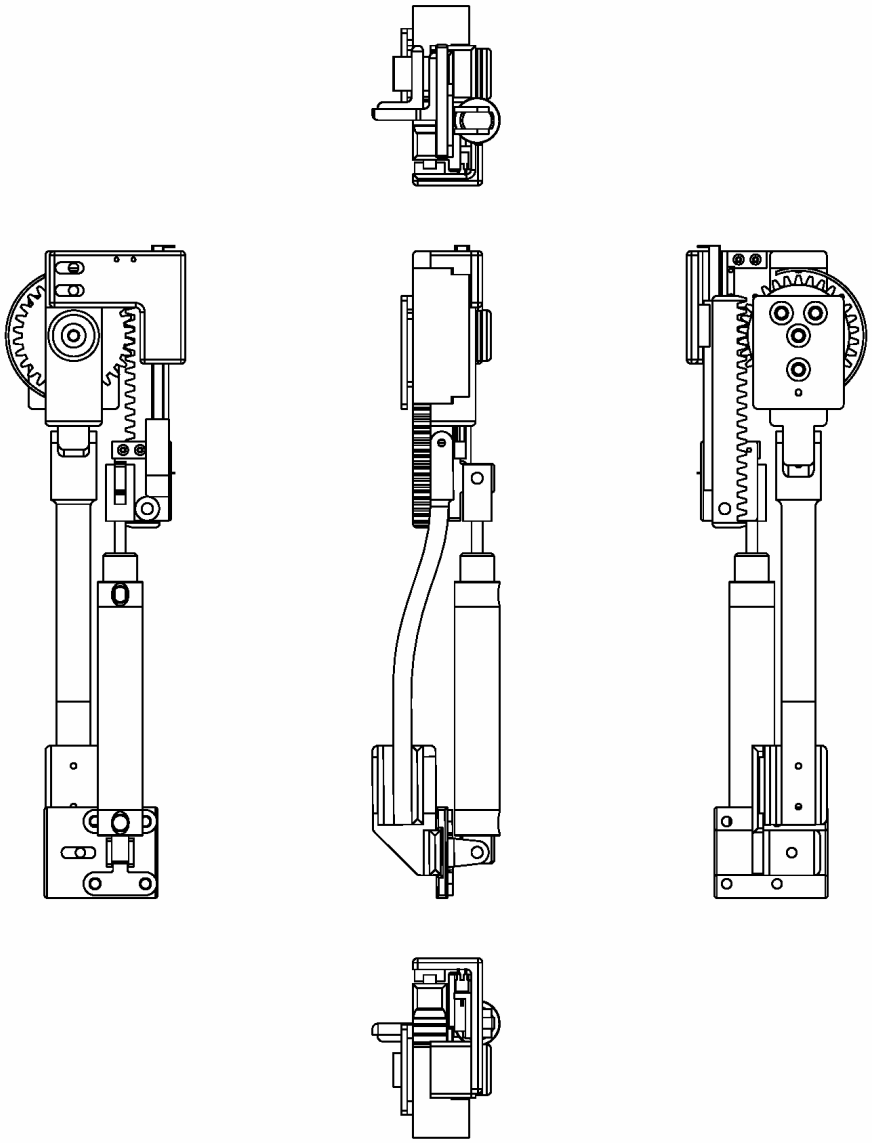

		DIMENSIONS ARE IN INCHES TOLERANCES: FRACTIONAL ± ANGULAR: MACH ± BEND ± TWO PLACE DECIMAL ± THREE PLACE DECIMAL ±		NAME	DATE
			DRAWN		
			CHECKED		
			ENG APPR.		
			MFG APPR.		
		MATERIAL	Q.A.		
			COMMENTS:		
NEXT ASSY	USED ON	FINISH			
APPLICATION		DO NOT SCALE DRAWING			

Cleveland FES Center

Hydraulic Rotary Actuator Concept 03 (left)

SIZE	DWG. NO.	REV.
A	HydraulicRotaryActuator_concept03	
SCALE: 1:3	WEIGHT:	SHEET 1 OF 1

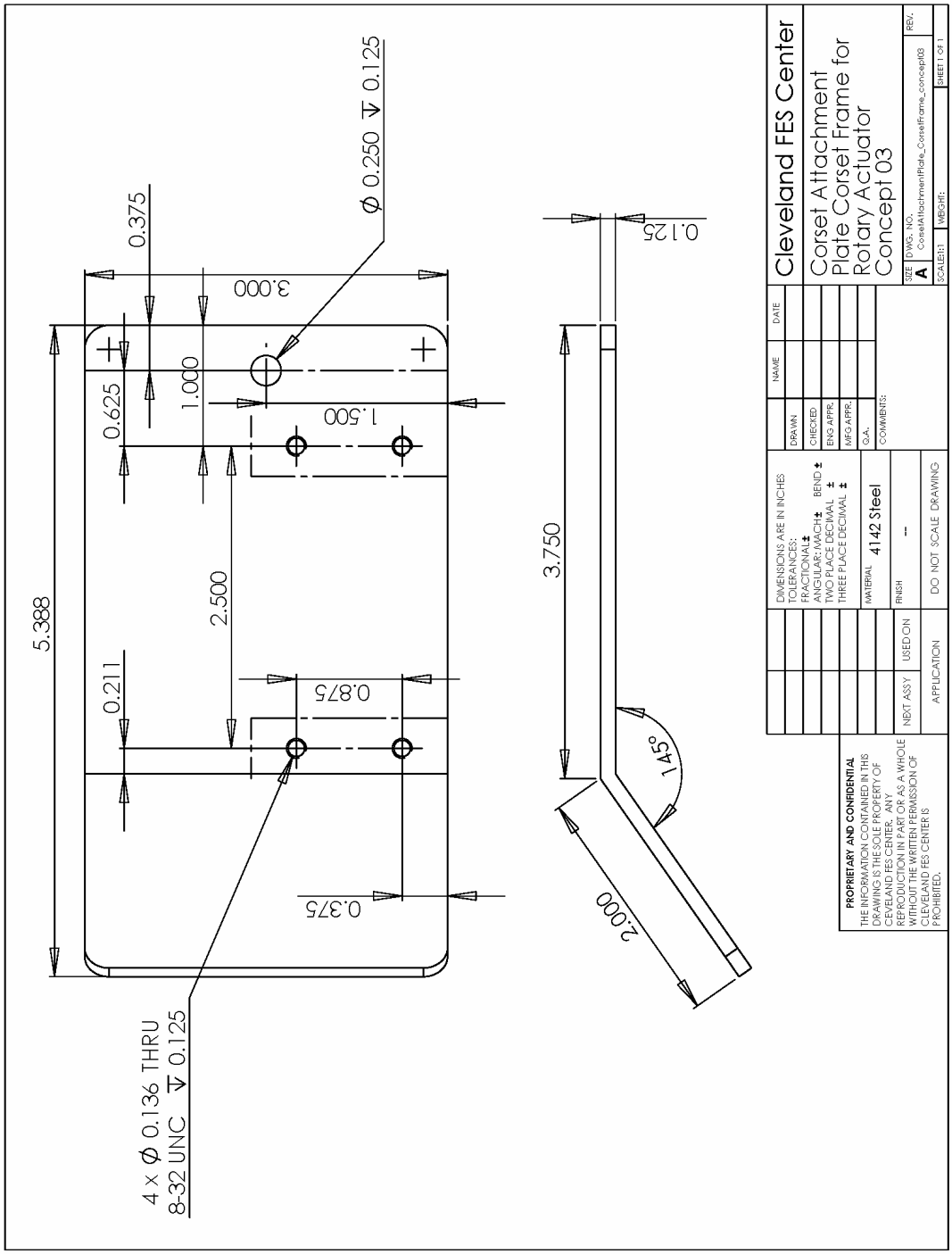
Cleveland FES Center
Corset Attachment Plate Corset Frame for Rotary Actuator Concept 03
DIMENSIONS ARE IN INCHES
TOLERANCES:
FRACTIONAL ±
ANGULAR: MACH ± BEND ±
TWO PLACE DECIMAL ±
THREE PLACE DECIMAL ±
MATERIAL 4142 Steel
FINISH --
DO NOT SCALE DRAWING
PROPRIETARY AND CONFIDENTIAL
THE INFORMATION CONTAINED IN THIS DRAWING IS THE SOLE PROPERTY OF CEVELAND FES CENTER. ANY REPRODUCTION IN PART OR AS A WHOLE WITHOUT THE WRITTEN PERMISSION OF CLEVELAND FES CENTER IS PROHIBITED.
5.388
3.000
0.375
0.625
1.000
1.500
2.500
0.211
0.875
0.375
Ø 0.250 ↧ 0.125
4 x Ø 0.136 THRU
8-32 UNC ↧ 0.125
3.750
0.125
145°
2.000

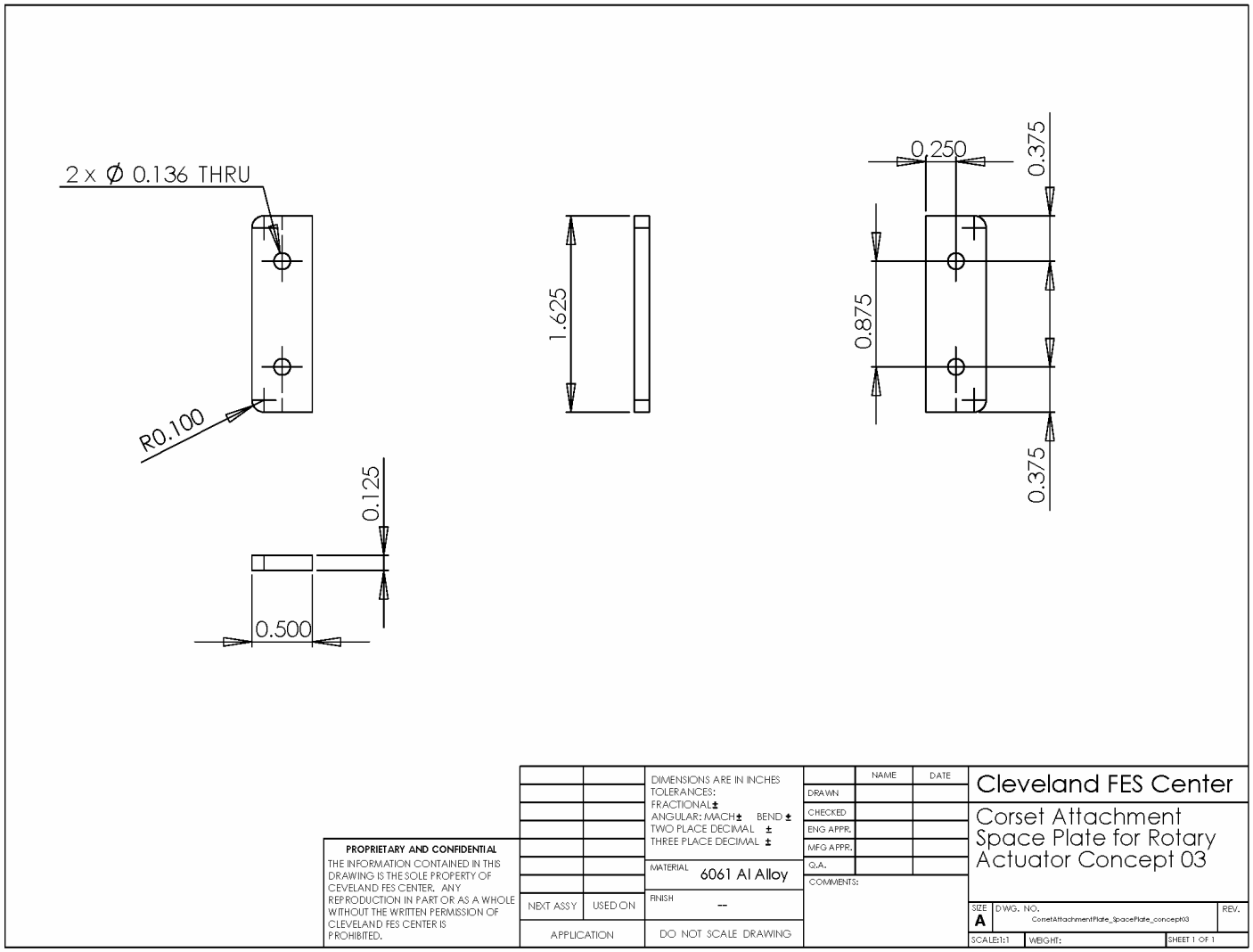
2 x Ø 0.136 THRU
R0.100
1.625
0.250
0.375
0.875
0.375
0.125
0.500
PROPRIETARY AND CONFIDENTIAL
THE INFORMATION CONTAINED IN THIS DRAWING IS THE SOLE PROPERTY OF CEVELAND FES CENTER. ANY REPRODUCTION IN PART OR AS A WHOLE WITHOUT THE WRITTEN PERMISSION OF CLEVELAND FES CENTER IS PROHIBITED.
NEXT ASSY
USED ON
APPLICATION
DIMENSIONS ARE IN INCHES
TOLERANCES:
FRACTIONAL ±
ANGULAR: MACH ± BEND ±
TWO PLACE DECIMAL ±
THREE PLACE DECIMAL ±
MATERIAL 6061 Al Alloy
FINISH --
DO NOT SCALE DRAWING
NAME
DATE
DRAWN
CHECKED
ENG APPR.
MFG APPR.
Q.A.
COMMENTS:
Cleveland FES Center
Corset Attachment Space Plate for Rotary Actuator Concept 03
SIZE A
DWG. NO. CorsetAttachmentPlate_SpacePlate_conceptK3
REV.
SCALE:1:1
WEIGHT:
SHEET 1 OF 1

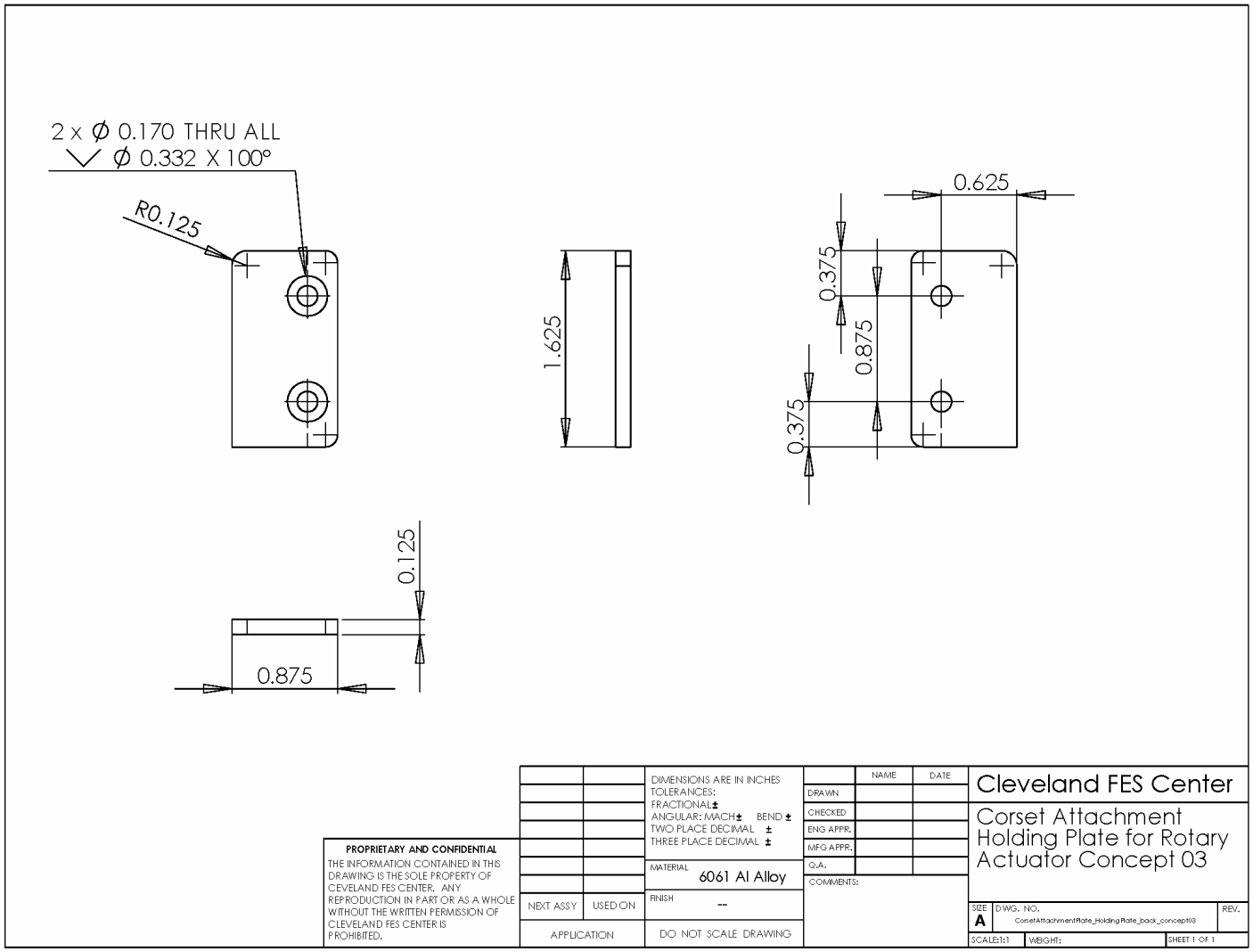

		DIMENSIONS ARE IN INCHES TOLERANCES: FRACTIONAL ± ANGULAR: MACH ± BEND ± TWO PLACE DECIMAL ± THREE PLACE DECIMAL ±	
		MATERIAL 6061 Al Alloy	
NEXT ASSY	USED ON	FINISH --	
APPLICATION		DO NOT SCALE DRAWING	

	NAME	DATE
DRAWN		
CHECKED		
ENG APPR.		
MFG APPR.		
Q.A.		
COMMENTS:		

PROPRIETARY AND CONFIDENTIAL

THE INFORMATION CONTAINED IN THIS DRAWING IS THE SOLE PROPERTY OF CEVELAND FES CENTER. ANY REPRODUCTION IN PART OR AS A WHOLE WITHOUT THE WRITTEN PERMISSION OF CLEVELAND FES CENTER IS PROHIBITED.

Cleveland FES Center

Corset Attachment Holding Plate for Rotary Actuator Concept 03

SIZE	DWG. NO.	REV.
A	CorsetAttachmentPlate_HoldingPlate_back_concept03	
SCALE:1:1	WEIGHT:	SHEET 1 OF 1

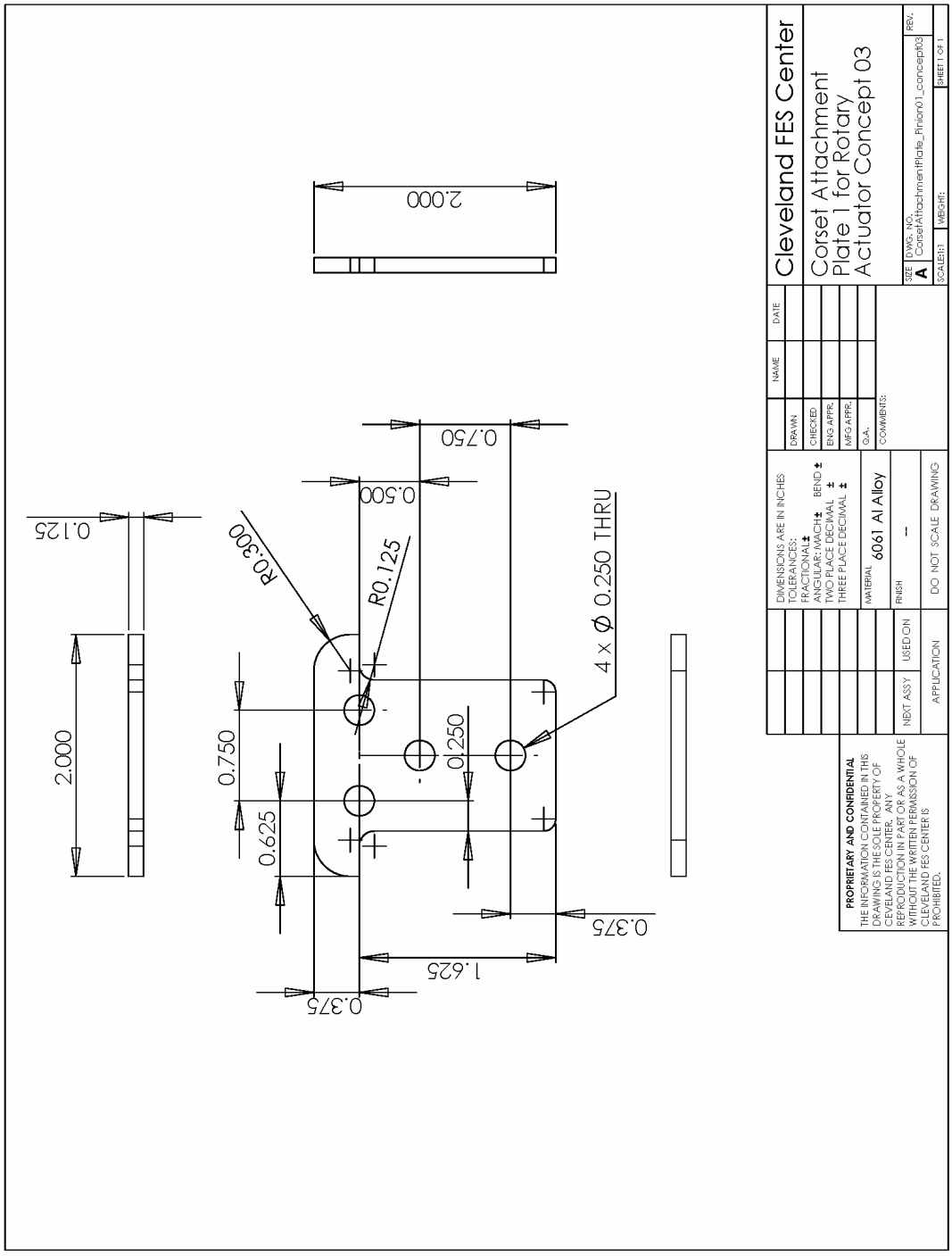
2.000
0.125
2.000
R0.300
R0.125
0.750
0.500
4 x Ø 0.250 THRU
0.750
0.625
0.250
0.375
1.625
0.375
Cleveland FES Center
Corset Attachment
Plate 1 for Rotary
Actuator Concept 03
DIMENSIONS ARE IN INCHES
TOLERANCES:
FRACTIONAL ±
ANGULAR: MACH ± BEND ±
TWO PLACE DECIMAL ±
THREE PLACE DECIMAL ±
MATERIAL 6061 Al Alloy
FINISH --
DO NOT SCALE DRAWING
DRAWN
CHECKED
ENG APPR.
MFG APPR.
Q.A.
COMMENTS:
NAME
DATE
NEXT ASSY
USED ON
APPLICATION
PROPRIETARY AND CONFIDENTIAL
THE INFORMATION CONTAINED IN THIS DRAWING IS THE SOLE PROPERTY OF CEVELAND FES CENTER. ANY REPRODUCTION IN PART OR AS A WHOLE WITHOUT THE WRITTEN PERMISSION OF CLEVELAND FES CENTER IS PROHIBITED.
SIZE A
DWG. NO. CorsetAttachmentPlate_Pinion01_concept03
REV:
SCALE:1:1
WEIGHT:
SHEET 1 OF 1

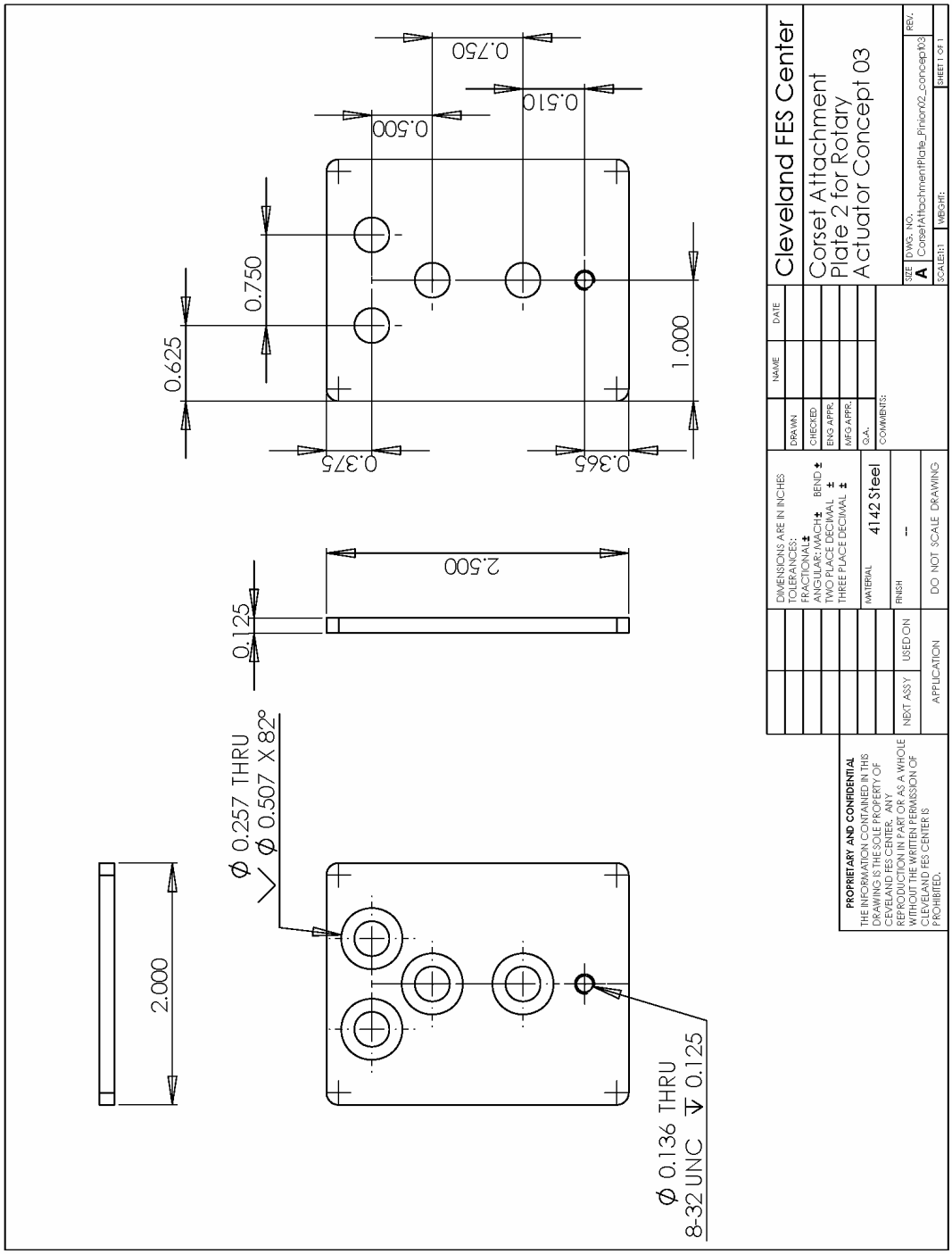
0.750
0.510
0.500
0.750
0.625
1.000
0.375
0.365
2.500
0.125
Ø 0.257 THRU
Ø 0.507 X 82°
2.000
Ø 0.136 THRU
8-32 UNC ↧ 0.125
Cleveland FES Center
Corset Attachment
Plate 2 for Rotary
Actuator Concept 03
DIMENSIONS ARE IN INCHES
TOLERANCES:
FRACTIONAL ±
ANGULAR: MACH ± BEND ±
TWO PLACE DECIMAL ±
THREE PLACE DECIMAL ±
MATERIAL 4142 Steel
FINISH --
DRAWN
CHECKED
ENG APPR.
MFG APPR.
Q.A.
COMMENTS:
NAME
DATE
NEXT ASSY
USED ON
APPLICATION
DO NOT SCALE DRAWING
SIZE A
DWG. NO. Corset Attachment Plate_Pinion02_concept03
REV:
SCALE 1:1
WEIGHT:
SHEET 1 OF 1
PROPRIETARY AND CONFIDENTIAL
THE INFORMATION CONTAINED IN THIS DRAWING IS THE SOLE PROPERTY OF CEVELAND FES CENTER. ANY REPRODUCTION IN PART OR AS A WHOLE WITHOUT THE WRITTEN PERMISSION OF CLEVELAND FES CENTER IS PROHIBITED.

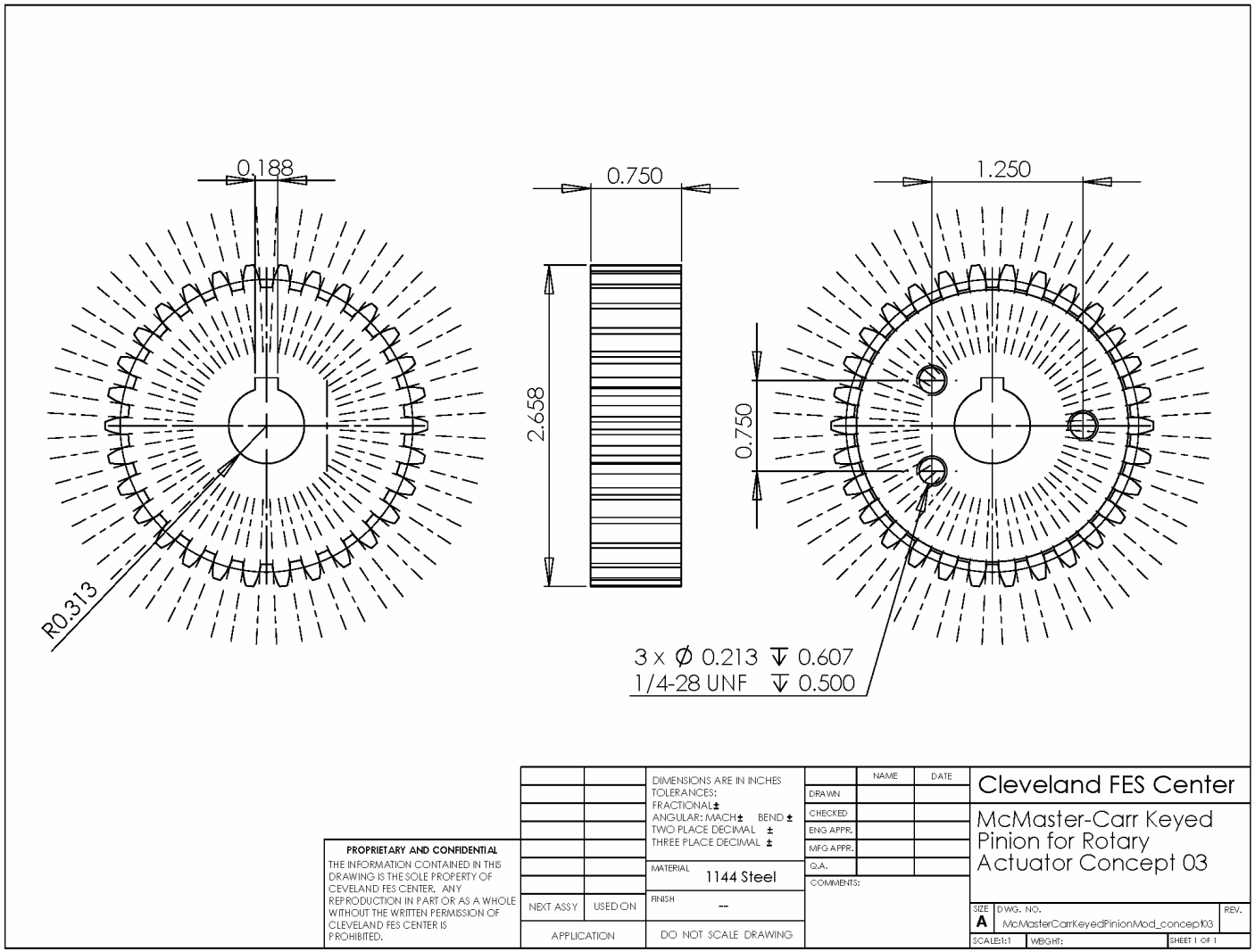
0.188
0.750
1.250
2.658
0.750
R0.313
3 x Ø 0.213 ↧ 0.607
1/4-28 UNF ↧ 0.500
PROPRIETARY AND CONFIDENTIAL
THE INFORMATION CONTAINED IN THIS DRAWING IS THE SOLE PROPERTY OF CEVELAND FES CENTER. ANY REPRODUCTION IN PART OR AS A WHOLE WITHOUT THE WRITTEN PERMISSION OF CLEVELAND FES CENTER IS PROHIBITED.
NEXT ASSY
USED ON
APPLICATION
DIMENSIONS ARE IN INCHES
TOLERANCES:
FRACTIONAL ±
ANGULAR: MACH ± BEND ±
TWO PLACE DECIMAL ±
THREE PLACE DECIMAL ±
MATERIAL 1144 Steel
FINISH --
DO NOT SCALE DRAWING
NAME
DATE
DRAWN
CHECKED
ENG APPR.
MFG APPR.
Q.A.
COMMENTS:
Cleveland FES Center
McMaster-Carr Keyed Pinion for Rotary Actuator Concept 03
SIZE A
DWG. NO. McMasterCarrKeyedPinionMod_concept03
REV.
SCALE:1:1
WEIGHT:
SHEET 1 OF 1

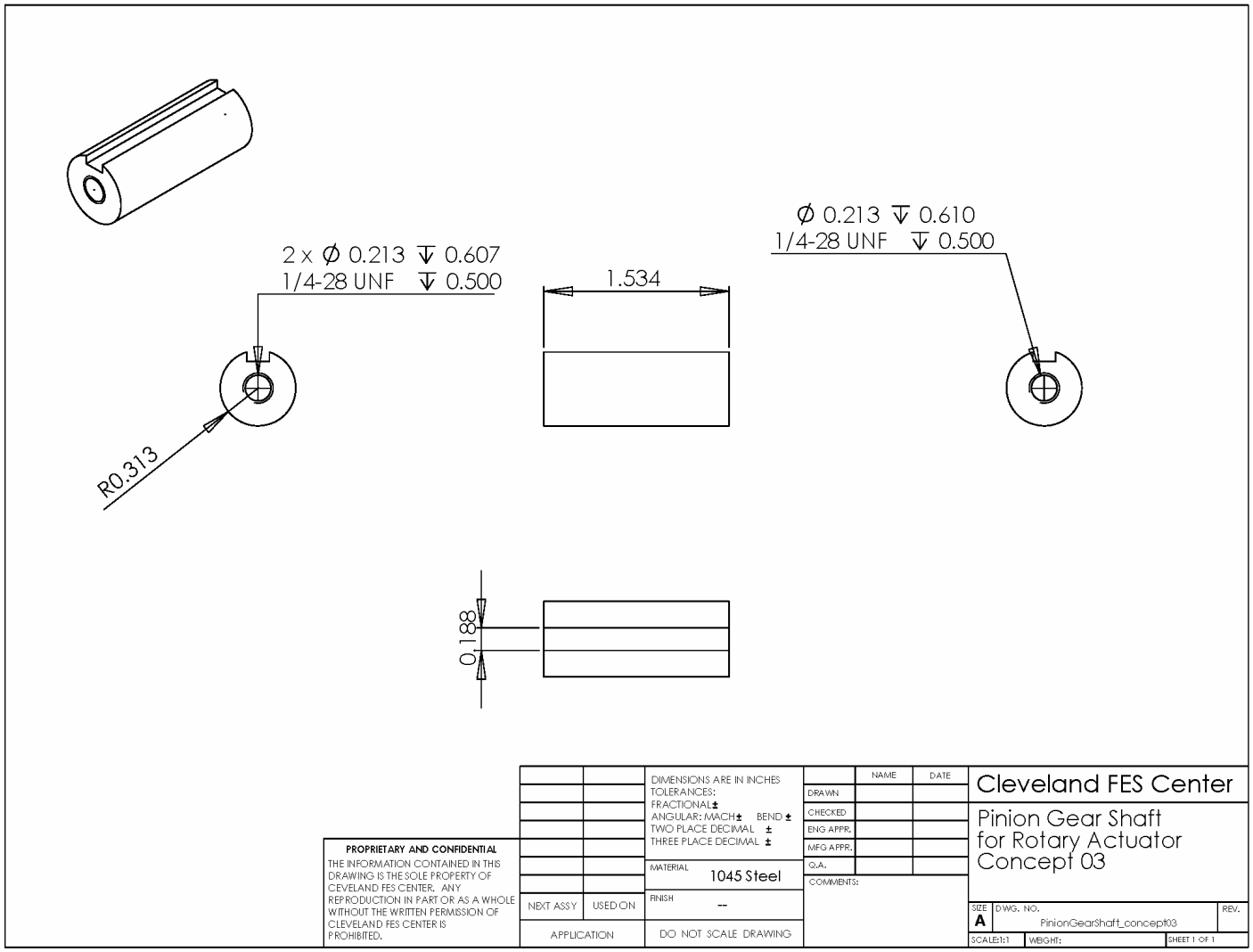
2 x Ø 0.213 ↧ 0.607
1/4-28 UNF ↧ 0.500
1.534
Ø 0.213 ↧ 0.610
1/4-28 UNF ↧ 0.500
R0.313
0.188
PROPRIETARY AND CONFIDENTIAL
THE INFORMATION CONTAINED IN THIS DRAWING IS THE SOLE PROPERTY OF CEVELAND FES CENTER. ANY REPRODUCTION IN PART OR AS A WHOLE WITHOUT THE WRITTEN PERMISSION OF CLEVELAND FES CENTER IS PROHIBITED.
NEXT ASSY
USED ON
APPLICATION
DIMENSIONS ARE IN INCHES
TOLERANCES:
FRACTIONAL ±
ANGULAR: MACH ± BEND ±
TWO PLACE DECIMAL ±
THREE PLACE DECIMAL ±
MATERIAL 1045 Steel
FINISH --
DO NOT SCALE DRAWING
NAME
DATE
DRAWN
CHECKED
ENG APPR.
MFG APPR.
Q.A.
COMMENTS:
Cleveland FES Center
Pinion Gear Shaft
for Rotary Actuator
Concept 03
SIZE A
DWG. NO. PinionGearShaft_concept03
REV.
SCALE:1:1
WEIGHT:
SHEET 1 OF 1

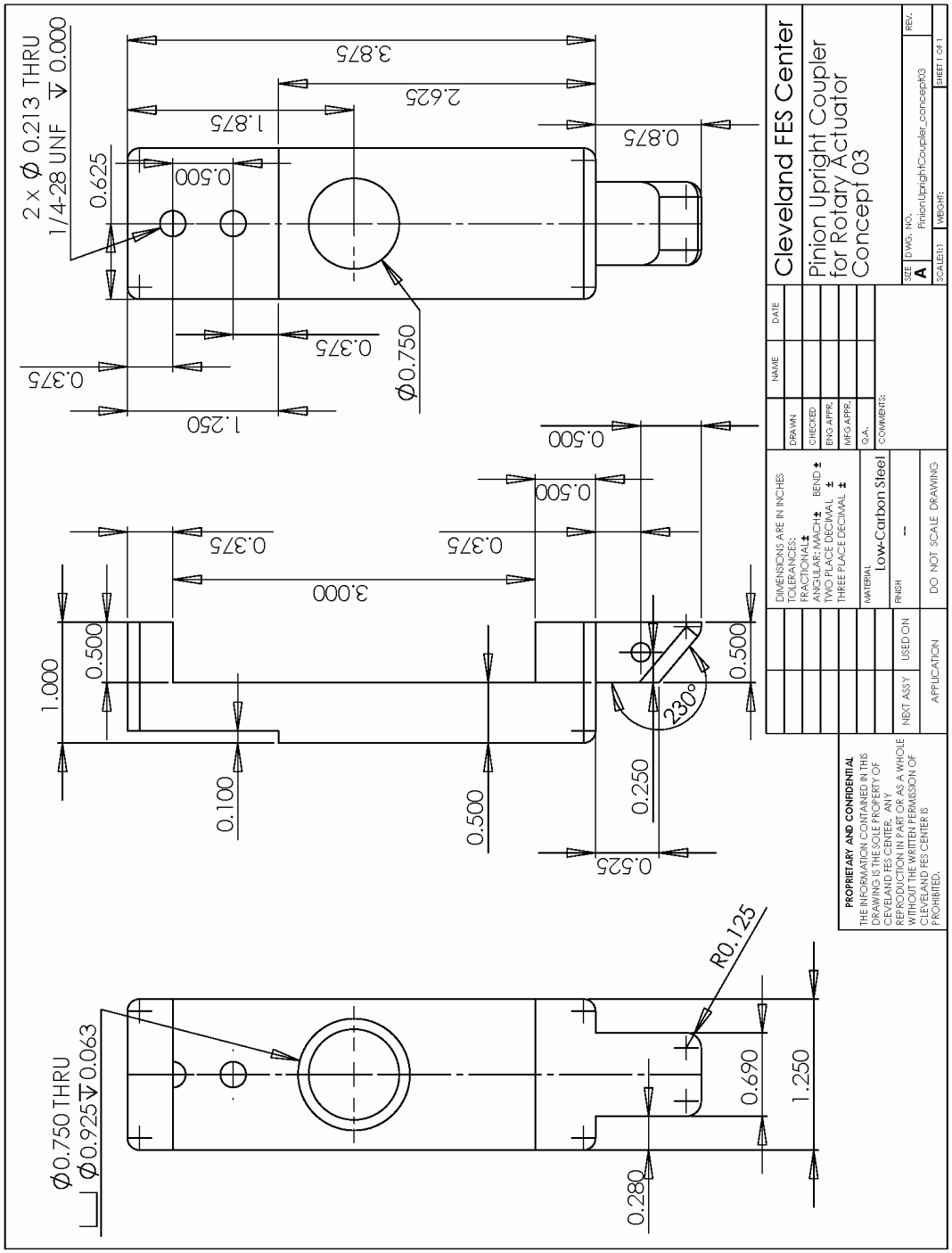
2 x Ø 0.213 THRU
1/4-28 UNF ⊽ 0.000
0.625
0.500
1.875
2.625
3.875
0.875
0.375
Ø0.750
1.250
0.375
0.500
0.500
0.375
0.375
3.000
1.000
0.500
0.500
230°
0.100
0.500
0.250
0.525
Ø0.750 THRU
⌴ Ø0.925⊽0.063
R0.125
0.690
1.250
0.280
Cleveland FES Center
Pinion Upright Coupler
for Rotary Actuator
Concept 03
DIMENSIONS ARE IN INCHES
TOLERANCES:
FRACTIONAL ±
ANGULAR: MACH ± BEND ±
TWO PLACE DECIMAL ±
THREE PLACE DECIMAL ±
MATERIAL
Low-Carbon Steel
FINISH
--
DO NOT SCALE DRAWING
DRAWN
CHECKED
ENG APPR.
MFG APPR.
Q.A.
COMMENTS:
NAME
DATE
NEXT ASSY
USED ON
APPLICATION
PROPRIETARY AND CONFIDENTIAL
THE INFORMATION CONTAINED IN THIS DRAWING IS THE SOLE PROPERTY OF CEVELAND FES CENTER. ANY REPRODUCTION IN PART OR AS A WHOLE WITHOUT THE WRITTEN PERMISSION OF CLEVELAND FES CENTER IS PROHIBITED.
SIZE
A
DWG. NO.
PinionUprightCoupler_concept03
REV.
SCALE: 1:1
WEIGHT:
SHEET 1 OF 1

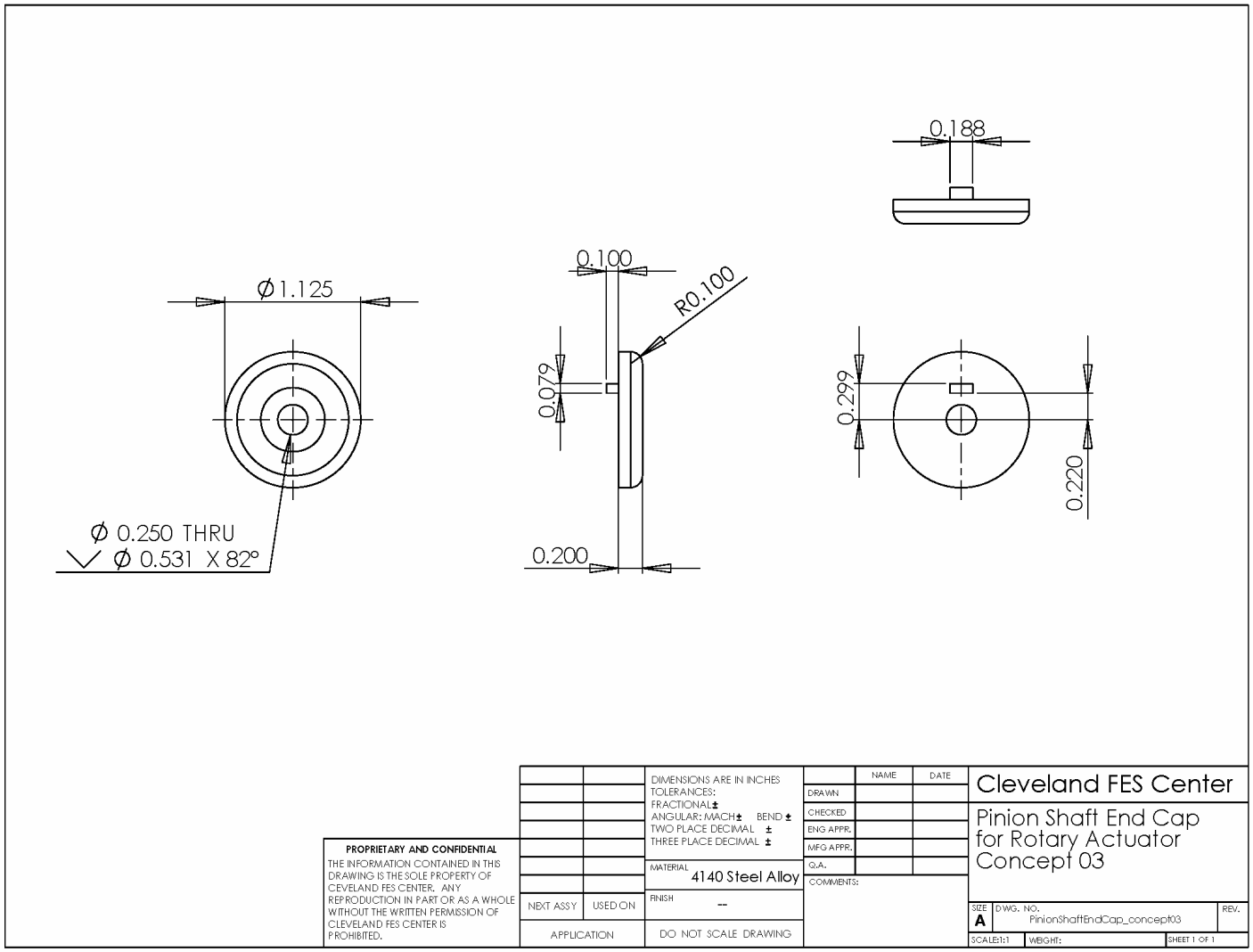
0.188
Ø1.125
0.100
R0.100
0.079
0.299
0.220
Ø 0.250 THRU
Ø 0.531 X 82°
0.200
PROPRIETARY AND CONFIDENTIAL
THE INFORMATION CONTAINED IN THIS DRAWING IS THE SOLE PROPERTY OF CEVELAND FES CENTER. ANY REPRODUCTION IN PART OR AS A WHOLE WITHOUT THE WRITTEN PERMISSION OF CLEVELAND FES CENTER IS PROHIBITED.
NEXT ASSY
USED ON
APPLICATION
DIMENSIONS ARE IN INCHES
TOLERANCES:
FRACTIONAL ±
ANGULAR: MACH ± BEND ±
TWO PLACE DECIMAL ±
THREE PLACE DECIMAL ±
MATERIAL
4140 Steel Alloy
FINISH
--
DO NOT SCALE DRAWING
NAME
DATE
DRAWN
CHECKED
ENG APPR.
MFG APPR.
Q.A.
COMMENTS:
Cleveland FES Center
Pinion Shaft End Cap for Rotary Actuator Concept 03
SIZE
A
DWG. NO.
PinionShaftEndCap_concept03
REV.
SCALE:1:1
WEIGHT:
SHEET 1 OF 1

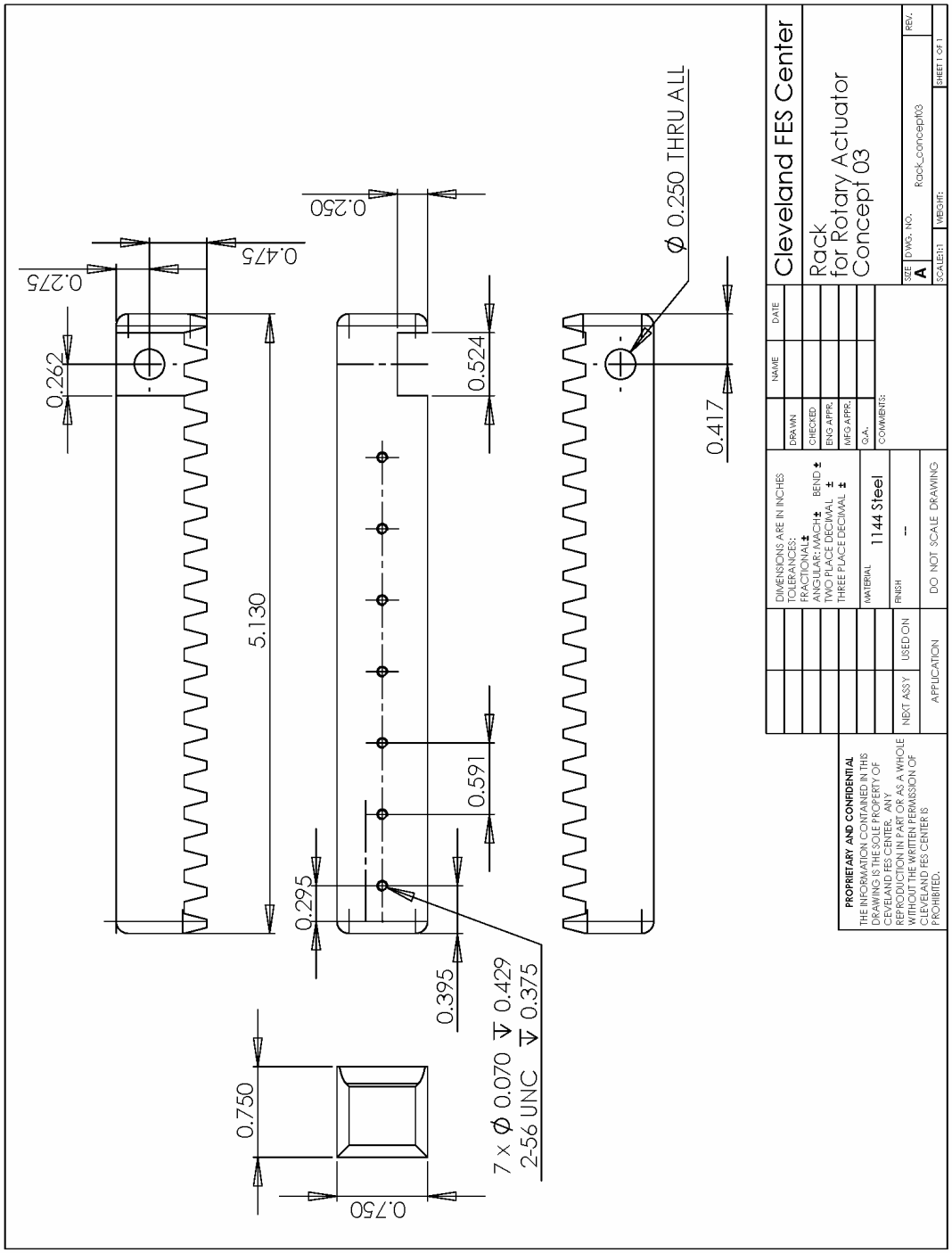
0.275
0.475
0.262
5.130
0.250
0.524
0.591
0.295
0.395
0.750
0.750
7 x Ø 0.070 ↧ 0.429
2-56 UNC ↧ 0.375
Ø 0.250 THRU ALL
0.417
Cleveland FES Center
Rack
for Rotary Actuator
Concept 03
DIMENSIONS ARE IN INCHES
TOLERANCES:
FRACTIONAL ±
ANGULAR: MACH ± BEND ±
TWO PLACE DECIMAL ±
THREE PLACE DECIMAL ±
MATERIAL 1144 Steel
FINISH --
DO NOT SCALE DRAWING
NAME
DATE
DRAWN
CHECKED
ENG APPR.
MFG APPR.
Q.A.
COMMENTS:
SIZE A
DWG. NO. Rack_concept03
REV.
SCALE 1:1
WEIGHT:
SHEET 1 OF 1
PROPRIETARY AND CONFIDENTIAL
THE INFORMATION CONTAINED IN THIS DRAWING IS THE SOLE PROPERTY OF CEVELAND FES CENTER. ANY REPRODUCTION IN PART OR AS A WHOLE WITHOUT THE WRITTEN PERMISSION OF CLEVELAND FES CENTER IS PROHIBITED.
NEXT ASSY
USED ON
APPLICATION

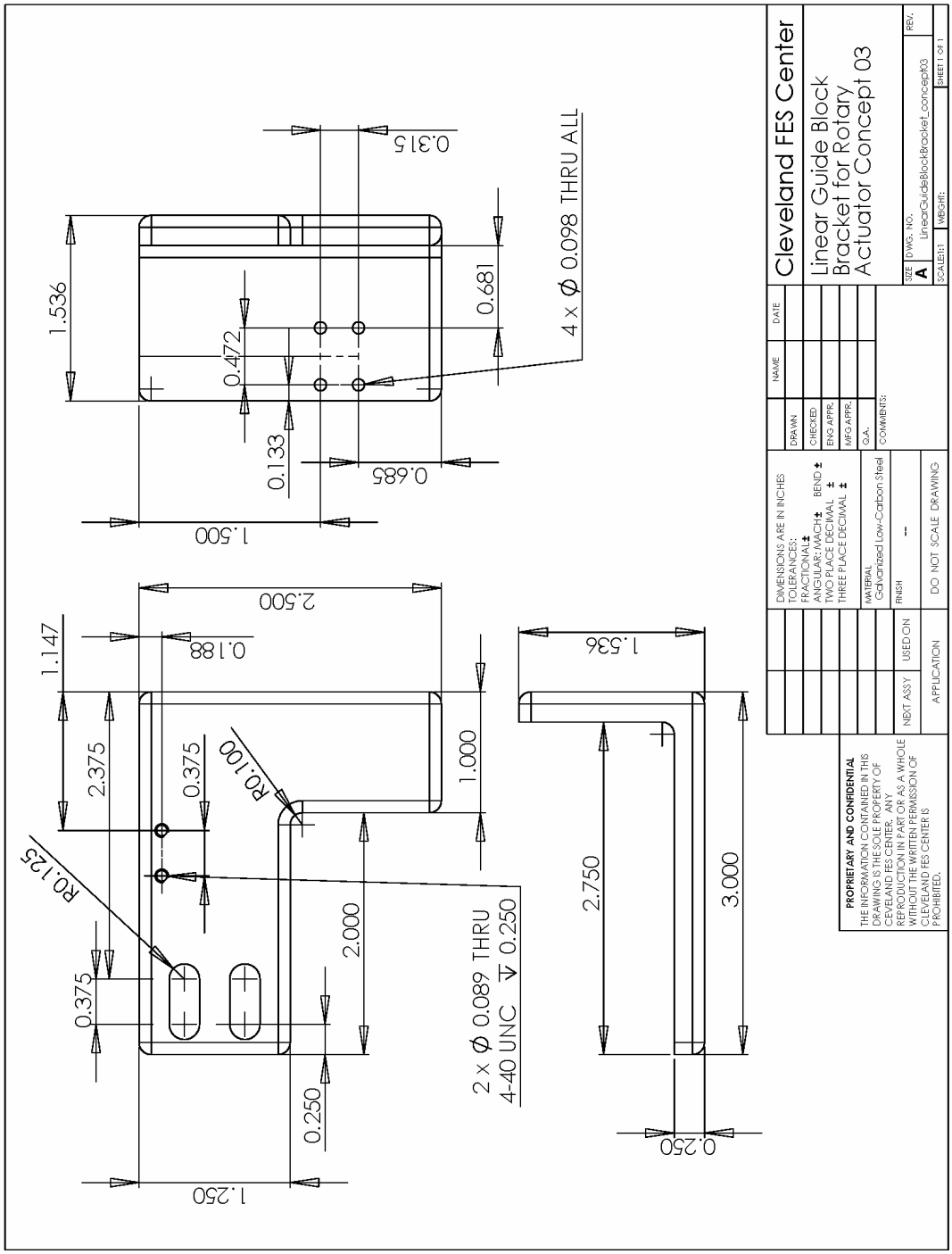
Cleveland FES Center
Linear Guide Block Bracket for Rotary Actuator Concept 03
LinearGuideBlockBracket_concept03
DIMENSIONS ARE IN INCHES
TOLERANCES:
FRACTIONAL ±
ANGULAR: MACH ± BEND ±
TWO PLACE DECIMAL ±
THREE PLACE DECIMAL ±
MATERIAL
Galvanized Low-Carbon Steel
FINISH
--
DO NOT SCALE DRAWING
PROPRIETARY AND CONFIDENTIAL
THE INFORMATION CONTAINED IN THIS DRAWING IS THE SOLE PROPERTY OF CEVELAND FES CENTER. ANY REPRODUCTION IN PART OR AS A WHOLE WITHOUT THE WRITTEN PERMISSION OF CLEVELAND FES CENTER IS PROHIBITED.
4 x Ø 0.098 THRU ALL
2 x Ø 0.089 THRU
4-40 UNC ↧ 0.250
R0.100
R0.125
0.315
0.681
1.536
0.472
0.133
0.685
1.500
2.500
0.188
1.147
2.375
0.375
1.000
0.375
2.000
0.250
1.250
1.536
2.750
3.000
0.250

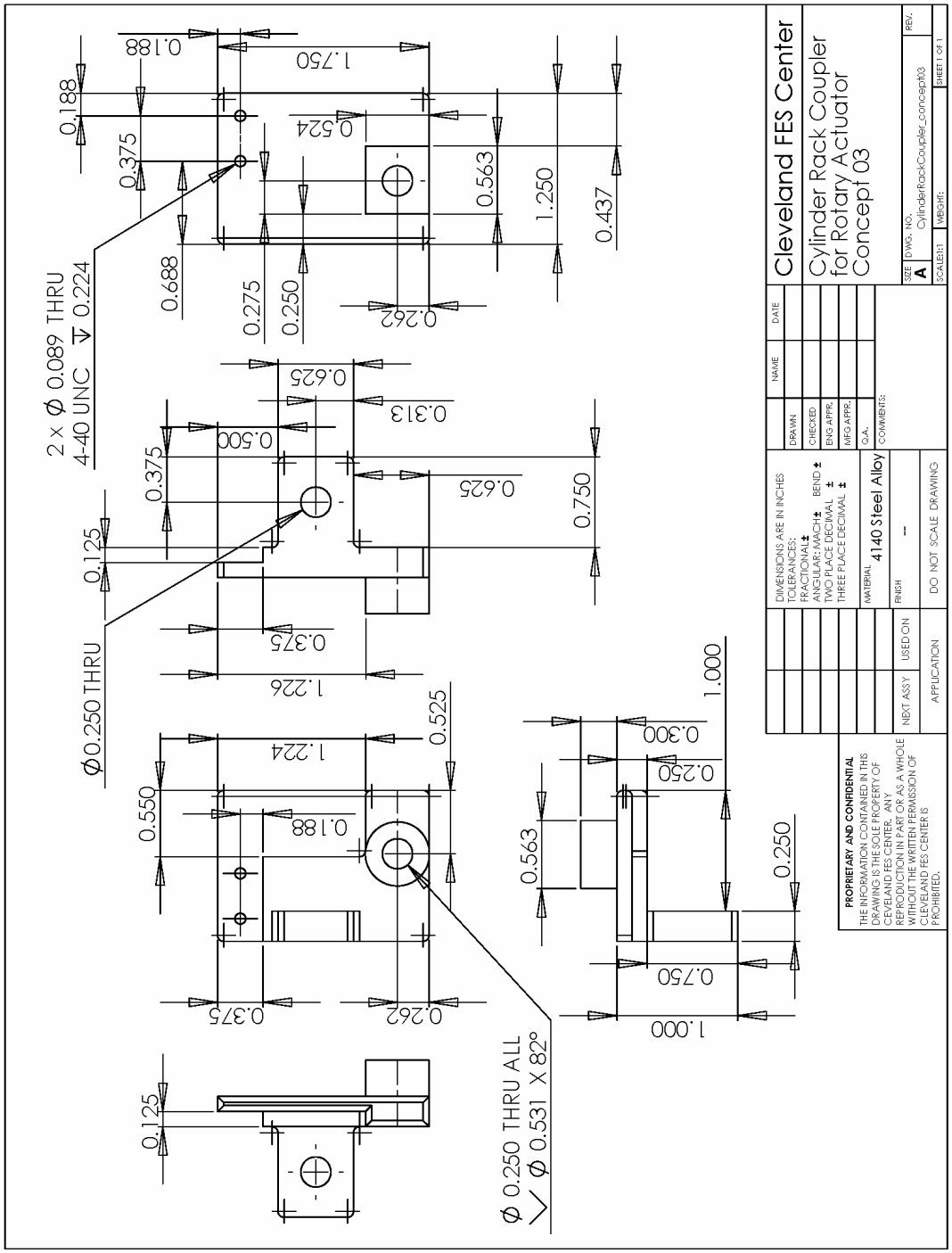
Cleveland FES Center
Cylinder Rack Coupler for Rotary Actuator Concept 03
DIMENSIONS ARE IN INCHES
TOLERANCES:
FRACTIONAL ±
ANGULAR: MACH ± BEND ±
TWO PLACE DECIMAL ±
THREE PLACE DECIMAL ±
MATERIAL 4140 Steel Alloy
FINISH --
DO NOT SCALE DRAWING
PROPRIETARY AND CONFIDENTIAL
THE INFORMATION CONTAINED IN THIS DRAWING IS THE SOLE PROPERTY OF CEVELAND FES CENTER. ANY REPRODUCTION IN PART OR AS A WHOLE WITHOUT THE WRITTEN PERMISSION OF CLEVELAND FES CENTER IS PROHIBITED.
2 × Ø 0.089 THRU
4-40 UNC ↧ 0.224
Ø0.250 THRU
Ø 0.250 THRU ALL
⌵ Ø 0.531 X 82°

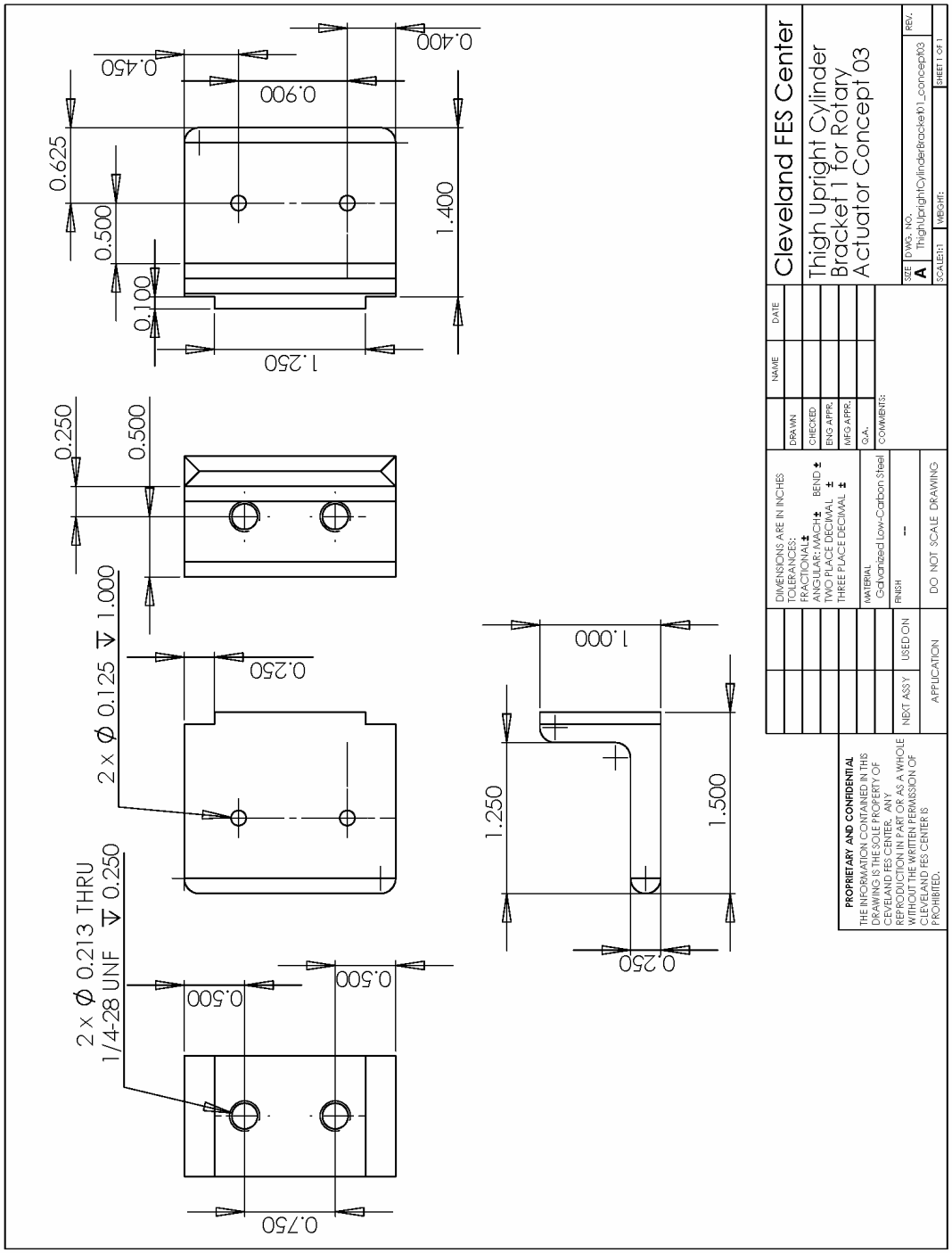
0.400
0.450
0.900
0.625
0.500
0.100
1.400
1.250
0.250
0.500
2 x Ø 0.125 ↧ 1.000
0.250
2 x Ø 0.213 THRU
1/4-28 UNF ↧ 0.250
0.500
0.500
0.750
1.000
1.250
1.500
0.250
Cleveland FES Center
Thigh Upright Cylinder Bracket 1 for Rotary Actuator Concept 03
DIMENSIONS ARE IN INCHES
TOLERANCES:
FRACTIONAL ±
ANGULAR: MACH ± BEND ±
TWO PLACE DECIMAL ±
THREE PLACE DECIMAL ±
MATERIAL
Galvanized Low-Carbon Steel
FINISH
--
DO NOT SCALE DRAWING
DRAWN
CHECKED
ENG APPR.
MFG APPR.
Q.A.
COMMENTS:
NAME
DATE
NEXT ASSY
USED ON
APPLICATION
PROPRIETARY AND CONFIDENTIAL
THE INFORMATION CONTAINED IN THIS DRAWING IS THE SOLE PROPERTY OF CEVELAND FES CENTER. ANY REPRODUCTION IN PART OR AS A WHOLE WITHOUT THE WRITTEN PERMISSION OF CLEVELAND FES CENTER IS PROHIBITED.
SIZE
A
DWG. NO.
ThighUprightCylinderBracket01_concept03
REV:
SCALE:1:1
WEIGHT:
SHEET 1 OF 1

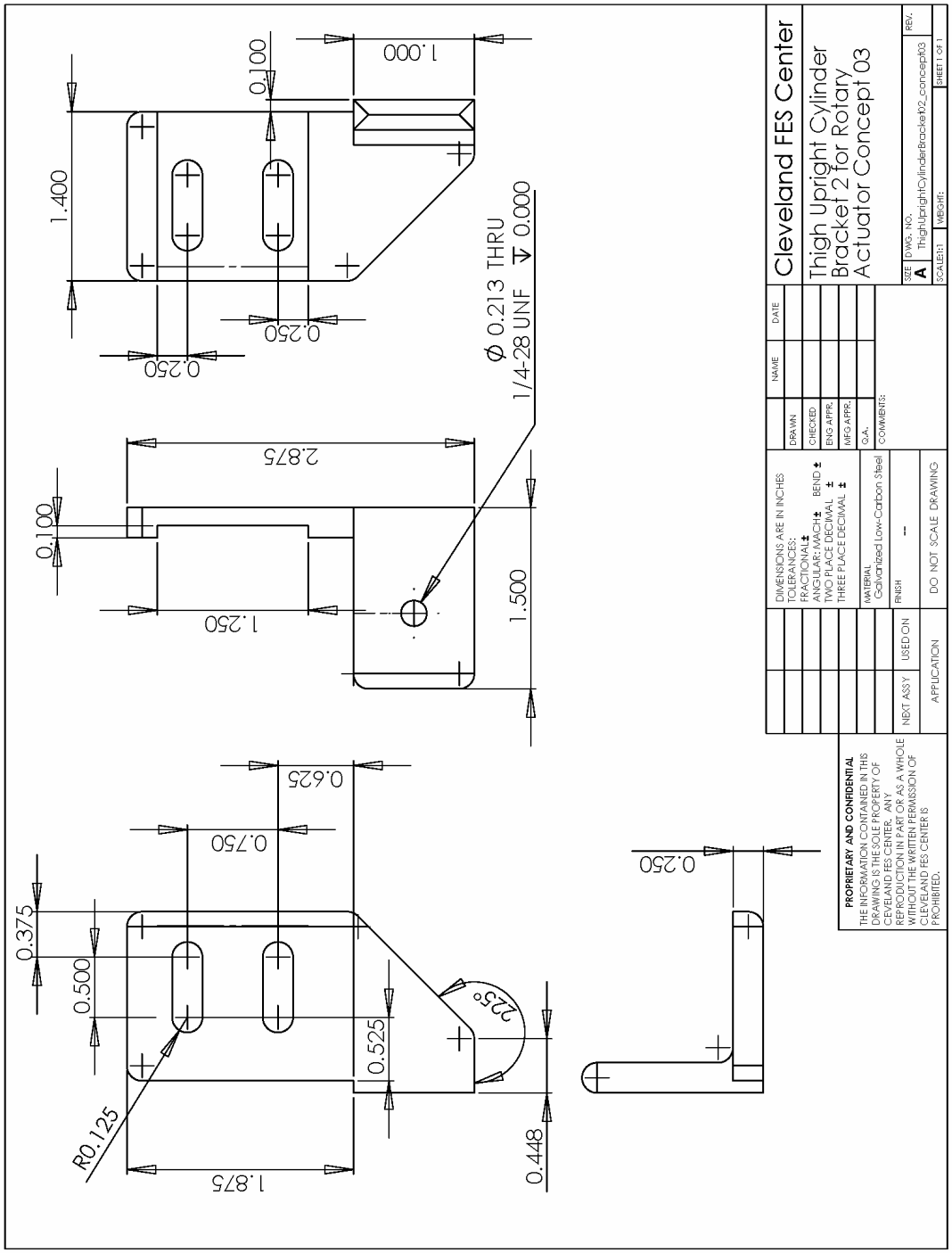
Cleveland FES Center
Thigh Upright Cylinder Bracket 2 for Rotary Actuator Concept 03
DIMENSIONS ARE IN INCHES
TOLERANCES:
FRACTIONAL ±
ANGULAR: MACH ± BEND ±
TWO PLACE DECIMAL ±
THREE PLACE DECIMAL ±
MATERIAL
Galvanized Low-Carbon Steel
FINISH
--
DO NOT SCALE DRAWING
PROPRIETARY AND CONFIDENTIAL
THE INFORMATION CONTAINED IN THIS DRAWING IS THE SOLE PROPERTY OF CEVELAND FES CENTER. ANY REPRODUCTION IN PART OR AS A WHOLE WITHOUT THE WRITTEN PERMISSION OF CLEVELAND FES CENTER IS PROHIBITED.
1.400
0.100
1.000
0.250
0.250
Ø 0.213 THRU
1/4-28 UNF ↧ 0.000
2.875
0.100
1.250
1.500
0.625
0.750
0.375
0.500
0.525
25°
R0.125
1.875
0.448
0.250

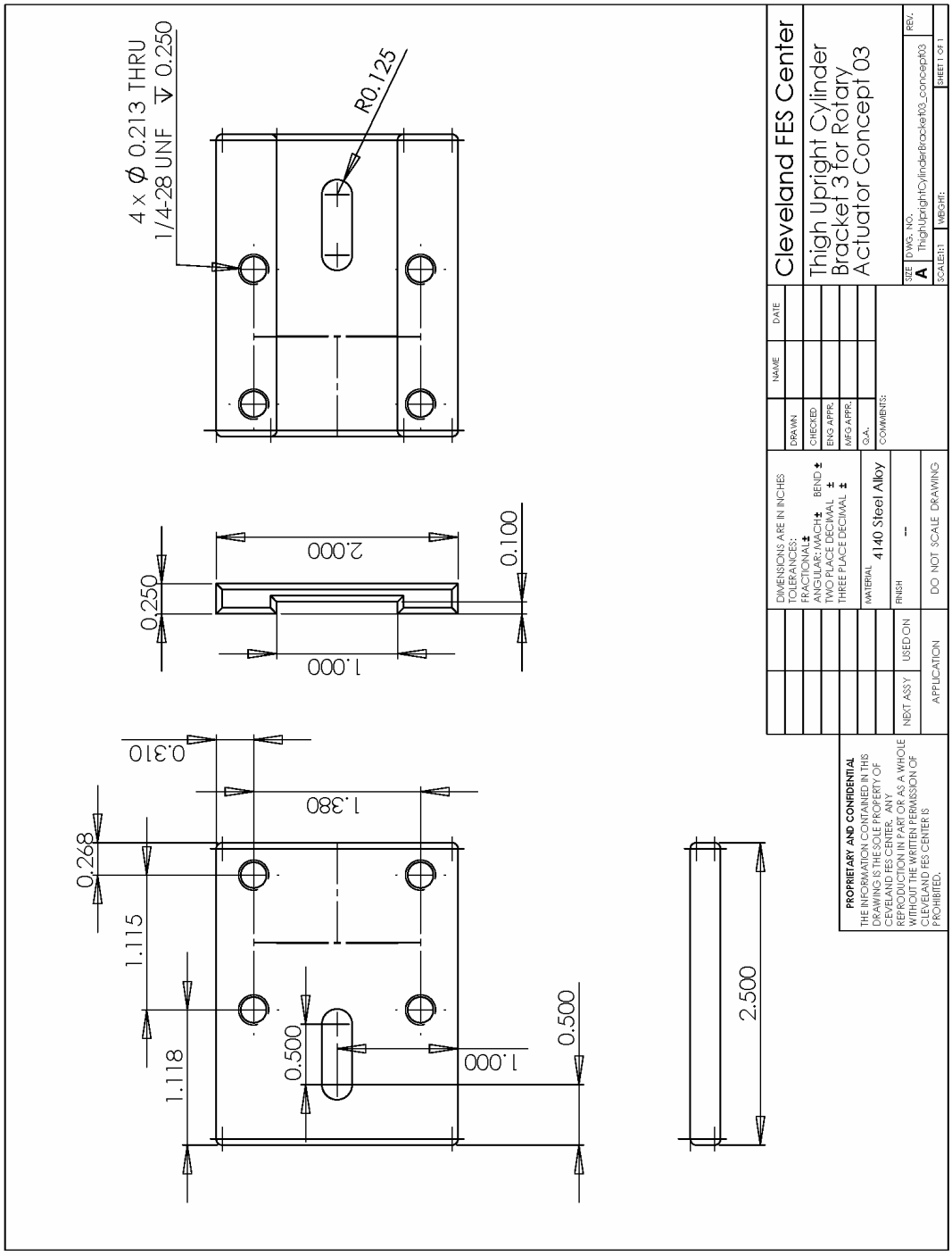
4 x Ø 0.213 THRU
1/4-28 UNF ⌀ 0.250
R0.125
2.000
0.250
0.100
1.000
0.310
1.380
0.268
1.115
1.118
0.500
0.500
1.000
2.500
Cleveland FES Center
Thigh Upright Cylinder Bracket 3 for Rotary Actuator Concept 03
DIMENSIONS ARE IN INCHES
TOLERANCES:
FRACTIONAL ±
ANGULAR: MACH ± BEND ±
TWO PLACE DECIMAL ±
THREE PLACE DECIMAL ±
MATERIAL 4140 Steel Alloy
FINISH --
DO NOT SCALE DRAWING
DRAWN
CHECKED
ENG APPR.
MFG APPR.
Q.A.
COMMENTS:
NAME
DATE
NEXT ASSY
USED ON
APPLICATION
PROPRIETARY AND CONFIDENTIAL
THE INFORMATION CONTAINED IN THIS DRAWING IS THE SOLE PROPERTY OF CEVELAND FES CENTER. ANY REPRODUCTION IN PART OR AS A WHOLE WITHOUT THE WRITTEN PERMISSION OF CLEVELAND FES CENTER IS PROHIBITED.
SIZE A
DWG. NO. ThighUprightCylinderBracket03_concept03
REV:
SCALE:1:1
WEIGHT:
SHEET 1 OF 1

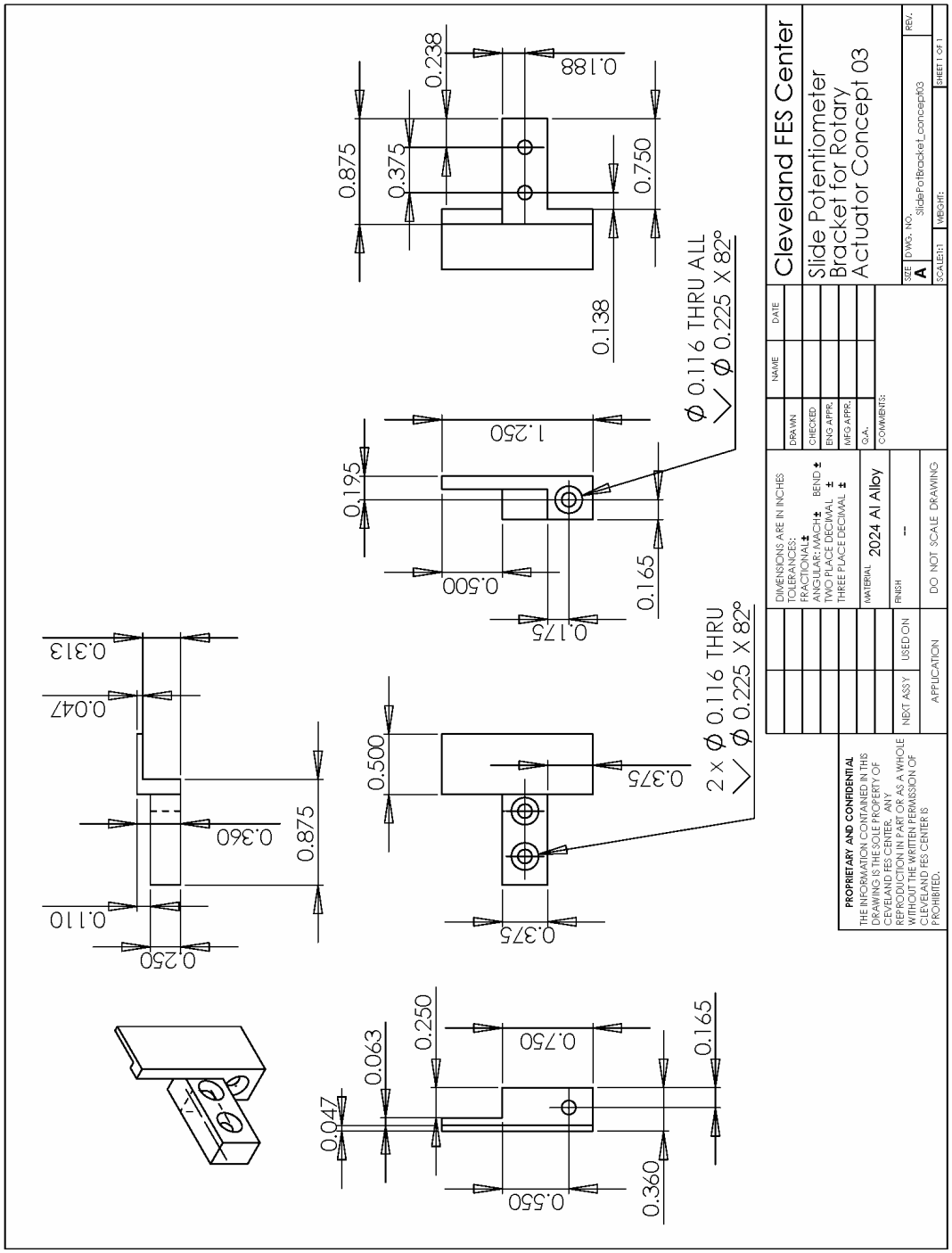
Cleveland FES Center
Slide Potentiometer Bracket for Rotary Actuator Concept 03
SIZE A
DWG. NO. SlidePotBracket_concept03
REV:
SCALE:1:1
WEIGHT:
SHEET 1 OF 1
DRAWN
CHECKED
ENG APPR.
MFG APPR.
Q.A.
COMMENTS:
NAME
DATE
DIMENSIONS ARE IN INCHES
TOLERANCES:
FRACTIONAL ±
ANGULAR: MACH ± BEND ±
TWO PLACE DECIMAL ±
THREE PLACE DECIMAL ±
MATERIAL 2024 Al Alloy
FINISH --
NEXT ASSY
USED ON
APPLICATION
DO NOT SCALE DRAWING
PROPRIETARY AND CONFIDENTIAL
THE INFORMATION CONTAINED IN THIS DRAWING IS THE SOLE PROPERTY OF CEVELAND FES CENTER. ANY REPRODUCTION IN PART OR AS A WHOLE WITHOUT THE WRITTEN PERMISSION OF CLEVELAND FES CENTER IS PROHIBITED.
0.875
0.375
0.238
0.188
0.750
0.138
Ø 0.116 THRU ALL
Ø 0.225 X 82°
1.250
0.195
0.500
0.175
0.165
2 X Ø 0.116 THRU
Ø 0.225 X 82°
0.500
0.375
0.375
0.313
0.047
0.360
0.875
0.110
0.250
0.047
0.063
0.250
0.750
0.165
0.550
0.360

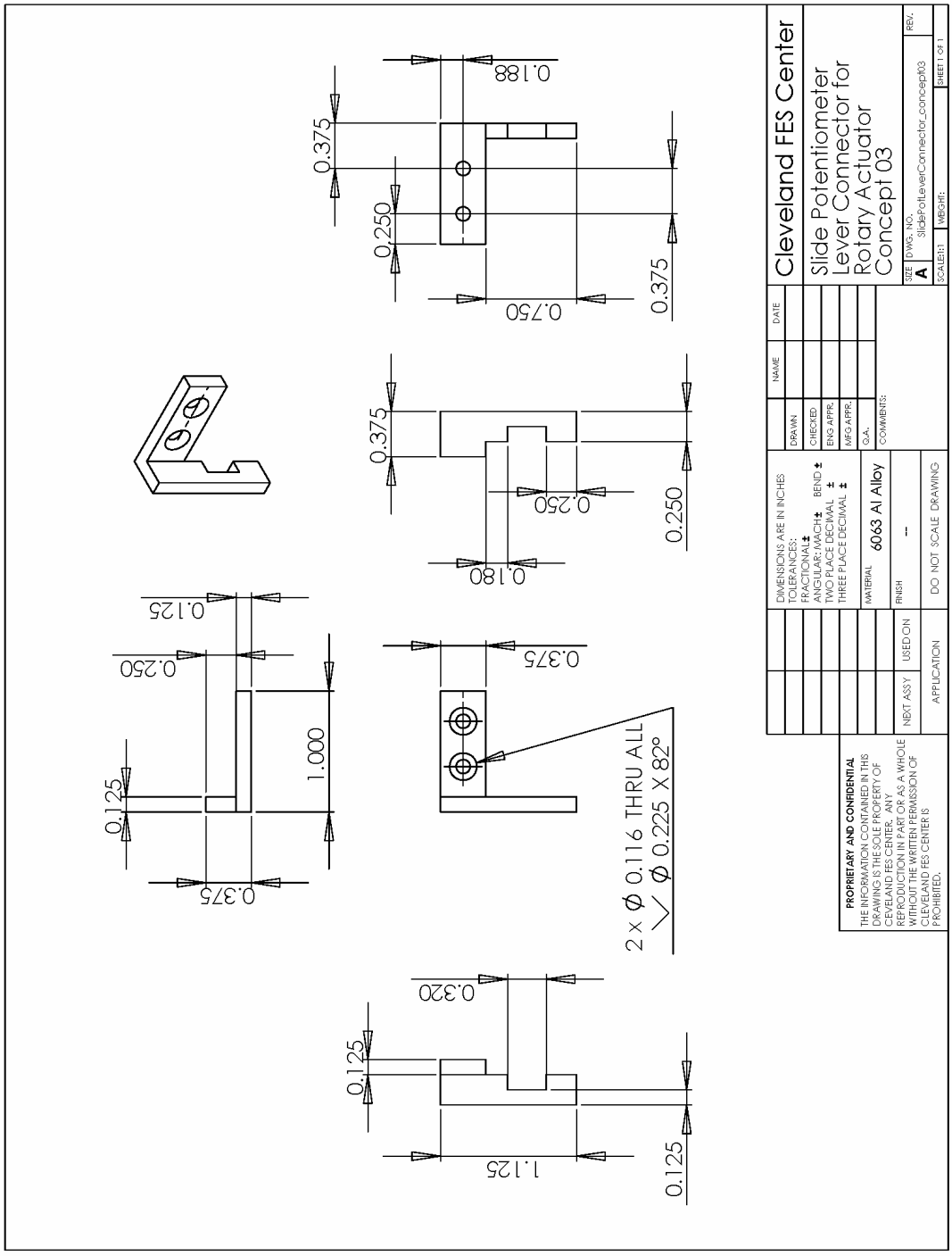
0.188
0.375
0.250
0.750
0.375
0.375
0.250
0.180
0.250
0.125
0.250
1.000
0.125
0.375
0.375
2 x Ø 0.116 THRU ALL
Ø 0.225 X 82°
0.320
0.125
1.125
0.125
PROPRIETARY AND CONFIDENTIAL
THE INFORMATION CONTAINED IN THIS DRAWING IS THE SOLE PROPERTY OF CEVELAND FES CENTER. ANY REPRODUCTION IN PART OR AS A WHOLE WITHOUT THE WRITTEN PERMISSION OF CLEVELAND FES CENTER IS PROHIBITED.
NEXT ASSY
USED ON
APPLICATION
DIMENSIONS ARE IN INCHES
TOLERANCES:
FRACTIONAL ±
ANGULAR: MACH ± BEND ±
TWO PLACE DECIMAL ±
THREE PLACE DECIMAL ±
MATERIAL 6063 Al Alloy
FINISH --
DO NOT SCALE DRAWING
DRAWN
CHECKED
ENG APPR.
MFG APPR.
Q.A.
COMMENTS:
NAME
DATE
Cleveland FES Center
Slide Potentiometer Lever Connector for Rotary Actuator Concept 03
SIZE A
DWG. NO. SlidePotLeverConnector_concept03
REV:
SCALE:1:1
WEIGHT:
SHEET 1 OF 1

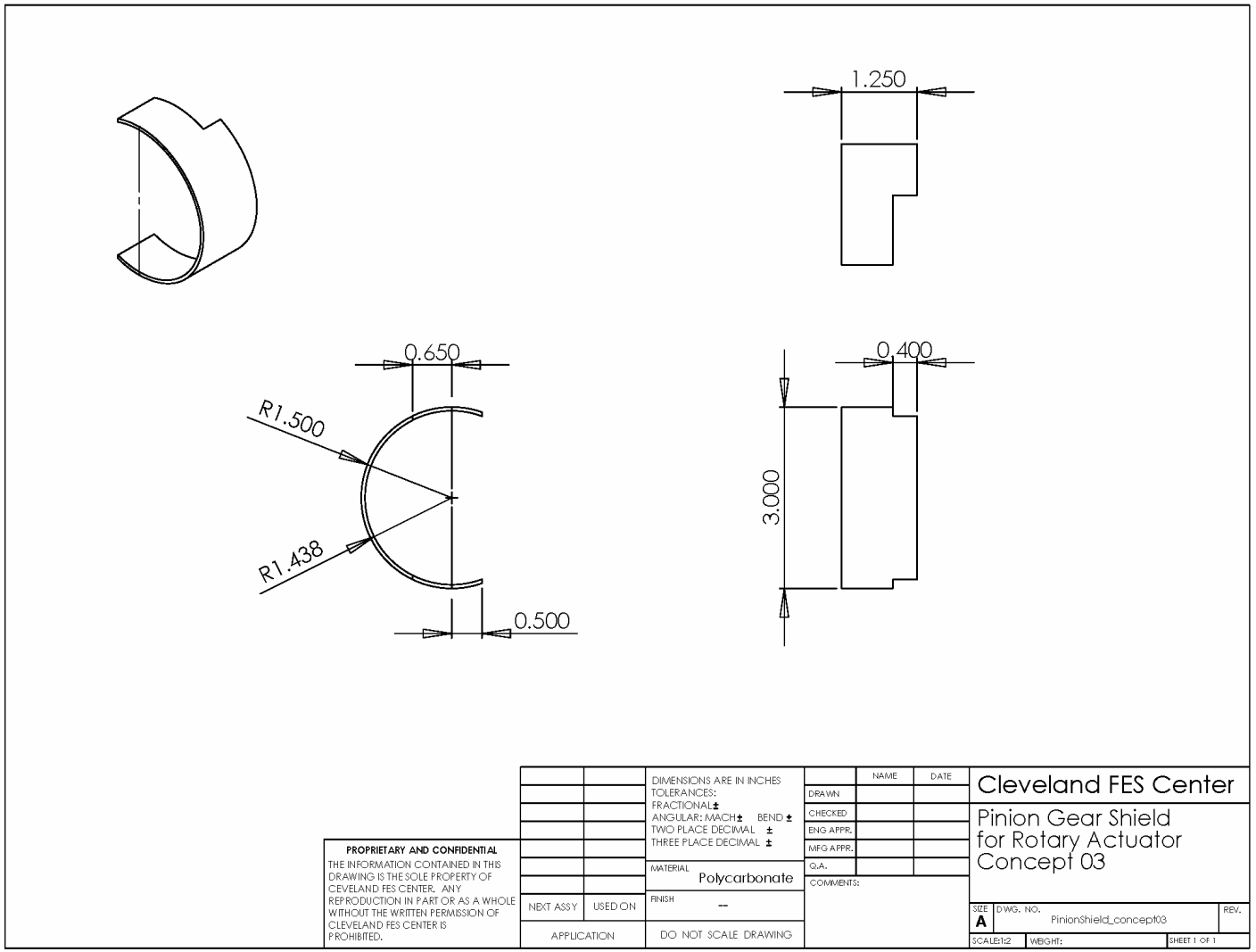

		DIMENSIONS ARE IN INCHES TOLERANCES: FRACTIONAL ± ANGULAR: MACH ± BEND ± TWO PLACE DECIMAL ± THREE PLACE DECIMAL ±		NAME	DATE
			DRAWN		
			CHECKED		
			ENG APPR.		
			MFG APPR.		
			Q.A.		
		MATERIAL: Polycarbonate	COMMENTS:		
NEXT ASSY	USED ON	FINISH: --			
APPLICATION		DO NOT SCALE DRAWING			

Cleveland FES Center

Pinion Gear Shield
for Rotary Actuator
Concept 03

SIZE	DWG. NO.	REV.
A	PinionShield_concept03	
SCALE:1:2	WEIGHT:	SHEET 1 OF 1

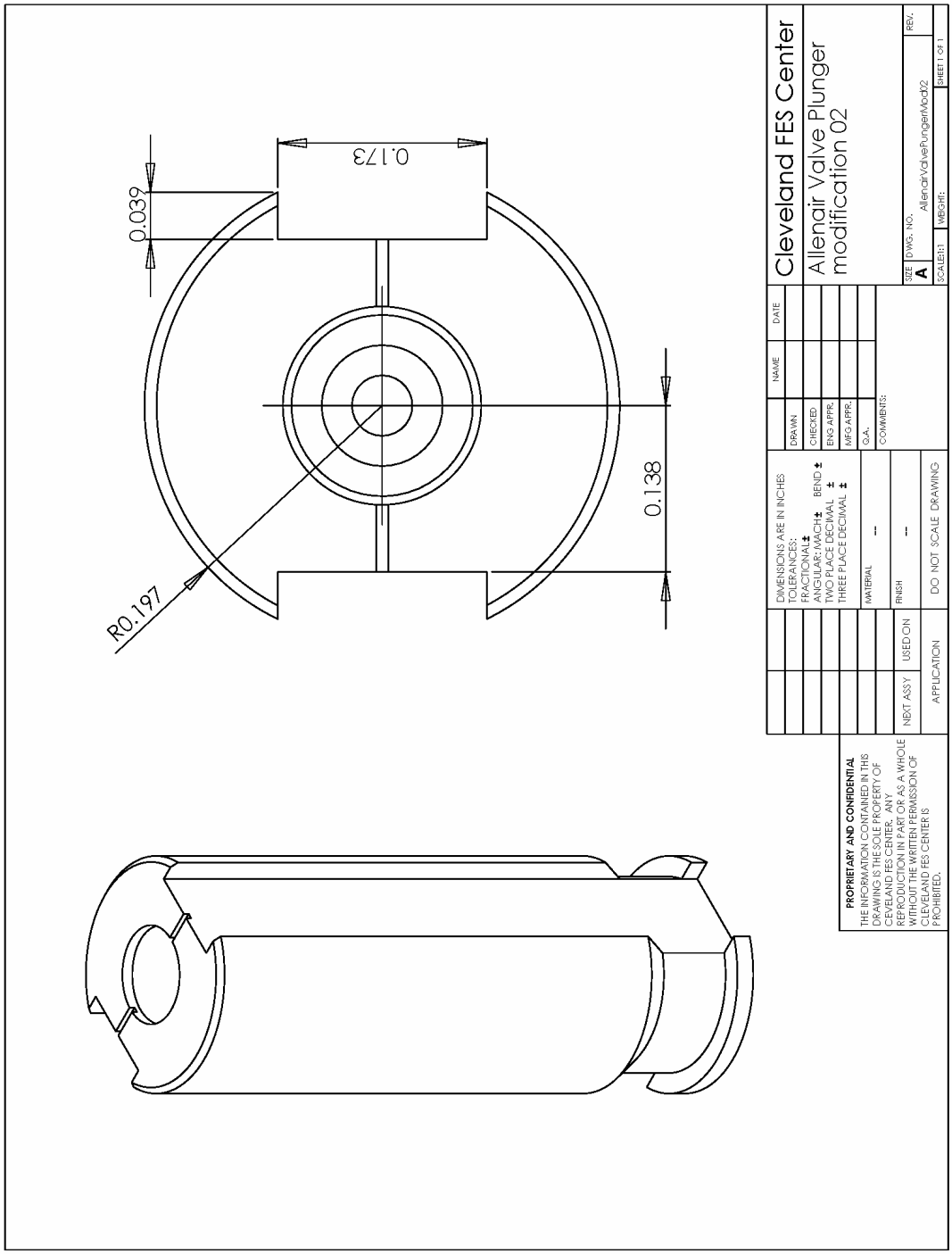
0.173
0.039
0.138
R0.197
Cleveland FES Center
Allenair Valve Plunger modification 02
DIMENSIONS ARE IN INCHES
TOLERANCES:
FRACTIONAL ±
ANGULAR: MACH ± BEND ±
TWO PLACE DECIMAL ±
THREE PLACE DECIMAL ±
MATERIAL ---
FINISH ---
NEXT ASSY
USED ON
APPLICATION
DO NOT SCALE DRAWING
DRAWN
CHECKED
ENG APPR.
MFG APPR.
Q.A.
COMMENTS:
NAME
DATE
PROPRIETARY AND CONFIDENTIAL
THE INFORMATION CONTAINED IN THIS DRAWING IS THE SOLE PROPERTY OF CEVELAND FES CENTER. ANY REPRODUCTION IN PART OR AS A WHOLE WITHOUT THE WRITTEN PERMISSION OF CLEVELAND FES CENTER IS PROHIBITED.
SIZE A
DWG. NO. AllenairValvePlungerMod02
REV.
SCALE 1:1
WEIGHT:
SHEET 1 OF 1

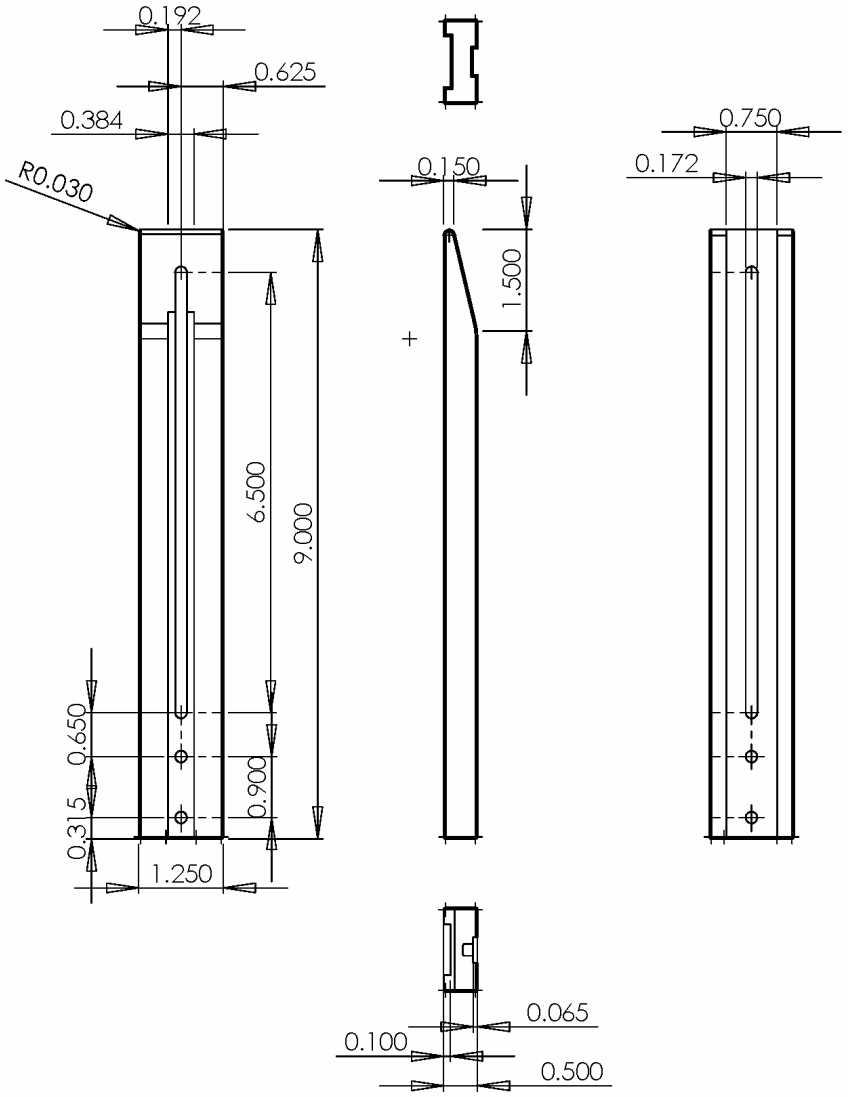

		DIMENSIONS ARE IN INCHES TOLERANCES: FRACTIONAL ± ANGULAR: MACH ± BEND ± TWO PLACE DECIMAL ± THREE PLACE DECIMAL ±		NAME	DATE	Cleveland FES Center
			DRAWN			
			CHECKED			Adjustable Thigh Upright Bracket
			ENG APPR.			
			MFG APPR.			
		MATERIAL 6061 Al Alloy	Q.A.			
			COMMENTS:			
NEXT ASSY	USED ON	FINISH				SIZE A DWG. NO. AdjustableThighUprightBracket REV.
APPLICATION		DO NOT SCALE DRAWING				SCALE:1:2 WEIGHT: SHEET 1 OF 1

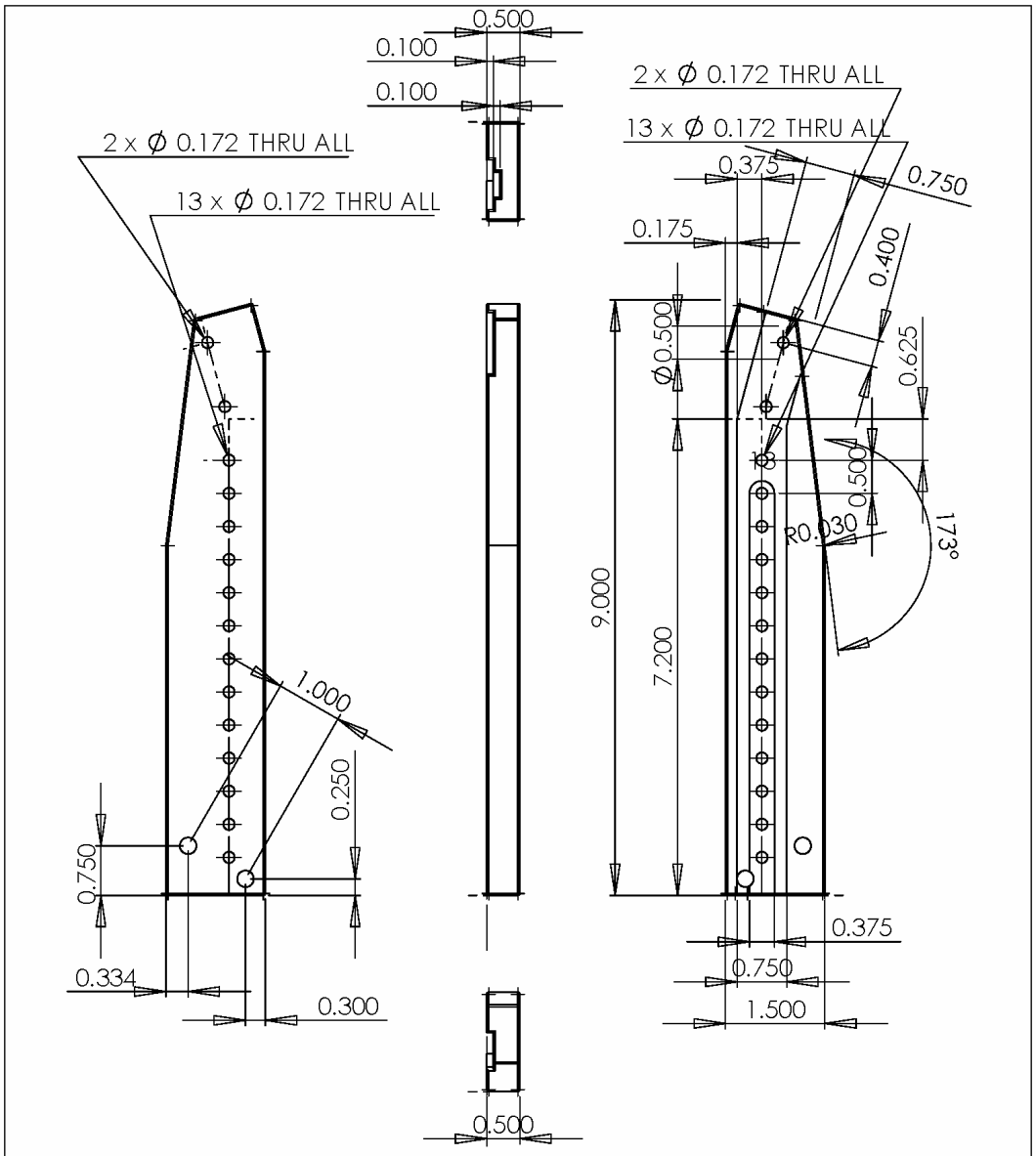

		DIMENSIONS ARE IN INCHES TOLERANCES: FRACTIONAL ± ANGULAR: MACH ± BEND ± TWO PLACE DECIMAL ± THREE PLACE DECIMAL ±		NAME	DATE
			DRAWN		
			CHECKED		
			ENG APPR.		
			MFG APPR.		
		MATERIAL 6061 Al Alloy	Q.A.		
			COMMENTS:		
NEXT ASSY	USED ON	FINISH			
APPLICATION		DO NOT SCALE DRAWING			

Cleveland FES Center

Adjustable Leg Upright Bracket (left)

SIZE A | DWG. NO. AdjustableLegUprightBracket_left | REV.

SCALE:1:2 | WEIGHT: | SHEET 1 OF 1

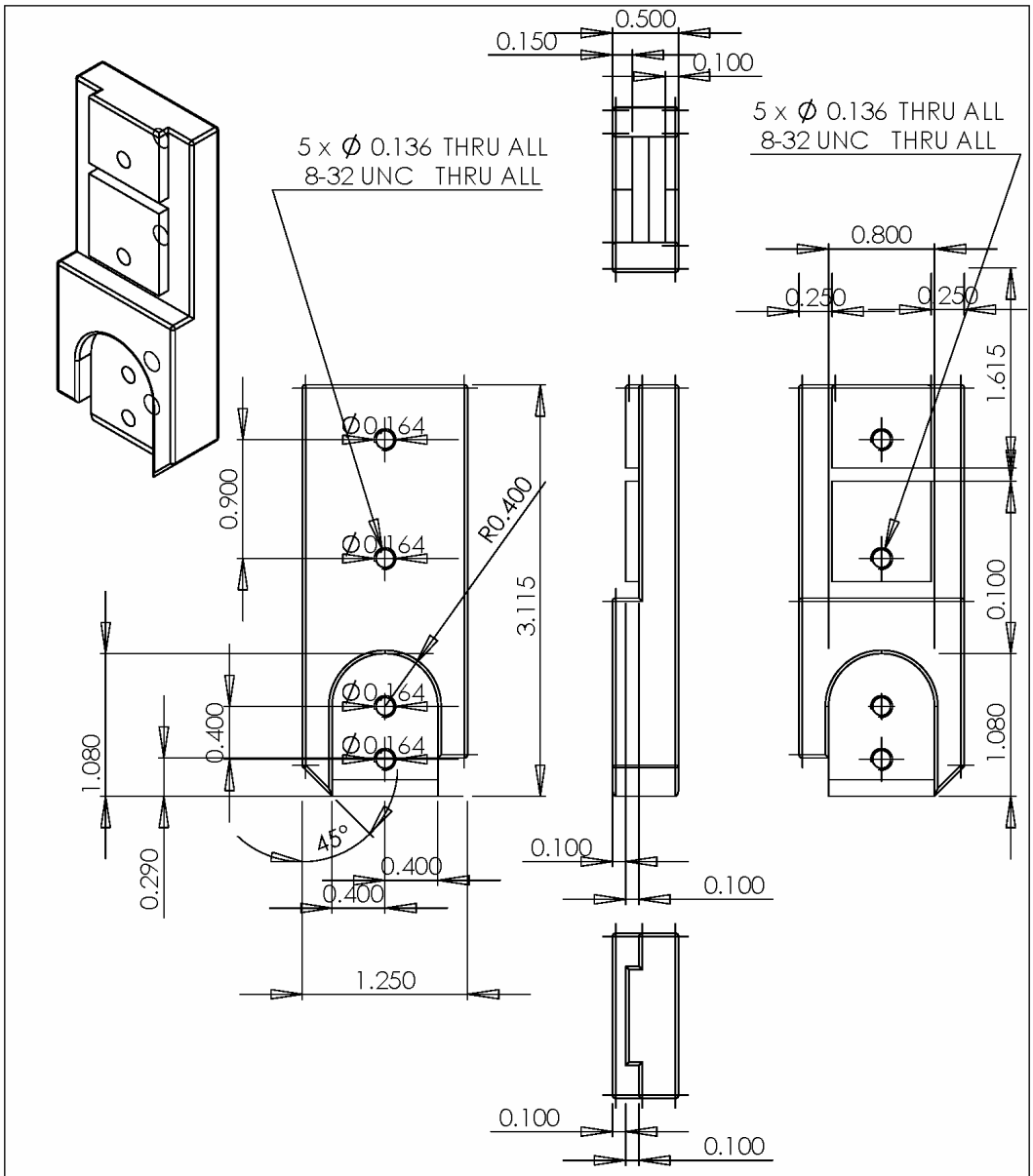

		DIMENSIONS ARE IN INCHES TOLERANCES: FRACTIONAL ± ANGULAR: MACH ± BEND ± TWO PLACE DECIMAL ± THREE PLACE DECIMAL ±		NAME / DATE	Cleveland FES Center
			DRAWN		Knee Thigh Upright with Latching Solenoid Mount (left)
			CHECKED		
			ENG APPR.		
			MFG APPR.		
		MATERIAL: 6061 Al Alloy	Q.A.		
			COMMENTS:		
NEXT ASSY	USED ON	FINISH			SIZE: A / DWG. NO.: KneeThighUpright_left02 / REV.
APPLICATION		DO NOT SCALE DRAWING			SCALE: 1:1 / WEIGHT: / SHEET 1 OF 1

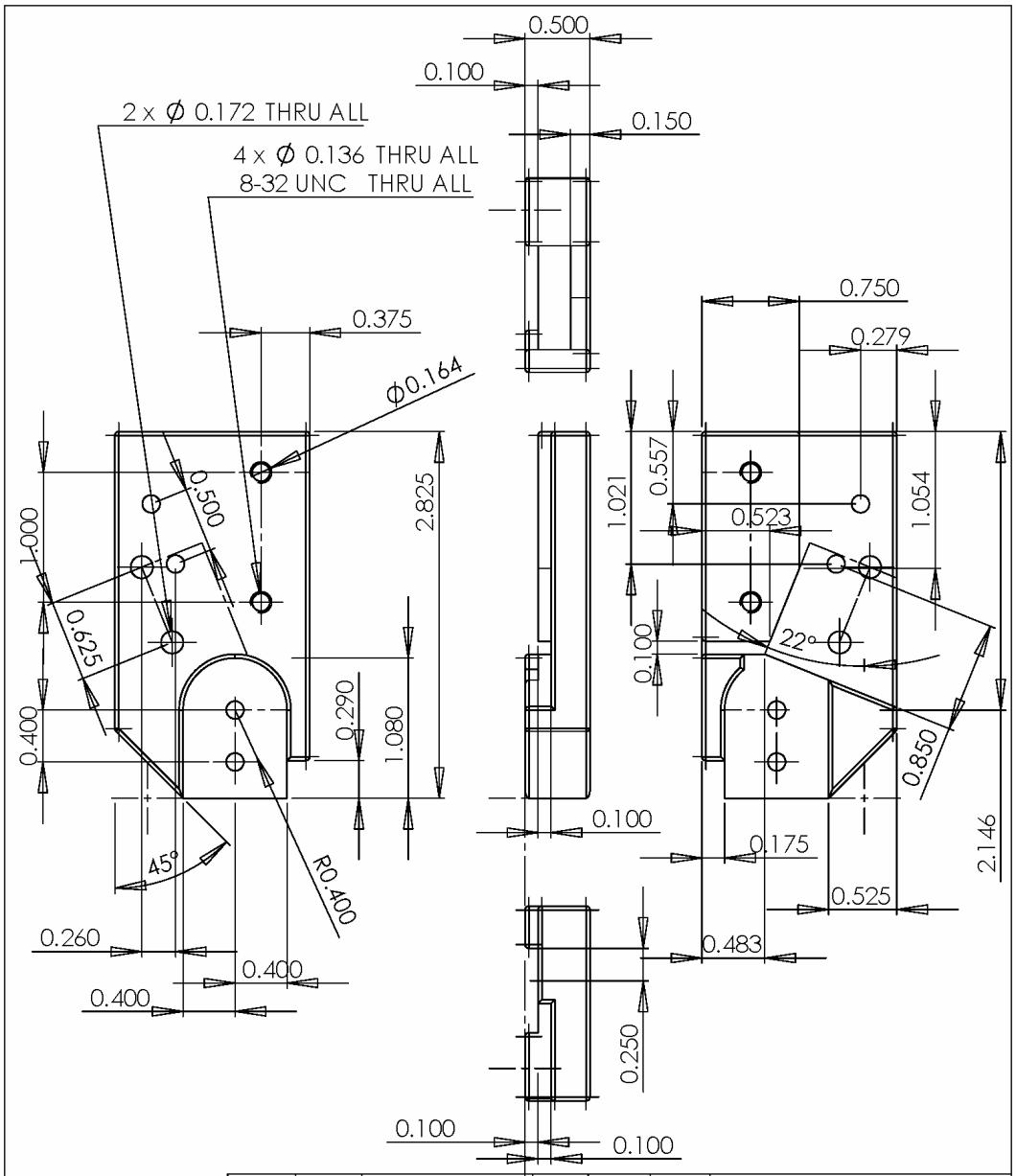
0.500
0.100
0.150
2 x Ø 0.172 THRU ALL
4 x Ø 0.136 THRU ALL
8-32 UNC THRU ALL
0.375
Ø0.164
0.750
0.279
0.557
1.021
0.523
1.054
0.500
2.825
1.000
0.625
0.400
0.290
1.080
22°
0.100
0.850
0.100
0.175
2.146
45°
R0.400
0.525
0.260
0.400
0.483
0.400
0.250
0.100
0.100
DIMENSIONS ARE IN INCHES
TOLERANCES:
FRACTIONAL ±
ANGULAR: MACH ± BEND ±
TWO PLACE DECIMAL ±
THREE PLACE DECIMAL ±
MATERIAL 6061 Al Alloy
FINISH
DO NOT SCALE DRAWING
NEXT ASSY
USED ON
APPLICATION
NAME
DATE
DRAWN
CHECKED
ENG APPR.
MFG APPR.
Q.A.
COMMENTS:
Cleveland FES Center
Knee Leg Upright with Latching Solenoid Mount (Left)
SIZE A
DWG. NO. KneeLegUpright_left
REV.
SCALE:1:1
WEIGHT:
SHEET 1 OF 1
PROPRIETARY AND CONFIDENTIAL
THE INFORMATION CONTAINED IN THIS DRAWING IS THE SOLE PROPERTY OF CLEVELAND FES CENTER. ANY REPRODUCTION IN PART OR AS A WHOLE WITHOUT THE WRITTEN PERMISSION OF CLEVELAND FES CENTER IS PROHIBITED.

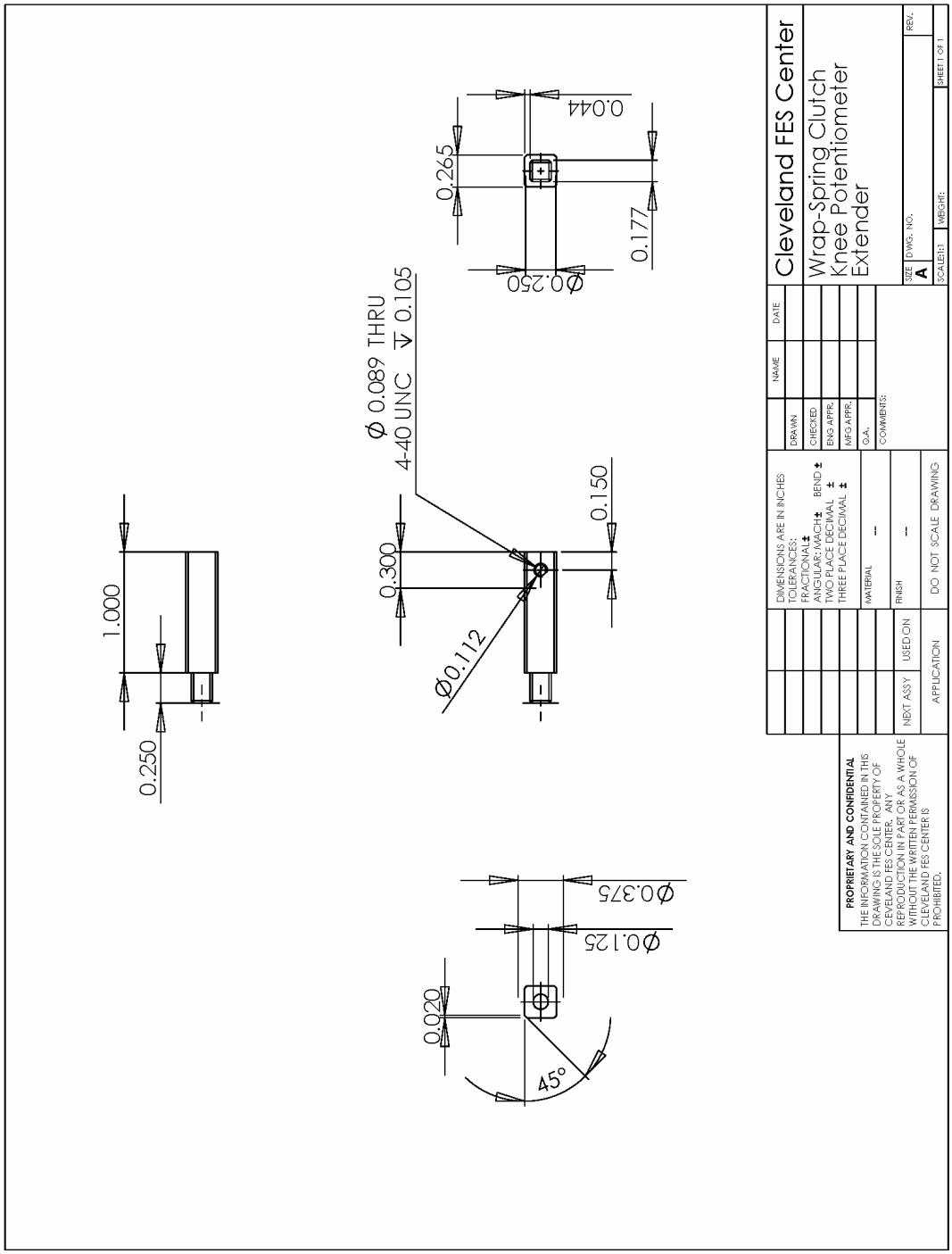
Cleveland FES Center
Wrap-Spring Clutch
Knee Potentiometer
Extender
PROPRIETARY AND CONFIDENTIAL
THE INFORMATION CONTAINED IN THIS DRAWING IS THE SOLE PROPERTY OF CEVELAND FES CENTER. ANY REPRODUCTION IN PART OR AS A WHOLE WITHOUT THE WRITTEN PERMISSION OF CLEVELAND FES CENTER IS PROHIBITED.
DIMENSIONS ARE IN INCHES
TOLERANCES:
FRACTIONAL ±
ANGULAR: MACH ± BEND ±
TWO PLACE DECIMAL ±
THREE PLACE DECIMAL ±
MATERIAL
FINISH
NEXT ASSY
USED ON
APPLICATION
DO NOT SCALE DRAWING
DRAWN
CHECKED
ENG APPR.
MFG APPR.
Q.A.
COMMENTS:
NAME
DATE
SIZE A
DWG. NO.
REV.
SCALE: 1:1
WEIGHT:
SHEET 1 OF 1
1.000
0.250
Ø 0.089 THRU
4-40 UNC ↧ 0.105
0.300
0.150
Ø0.112
0.265
0.044
Ø0.250
0.177
0.020
Ø0.125
Ø0.375
45°

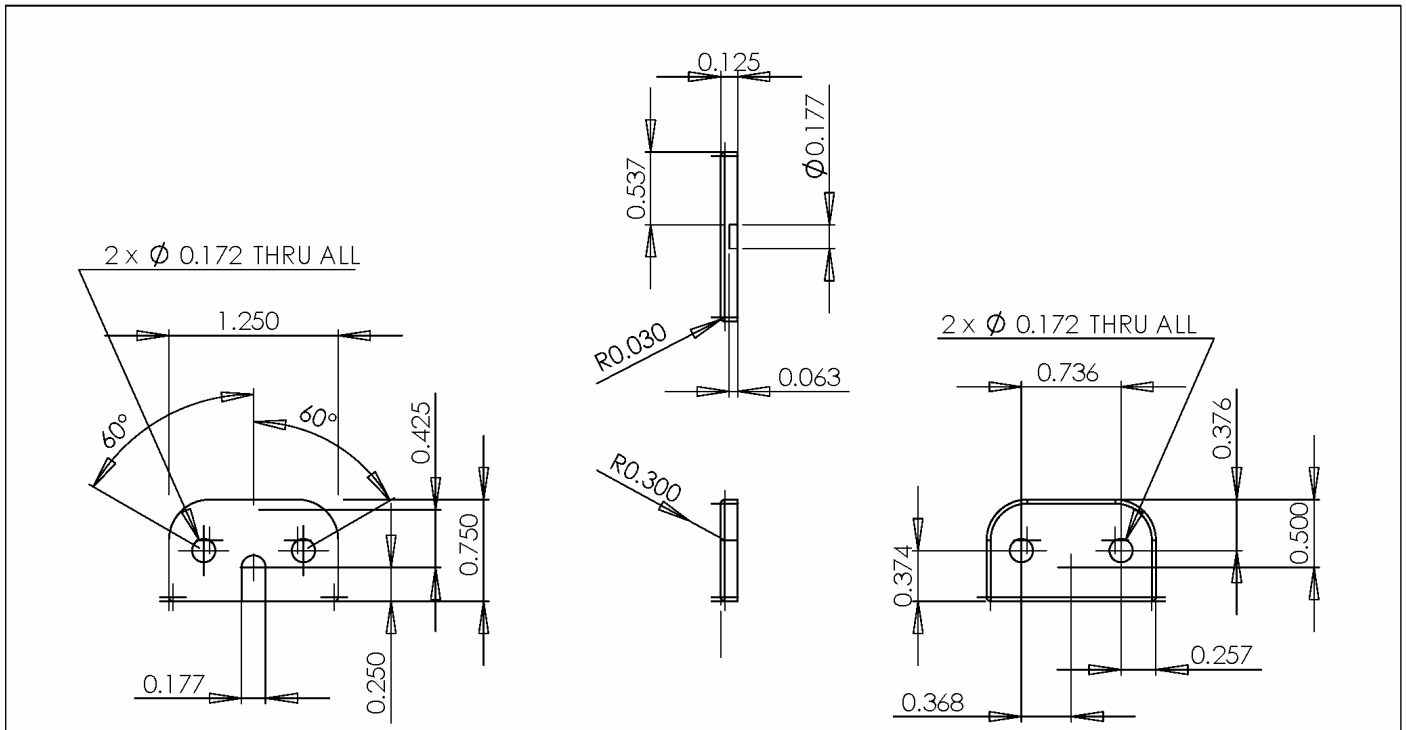

		UNLESS OTHERWISE SPECIFIED:		NAME	DATE	Cleveland FES Center
		DIMENSIONS ARE IN INCHES TOLERANCES: FRACTIONAL ± ANGULAR: MACH ± BEND ± TWO PLACE DECIMAL ± THREE PLACE DECIMAL ±	DRAWN			TITLE: Wrap-Spring Clutch Knee Potentiometer Mounting Bracket
			CHECKED			
			ENG APPR.			
			MFG APPR.			
		INTERPRET GEOMETRIC TOLERANCING PER:	Q.A.			
		MATERIAL	COMMENTS:			SIZE A | DWG. NO. PotentiometerBracket | REV
		FINISH				
NEXT ASSY	USED ON					SCALE: 1:1 | WEIGHT: | SHEET 1 OF 1
APPLICATION		DO NOT SCALE DRAWING				

5 4 3 2 1

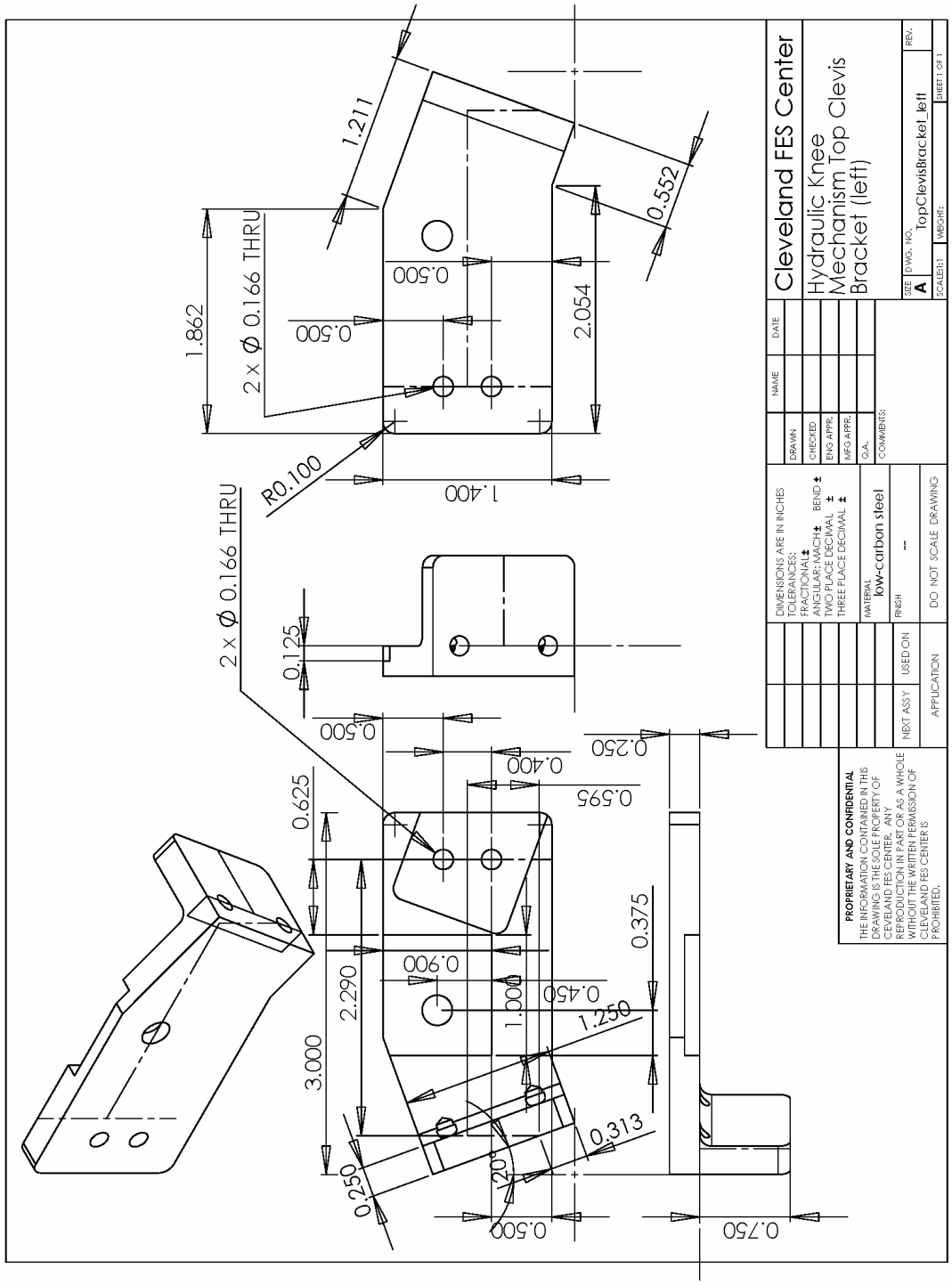
Cleveland FES Center
Hydraulic Knee Mechanism Top Clevis Bracket (left)
TopClevisBracket_left
low-carbon steel
1.211
0.552
1.862
2 x Ø 0.166 THRU
0.500
2.054
R0.100
1.400
0.125
0.250
0.400
0.595
0.625
0.375
0.900
0.450
1.000
1.250
2.290
3.000
0.313
20°
0.250
0.750

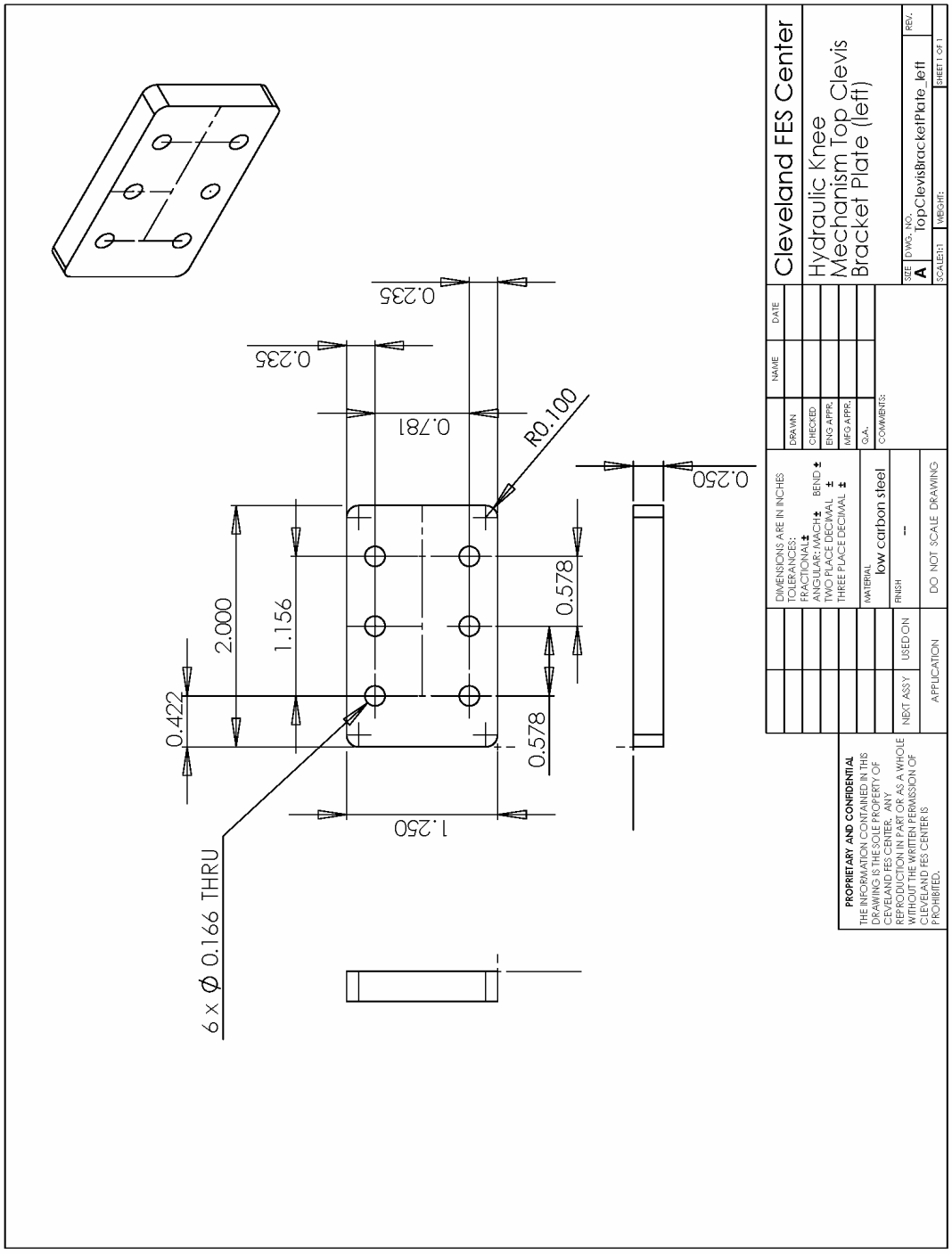
0.235
0.235
0.781
R0.100
0.250
0.578
2.000
1.156
0.422
0.578
1.250
6 x Ø 0.166 THRU
Cleveland FES Center
Hydraulic Knee Mechanism Top Clevis Bracket Plate (left)
DIMENSIONS ARE IN INCHES
TOLERANCES:
FRACTIONAL ±
ANGULAR: MACH ± BEND ±
TWO PLACE DECIMAL ±
THREE PLACE DECIMAL ±
MATERIAL
low carbon steel
FINISH
--
NEXT ASSY
USED ON
APPLICATION
DO NOT SCALE DRAWING
DRAWN
CHECKED
ENG APPR.
MFG APPR.
Q.A.
COMMENTS:
NAME
DATE
SIZE
A
DWG. NO.
TopClevisBracketPlate_left
REV.
SCALE: 1:1
WEIGHT:
SHEET 1 OF 1
PROPRIETARY AND CONFIDENTIAL
THE INFORMATION CONTAINED IN THIS DRAWING IS THE SOLE PROPERTY OF CEVELAND FES CENTER. ANY REPRODUCTION IN PART OR AS A WHOLE WITHOUT THE WRITTEN PERMISSION OF CLEVELAND FES CENTER IS PROHIBITED.

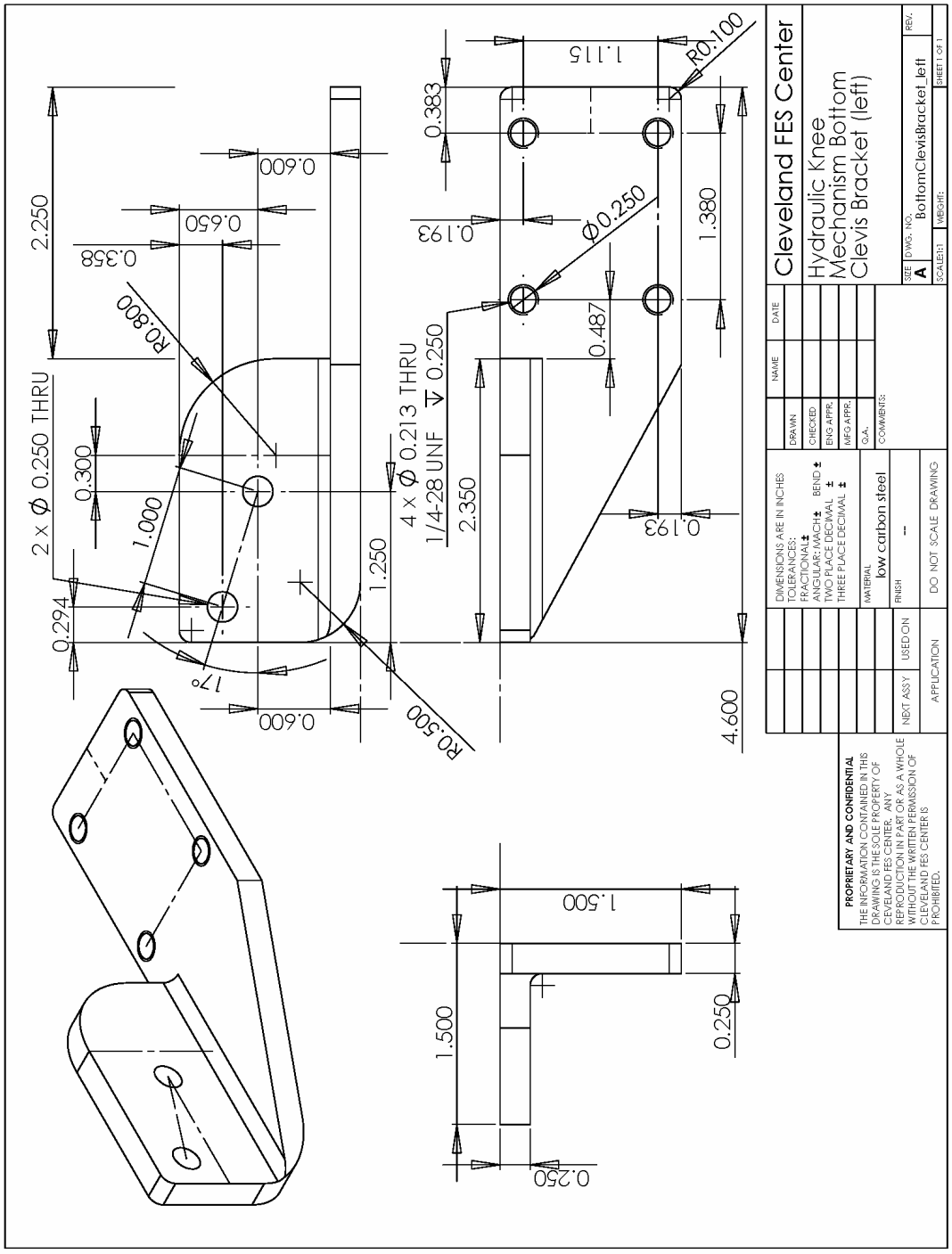
Cleveland FES Center
Hydraulic Knee
Mechanism Bottom
Clevis Bracket (left)
BottomClevisBracket_left
low carbon steel
DO NOT SCALE DRAWING
PROPRIETARY AND CONFIDENTIAL
2.250
0.600
0.650
0.358
R0.800
2 x Ø 0.250 THRU
0.300
1.000
0.294
17°
1.250
0.600
R0.500
4 x Ø 0.213 THRU
1/4-28 UNF ⊽ 0.250
2.350
0.383
1.115
R0.100
0.193
Ø0.250
1.380
0.487
0.193
4.600
1.500
1.500
0.250
0.250

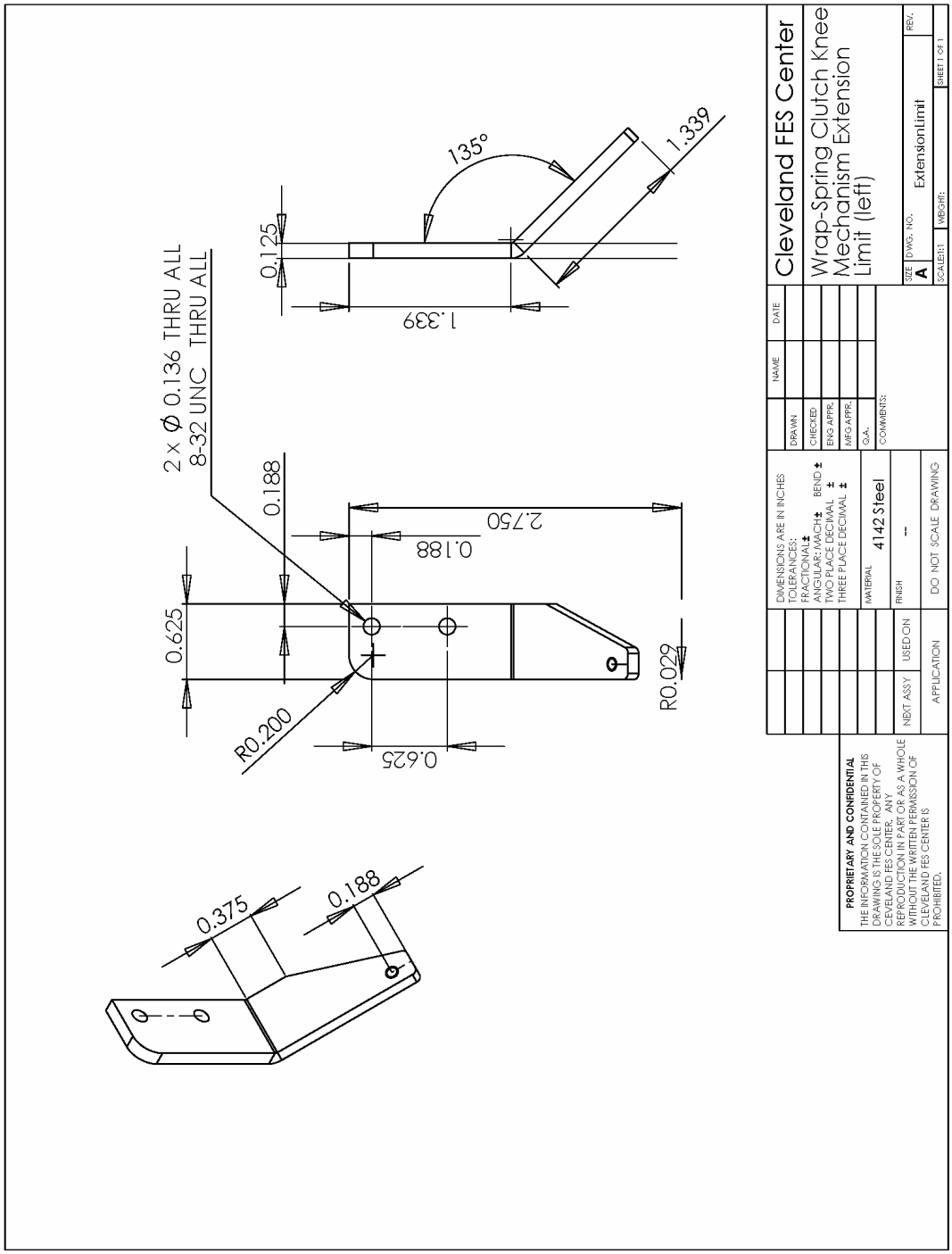
2 x Ø 0.136 THRU ALL
8-32 UNC THRU ALL
0.188
0.188
2.750
0.625
R0.200
0.625
R0.029
0.125
1.339
135°
1.339
0.375
0.188
PROPRIETARY AND CONFIDENTIAL
THE INFORMATION CONTAINED IN THIS DRAWING IS THE SOLE PROPERTY OF CEVELAND FES CENTER. ANY REPRODUCTION IN PART OR AS A WHOLE WITHOUT THE WRITTEN PERMISSION OF CLEVELAND FES CENTER IS PROHIBITED.
NEXT ASSY
USED ON
APPLICATION
DIMENSIONS ARE IN INCHES
TOLERANCES:
FRACTIONAL ±
ANGULAR: MACH ± BEND ±
TWO PLACE DECIMAL ±
THREE PLACE DECIMAL ±
MATERIAL
4142 Steel
FINISH
--
DO NOT SCALE DRAWING
NAME
DATE
DRAWN
CHECKED
ENG APPR.
MFG APPR.
Q.A.
COMMENTS:
Cleveland FES Center
Wrap-Spring Clutch Knee Mechanism Extension Limit (left)
SIZE
A
DWG. NO.
ExtensionLimit
REV.
SCALE:1:1
WEIGHT:
SHEET 1 OF 1

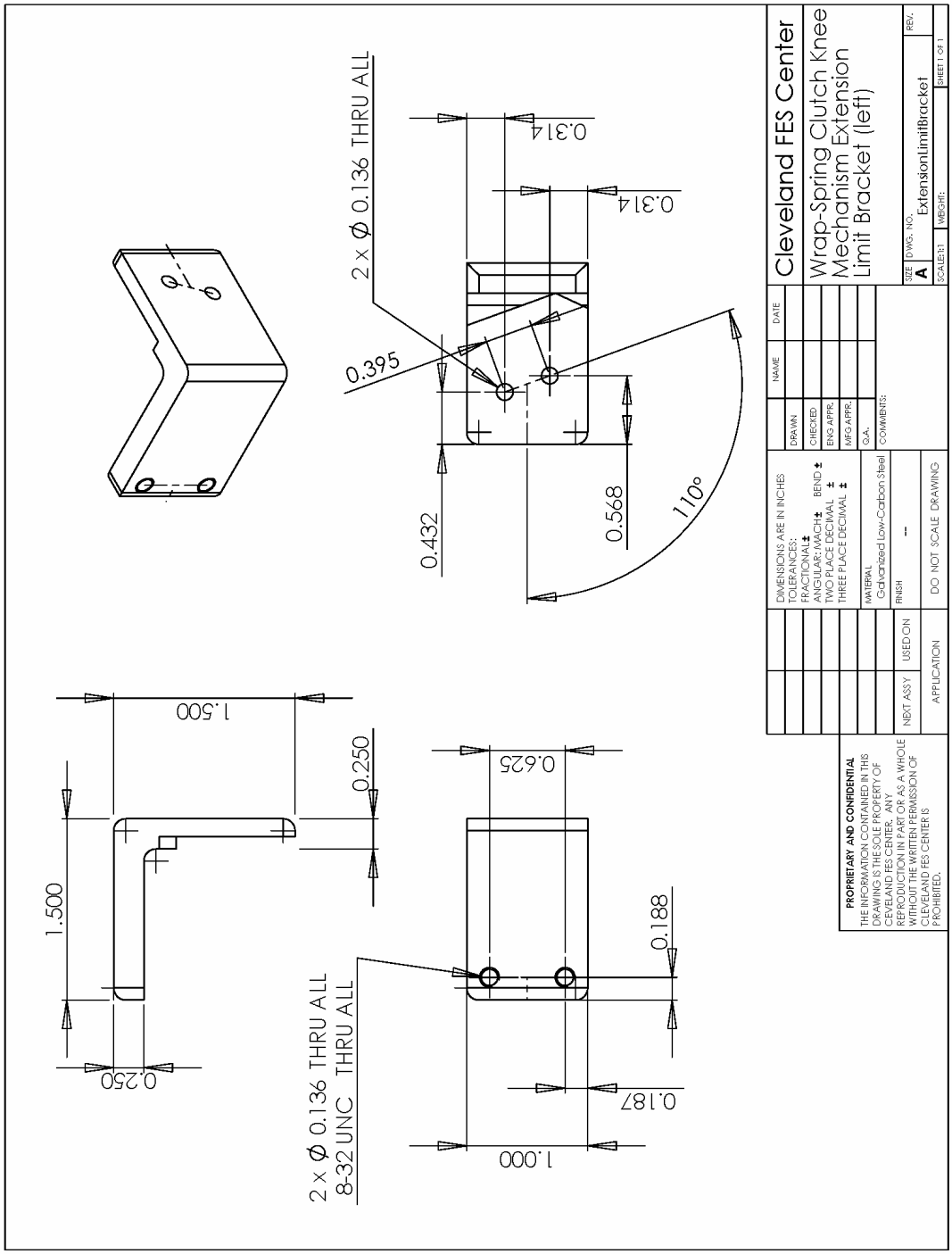
Cleveland FES Center
Wrap-Spring Clutch Knee Mechanism Extension Limit Bracket (left)
ExtensionLimitBracket
SIZE A
SCALE: 1:1
WEIGHT:
SHEET 1 OF 1
REV:
DWG. NO.
DRAWN
CHECKED
ENG APPR.
MFG APPR.
Q.A.
COMMENTS:
NAME
DATE
DIMENSIONS ARE IN INCHES
TOLERANCES:
FRACTIONAL ±
ANGULAR: MACH ± BEND ±
TWO PLACE DECIMAL ±
THREE PLACE DECIMAL ±
MATERIAL
Galvanized Low-Carbon Steel
FINISH
--
DO NOT SCALE DRAWING
NEXT ASSY
USED ON
APPLICATION
PROPRIETARY AND CONFIDENTIAL
THE INFORMATION CONTAINED IN THIS DRAWING IS THE SOLE PROPERTY OF CEVELAND FES CENTER. ANY REPRODUCTION IN PART OR AS A WHOLE WITHOUT THE WRITTEN PERMISSION OF CLEVELAND FES CENTER IS PROHIBITED.
2 x Ø 0.136 THRU ALL
0.314
0.314
0.395
0.432
0.568
110°
1.500
0.250
1.500
0.250
2 x Ø 0.136 THRU ALL
8-32 UNC THRU ALL
0.625
0.188
0.187
1.000

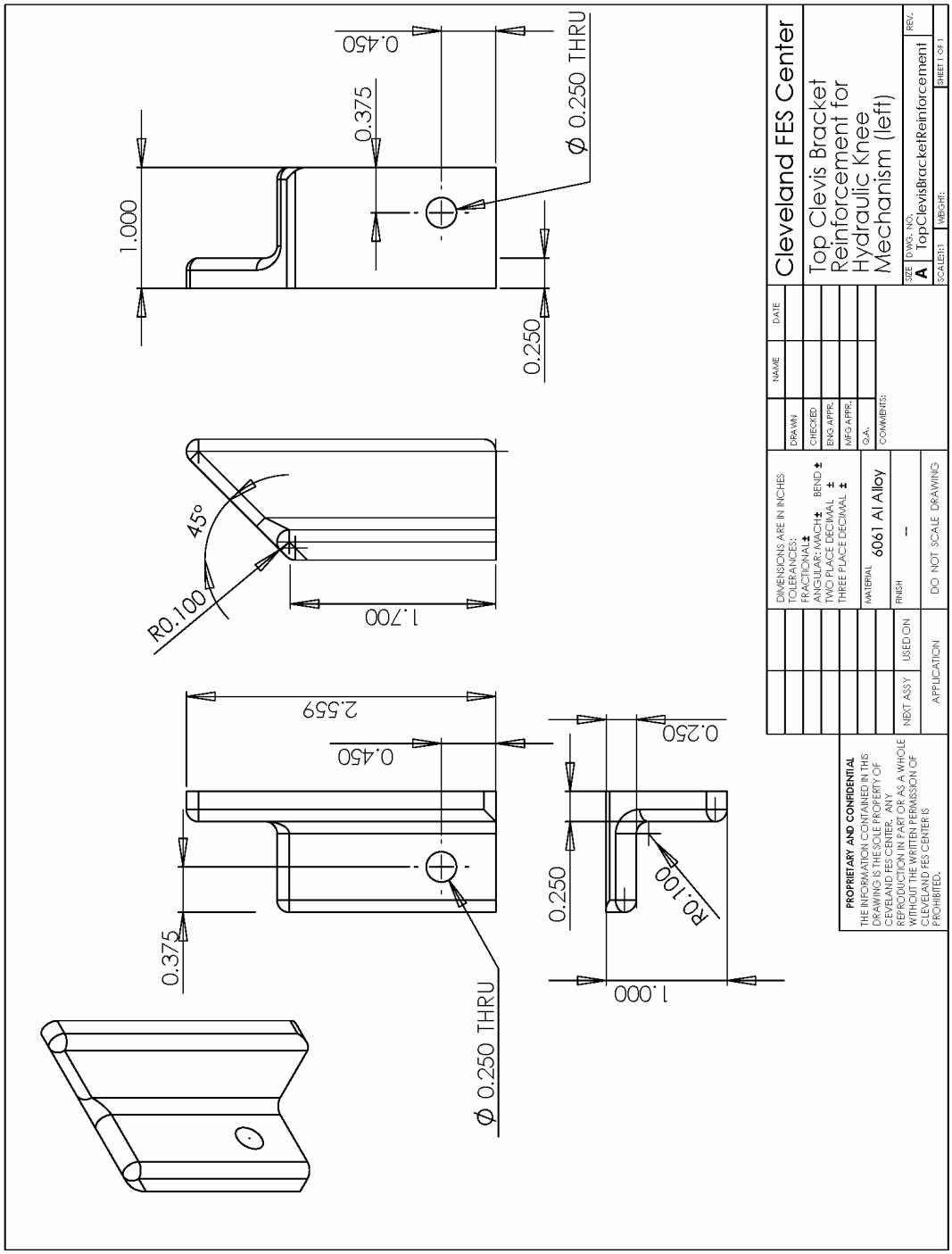
Cleveland FES Center
Top Clevis Bracket Reinforcement for Hydraulic Knee Mechanism (left)
SIZE A
DWG. NO. TopClevisBracketReinforcement
REV:
SCALE:1:1
WEIGHT:
SHEET 1 OF 1
DRAWN
CHECKED
ENG APPR.
MFG APPR.
Q.A.
COMMENTS:
NAME
DATE
DIMENSIONS ARE IN INCHES
TOLERANCES:
FRACTIONAL ±
ANGULAR: MACH ± BEND ±
TWO PLACE DECIMAL ±
THREE PLACE DECIMAL ±
MATERIAL 6061 Al Alloy
FINISH --
DO NOT SCALE DRAWING
NEXT ASSY
USED ON
APPLICATION
PROPRIETARY AND CONFIDENTIAL
THE INFORMATION CONTAINED IN THIS DRAWING IS THE SOLE PROPERTY OF CEVELAND FES CENTER. ANY REPRODUCTION IN PART OR AS A WHOLE WITHOUT THE WRITTEN PERMISSION OF CLEVELAND FES CENTER IS PROHIBITED.
1.000
0.375
0.450
Ø 0.250 THRU
0.250
45°
R0.100
1.700
2.559
0.450
0.375
Ø 0.250 THRU
0.250
R0.100
1.000

BIBLIOGRAPHY

CHAPTER 1

1. C. S. To, R. Kobetic, J. R. Schnellenberger, M. L. Audu, and R. J. Triolo, "Design of a variable constraint hip mechanism for a hybrid neuroprosthesis to restore gait after spinal cord injury," *IEEE/ASME Trans Mechatronics*, vol. 13, no. 2, pp. 197-205, 2008.

2. R. Kobetic, C. S. To, J. R. Schnellenberger, M. L. Audu, T. C. Bulea, R. Gaudio, G. Pinault, S. Tashman, and R. J. Triolo, "Development of a hybrid orthosis for standing, walking, and stair climbing after spinal cord injury" *J. Rehabil. Res. Dev.*, vol. 46, no. 3, pp. 447-462, 2009.

3. "Spinal Cord Injury Facts & Statistics." Spinal Cord Injury Information Pages. 25 June 2006. 23 Dec. 2007 <http://www.sci-info-pages.com/facts.html>.

4. H. O. Kent, "Vannini-Rizzoli Stabilizing Orthosis (Boot): Preliminary report on a new ambulatory aid for spinal cord injury," *Arch. Phys. Med. Rehabil.*, vol. 73, pp. 302-307, Mar. 1992.

5. M. Lyles and J. Munday, "Report on the evaluation of the Vannini-Rizzoli Stabilizing Limb Orthosis," J. *Rehab. Res. & Dev.*, vol. 29, no. 2, pp. 77-104, 1992.

6. J. F. Lehmann, C. G. Warren, D. Hertling, M. McGee, B. C. Simons, and A. Dralle, Craig-Scott orthosis: a biochemical and functional evaluation," *Arch. Phys. Med. Rehabil.*, vol. 57, no. 9, pp. 438-442, Sep. 1976.

7. K. D. Merkel, N. E. Miller, P. R. Westbrook, and J. L. Merritt, " Energy expenditure of paraplegic patients standing and walking with two knee-ankle-foot orthoses," *Arch. Phys. Med. Rehabil.*, vol. 65, pp. 121-124, Mar. 1984.

8. N. Rosman and E. Spira, "Paraplegic use of walking braces: A survey," *Arch. Phys. Med. Rehabil.*, vol. 55, pp. 310-314, July 1974.

9. R. Mikelberg and S. Reid, "Spinal cord lesions and lower extremity bracing: An overview and follow-up study," *Paraplegia*, vol. 19, pp. 379-385, 1981.

10. C. Hong, E. B. San Luis, and S. Chung, "Follow-up study on the use of leg braces issued to spinal cord injury patients," *Paraplegia*, vol. 28, pp. 172-177, 1990.

11. J. W. Middleton, J. D. Yeo, L. Blanch, V. Vare, K. Peterson, and K. Brigden, "Clinical evaluation of a new orthosis, the 'Walkabout', for restoration of functional

standing and short distance mobility in spinal paralysed individuals," *Spinal Cord*, vol. 35, pp. 574-579, 1997.

12. G. K. Rose, "The principles and practice of hip guidance articulations," *Prosth. & Orth. Intnl*., vol. 3, pp. 37-43, 1979.

13. A. V. Nene and J. H. Patrick, "Energy cost of paraplegic locomotion with the ORLAU Parawalker," *Paraplegia*, vol. 27, pp. 5-18, 1989.

14. P. Moore and J. Stallard, "A clinical review of adult paraplegia patients with complete lesions using the ORLAU Parawalker," *Paraplegia*, vol. 29, pp. 191-196, 1991.

15. R. Douglas, P. F. Larson, R. D'Ambrosia, R. E. McCall, "The LSU reciprocating gait orthosis," *Orthopedics*, vol. 6, pp. 834-839, 1983.

16. R. J. Jefferson, M. W. Whittle, "Performance of three walking orthosis for the paralyzed: a case study using gait analysis," *Prosth. & Orth. Intnl*., vol. 14, pp. 103-110, 1990.

17. W. M. Motloch, "Principles of orthotic management for child and adult paraplegia and clinical experience with the isocentric RGO," *Proc. 7th World Congress of the International Society for Prosthetics and Orthotics*, Chicago, pp. 28, Jun 28 - July 3, 1992.

18. S. Hirokawa, M. Grimm, T. Le, M. Solomonow, R. V. Baratta, H. Shoji, and R. D. D'Ambrosia, "Energy consumption in paraplegic ambulation using the reciprocating gait orthosis and electrical stimulation of the thigh muscles," *Arch. Phys. Med. Rehabil*., vol. 71, pp. 687-694, Aug. 1990.

19. L. Sykes, J. Edwards, E. S. Powell, and E. R. S. Ross, "The reciprocating gait orthosis: Long-term usage patterns," *Arch. Phys. Med. Rehabil.*, vol. 76, pp. 779-783, Aug. 1995.

20. J. L. Merritt, N. E. Miller, and T. J. Hanson, "Preliminary studies of energy expenditures in paraplegics using swing-thru and reciprocating gait patterns," *Arch. Phys. Med. Rehabil.*, vol. 64, pp. 510, Oct. 1983.

21. L. A. Harvey, G. M. Davis, M. B. Smith, and S. Engel, "Energy expenditure during gait using the Walkabout and Isocentric Reciprocating Gait orthoses in persons with paraplegia," *Arch. Phys. Med. Rehabil.*, vol. 79, pp. 945-949, Aug. 1998.

22. M. W. Whittle, G. M. Cochrane, A. P. Chase, A. V. Copping, R. J. Jefferson, J. Staples, P. T. Fenn, and D. C. Thomas, "A comparative trial of two walking systems for paralysed people," *Paraplegia*, vol. 29, pp. 97-102, 1991.

23. M. J. Ijzerman, G. Baardman, H. J. Hermens, P.H. Veltink, H. B. K. Boom, and G. Zilvold, "The influence of the reciprocal cable linkage in the advanced reciprocating gait orthosis on paraplegic gait performance," *Prosth. & Orth. Intnl*., vol. 21, pp. 52-61, 1997.

24. P. M. Dall, B. Muller, I. Stallard, J. Edwards, and M. H. Granat, "The functional use of the reciprocal hip mechanism during gait for paraplegic patients walking in the Louisiana State University reciprocating gait orthosis," *Prosth. & Orth. Intnl*., vol. 23, pp. 152-162, 1999.

25. S. Tashman, F. E. Zajac, and I. Perkash, "Modeling and simulation of paraplegic ambulation in a reciprocating gait orthosis," *J. Biomech. Eng.*, vol. 117, pp. 300-308, Aug. 1995.

26. J. S. Petrofsky and J. B. Smith, "Physiologic costs of computer-controller walking in persons with paraplegia using a Reciprocating-Gait Orthosis," *Arch. Phys. Med. Rehabil*., vol. 72, pp. 890-896, Oct. 1991.

27. R. Blessey, "Energy cost of normal walking," *Orthopedic Clinics of North America*, vol. 9, pp. 356-358, 1978.

28. H. Natvig, and R. McAdam, "Ambulation without wheelchairs for paraplegics with complete lesions," *Paraplegia*, vol. 16, pp. 142-146, 1978.

29. M. Solomonow, R. Baratta, S. Hirokawa, N. Rightor, W. Walker, P. Beaudette, H. Shoji, and R. D'Ambrosia, "The RGO Generation II: Muscle stimulation powered orthosis as a practical walking system for thoracic paraplegics," *Orthopedics*, vol. 12, pp. 1309-1315, 1989.

30. A. Kralj, T. Bajd, R. Turk, "Electrical stimulation providing functional use of paraplegic patient muscles," *Med. Prog. Technol*., vol. 7, pp. 3-9, 1980.

31. T. Bajd, A. Kralj, R. Turk, H. Benko, J. Sega, "The use of a four-channel electrical stimulator as an ambulatory aid for paraplegic patients," *Physical Therapy*, vol. 63, no. 7, pp. 1116-1120, July 1983.

32. E. B. Marsolais and R. Kobetic, "Development of a practical electrical stimulation system for restoring gait in the paralyzed patient," *Clin. Orthop.*, no. 233, pp. 64-74, Aug. 1988.

33. P. Gallien, R. Brissot, M. Eyssette, L. Tell, M. Barat, L. Wiart, H. Petit, "Restoration of gait by functional electrical stimulation for spinal cord injured patients," *Paraplegia*, vol. 33, no. 11, pp. 660-664, Nov. 1995.

34. R. Kobetic, R. J. Triolo, and E. B. Marsolais, "Muscle selection and walking performance of multichannel FES systems for ambulation in paraplegia," *IEEE Trans. Rehab. Eng.*, vol. 5, no. 1, pp. 23-29, Mar. 1997.

35. R. Kobetic, R. J. Triolo, J. P. Uhlir, C. Bieri, M. Wibowo, G. Polando, E. B. Marsolais, J. A. Davis, K. A. Ferguson, and M. Sharma, "Implanted functional electrical stimulation system for mobility in paraplegia: A follow-up case report," *IEEE Trans. Rehab. Eng.*, vol. 7, no. 4, pp. 390-398, Dec. 1999.

36. A. Kralj, R. J. Jaeger, and T. Bajd, "Posture switching enables prolonged standing in paraplegic patients functionally electrically stimulated," *Proc. Fifth. Ann. Conf. on Rehab. Eng.*, pp. 60, Houston, 1982.

37. Kralj, T. Bajd, R. Turk, J. Krajnik, and H. Benko, "Gait restoration in paraplegic patients: a feasibility demonstration using multichannel surface electrode FES," *J. Rehabil. Res. Dev.*, vol. 20, pp. 3-20, 1983.

38. D. Graupe and K. H. Kohn, "Transcutaneous functional neuromuscular stimulation of certain traumatic complete thoracic paraplegics for independent short-distance ambulation," *Neurol. Res.*, vol. 19, no. 3, pp. 323-333, June 1997.

39. D. Graupe and K. H. Kohn, "Functional neuromuscular stimulator for short-distance ambulation by certain thoracic-level spinal-cord-injured paraplegics," *Surg. Neurol.*, vol. 50, no. 3, pp. 202-207, Sep. 1998.

40. R. Brissot, P. Gallien, M. P. Le Bot, A. Beaubras, D. Laisne, J. Beillot, and J. Dassonville, "Clinical experience with functional electrical stimulation-assisted gait with Parastep in spinal cord-injured patients," *Spine*, vol. 25, no. 4, pp. 501-508, 2000.

41. M. S. Nash, P. L. Jacobs, B. M. Montalvo, K. J. Klose, R. S. Guest, and B. M. Needham-Shropshire, "Evaluation of a training program for persons with SCI paraplegia using the Parastep 1 ambulation system: part 5. Lower extremity blood flow and hyperemic response to occlusion are augmented by ambulation training," *Arch. Phys. Med. Rehabil*., vol. 78, no. 8, pp. 808-814, 1997.

42. R. S. Guest, K. J. Klose, B. M. Needham-Shropshire, and P. L. Jacobs, "Evaluation of a training program for persons with SCI paraplegia using the Parastep 1 ambulation system: part 4. Effect on physical self-concept and depression," *Arch. Phys. Med. Rehabil*., vol. 78, no. 8, pp. 804-807, 1997.

43. U. Stanic, R. Acimovic-Janezic, N. Gros, A. Trnkoczy, T. Bajd, and M. Kljajic, "Multichannel electrical stimulation for correction of hemiplegic gait," *Scand. J. Rehabil. Med.*, vol. 10, pp. 175-192, 1977.

44. J. S. Petrofsky and C. A. Phillips, "Closed-loop control of movement of skeletal muscle," *CRC Crit. Rev. Biomed. Eng*., vol. 13, pp. 35-96, 1985.

45. D. J. Nicol, M. H. Granat, S. J. Tuson, and R. H. Baxendale, "Variability of the dishabituation of flexion reflexes for FES assisted gait in spinal injured man," *Med. Eng. Phys.*, vol. 20, no. 3, pp. 182-187, 1998.

46. A. Scheiner, G. Polando, and E. B. Marsolais, "Design and clinical application of a double helix electrode for functional electrical stimulation," *IEEE Trans. Biomed. Eng.*, vol. 41, no. 5, pp. 425-431, 1994.

47. H. Kagaya, M. Sharma, G. Polando, and E. B. Marsolais, "Reliability of closed double helix electrode for totally implantable FES system," *Clin. Orthop.*, vol. 233, pp. 64-74, 1998.

48. E. B. Marsolais and R. Kobetic, "Functional electrical stimulation for walking in paraplegia," *J. Bone. Joint. Surg.*, vol. 69A, pp. 728-733, 1987.

49. E. B. Marsolais and R. Kobetic, "Implantation techniques and experience with percutaneous intramuscular electrodes in the lower extremities," *J. Rehabil. Res. Dev.*, vol. 23, pp. 1-8, 1986.

50. S. Nandurkar, E. B. Marsolais, and R. Kobetic, "Percutaneous implantation of iliopsoas for functional neuromuscular stimulation," *Clin. Orthop.*, vol. 389, pp. 210-217, 2001.

51. J. T. Mortimer, D. Kaufman, and U. Roessmann, "Intramuscular electrical stimulation: Tissue damage," *Ann. Biomed. Eng*., vol. 8, pp. 235-244, 1980.

52. R. J. Triolo, M. Q. Liu, R. Kobetic, and J. P. Uhlir, "Selectivity of intramuscular stimulating electrodes in the lower limbs," *J. Rehabil. Res. Dev.*, vol. 38, no. 5, pp. 533-544, 2001.

53. J. P. Uhlir, R. J. Triolo, and R. Kobetic, "The use of selective electrical stimulation of the quadriceps to improve standing function in paraplegia," *IEEE Trans. Rehabil. Eng.*, vol. 8, no. 4, pp. 514-522, 2000.

54. R. J. Triolo, M. Wibowo, J. Uhlir, R. Kobetic, and R. Kirsch, "Effects of stimulated hip extension moment and position on upper-limb support forces during FES-induced standing – A technical note," *J. Rehabil. Res. Dev.*, vol. 38, no. 5, pp. 545-555, 2001.

55. Y. Shimada, K. Sato, E. Abe, H. Kagaya, K. Ebata, M. Oba, M. Sata, "Clinical experience of functional electrical stimulation in complete paraplegia," *Spinal Cord*, vol. 34, pp. 615-619, 1996.

56. E. B. Marsolais and B. G. Edwards, "Energy costs of walking and standing with functional neuromuscular stimulation and long leg braces," *Arch. Phys. Med. Rehabil*., vol. 69, pp. 243-249, April 1988.

57. M. Gregory and C. S. Bickel, "Recruitment patterns in human skeletal muscle during electrical stimulation," *Physical Therapy*, vol. 85, no. 4, pp. 358-364, 2005.

58. J. H. Patrick and M. R. McClelland, "Low energy cost reciprocal walking for the adult paraplegic," *Paraplegia*, vol. 23, pp. 113-117, 1985.

59. J. Stallard, R. E. Major, R. Poiner, I. R. Farmer, and N. Jones, "Engineering design considerations of the ORLAU Parawalker and FES hybrid system," *Eng. Med.*, vol. 15, no. 3, pp. 123-129, 1986.

60. M. McClelland, B. J. Andrews, J. H. Patrick, P. A. Freeman, and W. S. El Masri, "Augmentation of the Oswestry Parawalker Orthosis by means of surface electrical stimulation: Gait analysis of three patients," *Paraplegia*, vol. 25, pp. 32-38, 1987.

61. A. V. Nene and J. H. Patrick, "Energy cost of paraplegic locomotion using the Parawalker – Electrical stimulation "hybrid" orthosis," *Arch. Phys. Med. Rehabil.*, vol. 71, pp. 116-120, Feb. 1990.

62. C. A. Phillips and D. M. Hendershot, "A systems approach to medically prescribed functional electrical stimulation. Ambulation after spinal cord injury," *Paraplegia*, vol. 29, pp. 505-513, 1991.

63. E. Isakov, R. Douglas, and P. Berns, "Ambulation using the reciprocating gait orthosis and functional electrical stimulation," *Paraplegia*, vol. 30, pp. 239-245, 1992.

64. L. Yang, M. H. Granat, J. P. Paul, D. N. Condie, and D. I. Rowley, "Further development of hybrid functional electrical stimulation orthoses," *Spinal Cord*, vol. 34, no. 10, pp. 611-614, Oct. 1996.

65. M. Solomonow, E. Aguilar, E. Reisin, R. V. Baratta, R. Best, T. Coetzee, and R. D'Ambrosia, "Reciprocating gait orthosis powered with electrical muscle stimulation (RGO II). Part I: Performance evaluation of 70 paraplegic patients," *Orthopedics*, vol. 20, no. 4, pp. 315-324, April 1997.

66. A. V. Nene and S. J. Jennings, "Hybrid paraplegic locomotion with the Parawalker using intramuscular stimulation: A single subject study," *Paraplegia*, vol. 27, pp. 125-132, 1989.

67. E. B. Marsolais, R. Kobetic, G. Polando, K. Ferguson, S. Tashman, R. Gaudio, S. Nandurkar, and H. R. Lehneis, "The Case Western Reserve University hybrid gait orthosis," *J. Spinal Cord Med*., vol. 23, no. 2, pp. 100-108, 2000.

68. R. Kobetic, E. B. Marsolais, R. J. Triolo, D. T. Davy, R. Gaudio, and S. Tashman, "Development of a hybrid gait orthosis: A case report," *J. Spinal Cord Med*., vol. 26, no. 3, pp. 254-258, 2003.

69. M. Goldfarb and W. Durfee, "Design of a controlled-brake orthosis for FES-added gait," *IEEE Trans. Rehab. Eng.*, vol 4, no. 1, pp. 13-24, Mar. 1996.

70. M. Goldfarb, K. Korkowski, B. Harrold, and W. Durfee, "Preliminary evaluation of a controlled-brake orthosis for FES-aided gait," *IEEE Trans. Neur. Sys. Rehab. Eng.*, vol. 11, no. 3, pp. 241-248, Sept. 2003.

71. P. J. Greene and M. H. Granat, "A knee and ankle flexing hybrid orthosis for paraplegic ambulation," *Med. Eng. Phys*., vol. 25, pp. 539-545, 2003.

72. S. Gharooni, B. Heller, and M. O. Tokhi, "A new hybrid spring brake orthosis for controlling hip and knee flexion in the swing phase," *IEEE Trans. Neur. Sys. Rehab. Eng.*, vol. 9, no. 1, pp. 106-107, Mar. 2001.

73. W. K. Durfee and A. Rivard, "Design and simulation of a pneumatic stored-energy, hybrid orthosis for gait restoration," *J. Biomech. Eng*., vol. 127, pp. 1014-1019, Nov. 2005.

CHAPTER 2

1. J. F. Lehmann and J. B. Stonebridge, "Knee lock device for knee ankle orthoses for spinal cord injured patients: an evaluation," *Arch. Phys. Med. Rehabil*., vol. 59, no. 5, pp. 207-211, 1978.

2. H. Kagaya, Y. Shimada, K. Sato, M. Sato, K. Iizuka, and G. Obinata, "An electrical knee lock system for functional electrical stimulation," *Arch. Phys. Med. Rehabil*., vol. 77, pp. 870-873, 1996.

3. R. Harrison, E. Lemaire, Y. Jeffreys, and L. Goudreau, "Design and pilot testing of an orthotic stance-phase control knee joint, *Orthopadie Technik,* pp. 2-4, 2001.

4. G. Kim, S. Kang, J. Ryu, M. Mun, and K. Kim, "Unlockable Knee Joint Mechanism for Powered Gait Orthosis," *Int, J. Precision Eng & Manufacturing*, vol. 10, no. 3, pp. 83-89, July 2009.

5. N. G. Van Leederdam, and E. E. Kunst, "New UTX-swing orthosis: Normal gait and safe standing," *Orthopadie Technik*, vol. 50, pp. 506-515, 1999.

6. G. Nijenbanning, J. A. Goudsmit, “Gravity operated locking hinge,” United States patent US 20030153854. Aug 14, 2003.

7. B. J. Hatton, D. L. Hatton, and Z. G. Wallace, “Articulating knee supports,” United States patent US 6635024. Oct 21, 2003.

8. T. Yakimovich, J. Kofman, and E. D. Lemaire, “Design and evaluation of a stance-control knee-ankle-foot orthosis knee joint,” *IEEE Trans. Neur. Sys. Rehab. Eng.*, vol. 14, no. 3, pp. 361-369, Sept. 2006.

9. R. B. McGhee, R. Tomovic, Y. Yang, and I. C. MacLean, “An experimental study of a sensor-controlled external knee locking system,” *IEEE Trans. Biomed. Eng.*, vol. 25, pp. 195-199, 1978.

10. S. E. Irby, K. R. Kaufman, R. W. Wirta, and D. H. Sutherland, “Optimization and application of a wrap-spring clutch to a dynamic knee-ankle-foot orthosis,” *IEEE Trans. Rehab. Eng.*, vol. 7, pp. 130-134, 1999.

11. N. Sclater, and N. P. Chironis, Mechanisms and Mechanical Devices Sourcebook. New York, NY: McGraw-Hill, 2001.

12. J. C. Moreno, F. Brunetti, E. Rocon, and J. L. Pons, “Immediate effects of a controllable knee ankle foot orthosis for functional compensation of gait in patients with proximal leg weakness,” *Med. Biol. Eng. Comp.*, vol. 46, no. 1, pp. 43-53, 2007.

13. T Yakimovich, E. D. Lemaire, and J. K. Kofman, “Engineering design review of stance-control knee-ankle-foot orthoses,” *J. Rehabil. Res. & Dev.*, vol. 46, no. 2, pp. 257-268, 2009.

14. J. Perry, Gait Analysis: Normal and Pathological Function, Thorofare, NJ: SLACK Incorporated, pp. 92, 94, 1992.

15. S. K. Ng and H. J. Chizeck, “Fuzzy model identification for classification of gait events in paraplegics,” *IEEE Trans. Fuzzy Syst.*, vol. 5, pp. 536–544, Nov. 1997.

16. M. M. Skelly and H. J. Chizeck, “Real-time gait event detection for paraplegic FES walking,” *IEEE Trans. Neural Systems Rehab. Eng.*, vol. 9, no. 1, pp. 59-68, March 2001.

17. R. Kobetic and E. B. Marsolais, “Synthesis of paraplegic gait with multichannel functional neuromuscular stimulation,” *IEEE Trans. Rehabil. Eng.*, vol. 2, no. 2, pp. 66–79, Jun. 1994.

CHAPTER 3

1. G. K. Rose, "The principles and practice of hip guidance articulations," *Prosth. & Orth. Intnl.*, vol. 3, pp. 37-43, 1979.

2. R. E. Major, J. Stallard, and G. K. Rose, "The dynamics of walking using the hip guidance orthosis (hgo) with crutches," *Prosth. & Orth. Intnl.*, vol. 5, pp. 19-22, 1981.

3. R. Douglas, P. F. Larson, R. D'Ambrosia, R. E. McCall, "The LSU reciprocating gait orthosis," *Orthopedics*, vol. 6, pp. 834-839, 1983.

4. Y. Ohta, H. Yano, R. Suzuki, M. Yoshida, N. Kawashima, and K. Nakazawa, "A two-degree-of-freedom motor-powered gait orthosis for spinal cord injury patients," *Proc. IMechE Part H: J. Engineering in Medicine*, vol. 221, no. 6, pp. 629-639, 2007.

5. R. J. Jefferson, M. W. Whittle, "Performance of three walking orthosis for the paralyzed: a case study using gait analysis," *Prosth. & Orth. Intnl.*, vol. 14, pp. 103-110, 1990.

6. W. M. Motloch, "Principles of orthotic management for child and adult paraplegia and clinical experience with the isocentric RGO," *Proc. 7th World Congress of the International Society for Prosthetics and Orthotics*, Chicago, pp. 28, Jun 28 - July 3, 1992.

7. A. Pedotti, M. Ferrarin, J. Quintern, and R. Riener, *Neuroprosthetics: from Basic Research to Clinical Application*, Germany: Springer-Verlag Berlin Heidelberg, pp. 493-502, 1996.

8. B. M. Y. Nouri and A. Zaidan, "Computer control of a powered two degree freedom reciprocating gait orthosis," *ISA Transactions*, vol. 45, no. 2, pp. 249-258, 2006.

9. G. Kim, S. Kang, S. Kang, J. Ryu, M. Mun, and K. Kim, "Unlockable knee joint mechanism for powered gait orthosis," *Int. J. Precision Engineering and Manufacturing*, vol. 10, no. 3, pp. 83-89, July 2009.

10. L. Yang, M. H. Granat, J. P. Paul, D. N. Condie, and D. I. Rowley, "Further development of hybrid functional electrical stimulation orthoses," *Spinal Cord*, vol. 34, no. 10, pp. 611-614, Oct. 1996.

11. P. M. Dall, B. Muller, I. Stallard, J. Edwards, and M. H. Granat, "The functional use of the reciprocal hip mechanism during gait for paraplegic patients walking in the Louisiana State University reciprocating gait orthosis," *Prosth. & Orth. Intnl*., vol. 23, pp. 152-162, 1999.

12. C. S. To, R. F. Kirsch, R. Kobetic, and R. J. Triolo, "Simulation of a functional neuromuscular stimulation powered mechanical gait orthosis with coordinated joint locking," *IEEE Trans. Neural Syst. Rehab. Eng*., vol. 13, no. 2, pp. 227-235, 2005.

13. D. W. Dudley, *Handbook of Practical Gear Design*, Boca Raton, FL: CRC Press LLC, pp. 3.74–3.115, 1994.

14. E. B. Marsolais, R. Kobetic, G. Polando, K. Ferguson, S. Tashman, R. Gaudio, S. Nandurkar, and H. R. Lehneis, "The Case Western Reserve University hybrid gait orthosis," *J. Spinal Cord Med.*, vol. 23, no. 2, pp. 100-108, 2000.

15. R. Kobetic, E. B. Marsolais, and P. C. Miller, "Function and strength of electrically stimulated hip flexor muscles in paraplegia," *IEEE Trans.Rehab. Eng*., vol. 2, no. 1, pp. 11-17, Mar. 1994.

16. R. Kobetic and E. B. Marsolais, "Synthesis of paraplegic gait with multichannel functional neuromuscular stimulation," *IEEE Trans. Rehab. Eng.*, vol. 2, no. 2, pp. 66-79, June 1994.

17. P. Krawetz and P. Nance, "Gait analysis of spinal cord injured subjects: Effects of injury level and spasticity," *Arch. Phys. Med. Rehabil.*, vol. 77, pp. 635-638, July 1996.

18. J. Perry, *Gait Analysis: Normal and Pathological Function*, Thorofare, NJ: SLACK Incorporated, pp. 10-16, 1992.

CHAPTER 4

1. M. Goldfarb, K. Korkowski, B. Harrold, and W. Durfee, "Preliminary evaluation of a controlled-brake orthosis for FES-aided gait," *IEEE Trans. Neur. Sys. Rehab. Eng.*, vol. 11, no. 3, pp. 241-248, Sept. 2003.

2. S. G. Caroll, R. J. Triolo, H. J. Chizeck, R. Kobetic, and E. B. Marsolais, "Tetanic response of electrically stimulated paralyzed muscle at varying interpulse intervals," *IEEE Trans. Biomed. Eng.*, vol. 36, no. 7, pp. 644-653, 1989.

3. J. T. Mortimer, D. Kaufman, and U. Roessmann, "Intramuscular electrical stimulation: Tissue damage," *Ann. Biomed. Eng*., vol. 8, pp. 235-244, 1980.

4. R. Kobetic and E. B. Marsolais, "Synthesis of paraplegic gait with multichannel functional neuromuscular stimulation," *IEEE Trans. Rehab. Eng*., vol. 2, no. 2, pp. 66-79, June 1994.

5. J. Perry, *Gait Analysis: Normal and Pathological Function*, Thorofare, NJ: SLACK Incorporated, pp. 10-16, 1992.

6. M. Goldfarb and W. Durfee, "Design of a controlled-brake orthosis for FES-added gait," *IEEE Trans. Rehab. Eng.*, vol 4, no. 1, pp. 13-24, Mar. 1996.

7. H. Kagaya, Y. Shimada, K. Sato, M. Sato, K. Iizuka, and G. Obinata, "An electrical knee lock system for functional electrical stimulation," *Arch. Phys. Med. Rehabil*., vol. 77, pp. 870-873, Sept. 1996.

8. S. Nandurkar, E. B. Marsolais, and R. Kobetic, "Percutaneous implantation of iliopsoas for functional neuromuscular stimulation," *Clin. Orthop.*, vol. 389, pp. 210-217, 2001.

9. R. B. Davis III, A. Ounpuu, D. Tybursji, and J. R. Gage, "A gait analysis data collection and reduction technique," *Human Movement Science*, vol. 10, pp. 575-587, 1991.

10. R. Kobetic, E. B. Marsolais, and P. C. Miller, "Function and strength of electrically stimulated hip flexor muscles in paraplegia," *IEEE Trans.Rehab. Eng*., vol. 2, no. 1, pp. 11-17, Mar. 1994.

CHAPTER 5

1. R. Kobetic, E. B. Marsolais, and P. C. Miller, "Function and strength of electrically stimulated hip flexor muscles in paraplegia," *IEEE Trans.Rehab. Eng*., vol. 2, no. 1, pp. 11-17, Mar. 1994.

2. E. B. Marsolais and B. G. Edwards, "Energy costs of walking and standing with functional neuromuscular stimulation and long leg braces," *Arch. Phys. Med. Rehabil*., vol. 69, pp. 243-249, April 1988.

3. R. Kobetic and E. B. Marsolais, "Synthesis of paraplegic gait with multichannel functional neuromuscular stimulation," *IEEE Trans. Rehab. Eng*., vol. 2, no. 2, pp. 66-79, June 1994.

4. C. S. To, R. F. Kirsch, R. Kobetic, and R. J. Triolo, "Simulation of a functional neuromuscular stimulation powered mechanical gait orthosis with coordinated joint locking," *IEEE Trans. Neural Syst. Rehab. Eng*., vol. 13, no. 2, pp. 227-235, 2005.

5. J. Perry, *Gait Analysis: Normal and Pathological Function.* Thorofare, NJ: SLACK Inc., 1992, pp. 61, 100, 120, 247.

6. H. M. Franken, P. H. Veltink, G. Baardman, R. A. Redmeyer, and H. B. K. Boom, "Cycle-to-cycle control of swing phase of paraplegic gait induced by surface electrical stimulation," *Med. Biol. Eng. Comp.*, vol. 33, pp. 440-451, 1995.

7. P. H. Veltink, "Control of FES-induced cyclical movements of the lower leg," *Med. Biol. Eng. Comp.*, vol. 29, pp. NS8-NS12, 1991.

8. H. M. Franken, P. H. Veltink, G. Baardman, R. A. Redmeijer, and H. B. K. Boom, "Experimental on/off control of the swing phase of paraplegic gait induced by surface electrical stimulation," *Proc. 15th IEEE EMBS Conf.*, San Diego, CA, USA, pp. 1324-1325, 1993.

9. H. M. Franken, W. de Vries, P. H. Veltink, G. Baardman, and H. B. K. Boom, "State detection during paraplegic gait as part of a finite state based controller," *Proc. 15th IEEE EMBS Conf.*, San Diego, CA, USA, pp. 1322-1323, 1993.

10. B. J. Andrews, R. W. Barnett, G. F. Phillips, C. A. Kirkwood, N. Donaldson, D. N. Rushton, and D. A. Perkins, "Rule-based control of a hybrid FES orthosis for assisting paraplegic locomotion," *Automedica*, vol. 11, pp. 175-199, 1989.

11. A. T. M. Willemsen, F. Bloemhof, and H. B. K. Boom, "Automatic stance-swing phase detection from accelerometer data for peroneal nerve stimulation," *IEEE Trans. Biomed. Eng.*, vol. 37, no. 12, pp. 1201-1208, Dec. 1990.

12. I. P. I. Pappas, M. Popovic, T. Keller, V. Dietz, and M. Morari, "A reliable gait phase detection system," *IEEE Trans. Neural Systems Rehab. Eng.*, vol. 9, no. 2, pp. 113-125, June 2001.

13. C. A. Kirkwood and B. J. Andrews, "Finite state control of FES systems: Application of AI inductive learning techniques," *Proc. 11th IEEE EMBS Conf.*, Seattle, WA, USA, pp. 1020-1021, 1989.

14. Z. M. Nikolic and D. B. Popovic, "Automatic rule determination for finite state model of locomotion," *Proc. 16th IEEE EMBS Conf.*, Baltimore, MD, USA, pp. 1382-1383, 1994.

15. A. Kostov, B. J. Andrews, D. B. Popovic, R. B. Stein, and W. Armstrong, "Machine learning in control of functional electrical stimulation systems for locomotion," *IEEE Trans. Biomed. Eng.*, vol. 42, pp. 541–551, June 1995.

16. R. Williamson and B. J. Andrews, "Gait event detection for FES using accelerometers and supervised machine learning," *IEEE Trans. Rehab. Eng.*, vol. 8, no. 3, pp. 312-319, Sept. 2000.

17. M. Hansen, M. K. Haugland, and T. Sinkjaer, "Evaluating robustness of gait event detection based on machine learning and natural sensors," *IEEE Trans. Neural Systems Rehab. Eng.*, vol. 12, no. 1, pp. 81-88, March 2004.

18. S. K. Ng and H. J. Chizeck, "A fuzzy logic gait event detector for FES paraplegic gait," *Proc. 15th IEEE EMBS Conf.*, San Diego, CA, USA, pp. 1238-1239, 1993.

19. S. K. Ng and H. J. Chizeck, "Fuzzy model identification for classification of gait events in paraplegics," *IEEE Trans. Fuzzy Syst.*, vol. 5, pp. 536–544, Nov. 1997.

20. M. M. Skelly and H. J. Chizeck, "Real-time gait event detection for paraplegic FES walking," *IEEE Trans. Neural Systems Rehab. Eng.*, vol. 9, no. 1, pp. 59-68, March 2001.

21. D. Graupe, K. H. Kohn, A. Kralj, and S. Basseas, "Patient controlled electrical stimulation via EMG signature discrimination for providing certain paraplegics with primitive walking functions," *J. Biomed. Eng.*, vol. 5, no. 3, pp. 220-226, July 1983.

22. B. J. Andrews, A. Kostov, and R. B. Stein, "Gait event and user intention detection for FES-control: Selecting sensors," *Proc. 17th IEEE EMBS Conf.*, Montreal, Que., Canada, vol. 2, pp. 1153-1154, 1995.

23. A. Zoss and H. Kazerooni, "Design of an electrically actuated lower extremity exoskeleton," *Advanced Robotics*, vol.20, no. 9, pp. 967-988, 2006.

24. H. Kawamoto, S. Kanbe, and Y. Sankai, " Power assist method for HAL-3 estimating operator's intention based on motion information," *Proc. IEEE International Workshop on Robot and Human Interactive Communication*, Millbrae, CA, USA, pp. 67-72, Oct. 2003.

25. H. Kazerooni, "Dynamics and control of instrumented harmonic drives," *ASME Trans. J. Dynamic Systems, Measurements, and Control*, vol. 117, pp. 15-19, Mar. 1995.

26. T. Nef and P. Lum, "Improving backdrivability in geared rehabilitation robots," *Med. Biol. Eng. Comput.*, DOI 10.1007/s11517-009-0437-0, Jan. 2009.

27. R. Kobetic, S. G. Carrol, and E. B. Marsolais, "Paraplegic stair climbing assisted by electrical stimulation," *39th Annual Conference on Engineering in Medicine and Biology*. pp. 265, 1986.